

Lawrence Berkeley National Laboratory

LBL Publications

Title

Performance Evaluation of Engineered Geothermal Systems Using Discrete Fracture Network Simulations

Permalink

<https://escholarship.org/uc/item/4168d73x>


Authors

Kennedy, Burton
Blankenship, Doug
Doe, Thomas
et al.

Publication Date

2021-04-06

Peer reviewed



The following report summarizes the findings of the EGS Validation Panel convened by the Geothermal Technology Office, Department of Energy to evaluate the feasibility of engineering a geothermal reservoir capable of generating electricity economically.

Panel Co-Chairs

Burton M. Kennedy, Lawrence Berkeley National Laboratory (LBNL)
Douglas A. Blankenship, Sandia National Laboratories (SNL)

Report Compilers

Thomas Doe, Golder Associates Inc. (Golder)
Azadeh Riahi, Itasca Consulting Group Inc. (Itasca)

Report Contributors

Branko Damjanac, Itasca Consulting Group (Itasca)
Pengcheng Fu, Lawrence Livermore National Laboratory (LLNL)
Eric Sonnenthal, Lawrence Berkeley National Laboratory (LBNL)
Aleta Finnila, Golder Associates Inc. (Golder)

Report Reviewers

Kate Baker, Consultant
Steve Ingebritsen, US Geological Survey (USGS)

Panel Members

Chad Augustine, National Renewable Energy Laboratory (NREL)
Kate Baker, Consultant
Douglas A. Blankenship, (co-chair) Sandia National Laboratories (SNL)
Charles Carrigan, Lawrence Livermore National Laboratory (LLNL)
Branko Damjanac, Itasca Consulting Group Inc. (Itasca)
Thomas Dewers, Sandia National Laboratories (SNL)
Thomas Doe, Golder Associates Inc. (Golder)
Derek Elsworth, Pennsylvania State University (PSU)
Charles Fairhurst, Itasca Consulting Group (Itasca)
Michael Fehler, Massachusetts Institute of Technology (MIT)
Pengcheng Fu, Lawrence Livermore National Laboratory (LLNL)
Steve Ingebritsen, US Geological Survey (USGS)
Burton M. Kennedy (co-chair), Lawrence Berkeley National Laboratory (LBNL)
Azadeh Riahi, Itasca Consulting Group Inc. (Itasca)
Eric Sonnenthal, Lawrence Berkeley National Laboratory (LBNL)
Norm Warpinski, Haliburton

This page intentionally left blank.

Performance Evaluation of Engineered Geothermal Systems Using Discrete Fracture Network Simulations

A Panel Report

April 9, 2021

This page intentionally left blank.

Summary

Purpose and Objectives

Electrical power production from geothermal energy has a solid record of success for permeable reservoirs such as The Geysers in northern California and geothermal systems in Iceland and New Zealand, among other places. Such permeable reservoirs, however, represent only a small fraction of the available heat energy in the earth's shallow crust. Most of the available energy resides in rocks with insufficient permeability and storage to produce commercial volumes of heated fluids.

Rather than produce the hot fluids in place, Enhanced (or Engineered) Geothermal Systems (EGS) create a permeable reservoir by creating new fractures or by stimulating pre-existing natural fractures. Cool water injected through the stimulated fractures draws heat from the rock as it circulates through the reservoir to a production well, which sends the heated water to the surface for power generation.

Geothermal heat is essentially ubiquitous at depth, and a major attraction of EGS systems is the possibility that geothermal power could be available anywhere (INL, 2006). Research studies and pilot electrical production projects beginning in the 1970s and continuing to the present time have proven that the EGS concept is capable of producing electricity, but not to commercial levels of power production either due to insufficient circulation rates or unexpectedly premature thermal decline in the production well.

Most methodologies for designing and assessing EGS performance use numerical simulators that treat the rock as a porous, continuous material (e.g., Sanyal and Butler, 2005). While porous, continuous approaches have had considerable success in geothermal development, fracture pathways are networks of discrete conductors that may be very discontinuous in addition to being heterogeneous and anisotropic. Furthermore, their flow behaviors may be very sensitive to coupled thermal, mechanical, and chemical effects.

Discrete fracture network models (DFN) were developed initially for radioactive waste disposal research and have subsequently had broader applications in

petroleum engineering and groundwater studies. To date, DFN models have not been widely applied for geothermal purposes.

The US Department of Energy (DOE) undertook a study of EGS behavior using DFN models and the DFN approaches. Sandia National Laboratories (Sandia) and Lawrence Berkeley National Laboratory (LBNL) directed the study, and they in turn selected the Itasca Consulting Group (Itasca), Golder Associates Inc. (Golder), Lawrence Livermore National Laboratory (LLNL), and LBNL to develop numerical experiments using DFN models to perform the following tasks:

- Help the DOE determine under what conditions EGS may or may not be viable,
- Guide analyses, including coupled hydro-thermomechanical-chemical modeling, to understand critical parameters and sensitivities, and
- Provide input to future field operations and EGS demonstrations.

Despite the considerable progress in developing DFN models over the past 40 years, at the start of this project there did not exist a widely applied or accepted DFN simulator that could handle coupled hydro-thermal-mechanical-chemical behaviors in fracture networks. Furthermore, simulation capabilities were often two-dimensional and not three-dimensional. Thus, a significant portion of the work performed for this study involved expanding the coupling capabilities of DFN models.

The overall organization of this report structures itself around DFN simulations that progress from simple to more complex, that is, from two-dimensional models with hydro-thermal coupling only to models having hydro-thermal-mechanical coupling in both two and three dimensions. Chemical coupling was included using porous continuum models with heterogeneous properties derived from DFN models.

Throughout these analyses, this study assumed some target values for a successful EGS operation. A commercial operation was assumed to have an output of at least 5 MW, which for reasonable thermal properties of the rock and water required a mass flow rate of 70 to 80 kg/s ($\sim .07 - .08 \text{ m}^3/\text{s}$) assuming 10% conversion efficiency. In addition to this flow rate, a successful EGS system was assumed to have thermal longevity, which means limiting production water thermal decline to either 10° C or

10% of the temperature differential between reservoir and injection fluid for a span of 20 to 30 years.

Two-Dimensional Hydro-Thermal Fracture Models (Golder)

The analytical solutions of Gringarten et al. (1975) describe heat transfer in two dimensions from parallel fractures having regular spacing and constant properties.

Analytical solutions using the Gringarten model and simple hydro-thermal numerical models extending the Gringarten model show that that EGS performance is influenced by the following:

- Surface area affects thermal breakthrough by a second power relationship.
- Flowrate affects thermal breakthrough by an inverse second power relationship.
- The definition of dimensionless time in Gringarten's solutions provides a simple and robust method of calculating the total fracture area required to meet performance targets (about 4 million m² for reasonable rock and fluid thermal properties).
- Multiple fractures improve thermal performance by having both enhanced surface area and decreased flow rates per fracture.
- At higher fracture intensities the combination of slower moving water and smaller block sizes results in delayed thermal breakthrough followed by rapid thermal depletion, along with high thermal recovery factors.
- Heterogeneity of both spacing and aperture within fracture networks leads to localization of thermal depletion and flow, resulting in poorer thermal performance.

Two- and Three-Dimensional Hydro-Mechanical Simulations (Itasca)

Itasca's initial simulations used their UDEC and 3DEC codes to perform hydro-mechanical simulations on two- and three-dimensional fracture networks. The studies focused on hydro-shear stimulation of natural fractures. Hydro-shearing is the preferential hydraulic shearing of the natural fractures by increasing pore pressures through hydraulic injection. The simulations looked at four performance indices: the pressure at the injection well as a measure of impedance, the total surface area of fractures that sees increased fluid pressure from injection, the total area of fractures that experience shear stimulation with more than 1 mm of slip,

and the average fracture aperture change due to the shear stimulation. The simulations were 2-dimensional using two fracture sets –, a primary and secondary, having different orientations with respect to the in-situ stresses and thus having different potentials for shear stimulation.

The fracture size distribution and the exponent of the negative power-law used to generate the fracture in the simulations will affect fracture connectivity and clustering. Distributions with larger fracture size frequencies have higher connectivity regardless of the average size of the fracture population. Smaller power law exponents weight the total population of fractures into longer fractures, while larger power law exponents weight towards shorter fractures. The greater fracture connectivity associated with longer fractures increases the total fracture area affected by injection, and it is also more efficient at diffusing pressure through the system, thus reducing the portion of the fracture network that reaches pressures sufficient for hydro-shearing. The probability of flow localization increases when connectivity is controlled by large fractures rather than a network of small fractures.

Rougher fractures with larger dilation angles have a greater increase in transmissivity with shearing but produce a smaller shear-affected area than fracture networks with smaller dilation angles.

The magnitude of in-situ deviatoric stress and orientation of in-situ principal stresses relative to fracture orientation are very important factors affecting the potential for fracture stimulation. DFNs almost always consist of multiple fracture sets. When multiple fracture sets compared to a single undergo hydro-shearing due to fluid pressure increase, the stimulated fracture surface area will be greater forming a better-connected network of permanently dilated fractures.

The three-dimensional hydro-mechanical simulations describe effects of staged injection versus injection through the entire length of the horizontal segment of the borehole. They show clear advantage of multi-stage stimulation in reducing localization of flow. Staged injection focuses the injection (sequentially) into shorter segments of the borehole length, leading to a greater shear stimulated area, and better chances of stimulating greater volume of the reservoir. Investigation of the effect of well completion design (i.e., open borehole versus cased completion with

perforation clusters) suggests that the cased completion, which relies on hydraulic fracturing to connect the injection well to the pre-existing DFN, leads to a larger stimulated area, but it also requires higher injection pressures during production to keep hydraulic fractures open.

2-D Studies with Vertical Wells Using Coupled Hydro-Thermal-Mechanical Models (Itasca)

The UDEC code was expanded during the term of this panel project to include heat exchange between the rock and the fractures, thus simulating the thermal aspects of EGS performance. Itasca verified the UDEC hydrothermal simulator against the Gringarten solutions.

As with the hydro-mechanical simulations, the hydro-thermal-mechanical simulations employed a primary fracture set and a secondary fracture set, where the primary set has a larger initial fracture aperture.

A major focus was an investigation of well positioning and well spacing. The well positioning considered three cases of alignment: alignment of the production and injection well with the direction of the primary fracture set, alignment in the direction of the secondary fracture set, and alignment in an intermediate orientation between the two sets. Along with these three alignment directions the study considered three different well spacings: 250 m, 500 m, and 800 m. Alignment with the primary fracture set direction focused the flow with a relatively small number of fractures directly connecting injection and production well and produced a short-circuiting behavior. Alignment along secondary and intermediate position forced the flow to take more tortuous paths and improves surface area, but it comes with the risk of fluid loss, especially as well distances increase.

Increasing the well spacing, especially in the intermediate direction, improves thermal performance and delays thermal breakthrough. The simulation results were compared with Gringarten analytical solutions for equally spaced parallel fractures. Although the cases are geometrically quite different, the Gringarten comparison provides an indicator of the effective surface area contributing to heat exchange through the network. The surface area, if assigned to a single fracture, implies a well spacing that is much larger than the physical distance between the wells. Similarly, if one uses the actual well spacing one can then determine, for the same

total exchange area, how many fractures are required for the heat exchange. Alignment of the wells in the primary fracture direction produces a relatively small heat exchange area that is more similar to a single fracture connecting two wells of the actual spacing. Simulations show that aligning well pairs in the intermediate direction promotes engages a larger surface area, either through a larger number of participating fractures or through a much greater tortuosity of the fracture pathways between the wells. In either case this larger exchange area is highly beneficial to EGS development.

Simulations varying thermal diffusivity showed models improvement in thermal performance for higher thermal diffusivity cases.

The simulations also looked at the effects of fracture spacing. Having a smaller fracture spacing creates a higher fracture intensity, that is, more surface area in a given volume. The greater surface area associated with smaller fracture spacings has a strong positive effect on EGS performance.

EGS Well Layouts to Mitigate Thermal-Drawdown-Induced Flow Channeling (LLNL)

LLNL addressed the optimization of well layouts by coupling DFN flow models in its GEOS mechanical code and heat transport model, NUFT. The process begins with a DFN model that calculated permeability and flow fields, which were then mapped into mechanical and thermal continuum models for solution of stress and temperatures. These output stresses and temperatures were used to adjust fracture properties for stress and temperature in the initial DFN model. The adjusted DFN model becomes a basis for repeating this loop through further time steps.

The well layout simulations run by LLNL used two fracture sets, a primary fracture set running 20° clockwise to the maximum stress direction and a secondary set running in the direction of the minimum stress, or perpendicular to the maximum stress. Two basic well layouts were tested – a four-well scheme with two injector-producer pairs and a five-spot configuration, with a central injector and four outlying producers on corners of a square. The four-well scheme considered several variations, where the alignment of the injector-producer pairs was either in the direction of the maximum stress and primary fracture set or perpendicular to it. For the simulations in which the injector-producer directions were aligned with the

maximum stress, alternative simulations considered the distance between the two injector-producer pairs.

The main findings of the simulations were the following:

- Thermomechanical effects concentrate the flow into preferential flow paths or channels due to a positive feedback loop between cooling and local fracture aperture enhancement.
- Alignments of injector-producer pairs in the direction of the primary fracture set and the maximum stress create fast paths that have earlier thermal breakthrough than alignments in the minimum stress direction where the flow gradient crosses the more conductive fractures
- Closer distances between injector-producer pairs create more likelihood of thermal interference, while larger distances create separate regions of thermal perturbation
- The five-spot layout reduces thermomechanical channeling effects. The five-spot reduces the distances between the injector and the producers compared with the injector-producer pairs, which is good for connectivity, and flow rates of each pathway carry lower flow rates than the injector-producer pairs, which is good for thermal longevity.

Flow Channeling in 2-D Fracture Networks Using a Single Well Pair (LLNL)

LLNL also performed a systematic suite of simulations using a single injector-producer pair aligned in the maximum horizontal stress direction. The simulations used several fracture networks including regularly spaced infinite fractures, fractures with random orientations, and networks with two sets similar to those of the well layout study but using different combinations of longer and shorter fractures in the two sets. The objective was to represent a wide range of possible DFN distributions in the field.

The major conclusions of single injector-producer pairs were:

- As with the well layout studies, thermomechanical effects are significant and enhance channeling that leads to early thermal breakthrough except for orthogonal networks with regular spacing.

- Aligning longer fractures in the direction of maximum stress (and the alignment of the injector-producer pair) increases the connectivity of the wells, leading to short-circuiting and early thermal breakthrough, while having longer, better connected fractures in the minimum stress direction and perpendicular to the alignment of the injector-producer pair spreads the flow through the fracture networks and produces better sweep and delayed thermal breakthrough
- Well spacings of 400 m and 800 m (in addition to the 600 m base case) show that increasing the well spacing delays thermal breakthrough
- Thermomechanical coupling lowers the impedance of flow between the injector and producer over time as fractures cool and apertures open. However, such benefits cannot be realized in production because the overall hydraulic impedance only decreases substantially near or after thermal breakthrough.

Thermally Induced Channeling in a Single Fracture (LLNL)

GEOS simulations in three-dimensions using a single horizontal fracture with an injector-producer pair were run with and without thermomechanical coupling and with a range of heterogeneity values for conductivity within the fracture. As with the fracture network simulations discussed above, the thermomechanical coupling creates flow channelization. This effect appears in a homogeneous-conductivity fracture and becomes more pronounced as conductivity values become more heterogeneous. The channeling effects reduce effective conducting surface area for heat transfer and reduce the time to thermal breakthrough.

Studies on Horizontal Wells with Multiple Stimulation Zones and Completions (LLNL)

LLNL developed a GEOS model for multiple parallel hydraulic fractures created from horizontal wells in a scheme similar to multi-staged stimulation in modern oil and gas production practices in tight, unconventional reservoirs. The simulations used eleven fractures with variable conductivity values.

The simulations produced flow rates that were concentrated in higher conductivity fractures. The thermomechanical effects further concentrated the flows in these

fractures. Without any intervention thermal breakthrough occurs along these fractures, resulting in early thermal breakthrough at the production well.

An active reservoir management (ARM) approach was used to block the most conductive fractures as they cooled and divert flow to less conductive fractures. This blocking and diversion could be repeated as the fractures begin to pass cool water to the production well. Diverting flow from higher conductivity fractures to lower conductivity ones would significantly increase the impedance between injection and production were it not for the thermomechanical effects that increase fracture conductivity with cooling over time. The simulations showed that an active reservoir management approach could significantly extend the production life of the horizontal injection-production well pairs.

Coupled Hydro-Thermal-Chemical Simulations (LBNL)

LBNL developed a hybrid DFN-continuum approach using fractures from Itasca's UDEC mapped into a continuum mesh in TOUGH, allowing the TOUGHREACT solver to simulate coupled chemistry along with hydro-thermal-mechanical effects. Demonstration simulations show changes in porosity that accompany dissolution and precipitation of quartz and calcite. Codes with coupled chemistry also can simulate tracer tests, which provide a non-thermal method of determining the fracture surface area.

Three-Dimensional Hydro-Thermal Simulations Focusing on the Role of In Situ Stress State (Golder)

Geothermal energy exists everywhere in the world, and a major attraction of EGS is the possibility of tapping this energy resource anywhere regardless of whether there are naturally conductive rocks. A Golder study using FracMan and HydroGeoSphere developed three dimensional models for archetypical faulting terrains in the US. "Faulting terrains" refer to the relative magnitudes of the vertical and horizontal stresses. Regions where the vertical stress is the greatest principal stress deform by normal faulting; regions where the vertical stress is the least principal stress deform by thrust faulting; and regions where the vertical stress is the intermediate stress (and the greatest and least principal stresses are horizontal) deform by strike-slip faulting.

The pathways for EGS circulation develop either on induced hydraulic fractures or on natural fractures that become critically stressed on injection and shear due to elevated pore pressure. For either fracture type, the optimal orientation for drilling EGS wells is the minimum stress direction, hence horizontal wells are favored for normal and strike-slip faulting regimes where the minimum stress is horizontal and vertical wells are favored for thrust faulting regimes where the minimum stress is vertical.

Golder carried out two sets of three-dimensional simulations for archetypical faulting terrains. The first used heat flow and thermal conditions appropriate for a typical location in each of the three faulting terrains. A northeastern US site was used for thrust faulting, a Basin and Range site in the western US was used for normal faulting, and a site near the San Andreas fault in California was used for

strike-slip faulting. A second set of simulations used a simpler experimental design in which rock properties and thermal gradients were fixed, and only the faulting and stress conditions were varied.

A significant finding of the studies was that three-dimensional effects arise from the fact that stresses, fluid pressures, and geothermal heat have vertical gradients. First, the thrust faulting regimes tend to correlate with low heat flow in the US, hence regions subject to thrust faulting require greater depths to reach rock with sufficient temperature, and rock stresses are very high, requiring high pressures for reservoir stimulation. Second, both hydraulic fractures and critically stressed natural fractures may grow preferentially up or downward depending on the relative magnitudes of the stress and fluid pressure gradients. For the Golder simulations, the gradients drove created fractures that propagated preferentially upwards with larger apertures at shallower depth. The combination of preferential fracture growth and fracture opening at shallower depths created preferred circulation on average at depths shallower than that of the injector would suggest, reducing the temperature of the production water from what one would expect without gradient effects.

Synthesis of DFN Modeling Results

The most important success factors for an EGS development are

- Having sufficient total fracture surface area connecting the injection and the production wells for heat exchange to produce commercial levels of electrical energy
- Controlling the flow rate through the stimulated fractures to control thermal longevity and avoid premature thermal breakthrough.

An EGS development based on individual hydraulic fractures will require a very large surface area, on the order of several million square meters. If the EGS is a single hydraulic fracture, this requires circulation distances of several kilometers, which is considerably longer than what is achieved in current fracturing either in geothermal or fossil energy practice. Since a single hydraulic fracture of this size is impractical, achieving this total surface area will likely require multiple fractures or stimulations. Such an EGS system may look very similar to an unconventional oil

and gas development with multiple fracturing stages along a well drilled horizontally or in the minimum stress direction.

The conductivities of multiple stimulated fractures along a well will not be uniform. The highest conductivity fractures will carry more flow and experience earlier thermal breakthroughs. To mitigate this result the flow to the individual stimulations will require active management, either by controlling the flow to each stimulation separately or by blocking flow to the higher conductivity fractures as they start producing cooler water.

The other approach to multiple fractures involves developing the EGS system along critically stressed natural fractures. Both Itasca and LLNL stimulations demonstrate the feasibility of creating complex fracture pathways by hydro-shearing. The success of this approach requires knowing the in-situ stresses and key aspects of the fracture network geometry. With this information the EGS designer can optimize expected performance using layouts of the injector and producer wells that exploit complex rather than direct fracture pathways. In addition to the well alignment, greater spacing enhances EGS performance, albeit with greater risk of not establishing injection-production well connections.

The key fracture geometry parameters for design are the fracture orientations, density, and length distributions. While simulations show that length can be important, fracture length is virtually impossible to characterize at depth, hence the main factors for design will be fracture set orientation and the in-situ stresses, which control the orientations of both hydraulic fractures and fracture sets that are oriented preferentially for shear stimulation.

Both the Itasca and LLNL simulations show that well layouts that avoid injector-producer alignment with the maximum stress direction or a conductive natural fracture set perform more poorly with respect to layouts that mobilize secondary sets or combinations of the primary and secondary sets.

Major Conclusions

1. A successful EGS system will likely involve multiple fractures and multiple stimulation zones. These may be achieved either by multi-staged stimulations, like unconventional oil and gas developments, or by using

stimulation methods that develop critical shearing stresses on natural fractures.

2. Optimizing well layouts to develop EGS by stimulating natural fractures needs to consider the geometry of the natural fractures and the in-situ stress field; alignment of wells with the most transmissive fractures will likely cause short-circuiting, while well alignments that cross multiple fracture sets will encourage more complex networks with more fracture area, albeit at the risk of reducing the likelihood of connectivity between the wells or increasing impedance.
3. A multiple fracture or stimulation system will require either separate management of each stimulation to avoid premature breakthrough on the most transmissive pathways or will require an active management approach that shuts down the more permeable pathways as they experience thermal breakthrough at the production well.
4. Chemical effects are important, particularly to reservoir longevity, but were not addressed in detail in this report other than to demonstrate some hybrid DFN and continuum methods that could provide a way forward.
5. Most of the simulations in this report were two dimensional; however, three-dimensional effects may be important, particularly in the presence of gradients of temperature and stress with depth. Simulations showed that both fracture propagation and fracture opening could occur at shallower depth than the injection point, resulting in circulation pathways that preferentially travel through cooler rock.

Table of Contents

Summary.....	i
1 Background and Introduction.....	1
1.1 Panel Mission.....	1
1.2 Porous Continuum versus Discrete Fracture Network Models.....	3
1.3 Modeling Teams.....	6
1.4 EGS Performance Criteria.....	7
1.5 Coupled Processes.....	8
1.5.1 Hydrothermal coupling.....	8
1.5.2 Hydro-mechanical coupling.....	9
1.5.3 Hydro-thermomechanical coupling.....	9
1.5.4 Hydro-thermomechanical-chemical coupling.....	9
1.6 Geologic Setting.....	10
2 Two-Dimensional Hydro-Thermal Fracture Models.....	11
2.1 Objective of Hydro-Thermal Calculations and Models.....	11
2.2 Analytical Solutions.....	11
2.2.1 Description of Gringarten analytical solution.....	11
2.2.2 Effect of rate and surface area on thermal performance.....	13
2.2.3 Effect of fracture spacing on thermal performance.....	14
2.2.4 EGS feasibility space based on analytical solutions.....	15
2.3 Hydro-Thermal Numerical Simulations Using Parallel Fractures.....	17
2.3.1 Parallel fracture numerical simulation verification.....	17
2.3.2 Parallel fracture numerical simulation, variable spacing and aperture..	18
2.3.3 Complex fracture network simulations.....	19
2.4 Summary of Hydro-Thermal Analytical Solutions and Numerical Simulations	20
3 Two- and Three-Dimensional Hydro-Mechanical Simulations (Itasca).....	35
3.1 Objectives of Hydro-Mechanical Simulations.....	35
3.2 Background and Simulation Approach.....	35
3.3 Two-Dimensional Simulations.....	36
3.3.1 Computational approach.....	36
3.3.2 DFN model.....	37
3.3.3 Base model fracture network description.....	38
3.3.4 Flow conditions.....	39
3.3.5 Creation of hydraulic fractures.....	40
3.3.6 Performance indices.....	40
3.4 Results of the Two-Dimensional Model.....	40
3.4.1 Effect of connectivity.....	40

3.4.2	Effect of fracture size distribution.....	41
3.4.3	Effect of dilation angle.....	42
3.4.4	Effect of orientation of in situ stresses.....	43
3.5	Three-Dimensional Hydro-Mechanical Simulations.....	54
3.5.1	Three-dimensional DFN representation.....	54
3.5.2	Injection method.....	55
3.5.3	Multi- versus single stage stimulation.....	55
3.5.4	Cased borehole versus open borehole completion.....	57
4	2-Dimensional Studies With Vertical Wells Using Coupled Hydro-Thermal-Mechanical Models (Itasca).....	59
4.1	Objective.....	59
4.2	Thermomechanical behavior of fracture networks using UDEC.....	59
4.2.1	UDEC thermal verification.....	59
4.2.2	Model description.....	59
4.2.3	Effects of well positioning and spacing.....	60
4.2.4	Effects of thermo-mechanical coupling during production.....	61
4.2.5	Effective surface area.....	62
4.2.6	Effects of thermal conductivity.....	64
4.2.7	Effects of fracture spacing.....	64
5	LLNL Simulations with Thermomechanical Coupling.....	77
5.1	EGS Well Layouts to Mitigate Thermal Drawdown Induced Flow Channeling Overview.....	77
5.2	EGS Well Layouts to Mitigate Thermal Drawdown Induced Flow Channeling	77
5.2.1	Description of the well-layout study model.....	77
5.2.2	Single well pair simulations.....	78
5.2.3	Well doublet simulations.....	78
5.2.4	Five-spot layout.....	80
5.3	Flow Channeling in 2-D Fracture Networks Using a Single Well Pair With and Without Thermomechanical Coupling.....	87
5.3.1	Model description.....	87
5.3.2	Importance of multiple realizations.....	88
5.3.3	Effects of single pair well spacing.....	89
5.3.4	Effect of thermomechanical coupling on impedance.....	89
5.4	Thermally Induced Channeling in a Single Fracture (LLNL).....	89
5.4.1	Model description.....	89
5.4.2	Model results.....	90
5.5	Studies on Horizontal Wells with Multiple Stimulation Zones and Completions.....	98
5.5.1	Description of EGS using horizontal wells.....	98
5.5.2	Horizontal well simulation results.....	99
6	Thermal-Hydrological-Chemical Processes Simulations Using Discrete Fracture Networks (LBNL).....	105
6.1	Overview.....	105

6.2	Coupled Thermal-Hydrological-Chemical (THC) Model Development.....	106
6.3	Simulations using Newberry Volcano EGS Site Geochemical Data.....	109
6.4	Coupled THC Simulation Conclusions.....	114
7	Three-Dimensional Hydro-Thermal Simulations Focusing on the Role of In Situ Stress State.....	123
7.1	Stress State and EGS Development.....	123
7.2	Stress State, and EGS Development.....	124
7.2.1	Description.....	124
7.2.2	Regional stress and heat flow.....	125
7.2.3	Archetypical faulting terrain simulation results.....	126
7.2.4	Simulations with constant material properties and depths.....	129
8	Synthesis and Conclusions.....	145
8.1	Objectives and Basic Criteria of EGS Performance.....	145
8.1.1	Purpose of this Panel Report.....	145
8.1.2	Criteria for EGS Viability.....	146
8.2	Fracture surface area required for an EGS Heat Exchanger and need for multifracture EGS.....	148
8.2.1	Lessons from analytical solutions.....	148
8.2.2	Second power dependency of thermal breakthrough on rate and area and need for a multifracture EGS.....	148
8.2.3	Input for future field operations and EGS demonstrations.....	149
8.3	Effects of Heterogeneity Between Fractures and within a Single Fracture	150
8.3.1	The problem of heterogeneity.....	150
8.3.2	Heterogeneity within a single fracture.....	150
8.3.3	Heterogeneity between fractures in a multiple stimulation EGS.....	150
8.3.4	Input for future field operations and EGS demonstrations.....	151
8.4	Stimulation of Natural Fracture Networks and Optimizing EGS Performance	152
8.4.1	Natural fractures and EGS.....	152
8.4.2	Well positioning and fracture networks.....	152
8.4.3	Optimizing shear stimulation for fracture surface area.....	154
8.4.4	Three-dimensional DFN simulation of multi-stage stimulation.....	155
8.4.5	Effects of Thermal-Hydro-Mechanical Coupling.....	155
8.4.6	Input for future field operations and EGS demonstrations.....	157
8.5	Simulation of Coupled Chemical Effects.....	157
8.5.1	Importance of chemical effects.....	157
8.5.2	Input for future field operations and EGS demonstrations.....	158
8.6	Three-Dimensional DFN Models in Different Regional Settings.....	158
8.6.1	Regional settings.....	158
8.6.2	Estimating the effect of shear stimulation on transmissivity.....	159
8.6.3	Three dimensional behaviors.....	159
8.6.4	Input for future field operations and EGS demonstrations.....	159
9	Acknowledgements.....	165
10	References.....	166

This page intentionally left blank.

Table of Figures

Figure 1. Conceptual model of EGS (INL, 2006).....	2
Figure 2. EGS thermal production experience compared with a 5 MW _e economic viability criterion.....	3
Figure 3. Computational grid for porous continuum model of EGS performance (Butler et al., 2004).....	5
Figure 4. Discrete fracture network model of EGS performance.....	5
Figure 5. Geometry and assumptions of the Gringarten analytical solution.....	22
Figure 6. Gringarten et al. (1975) type curves for five values of dimensionless rock block thickness, X_{eD} , with conversion to real time for properties in Table 2.....	22
Figure 7. Effect of fracture length and flow rate on thermal performance. Each curve can be produced with different combinations of rate and total area. Hence each curve has a label for variable length, z , at constant rate of 0.08 m ³ /s (upper label box) and variable rate at constant length, $z=500$ m (lower label box). Height, y , is constant at 500 m. Thermal longevity depends on the square of surface area and inverse square of flow rate.....	23
Figure 8. Delay in thermal decline (10% of initial T) versus fracture area and flow rate for cases in Figure 7. Time to 10% decline increases with larger area and decreases with higher rate.....	24
Figure 9. Effect of multiple fractures on thermal performance. Flow rate 0.08m ³ /s. Increasing the numbers of fractures increases the surface area for heat transfer and reduces flow rate per fracture. Both effects increase thermal longevity. Further improvement with number of fractures stops when the thermal front in the rock does not lag the thermal front in the fractures (see Figure 11).....	25
Figure 10. Effect of multiple fractures on thermal breakthrough and energy production. Flow rate, 0.08 m ³ /s. A higher number of fractures delays thermal decline. For large numbers of fracture with small spacings, most of the energy has been produced from the rock when thermal breakthrough (10% decline) is reached.	26
Figure 11. Role of flow rate in thermal breakthrough and thermal sweep efficiency (Doe et al., 2014). At high rate, the thermal front advances without cooling the rock; at low rate the thermal front in the rock advances with thermal front in the fracture. (red = hot, blue = cold).....	26
Figure 12. Using dimensionless type curves for feasibility space calculation. (1) determine the target thermal decline and its associated dimensionless temperature. A 10-degree decline when the difference of the injection and rock temperatures is 150 degrees corresponds to dimensionless temperature, T_D , of 0.067. (2) That dimensionless temperature is achieved at a dimensionless time, t_D , of 0.6. (3) Using the definition of dimensionless time and setting the real time value to the target thermal longevity (e.g., 20 years), allows one to calculate the combinations of flow rate and area necessary to achieve the target. This calculation uses the infinite dimensionless spacing curve (single fracture). Similar analyses for multiple fractures	

(finite fracture spacing) will use the other dimensionless spacing curves. For this thermal decline, dimensionless spacing values >2 still follow the infinite curve.....27

Figure 13. Verification of HydroGeoSphere (symbols) with analytical solutions (lines). Points are HydroGeoSphere simulation results superposed on Gringarten et al. (1975) Figure 5 for the same property and geometry conditions.....28

Figure 14. Visualizations of parallel fracture numerical simulations from uniform spacing and aperture to variable spacing and aperture. Increased heterogeneity (variable spacing and variable aperture) focuses the flow into “short circuits”.....29

Figure 15. Production temperature results for parallel fracture models shown in Figure 14. Variable spacing results in earlier thermal breakthrough compared with the uniform spacing and aperture case. Varying the aperture further hastens thermal breakthrough creating “short circuits”. Temperature given as dimensionless values with actual temperature in parentheses. Red lines show a 10% thermal decline with corresponding time in years for each simulation.....30

Figure 16. Stimulated subset of DFN model based loosely on Newberry EGS site data for fracture orientations. Red fractures are stimulated by the hydraulic injection. Gray fractures are unaffected. Stimulation simulated in FracMan.....31

Figure 17. Production temperature versus time with comparison to Gringarten-type curves for a complex fracture network model. The inset shows a map view of the fracture network with a temperature snapshot at 30 years. The early time follows a dimensionless spacing type curve with a value of 1, as the rock between closely spaced fractures thermally depletes. Once these rock blocks are depleted, the entire stimulated volume acts as a single sink and the temperature curve deviates toward the single fracture, infinite spacing case. Temperature profile at 30 years, well spacing is 1074 m. A is the injector and B is the producer. From Doe et al., 2014..... 32

Figure 18. Conceptual model of dilation on fractures as implemented in UDEC.....44

Figure 19. Effect of length exponent on fracture clustering. Left column: fractures colored based on their relative size to reservoir size, red indicates longest fractures in the reservoir while dark blue indicates shortest, right column: cluster geometry, each color within a reservoir indicates a cluster.....45

Figure 20. UDEC Model setup, DFN (core) and outer region. Red dot indicates location of injection well, and blue line is the trajectory of the potential hydraulic fracture..... 46

Figure 21. (a) Fracture networks for connectivity sensitivity, (b) contours of aperture increase..... 47

Figure 22. Performance indices for connectivity study.....48

Figure 23. Fracture size exponent sensitivity study, fractures colored by their relative length to reservoir size (red indicate the longest while dark blue indicate the shortest) connectivity, fracture apertures, and fracture slip.....49

Figure 24. Effect of fracture length exponent on performance indices.....50

Figure 25. Permanent aperture increases after stimulation (evaluated after pressures are decreased to the in-situ value) with dilation angle.....51

Figure 26. Effect of dilation angle on shear stimulated area and aperture.....51

Figure 27. Effect of fracture set orientation relative to in situ stresses. (Left: fractures colored based on their relative length to reservoir size). Strike is relative to σ_{HMAX} , middle. Aperture contours, right: slip on fractures.....52

Figure 28. DFN affected and DFN shear-stimulated area for stress case.....53

Figure 29. Three-dimensional DFNs for study.....56

Figure 30. Multistage stimulations with horizontal borehole. Top row is multistage with cased borehole, bottom row is multi stage in an open borehole completion. Circles indicate the three stages, red lines are potential location of production well 56

Figure 31. Shear stimulated area for multistage versus single stage stimulation, injection rate of 70 kg/s.....57

Figure 32. Visualization of multi-stage versus single stage stimulation.....57

Figure 33. Comparison of shear stimulated area for cased well completion vs. open borehole completion..... 58

Figure 34. Comparison of infectivity during production for cases with cased borehole and open borehole completion, Left column: multi-stage stimulation, right column single stage..... 58

Figure 35. Single-fracture hydro-thermal verification of UDEC with Gringarten et al. (1975) solution. Mismatch due either to meshing coarseness and minor differences in Gringarten and model boundary conditions. Gringarten domain ends at fracture tip, simulation continues 500 m on either side.....65

Figure 36. Temperature contours in the reservoir after 32 months of production in the well positioning study. From left to right the columns are Case I, Case II, and Case III. Cases I and II did not have well connectivity for the 800 m well spacing. Circle points out single pathway for short well spacing and orientation along primary fracture set..... 66

Figure 37. Production temperature, well positioning study, 250 m well spacing (gray lines are without thermomechanical coupling) Case II and III have improved performances due to pathway tortuosity compared with the direct connection along the primary fractures in Case I.....67

Figure 38. Production temperature, well positioning study, 500 m well spacing (gray lines are without thermomechanical coupling) Case II and III have improved performances due to pathway tortuosity compared with the direct connection along the primary fractures in Case I.....68

Figure 39. Effect of well spacing on thermal performance. Blue symbols are coupled thermal-mechanical model results. Gray lines are without thermomechanical coupling. Increased well spacing has better performance due to added surface area to the heat exchange..... 68

Figure 40. Time to 10% thermal decline by well position and spacing. Case II and III have improved performances due to pathway tortuosity compared with the direct connection along the primary fractures in Case I.....69

Figure 41. Comparison of thermal behavior with and without thermomechanical coupling (500 m well spacing). Coupling does not significantly affect the pathways

or pattern of thermal drawdown. Comparisons of thermal performance appear in Figure 37 to Figure 39..... 70

Figure 42. Match of simulation for Case III, well spacing = 500m for Gringarten et al. (1975) analytical solution. Curves are for various values of dimensionless fracture spacing, X_{eD} and inset table shows correspondence to spacing, X_e , in meters. The simulation is for a complex fracture network. The thermal behavior suggests a total interchange area of $1.05E6 \text{ m}^2$ (Area times number of fractures times 350m height). If the length is the well spacing ($d=500$), there are effectively $n=6$ fractures. If there is a single, highly tortuous, fracture, it has an effective length of 3000 m..... 71

Figure 43. Sensitivity study to thermal conductivity and rock density for Case III, wells positioned intermediate to the direction of the two fracture sets. Increased density and thermal conductivity improve thermal performance..... 72

Figure 44. Visualization of thermal drawdown for fracture spacing study. Smaller spacing provides more conducting pathways between the wells. With increasing spacing the stimulated volume evolves towards pathways along individual fractures rather than through a network..... 73

Figure 45. Production temperature versus time for fracture spacing study. The smaller spacing creates stimulated regions with more pathways and surface area for heat exchange, thus improving thermal performance. Inset shows the time to 10% production temperature decline..... 74

Figure 46. GEOS modeling approach for coupled hydro-thermal-mechanical simulation. GEOS involves the interaction of three separate codes, a fracture network model, continuum heat and fluid flow mode (TH flow mode), and a finite-element mechanical code (Solid FEMO. Each time step starts with the DFN/rock joint model, passes through a hydro-thermal calculation, determines the stress changes due to temperature, and finally updates the DFN model with apertures that are updated for thermomechanical effects. (Fu et al., 2016)..... 81

Figure 47. Fracture network for well positioning study (left); pathways from Scheme A (center) where the wells are aligned with the maximum horizontal stress, and Scheme B (right) where wells are aligned with the minimum horizontal stress..... 81

Figure 48. Well layouts and flow rates for well layout study. Injection is positive in kg/s, production is negative. Injection wells are blue, production wells are red. North is up on the page. The y well spacing is 800 m. The x well spacing is 800 m except for variants of C and D that are 400 m..... 82

Figure 49. Well positioning study, single pairs, Scheme A (top) in the direction of the major stress, Scheme B (bottom) in the direction of the minor stress. Left, production temperature. Right, temperature visualization at 20 years with pathways. Visualizations show flow pathways as black lines. Stresses are acting N-S (N up on the page) and preferentially open the N20E set rather than the E-W set. Scheme A follows the open fractures and has early thermal breakthrough. Scheme B forces flow through the E-W set and has a much better sweep with no thermal decline in 30 years..... 82

Figure 50. Well positioning study, two well pairs. Scheme C producer and injector are flowing in parallel direction with 400 and 800 m spacings on the pairs. Scheme

D, injection and production are at opposite corners. Left, production temperature, Right, temperature visualization at 20 years with pathways. Scheme C with the 400-m doublet spacing shows a single pathway connecting the SW injection well with the east well pair. This capture of SW injection water results an early breakthrough at the NE producer and later breakthrough at the NW producer. Other doublet simulations show similar breakthrough times.....83

Figure 51. Well positioning study, Scheme E - center well injection well with four production wells and a central injector. Left, production temperature, Right, temperature visualization at 20 years with pathways.....84

Figure 52. Fracture networks for Flow Channeling Study (Fu et al., 2016). The injection well (blue) and production well (red) are 600 m apart. All networks have the same intensity 0.1 m^{-1} . Network A (not shown) uses regularly spaced fractures with lengths that extend to the model boundaries. Top: central portion of network with descriptions, Middle: Temperature at 20 years with no thermomechanical coupling, Bottom: Temperature at 20 years with thermomechanical coupling. n_i is the average number of intersections along each fracture and is a measure of connectivity with the subscripts indicating primary and secondary sets.....91

Figure 53. Thermal performance of networks for single well-pair study (Fu et al., 2016). Left: no thermomechanical coupling; right, thermomechanical coupling.....92

Figure 54. Left: Effect of thermomechanical coupling on time to 10% thermal decline for each fracture network. Except of for Network A, the coupling significantly reduces time to thermal decline. Right: Comparison of time to 10% thermal decline for all networks with six realizations of Fracture Network B. Variability of different realizations of a single network is similar to variability among single realizations of six different networks. Data are replotted from Fu et al. (2016).....92

Figure 55. Effect of well spacing on time to 10% thermal decline for Fracture Networks B - E. Increasing well spacing improves EGS performance. Decrease in Fracture Network E time is from a spacing of 600 m to 800 m is likely an effect of a single realization. Data replotted from Fu et al. (2016).....93

Figure 56. Evolution of injection well impedance over time. Decrease in impedance reflects the increasing apertures of fractures with cooling due to thermomechanical coupling. Impedance measured as the pressure difference between the wells at a given time divided by the initial pressure difference (Fu et al., 2016).....93

Figure 57. Single fracture channeling simulation sketch (Guo et al., 2016).....94

Figure 58. Visualizations of single fracture channeling study.....94

Figure 59. Production temperature versus time, channeling study.....95

Figure 60. Variation in production life (defined as 53% thermal decline) versus correlation length and aperture standard deviation.....95

Figure 61. Comparison of unconventional natural gas system of hydraulic fractures with a multiple fracture EGS system using horizontal wells.....101

Figure 62. Well layout for multiple fracture EGS simulations.....101

Figure 63. Production temperature and pressure difference versus time.....102

Figure 64. Exit temperature and flow rate for each fracture.....102

Figure 65. Thermal drawdown visualization for production with no fracture blocking. 103

Figure 66. Production temperature and pressure versus time blocking single fractures as they have thermal breakthrough.....103

Figure 67. Single fracture exit temperature blocking single fractures as they exhibit thermal breakthrough..... 104

Figure 68. Temperature visualization at 30 years for a reservoir with no management intervention (left) and active reservoir management (right) which blocks fractures #6 and #8 at 15 years and fractures #3 and #5 at 20 years)....104

Figure 69. (a) 2D TOUGHREACT mesh generation using Delauney triangulation of UDEC subcontacts. (b) Remeshing using Centroidal Voronoi Tessellation with 5 Lloyd's iterations. (c) Final smoothed mesh after 10 Lloyd's iterations.....115

Figure 70. (a) Final 2D TOUGHREACT mesh of entire domain showing overlain UDEC stimulated fracture network. (b) Blow-up of edge of fractured region showing smoothed TOUGHREACT mesh with original UDEC subcontacts (red points) and UDEC fracture network (blue lines)..... 116

Figure 71. Contoured equivalent permeability field of interior stimulated reservoir region. UDEC fracture network superimposed (dark red). Equivalent permeability was field calculated using the cubic law applied to the UDEC fracture aperture distributions weighted over polygonal TOUGHREACT mesh elements. The permeabilities vary from about 10^{-9} m² (dark blue) to 10^{-17} m² (brown).....116

Figure 72. Sodium 1,5-napthalene disulfonate tracer concentrations after 3 weeks, 1 year, and 2 years of injection and production. The figure shows the simulation grid for TOUGH as well as in dark red the DFN model developed in UDEC. At lower right, the napthalene sulfonate-2,15 tracer concentration at the producing well is shown over nine years of injection and production..... 117

Figure 73. a) Temperature at producing well over 30 years injection and production at 80 kg/s. Note that temperatures only start declining after 20 years, and by 30 years have only dropped to 196 °C. b) Pressure at producing well over 30 years. Note the early pressure drop, followed by fairly stable pressures, and then a more gradual decline after 15 years.....118

Figure 74. Temperature field in reservoir with simulated injection and production. Note that even though a large region around the injector has cooled significantly after 30 years, the production well is still close to the initial reservoir temperature. a) 2 years. b) 30 years..... 119

Figure 75. Temperature field around injector of simulated injection and production. Flux vectors show fluid flow focused in preferred permeability pathways. UDEC fracture network superimposed (dark red). a) 10 years. b) 30 years.....119

Figure 76. Calcium and magnesium concentrations (mg/kg H₂O) in reservoir after 30 years..... 120

Figure 77. Calcite precipitation after 2, 10, 20, and 30 years.....121

Figure 78. Plagioclase (albite+anorthite) and potassium feldspar (microcline+sanidine) dissolution after 30 years..... 121

Figure 79. Chlorite (daphnite+clinochlore) and pyrite precipitation after 30 years. 122

Figure 80. Permeability ratio (k/k_0) after 10 and 30 years.....122

Figure 81. In situ stress states and their relationship to faulting, hydraulic fracturing, and favorability of natural fracture orientation for hydro-shearing. The three regional stress regimes appear in the upper panel with the orientation of principal stresses (σ_1 largest) and the associated fault geometries. The lower panel shows the orientation of hydraulic fracture for each regime (perpendicular to the least principal stress, σ_3) and the most favorable orientation to create hydro-shearing, which is two orientations at an acute angle to the maximum principal stress (σ_1).132

Figure 82. Maps of heat flow (top) and stress state (below) (Reinecker et al., 2005) in the lower 48 states of the United States (from Williams and DeAngelo, 2015). Higher heat flows are in red. Regional stress regimes are divided into normal faulting (red), strike-slip (green) and thrust faulting (blue) on the figure on the right. High heat flows associate most with normal faulting (west, basin-and range province) and least with thrust faulting (east and north-east).....133

Figure 83. DFN model for Normal, Strike-Slip, and Thrust faulting with stereographic plots of fracture poles and orientations of wells.....134

Figure 84. Critically stressed (hydro-sheared) fractures in archetypical models. Upper: pole stereographic plots of all fractures (green) and critically stressed fractures (red). Lower: Mohr diagrams of shear and normal stress with shear and normal stresses on all fractures (green) and critically stressed fractures (red)....135

Figure 85. Extracted fractures for flow and thermal simulation in thrust faulting model. Color shows pressure, and dashed lines are flow lines. Note the preferential flow due to larger fracture opening (apertures) at shallower depth. The major portion of the production passes through shallower, cooler rock and enters the production at a shallower depth than the injection point.....136

Figure 86. Water temperature in vertical hydraulic fractures of normal faulting regional model after 10 years. Injection well located on right side with Production well located on left side of figure (scale is in meters). Note preferential cooling due to larger opening (apertures) of fractures at shallow depths. (Finnila et al., 2015). 137

Figure 87. Left: Comparison of pore pressure gradient in the fracture with minimum stress. To open fractures, pore pressure (or pressure inside fractures) must equal the minimum stress. However, the pressure gradient within the fracture is based on the fluid density and parallels the hydrostatic gradient. The difference between the fluid pressure in the fracture and the stress normal to the fracture increases with shallower depth causing the fracture to be more open at shallow depth. Right: Illustration of apertures opening with shallower depth from Secor and Pollard (1975). P_0 is the gradient of fluid pressure and S_{x0} is the gradient of rock stress. The “teardrop” shape shows the variation in fracture aperture with depth, which is controlled by relative difference between fluid pressure and rock stress.....138

Figure 88. Thermal performance of hydraulic fracture and hydro-sheared fracture models for each faulting terrain. Poor performance of the Normal faulting hydraulic

fracture model comes from preferential circulation in shallower, cooler parts of the model due to enhanced fracture aperture at shallower depth.....139

Figure 89. Summary of Constant Material Property model. For each stress state (normal, strike-slip, thrust), there is a DFN model with two sets aligned for shear stimulation, one set aligned and one not, and no sets aligned (top row of stereographic projections). The second row for each stress state shows a Mohr diagram of shear versus normal stress with critically stressed fractures (red) and non-critically stressed fractures (green) with percent critically stressed. The bottom row for each stress state is a stereographic projection of poles to the fractures with critically stressed in red and not critically stressed in green.....140

Figure 90. Thermal behaviors in three regional faulting terrains (normal, strike-slip, and thrust) for constant material properties and thermal conditions. There are a total of nine combinations of stress state and fracture orientation. Simulations assume two fracture sets where both sets are optimally aligned for shear stimulation (two aligned sets), one set is optimally aligned and the other set is not (one aligned set), and where neither set is optimally aligned (no aligned sets). The normal stress model with no aligned sets produced no connectivity and has no thermal curve.....141

Figure 91. Example of a single fracture EGS capable of producing 5 MW_e for 20 years.....161

Figure 92. Example of multifracture EGS capable of producing 5 MW_e for 20 years.161

Figure 93. Comparison of production temperature histories for an EGS using multiple homogenous fractures, multiple heterogeneous fractures, and a single fracture with same dimensions as one of the fractures in the multiple fracture case. Arrows point out the time to thermal breakthrough (10% production temperature decline or dimensionless temperature equals 0.9). The heterogeneous and single fracture cases see much earlier thermal breakthrough than the homogenous case.162

Figure 94. Thermal performance in a homogeneously and heterogeneously transmissive fracture with and without thermal-mechanical coupling. Heterogeneity channelizes the flow resulting in earlier thermal breakthrough. This channelization increases with thermal-mechanical coupling. Results from Fu et al. (2016).....163

Figure 95. Conceptual model of the effects of well positioning with respect to major and minor fracture sets. Thermal performance improves when the well layout exploits tortuous pathways through multiple fracture sets.....164

This page intentionally left blank

Table of Tables

Table 1. Property definitions, symbols, and values.....	33
Table 2. Results of multiple fracture calculations for thermal breakthrough and energy production.....	34
Table 3. Properties for complex DFN simulation based on Newberry (Cladouhos et al. 2011).....	34
Table 4. Properties for UDEC verification with Gringarten solution.....	79
Table 5. Input Rock and water mechanical and thermal properties for Itasca THM simulations.....	79
Table 6. Time to 10% thermal decline or three well positioning cases and well spacings.....	79
Table 7. Effective surface area for well position simulations.....	80
Table 8. Rock thermal properties used in evaluating the effect of thermal diffusivity.	80
Table 9. Properties for LLNL well layout study.....	90
Table 10. Dimensions and injection/production pressures for LLNL well layout study.	90
Table 11. Well layout study, time to 10% production temperature decline.....	91
Table 12. Model descriptions for 2-D channeling studies (data from Fu et al. 2016). Fracture network parameters from the well layout study (Fu and Carrigan, 2014) are given at the bottom of the table for comparison.....	103
Table 13. Properties for single fracture channeling study (Guo et al., 2016).....	104
Table 14. THM Input Parameters.....	118
Table 15. Primary Mineral Volume Fractions and Kinetic Data used in the THC Model (based on Bargar and Keith, 1999; Keith and Bargar, 1988). Kinetic data include the rate constant at 25°C (k_0), activation energy EA, the transition state law exponents (n and m), and the reactive surface area A_i	119
Table 16. Potential Secondary Mineral Kinetic Data used in the THC Model (based on Bargar and Keith, 1999; Keith and Bargar, 1988).....	120
Table 17. Initial, Stimulation (Parentheses), Final Reservoir Injector and Producer Water Chemistry.....	121
Table 18. Parameters and impedance results for Archetypical Faulting Terrain models.....	153
Table 19. Description of Constant Material Property models with impedance results.	154

This page intentionally left blank.

1 Background and Introduction

1.1 Panel Mission

In 2013 the Department of Energy through Sandia and Lawrence Berkeley National Laboratories formed an expert panel to assess the status of Enhanced (or Engineered) Geothermal Systems (EGS). The panel was focused on bridging the gaps between expectations and outcomes for EGS development.

The production of electrical power from geothermal energy is well established based on the production of hot fluids from permeable reservoirs with significant fluid storage. For example, The Geysers in northern California and geothermal systems in Iceland and New Zealand among others have provided significant contributions to local electricity generating networks.

The portion of heat in the Earth's upper crust, which such permeable systems can access, is a tiny fraction of the total heat available. Yet, geothermal heat is essentially ubiquitous at depth, and a major attraction of EGS systems is the possibility that geothermal power could be available anywhere (INL, 2006). Most of the crust's heat energy is stored in rocks that lack both the fluid permeability and storage to be viable electricity generating reservoirs. These low permeability thermal reservoirs require either enhancing the flow capacity of natural non-conducting fractures or creating new conductive fractures in the rock. Both situations require fluid injection at elevated pressures. Once the reservoir is enhanced, cool water enters the reservoir through an injection well, collects thermal energy from the rock, leaves the reservoir through a production well, and finally produces power at a surface power plant (Figure 1).

The main challenge of EGS development has been (INL, 2006) creating an optimal level of connectivity between the injection and production wells. Without connectivity the injection-production system cannot produce a sufficient water circulation to produce commercial power, or it may require excessive injection pressures to be feasible. On the other hand, excessive connectivity along highly conductive preferred pathways within the fracture network may create a "short-

circuit” between the injection and production wells that causes rapid thermal breakthrough and premature temperature decay of the production water.

Beginning in the 1970’s at Fenton Hill in New Mexico, numerous pilot projects have attempted to demonstrate the feasibility of creating an EGS system. These projects have created permeable fracture networks by either enhancing the permeability of the natural fractures or by creating new hydraulic fractures. To date, the results of pilot projects in North America, Europe, Asia, and Australia, have successfully shown that EGS systems can produce electricity; however, they have been unable to produce at commercial levels of power either due to insufficient circulation rates or unexpectedly premature thermal decline (Figure 2). This experience has led to efforts such as JASON (2013) and Breede et al. (2013) to more deeply understand the factors that affect the development of viable EGS systems. The focus of this panel has been the influence of discrete fracture networks.

The panel was charged with the following tasks:

- Help the DOE determine the viability of EGS creation and operation and under what conditions EGS may or may not be viable,
- Guide analyses, including coupled hydro-thermomechanical-chemical analyses, to understand critical parameters and sensitivities,
- Provide input to future field operations and EGS demonstrations.

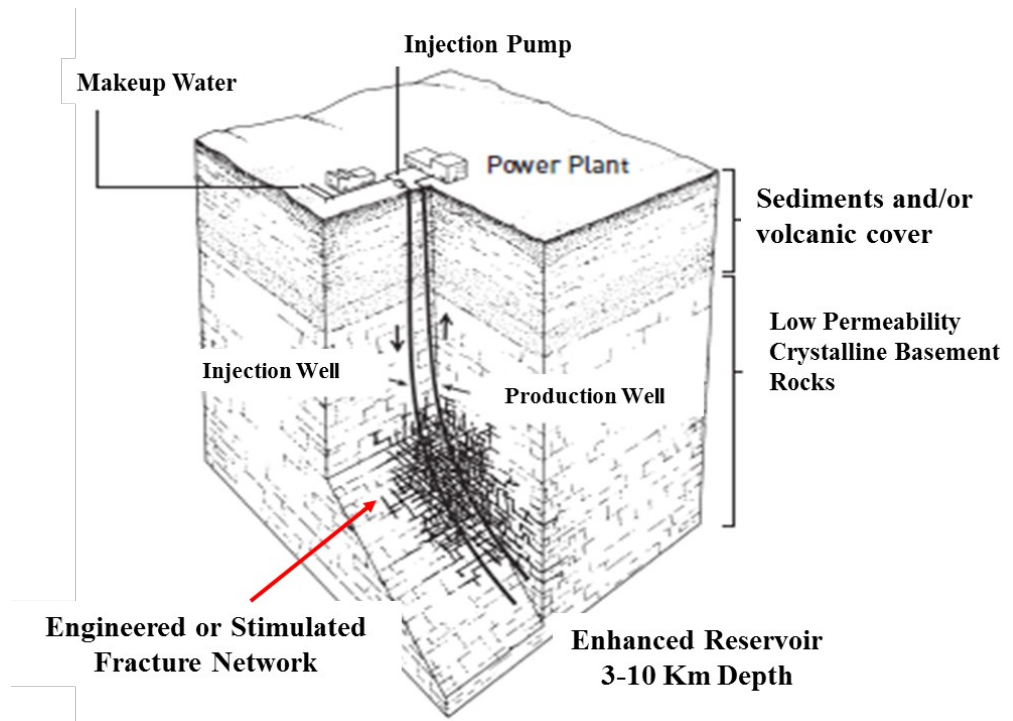


Figure 1. Conceptual model of EGS (INL, 2006)

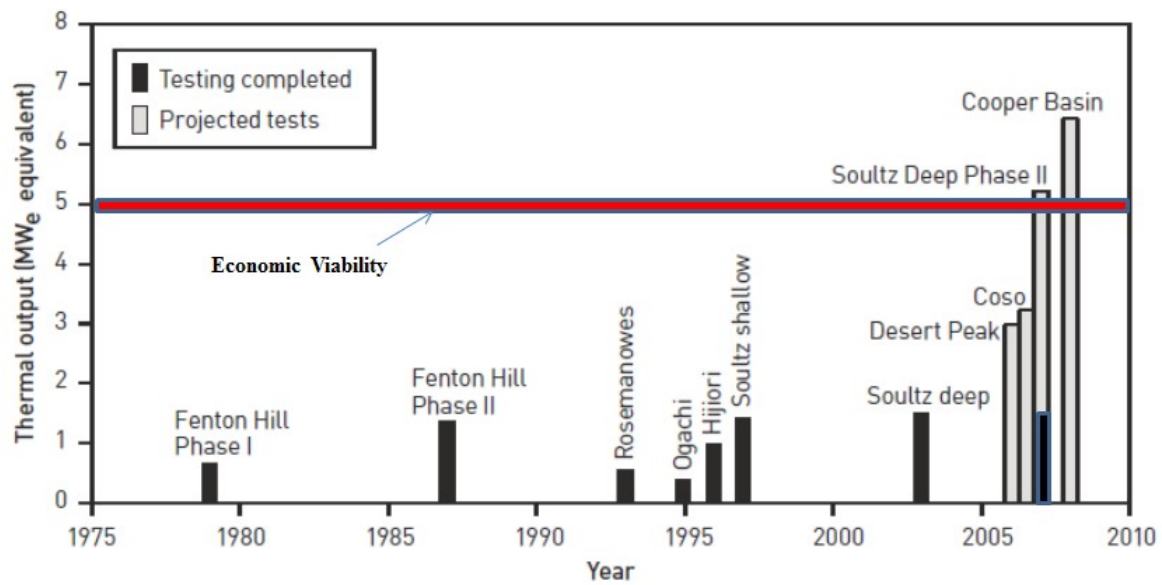


Figure 2. EGS thermal production experience compared with a 5 MW_e economic viability criterion.

1.2 Porous Continuum versus Discrete Fracture Network Models

The panel decided to focus on whether the creation and maintenance of fracture pathways through an EGS reservoir may have been oversimplified in the past. Specifically, most analyses of production in EGS reservoirs have used well-accepted numerical methods from the geothermal and fossil fuel reservoir industry, which treat the subsurface as a porous medium with a high degree of homogeneity. Rather than look at the details of fracture geometry and connectivity, these porous media models reduce the hydraulic properties of the fractured reservoir to averaged or upscaled porous flow properties.

Porous continuum models represent flow in fractures using either an equivalent porous medium, which has the same permeability as the fracture network, or as a multi-porosity system. Most commonly in the dual porosity models the main permeability is provided by an equivalent porous medium representing the fractures, and the rock between the fractures provides additional storage, both hydraulic and thermal. The fractures are not represented as individual features, but as an equivalent anisotropic medium with constant fracture spacing and infinite fracture length. An example of a computational grid for a porous continuum model appears in Figure 3 (Butler et al., 2004; Sanyal and Butler, 2005). In this model, the red region in the figure is the stimulated volume from the EGS development and has enhanced fracture flow properties. The milestone report on EGS produced by the MIT panel (INL, 2006) refers only to porous continuum models, citing the Sanyal-Butler model as a basis for estimating thermal recovery factors.

In recent years alternative numerical methods that represent more realistic fracture-network behaviors have been introduced to reservoir engineering and hydrogeologic practice. These methods are called discrete-fracture network (or DFN) models because they represent the medium as a heterogeneous fracture network of conductors having variable properties of orientation, transmissivity, size, and intensity. Figure 4 shows an example of a discrete fracture network model with an injection-production well pair. For thermal calculations flow may be calculated

using the discrete fracture network, which is embedded in a continuum model for calculating the heat flow. Unlike a porous continuum model, which uses constant fracture spacing and therefore constant block sizes, the DFN model incorporates the effects of heterogeneity of fracture properties and spacing and produces a distribution of block sizes that may be important for the rate of thermal depletion from the rock.

DFN models were first developed for radioactive waste disposal research sites (Hartley and Roberts, 2012), and have subsequently seen wide application and assessments of fractured oil and gas reservoirs (Dershowitz et al., 2010; McClure and Horne, 2013). Fracture networks introduce variable connectivity, preferred pathways, and high levels of heterogeneity. These are exactly the concerns that arise with connectivity within EGS reservoirs. The primary criticism of DFN models has been whether it is possible to develop the database required for their application. Whether or not this is the case, insights into EGS performance can be obtained through numerical experiments using realistic, if hypothetical, parameters, for example, Doe and McLaren (2016).

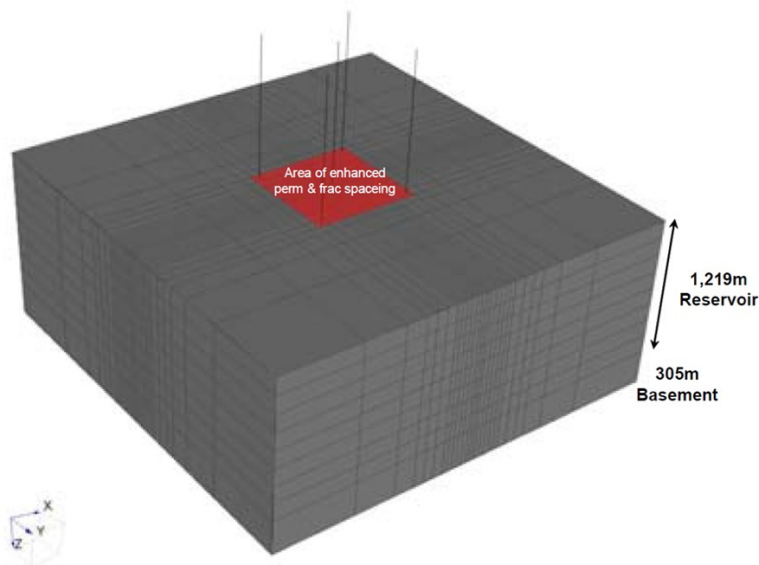


Figure 3. Computational grid for porous continuum model of EGS performance (Butler et al., 2004)

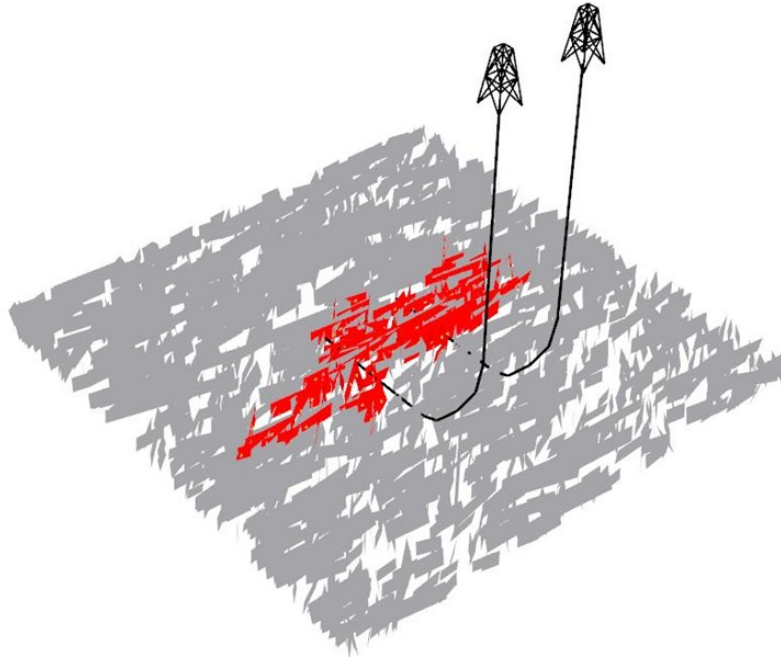


Figure 4. Discrete fracture network model of EGS performance

1.3 Modeling Teams

The panel contacted four modeling teams with experience in using DFN models for hydrogeologic, reservoir engineering, and rock stability modeling. The teams were Golder Associates (Golder), Itasca Consulting Group (Itasca), and Lawrence Livermore National Laboratory (LLNL). Lawrence Berkeley National Laboratory (LBNL) was also engaged to add geochemical insight to the modeling work. Each modeling team was given relatively free rein to define and conduct numerical experiments to address EGS performance issues. Golder Associates has a strong reputation for its FracMan discrete fracture network modeling code, which has seen wide application in nuclear waste, mining, and petroleum reservoir engineering. Itasca has been a leader in geomechanical modeling, simulating the behaviors of the rock blocks in slopes and around underground openings. Their UDEC code has become a standard for mechanical simulation of rock masses containing rock blocks defined by fractures. Prior to this study, these codes had been adapted for coupled hydro-mechanical flow, including simulation of hydraulic fracturing in unconventional oil and gas reservoirs. Neither the Golder nor Itasca codes had been

used extensively for geothermal work. Rather than being viewed as a weakness, the panel considered this lack of prior experience to be conducive to developing fresh insights into EGS questions. Lawrence Livermore National Laboratory has more recently developed DFN models ranging from heterogeneous single fractures to large scale DFN networks consisting of tens of thousands of fractures. Their models utilize the GEOS high-performance computing platform developed at the laboratory. Their particular focus has been simulating coupled behaviors in an EGS reservoir. Lawrence Berkeley National Laboratory also performed complimentary simulations primarily focusing on chemical coupling, using porous medium models (TOUGHREACT) with heterogeneous permeability fields based on upscaling a DFN generated using Itasca's UDEC codes.

At the beginning of this project, neither the Golder nor the Itasca codes were capable of simulating coupled hydro-thermal flow. The Itasca codes included hydro-mechanical coupling, while the Golder codes primarily simulated fluid flow with limited mechanical influence. Over the course of the work both Golder and Itasca developed hydro-thermal coupling, as well progressing from two to three-dimensional simulation capabilities. LLNL's effort ran partly parallel to an internal LDRD (Lab-Directed Research and Development) project, Creating Optimal Fracture Networks (2011 - 2014), and used modeling capabilities (e.g., Settgest et al., 2017) emerging from that effort.

Most of the work performed for this panel has been published in a variety of venues including the proceedings of the Stanford Geothermal Workshops, the proceedings of the Geothermal Resources Council, and refereed journal articles in *Geothermics* and *Rock Mechanics and Rock Engineering*. This panel report summarizes the findings of the numerical experiments and, unlike the publications, provides some comparison between the different modeling groups' efforts, with the goal of extracting generalized findings with respect to EGS performance.

This introductory section reviews some of the performance criteria (flow rate and thermal longevity) that would define a commercially successful EGS operation and provided a target for the numerical simulations to achieve.

A key part of the work, and a distinction between the different modeling groups' activities, is different uses of coupled approaches. Coupling refers to the

simultaneous simulation of different physical processes that have mutual interactions, specifically hydraulic, thermal, mechanical, and chemical behaviors that may have a very strong influence on EGS performance. Some distinctions between the modeling results involve the level and types of coupling behaviors. Coupling provides one basis for organizing the reporting of the model results, and the subsequent chapters address EGS behaviors starting with relatively simple analytical solutions with hydro-thermal coupling, proceeding then to hydro-mechanical coupling, and finally to results that involve hydro-thermomechanical coupling.

1.4 EGS Performance Criteria

For the purposes of this study the modeling teams were given a set of performance criteria in terms of the power output and thermal longevity of an EGS system.

A commercial EGS power plant is likely to use a binary system where the hot produced fluids heat a secondary fluid, which drives the power-generating turbines. The power output, W_e , in watts is the product of the fluid's specific heat capacity, c_w (J/kg/°C), the flow rate, q (m³/s), the temperature difference, ΔT , the fluid density, ρ_f , and a factor that represents the thermal efficiency of the system, η , or

$$W_e = \eta \rho_f q \Delta T c_w.$$

Assuming one is recirculating the output fluid of the power plant into the injection well, the temperature difference for the power calculation will be the difference in temperature between the injector and producer fluids. Using a density of 1000 kg/m³, heat capacity of 4180 J/kg/°C, temperature difference of 150°C, and efficiency of 10%, a target output of 5 MW would be achieved with a volumetric flow rate of 0.08 m³/s or mass flow rate of 80 kg/s.

Given the large capital investment in the subsurface system and the power plant, there is also a performance criterion for thermal longevity. The binary system will be most efficient over a restricted range of temperature conditions; therefore, successful operation requires that the production temperature not fall too far below the design value. For the purposes of the numerical experiments, the modeling

groups used a range of conditions of either a 10% thermal decline or a 10°C thermal decline over a time period of 20 to 30 years.

A significant part of the simulation work was focused on defining a range of conditions that will produce an economic power output in terms of flow rate while sustaining production water temperature for a sufficient time to recover capital investments (thermal longevity). The initial expectation was that such a reservoir would require a volume of at least a cubic kilometer with a well spacing of about 500 m. Additional criteria, which were less defined, included minimizing the flow impedance, that is, having a system with sufficient permeability that would not require excessive injection pressures. Some other criteria that were secondary included keeping fluid losses from the injection to acceptable levels, that is, most injected fluid returns as production fluid, and chemical effects that would neither cause the fractures to close or to channelize, while not adversely affecting power plant performance through scaling of pipes and other flow conductors.

1.5 Coupled Processes

2 Hydrothermal coupling

As discussed above an EGS is a heat exchanger. The heat exchange occurs between cooler fluid in fractures and hotter rock in the fracture walls. As we will explore in subsequent sections, the performance of the heat exchanger depends on the flow rate of the fluid, the total surface area of the fractures, the volume of hot rock between the fractures, and thermal conductivity of the rock. This heat exchange is therefore a coupled process of fluid flow in the fractures, heat transport in the fluid, and heat flow from the rock to the fluid, in other words, a coupled hydro-thermal process. Chapter 2 of this panel report uses analytical solutions and simple DFN models to explore how the heat exchanger works and identifies some of the critical controls on EGS performance.

3 Hydro-mechanical coupling

The original concept of EGS involved artificial fractures created by injecting water at pressures that exceeded the strength of the rock and the stresses in the rock mass, also known as hydraulic fractures. The use of microseismic data from the hydraulic

stimulations at Rosemanowes (Pine and Batchelor, 1984) contributed to the concept that fluid injection could also open natural fractures in shear according to the principles of critical stress analysis (Zoback, 2007) or hydro-shearing (Cladouhos et al., 2011). In contrast with simple hydraulic fracturing, which may create a single conductive zone perpendicular to the minimum rock stress direction, hydro-shearing may create connections among pre-existing fractures. These fracture networks that were previously unconnected or only sparsely connected, may have considerably larger surface area than could be achieved by creating a single extensile fracture. An important complement of the panel work involved using DFN models with hydro-mechanical coupling to investigate how fracture surface area could be enhanced through an understanding of the natural fracture networks and by judicious placement of wells within those networks. Chapter 3 of this panel report looks at the application of coupled hydromechanical DFN modeling to understand better these processes.

4 Hydro-thermomechanical coupling

In addition to the pressure dependence of fracture opening, the EGS heat exchange causes rock cooling and therefore thermomechanical contraction. This contraction of the rock alters the stress field and locally causes the fractures to open, which increases their flow capacity. Depending on the geometry of the flow, this fracture opening may not necessarily be evenly distributed throughout the heat exchanger. By preferentially opening some parts of the fracture network and not others, flow may become concentrated in only a portion of the fracture network, thus reducing the effective surface area for heat exchange. Chapter 4 looks at the fracture networks that were studied in Chapter 3 with the addition of the thermal-mechanical coupling. Additional studies of single fractures further show how thermomechanical fracture opening can create flow channels within single fractures.

5 Hydro-thermomechanical-chemical coupling

In addition to the thermal and mechanical processes, chemical processes influence the heat exchanger. Natural and introduced fluids in an EGS heat exchanger usually contain dissolved chemical constituents and are themselves chemically reactive. Over time, temperature and pressure changes can cause dissolution or precipitation

of chemical constituents along the fracture walls. Dissolution enhances the opening of fractures along channel like pathways, thus reducing the heat exchange area per unit fluid volume. Similarly, precipitation tends to occur in those parts of the fractures where the openings are smaller, also creating a heterogeneous channelized effect as well as adding to the flow resistance of the system. The investigation of chemical coupling for the panel work used DFN models indirectly by upscaling properties from Itasca's DFN code, UDEC, to LBNL's porous continuum code, TOUGHREACT. The models were based on the EGS research site at Newberry crater in Oregon. This work is reported in Chapter 5.

5.1 Geologic Setting

In addition to looking at coupled processes, the panel looked at EGS performance in different geologic and tectonic settings. A specific attraction of EGS for power generation is the recognition that EGS resources may be widespread if not ubiquitous. That said, the ability to extract that resource will depend on the geothermal gradients, which determine the depth required to find an exploitable geothermal resource, as well as the in-situ stress conditions which will determine the characteristics of the hydraulic fractures and critically stressed natural fractures. Chapter 7 looks at the interplay of rock stress and geothermal gradient in terms of the economics and optimization of EGS development in different geologic settings.

6 Two-Dimensional Hydro-Thermal Fracture Models

6.1 Objective of Hydro-Thermal Calculations and Models

In this section we will start with the well-known analytical solution developed by Gringarten et al. (1975) to develop some basic understandings of the EGS heat exchanger and define a set of parameters that meet the heat production and thermal longevity requirements described in the previous section. We then expand this into some simple numerical simulations that incorporate the effects of heterogeneity.

6.2 Analytical Solutions

7 Description of Gringarten analytical solution

The Gringarten solution describes the two-dimensional heat flow in a single fracture that has a length in the direction of fluid flow, z , and a unit height in the y direction (Figure 5). Gringarten defines his flow rate, Q , as the flow per fracture per unit height, f . The total flow rate, which we define here as q , is the product of Q , the fracture height and the number of fractures. The utility of expressing flow as Q is that the temperature solution holds regardless of the number of fractures and fracture height, but q is useful if one wants to express results in terms of a total flow rate from a set of fractures.

By symmetry, the fracture draws heat from two rock blocks having a thickness, x_e , one on each fracture face, which are the dark blue blocks in Figure 5. The fracture spacing is twice the thickness of the rock block contributing heat to the adjacent fracture face. The outermost block has infinite thickness. The discrepancy that results from using a finite versus an infinite outer block appears in later time behaviors, which occur after the production temperature would have dropped below commercially viable values, as we will discuss in later sections.

The solutions appear as type curves in Figure 6. Type curves use dimensionless parameters, that is, lumped parameters with no units, to provide an efficient expression of the results of an analytical solution. The solutions use three

parameters -- dimensionless temperature, T_D , dimensionless time, t_D , and dimensionless block thickness, x_{eD} .

Gringarten et al. (1975) analytical solution defines dimensionless time as

$$t_D = \frac{(\rho_w c_w)^2}{K_r \rho_r c_r} \left(\frac{Q}{z} \right)^2 t = C_1 \left(\frac{2x_e q}{xyz} \right)^2 t$$

and dimensionless spacing as

$$x_{eD} = x_e \frac{\rho_w c_w Q}{K_r z} = x_e C_2 \frac{2x_e q}{xyz}$$

Where C_1 and C_2 are lumped parameters containing the rock and fluid properties.

The curves can be readily transformed into solutions with real time though conversions that include the rock and water properties, the block thickness, x_e , and the length dimensions, x , y , and z using:

$$t = \frac{t_D}{C_1} \left(\frac{xyz}{2x_e q} \right)^2$$

$$x_e = \frac{x_{eD}}{C_2} \frac{xyz}{2x_e q}$$

where terms and values appear in Table 2. Figure 6 shows an example conversion to real time for a single fracture with $y=250\text{m}$, $z=1000\text{m}$, and $q=.01 \text{ m}^3/\text{s}$ and a range of x_e values. The real time values show the thermal depletion effects of smaller block size values.

The dimensionless temperature simply expresses the relative cooling of the production water over time. Initially the production water temperature is that of the rock, T_{R0} . A dimensionless temperature value of zero means there has not yet been a decline in the production water temperature, $T_p(t)$.

The production water temperature declines with time as either the rock cools or a cooler thermal front from the injection well reaches the production well. Over time, all curves move to a dimensionless temperature of 1, which means the production

water temperature is the same as that of the injection water, T_i , and there is no net production of heat. Note that the solution assumes the injection water temperature is constant over time.

One can convert dimensionless temperature to real temperature using:

$$T_p(t) = T_{R0} - T_D (T_{R0} - T_i),$$

although it is often convenient to express simulation results as the fraction of thermal decline in an EGS system, which is identical to the dimensionless temperature.

Before going to some examples of calculations using the Gringarten curves, we describe some general characteristics of the curves in Figure 6. First, as mentioned above, the curves start with a period of thermal stability during which the reservoir inflow into the, producing well is water at the rock temperature with negligible thermal decline. Then, at some point the production temperature begins to drop significantly, which is the thermal breakthrough. This decline starts somewhere between dimensionless times of 0.1 and 0.3. A 10% decline occurs between dimensionless times of 0.6 and 1 depending on the dimensionless rock block thickness. For smaller block size values, the thermal decline results from the thermal depletion of the rock blocks. For larger block sizes, the thermal decline reflects decreasing heat flow from rock to the fracture, and the advance of the cooling front within the fracture from the injection well to the production well.

8 Effect of rate and surface area on thermal performance

The analytical solutions can provide some useful insights to the key factors that affect thermal performance. The main objective of an EGS design is to maximize the power while delaying the thermal decline. In terms of the analytical solution, we wish the conversion factor from dimensionless to real time to be large.

The conversion factor contains terms for the rock and fluid properties, C_1 , the flow rate per fracture per unit height, Q , and the fracture area, xy , times the number of fractures, which is x/x_e . Looking at the rock and fluid properties, there is some benefit to hosting EGS systems in rocks with high thermal conductivity, however, except for some rocks with very high quartz contents, the thermal properties of

rocks are generally not sufficiently variable to be a major factor in design. Thermal drawdown of the reservoir will increase as the square root the flow rate and decreases as the square root of the contacted heat exchanger surface area.

Figure 7 shows this with two sets of curves: one for variable rates at a constant length (500 m) and the other for variable lengths at a constant rate. The solutions are for a single fracture with infinite block thickness. The two sets of curves overlies one another; hence, there are two sets of curve identifiers. The results show clearly the effect of increasing area or length (with constant height) or decreasing flow rate on improving thermal performance. The log slopes in Figure 8 show this is a second power relationship, hence adding area or decreasing flow rate strongly improves thermal longevity. It is worth noting that the only single fracture simulations that meet the 10-degree decline in 20 years criterion are the cases with the largest area (8000m x 500m) at 80 kg/s or the 500m by 500m fracture with a flow rate of 5 kg/s. In order to meet the target rate of $.08 \text{ m}^3/\text{s}$, the latter fracture with the 5 kg/s rate would have to be replicated sixteen times.

9 Effect of fracture spacing on thermal performance

The next case considers the effect of fracture spacing on thermal performance (Figure 9). To illustrate this case, we consider a stimulated volume that is 500 m in height, 200 m in width, and 500 m in length between the injection and production locations. We use the properties contained in Table 2.

There are two striking features of the temperature versus time plots in Figure 9. First, increasing the number of fractures dramatically improves the thermal performance. Increasing the number of fractures not only increases the surface area for heat transfer, but also reduces the flow rate per fracture. As the previous section discusses, surface area and flow rate have second power effects on the time to thermal breakthrough (Figure 10). This increase in surface area and decrease in flow rate more than offset the effect of smaller block thickness on thermal decline. Smaller block thicknesses breakthrough later than larger block thicknesses.

The second interesting feature of these curves is the small improvement from 16 to 24 fractures. This behavior was also observed in spacing-sensitivity calculations reported in Doe et al. (2014). This behavior reflects how flow rate affects the advance of the thermal front in the fractures compared with the rock blocks. At the

high flow rates required in calculations with only a few fractures, the thermal front advances rapidly within the fracture without significantly depleting energy from the rock blocks. This behavior results in earlier thermal breakthrough and a long gradual decline in the temperature. By contrast, calculations for larger number of fractures have lower flow rates, and the thermal front advances more slowly in the fractures, closer to the rate of advance of the thermal front in the rock blocks. This behavior is illustrated in Figure 11 (Doe et al., 2014).

For the system with 16 fractures, the thermal front in the rock blocks is not far behind that in the fracture, and once thermal breakthrough occurs the decline is relatively steep. Adding more fractures to the calculations, such as going from 16 to 24 fractures, does not change thermal behavior very much, because the thermal behavior becomes dominated by depletion of the rock blocks.

The effects of thermal depletion are further illustrated in Figure 10 and Table 3 which show the percent of the thermal energy in the volume that has been produced when the temperature has declined by 10% of the difference between the injection and production values. For the single fracture, only one percent of the thermal energy in the system has been produced when the 10% thermal decline has been reached at 0.9 years. By contrast, the calculations using 16 and 24 fractures reached 10% thermal decline at 8.6 and 9.7 years having produced 65% and 72% of the available thermal energy stored above the injection temperature.

Another way to look at the question of energy depletion is to think in terms of production temperature behaviors that are dominated by cooling within the fracture and those that reflect depletion of heat in the matrix. The point where adding fractures or reducing rate no longer affects the production temperature curves is an indicator of matrix domination. The transition from fracture to matrix domination may be defined by the dimensionless fracture spacing, x_{eD} . Using the results in Figure 9 and converting to dimensionless values, it appears that matrix depletion takes over when x_{eD} is less than 0.2. The definition of dimensionless spacing defines the parameter space for matrix domination.

In summary, multiple fractures within the stimulated volume significantly improve thermal performance by having both increased surface area and lower flow rate per fracture. There is a limit to how much increasing the number of fractures improves

thermal performance which is determined by the fracture intensity once thermal depletion of the rock blocks becomes dominant.

10 EGS feasibility space based on analytical solutions

The analytical solutions provide a relatively simple basis for determining EGS feasibility space. This example follows the approach presented in Doe et al. (2014), which starts with the thermal longevity requirement. Section 1.4 defines the following criteria for a 5 MW EGS system:

- Flow rate of 80 kg/s or 0.08 m³/s
- Initial injection-production temperature difference of 150 °C
- Thermal decline less than 10°C in 20 years (6.3E8 s).

The thermal decline criterion of 10°C for a system with a 150° differential temperature translates into a dimensionless temperature of 0.067. The first step to calculate feasibility space is to inspect the type curve for the dimensionless time value corresponding to this dimensionless temperature as shown in Figure 12, which is a detail of the type curves in Figure 9. The dimensionless time corresponding to a dimensionless temperature of 0.067 is 0.6.

The feasible space for flow rate and fracture area comes directly from the definition of dimensionless time, or

$$\frac{A}{q} = \sqrt{\frac{C_1 t}{t_D}}$$

$$A = yz n_f$$

If we use the target flow rate of 0.080 m³/s we can obtain the required fracture area, A , for a feasible EGS. Rearranging the definition of dimensionless time and including the appropriate values gives us the following relationship, where n_f is the number of fractures.

$$A = yz n_f = q \sqrt{C_1 \left(\frac{t}{t_D} \right)_{required}}$$

$$A = yz n_f = 0.08 \text{ m}^3/\text{s} \sqrt{2.52 \times 10^6 \text{ s/m}^2 \frac{6.3 \times 10^8 \text{ s}}{0.6}} = 4.1 \times 10^6 \text{ m}^2$$

If the target is to have a 1 km³ reservoir with fractures that are 1 x 10⁶ m² in area, then the number of fractures would be

$$n_f = \frac{4.1 \times 10^6 \text{ m}^2}{1 \times 10^6 \text{ m}^2} \approx 4$$

By choosing the infinite x_{eD} type curve, we assume the fractures are not thermally interacting. As the type curves for $x_{eD} > 2$ have not diverged from the infinite type curve at the dimensionless time of interest, this analysis holds for fracture spacings corresponding to $x_{eD} > 2$. We can calculate the spacing for these four fractures by rearranging the definition of x_{eD} and substituting the appropriate values:

$$x_c = \frac{x_{eD} \sqrt{2} n_f}{q C_2} = \frac{2 \times 1 \times 10^6 \text{ m}^2 \times 4}{0.08 \text{ m}^3/\text{s} \times 1.67 \times 10^6 \text{ s}/\text{m}^2} = 60 \text{ m}$$

fracture spacing = $2x_c = 120 \text{ m}$

For smaller fracture spacings, the same analysis would use the dimensionless time values from a type curve with a smaller value of x_{eD} .

For this example, we assumed the flow rate and calculated the necessary total surface area. Conversely, we can do the same analysis assuming a surface area and determining the maximum flow rate allowable to meet the thermal longevity criterion.

10.1 Hydro-Thermal Numerical Simulations Using Parallel Fractures

11 *Parallel fracture numerical simulation verification*

The Gringarten analytical model for EGS performance is a useful starting place for understanding some of the basic thermal transfer mechanisms between rock blocks and flowing fractures. The analytical model, however, has several inconsistencies with realistic discrete fracture networks. The development of discrete fracture network methods arose from an understanding that natural fracture networks are highly heterogeneous. The Gringarten model assumes uniform fracture spacing and rock block size, parallel fractures with no deviation in orientation, and uniform fracture apertures and flow properties. As a first step from analytical solutions to more realistic fracture network models, we perform a series of simulations using

parallel fractures, like the Gringarten model, starting with a uniform-fracture verification case for the numerical model and proceeding to parallel fracture networks with increasing heterogeneity. The results of these models have been presented in Doe et al. (2014).

The modeling approach used the Golder Associates FracMan DFN code for fracture generation and for creating complex fracture networks (Dershowitz et al., 2010; Cottrell et al., 2013). While the FracMan code includes flow solutions, it does not include coupled hydrothermal calculation. For this purpose, we turn to HydroGeoSphere (Therrien and Sudicky, 1996; Brunner and Simmons, 2012), which was originally developed at the University of Waterloo and the University of Laval and is currently being commercialized by Aquanty Ltd. of Waterloo, Ontario Canada. The HydroGeoSphere code is a control-volume, finite-element simulator particularly adapted to interactions between rock blocks and fractures both for thermal calculations and for contaminant transport. The work undertaken for this panel utilized an interface which maps fracture networks from FracMan into HydroGeoSphere.

The first HydroGeoSphere model was developed as a verification case using a 1000 m domain in the x and z directions continuing with Gringarten's convention for using z to denote the direction parallel to flow. The simulations reproduce the four cases in Figure 5 of Gringarten et al. (1975). The verification case from Gringarten uses an initial rock temperature of 300°C with an injection water temperature of 65°C and total flow rate of $0.145\text{ m}^3/\text{s}$. The model uses a 1 km cube with constant head boundaries of 100 m on the injection face and zero on the production face. The comparison of simulation results and Gringarten's solution provides a verification of HydroGeoSphere's performance (Figure 13).

12 Parallel fracture numerical simulation, variable spacing and aperture

With the HydroGeoSphere results verified, the next step looks at the effect of heterogeneity of both spacing and aperture. The heterogeneity study retains the properties and geometries of the Gringarten example. Keeping the number of fractures and the model region the same as those of the example, four simulations produce the following conditions:

- Uniform spacing and aperture (verification case)
- Random spacing, constant aperture
- Random spacing, moderately variable aperture (mean= $2.9E-4$ m; variance= $1E-4$ m)
- Random spacing, highly variable aperture (mean= $2.9E-4$ m; variance= $2E-4$ m)

The temperature visualizations for the four parallel fracture cases appear in Figure 14. The bar chart beneath each visualization shows the relative magnitude of the aperture for each fracture. The uniform spacing and aperture case develops uniform cooling both along the fractures and symmetric to each fracture in the rock blocks, which represents the conditions of the analytical solution. Introducing variable spacing, even with constant aperture, produces thermal results with considerable non-uniformity of cooling, which occurs preferentially in rock blocks that are bounded by closely spaced fractures.

The third and fourth cases in Figure 14 have non-uniform apertures in addition to non-uniform spacing. The combination of variable spacing and non-uniform aperture produces an even greater non-uniformity to the distribution of cooling within the system. Thermal depletion occurs preferentially between fractures that are closely spaced while significant volumes of rock between the widely spaced fractures do not contribute to power production.

The effect of variable spacing and aperture on thermal performance is very significant (Figure 15). As a measure of performance, we may choose the time to reach a 10° thermal decline, as given by the 0.1 dimensionless temperature value. The uniform spacing and aperture case after about 20 years and reaches the 10° decline mark at about 43 years. Adding variable spacing, while leaving the apertures constant, degrades the thermal performance, reaching 10° decline at about 25 years.

The two cases with both variable spacing and aperture show further degradation to the thermal performance. The case with moderate variability of aperture begins to decline before five years and has cooled 10% in 16 years, while the high variability case reaches 10% decline in about 8 years.

Adding variability in spacing and transmissivity of the parallel fractures degrades thermal performance relative to the uniform case. For the variable spacing, uniform aperture cases this degradation occurs due to local thermal depletion of the rock mass between closely spaced fractures. The non-uniform aperture cases concentrate flow rate in a smaller number of fractures. As shown previously with Gringarten analytical calculations, flow rate has a strong effect on early thermal breakthrough. The combined effect of spacing and aperture reflects, therefore, both localized thermal depletion of rock blocks and accelerated migration of cooler injection water to the producing wells along the larger-aperture fractures that are carrying the higher flow rates.

13 Complex fracture network simulations

Up to this point the numerical simulations used only parallel fractures, while realistic fracture networks have multiple sets in different orientations. We developed a model with variable fracture orientations based on image logs from the Newberry EGS site (Cladouhos et al., 2011). Rather than defined fracture sets, we sampled directly from the orientations at Newberry site. We used a variable size distribution. We then used FracMan's hydraulic fracturing simulator to inject fluid and create a set of stimulated fractures that was a subset of the entire fracture set. The inset to Figure 16 shows the fracture network. The well spacing for this model is 1074 m within a 2.2 km long by 724 m wide region with a thickness of 500 m. The flow rate is 70 kg/s. Properties for the simulations are based on Newberry and appear in Table 3.

The hydraulic fracturing simulations define two rock regions - a stimulated volume, which is roughly the rock volume inside a line drawn around the fracture network and an unstimulated volume of rock without fractures or fractures that remain closed. The circulation of water in the EGS system is entirely within the fractures of the stimulated volume.

The two volumes influence the production temperature history and produce two distinct phases of production temperature decline, an initial phase when the heat is being drawn from the stimulated volume and a second phase when the heat is being drawn from the unstimulated volume. The first phase follows the Gringarten-type curve for a dimensionless spacing of 1. That curve deviates from the infinite

spacing curve at about 15 years, and the more rapid thermal decline is an indication that the stimulated volume is depleting of available energy.

Then at 40 years the rate of decline in the production temperature slows. At this point in time, the stimulated volume is depleted, and the energy is being extracted from the unstimulated volume. The stimulated volume is acting as a single thermal sink, which is essentially Gringarten's single fracture, infinite spacing condition. In the second phase, thermal production from the unstimulated volume, the thermal decline runs roughly parallel to infinite spacing case. The inset to Figure 17 shows the temperature in the rock volume at 30 years, which is a time when the stimulated volume is approaching depletion.

The simulations using a stimulated volume point out one deficiency in the Gringarten solutions. The solutions for finite fracture spacing assume that each of the two faces of each fracture draws energy from a rock block with a thickness that is half the fracture spacing. If one has a finite number of fractures, then outside fractures in the parallel array actually have an infinite block on their outside faces (see Figure 5). Hence, any realistic Gringarten-like system is a composite of a finite fracture spacing within the parallel fracture array and an infinite fracture spacing system for the two outside fractures. Production temperature behaviors will have two phases like the complex network simulations where the finite blocks will deplete first, and the longer-term thermal decline will be controlled by the infinite rock blocks facing the two outer fractures.

13.1 Summary of Hydro-Thermal Analytical Solutions and Numerical Simulations

Analytical solutions using the Gringarten model and simple hydro-thermal numerical models extending the Gringarten model show that that EGS performance is influenced by the following:

- Surface area affects thermal breakthrough by a second power relationship
- Flowrate affects thermal breakthrough by an inverse second power relationship
- Multiple fractures improve thermal performance by having both enhanced surface areas and decreased flow rates per fracture

- At higher fracture intensities the combination of slower moving water and smaller block sizes results in delayed thermal breakthrough followed by rapid thermal depletion, along with high thermal recovery factors.
- Heterogeneity within fracture networks (both spacing and aperture) leads to localization of thermal depletion and flow, resulting in poorer thermal performance
- Complex fracture systems have early time behaviors consistent with thermal depletion of multi-fracture networks, followed by later slower decline as the stimulated volume acts as a single thermal sink.

EGS performance is improved when flow is distributed into networks of multiple fractures rather than a single hydraulic fracture. Shear stimulation of natural fractures at pressures below the minimum in situ stress is one way to achieve this objective. The following section looks at coupled hydro-mechanical simulations using discrete fracture network models to determine factors that are favorable to shear stimulation.

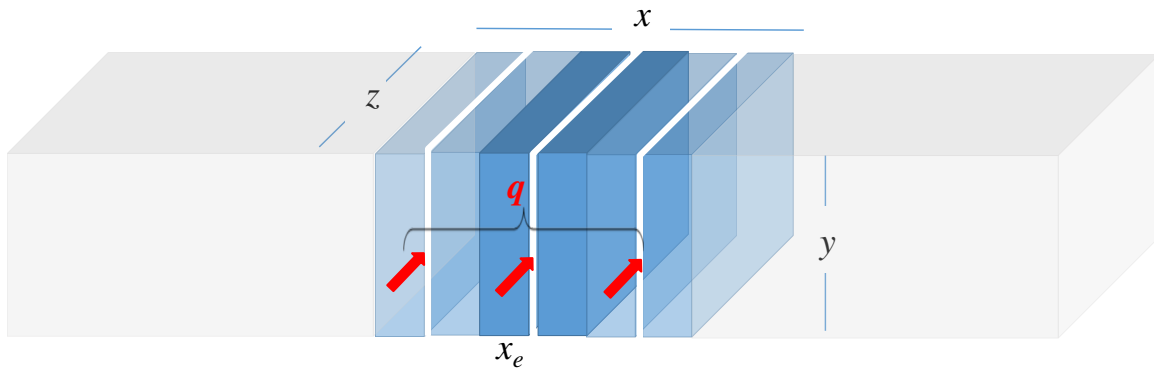


Figure 5. Geometry and assumptions of the Gringarten analytical solution.

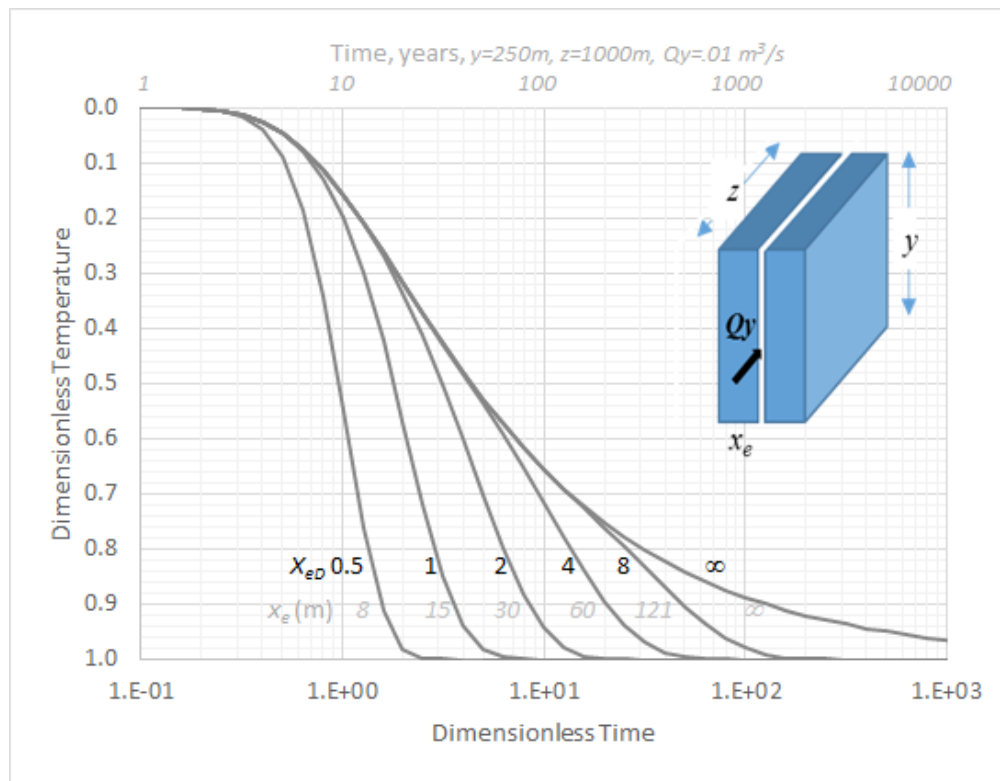


Figure 6. Gringarten et al. (1975) type curves for five values of dimensionless rock block thickness, X_{eD} , with conversion to real time for properties in Table 2.

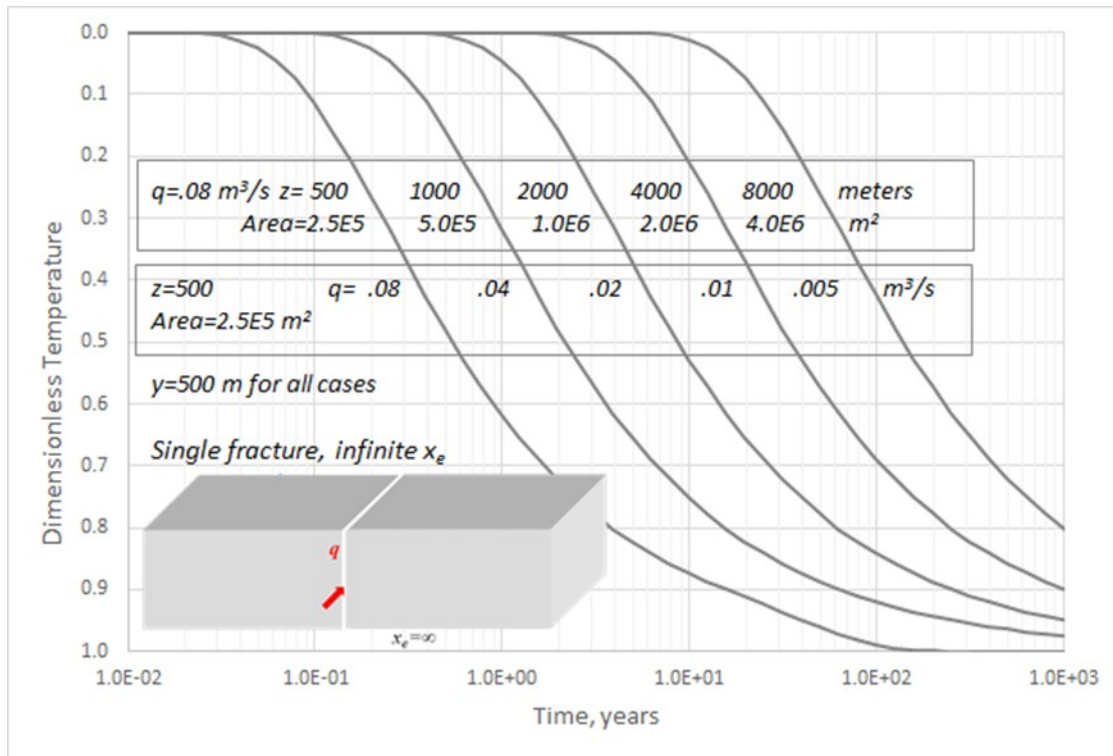


Figure 7. Effect of fracture length and flow rate on thermal performance. Each curve can be produced with different combinations of rate and total area. Hence each curve has a label for variable length, z , at constant rate of $0.08 \text{ m}^3/\text{s}$ (upper label box) and variable rate at constant length, $z=500 \text{ m}$ (lower label box). Height, y , is constant at 500 m . Thermal longevity depends on the square of surface area and inverse square of flow rate.

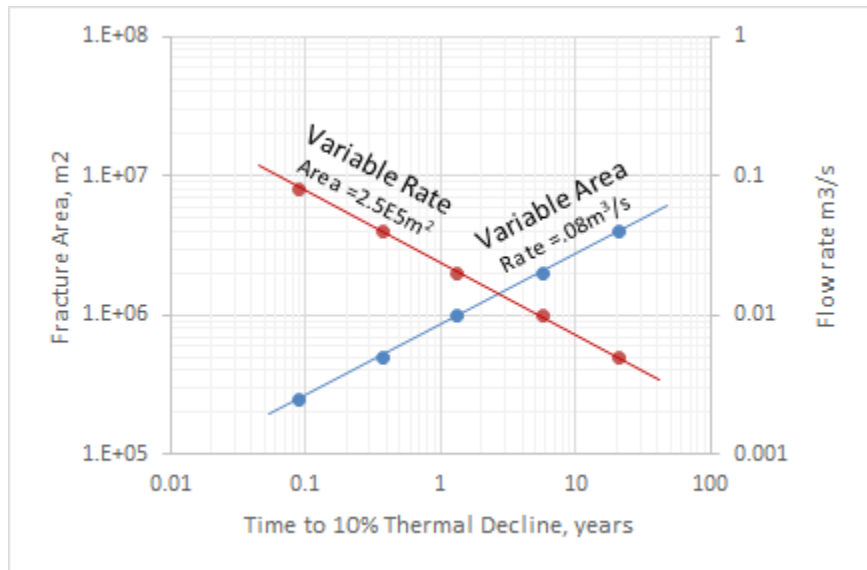


Figure 8. Delay in thermal decline (10% of initial T) versus fracture area and flow rate for cases in Figure 7. Time to 10% decline increases with larger area and decreases with higher rate.

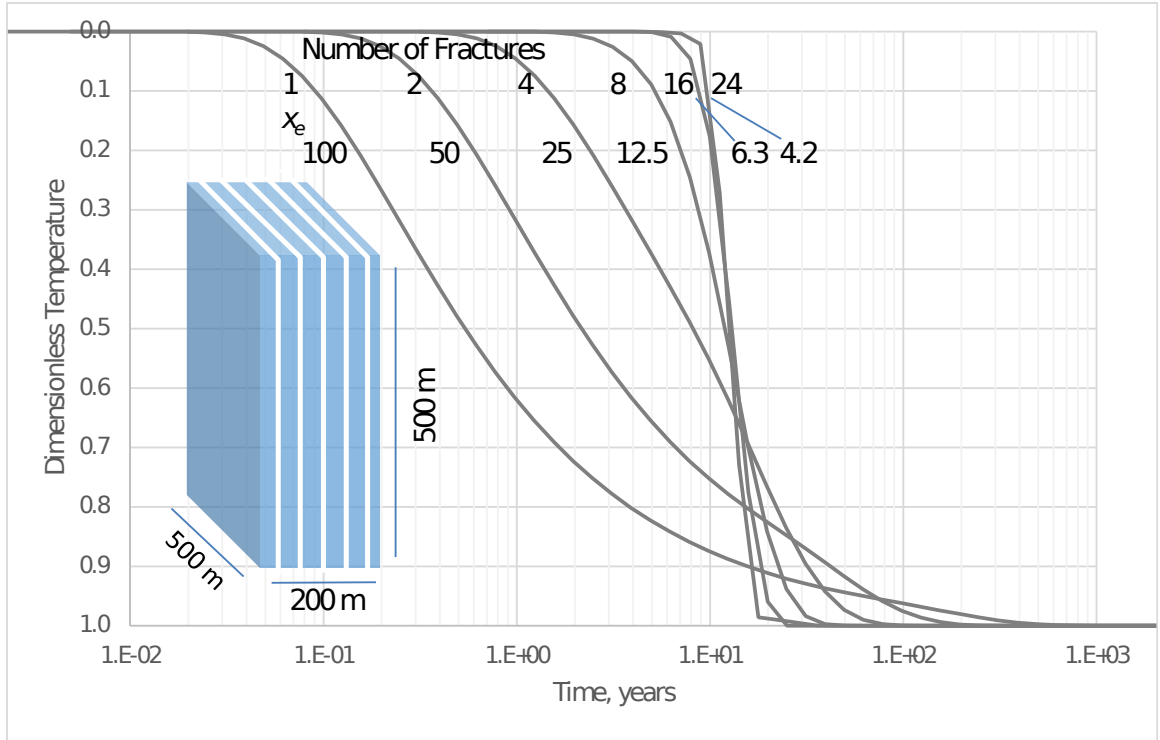


Figure 9. Effect of multiple fractures on thermal performance. Flow rate $0.08\text{m}^3/\text{s}$. Increasing the numbers of fractures increases the surface area for heat transfer and reduces flow rate per fracture. Both effects increase thermal longevity. Further improvement with number of fractures stops when the thermal front in the rock does not lag the thermal front in the fractures (see Figure 11)

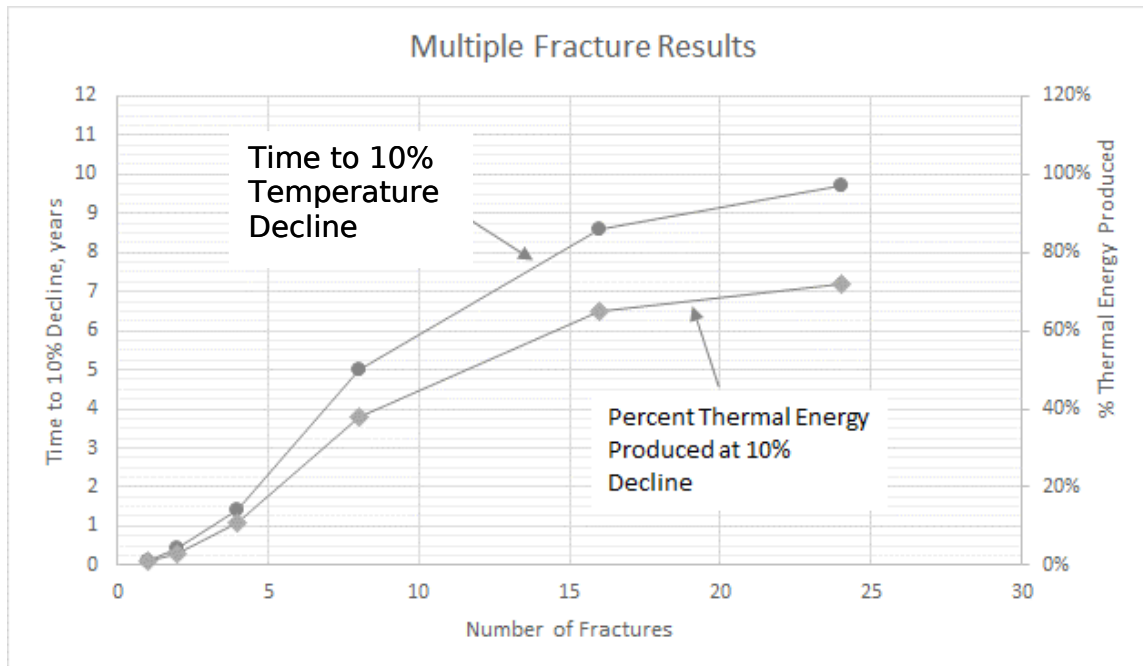


Figure 10. Effect of multiple fractures on thermal breakthrough and energy production. Flow rate, 0.08 m³/s. A higher number of fractures delays thermal decline. For large numbers of fracture with small spacings, most of the energy has been produced from the rock when thermal breakthrough (10% decline) is reached.

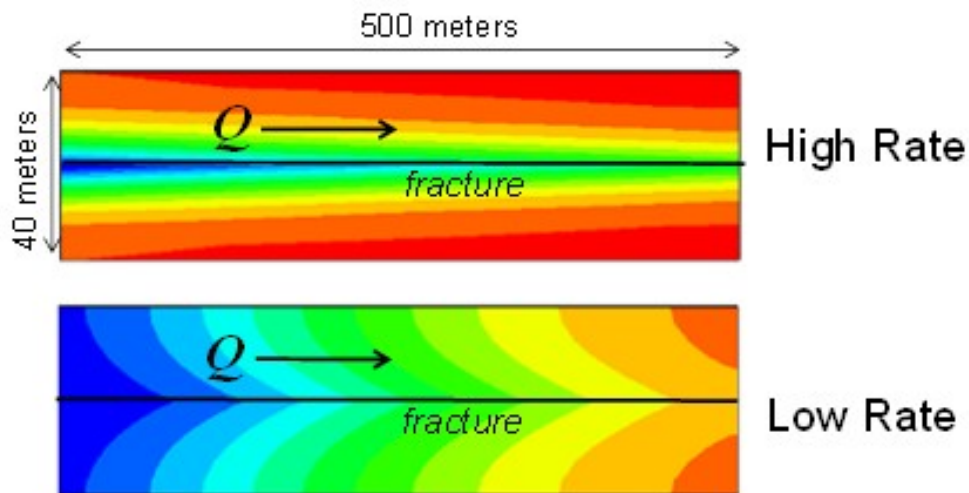


Figure 11. Role of flow rate in thermal breakthrough and thermal sweep efficiency (Doe et al., 2014). At high rate, the thermal front advances without cooling the rock; at low rate the thermal front in the rock advances with thermal front in the fracture. (red = hot, blue = cold)

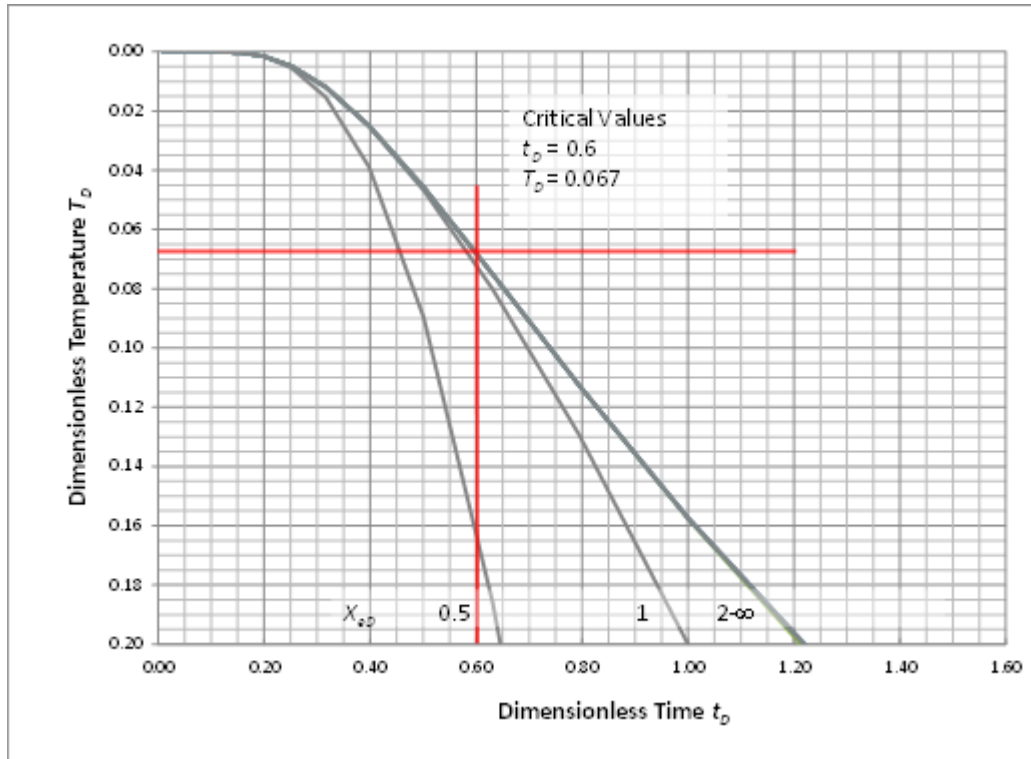


Figure 12. Using dimensionless type curves for feasibility space calculation. (1) determine the target thermal decline and its associated dimensionless temperature. A 10-degree decline when the difference of the injection and rock temperatures is 150 degrees corresponds to dimensionless temperature, T_D , of 0.067. (2) That dimensionless temperature is achieved at a dimensionless time, t_D , of 0.6. (3) Using the definition of dimensionless time and setting the real time value to the target thermal longevity (e.g., 20 years), allows one to calculate the combinations of flow rate and area necessary to achieve the target. This calculation uses the infinite dimensionless spacing curve (single fracture). Similar analyses for multiple fractures (finite fracture spacing) will use the other dimensionless spacing curves. For this thermal decline, dimensionless spacing values >2 still follow the infinite curve.

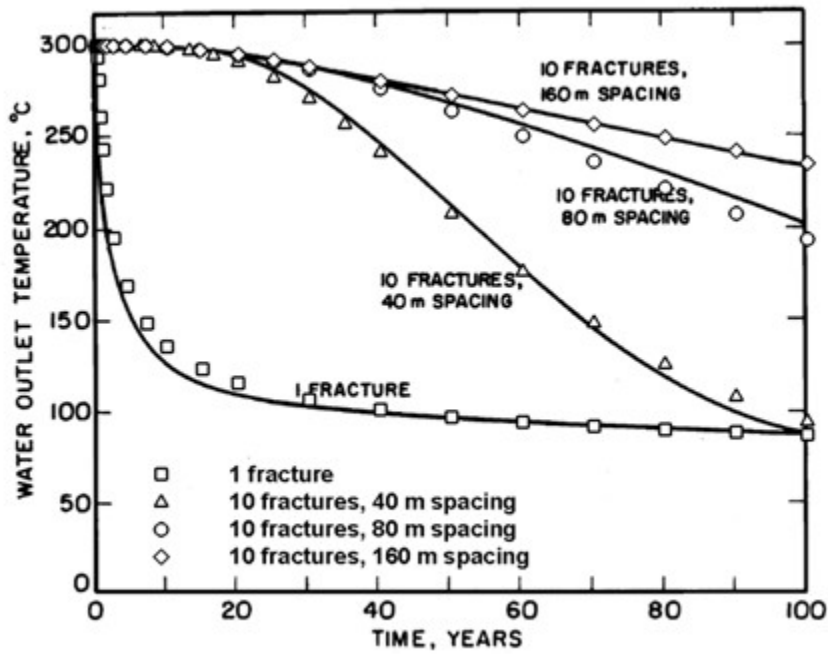


Figure 13. Verification of HydroGeoSphere (symbols) with analytical solutions (lines). Points are HydroGeoSphere simulation results superposed on Gringarten et al. (1975) Figure 5 for the same property and geometry conditions.

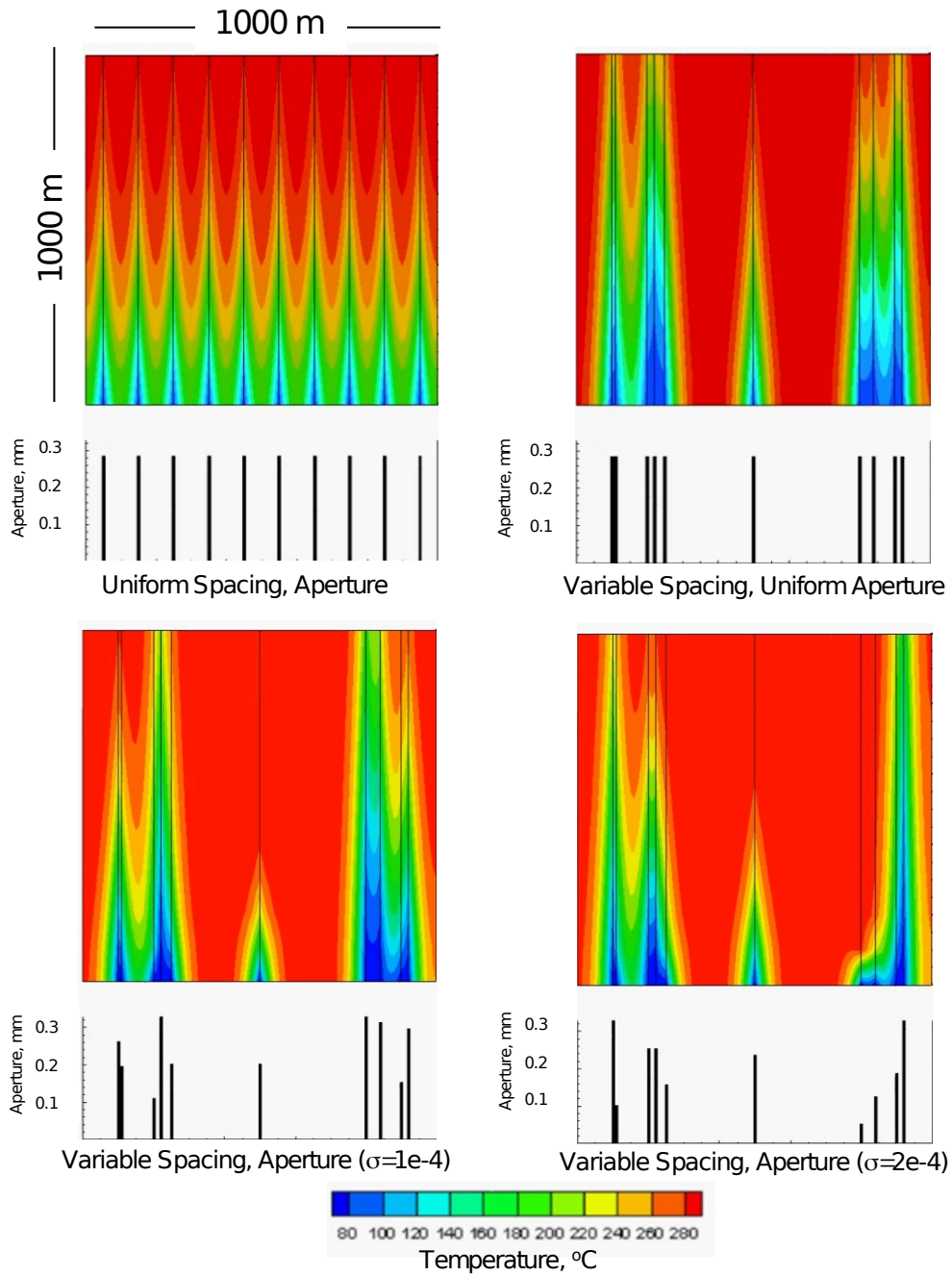


Figure 14. Visualizations of parallel fracture numerical simulations from uniform spacing and aperture to variable spacing and aperture. Increased heterogeneity (variable spacing and variable aperture) focuses the flow into "short circuits".

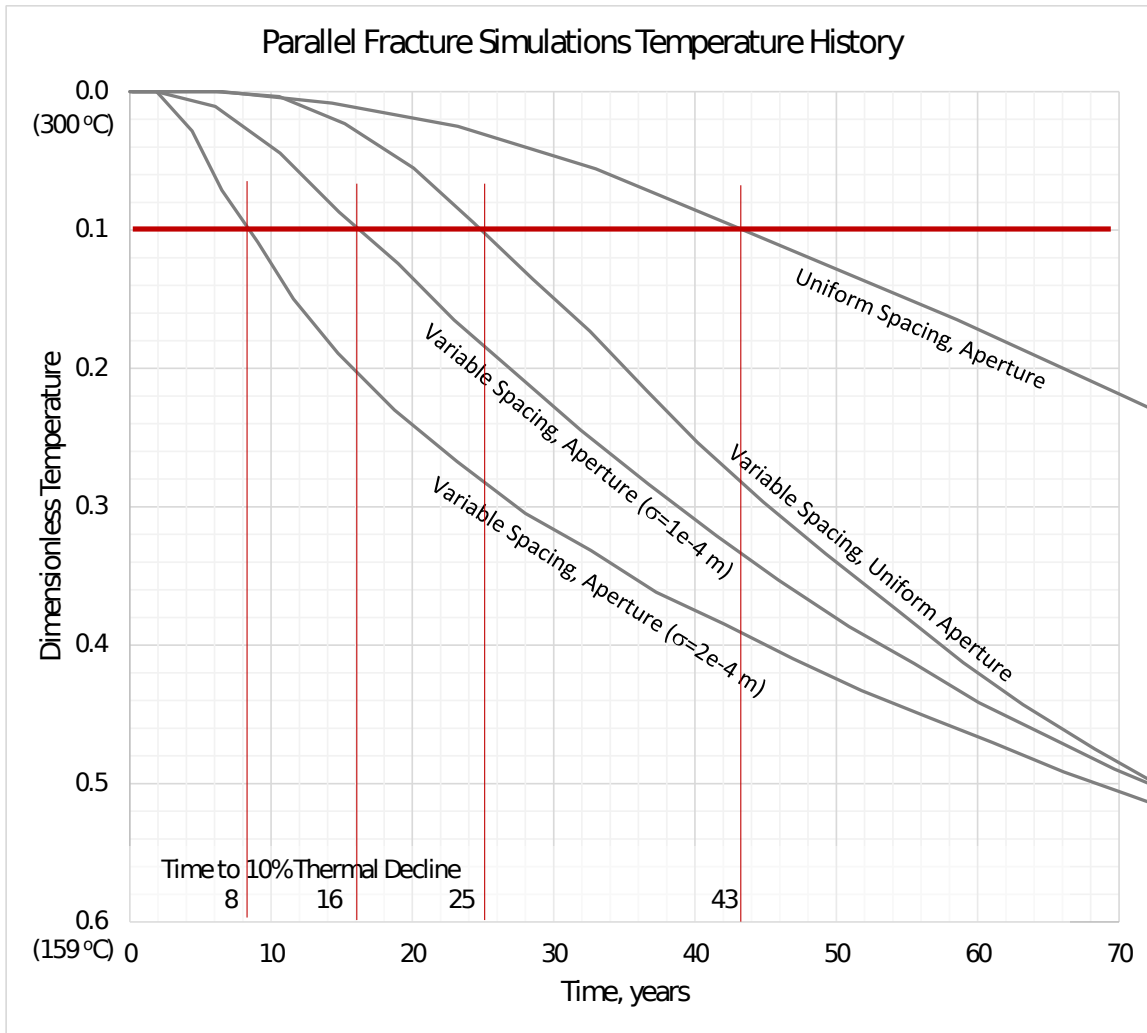


Figure 15. Production temperature results for parallel fracture models shown in Figure 14. Variable spacing results in earlier thermal breakthrough compared with the uniform spacing and aperture case. Varying the aperture further hastens thermal breakthrough creating “short circuits”. Temperature given as dimensionless values with actual temperature in parentheses. Red lines show a 10% thermal decline with corresponding time in years for each simulation.

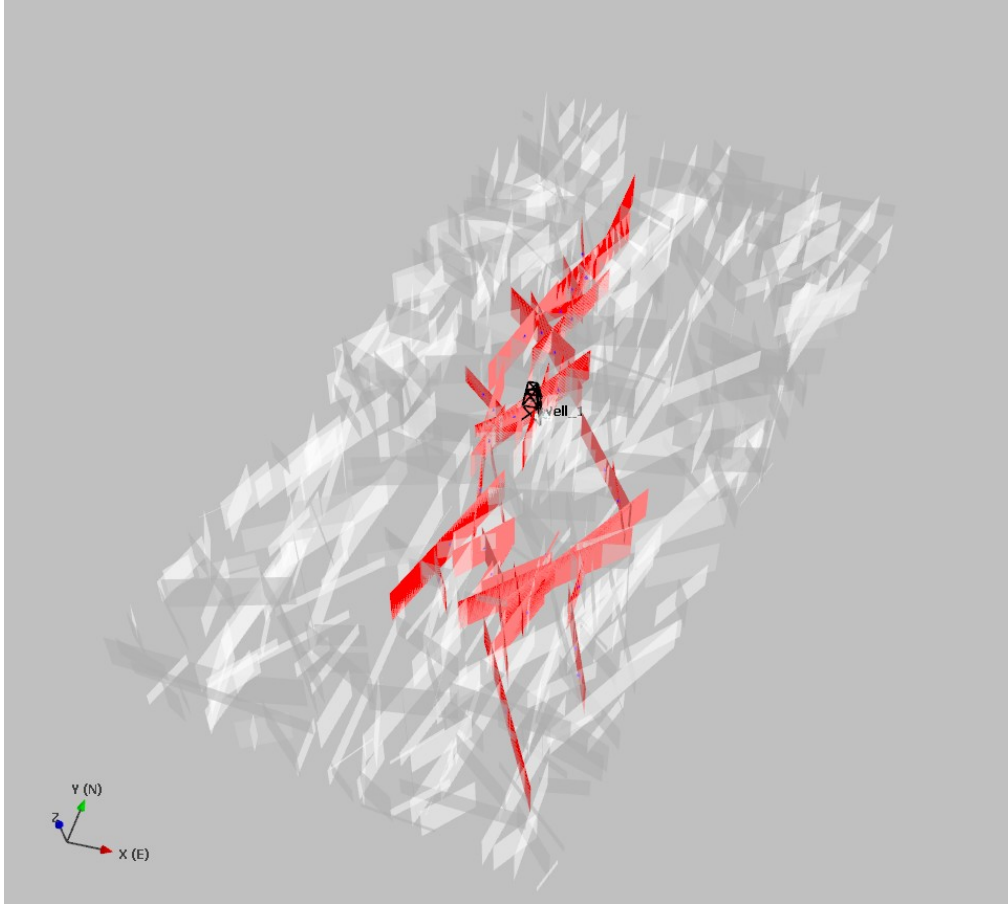


Figure 16. Stimulated subset of DFN model based loosely on Newberry EGS site data for fracture orientations. Red fractures are stimulated by the hydraulic injection. Gray fractures are unaffected. Stimulation simulated in FracMan.

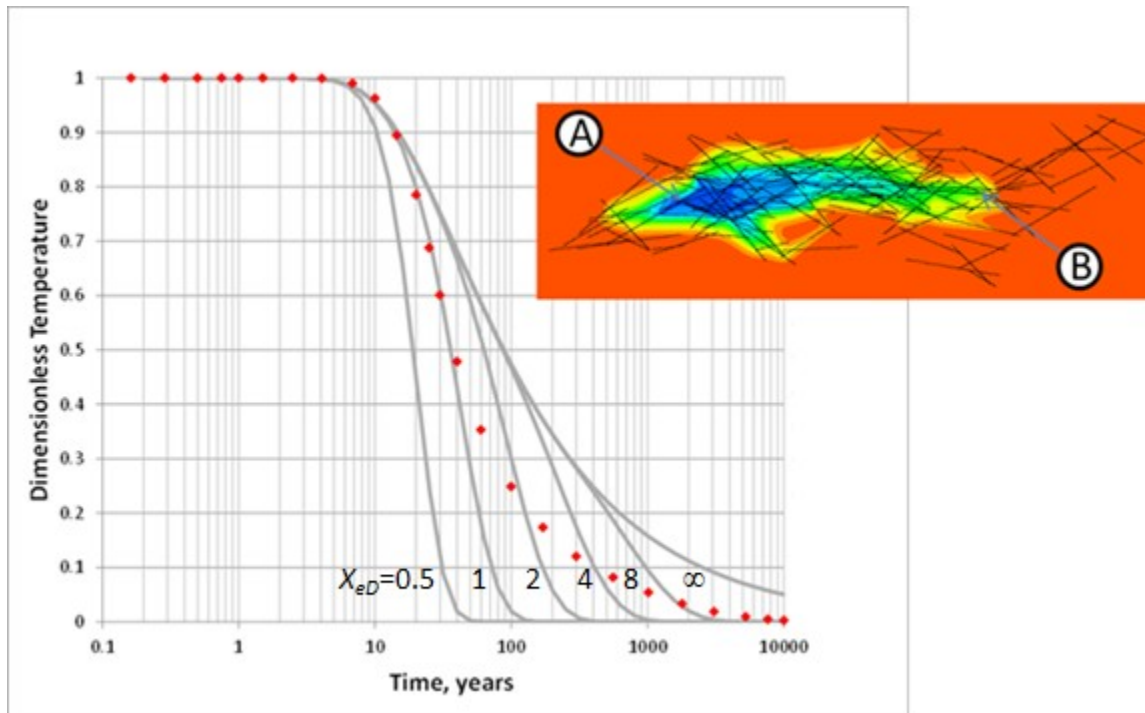


Figure 17. Production temperature versus time with comparison to Gringarten-type curves for a complex fracture network model. The inset shows a map view of the fracture network with a temperature snapshot at 30 years. The early time follows a dimensionless spacing type curve with a value of 1, as the rock between closely spaced fractures thermally depletes. Once these rock blocks are depleted, the entire stimulated volume acts as a single sink and the temperature curve deviates toward the single fracture, infinite spacing case. Temperature profile at 30 years, well spacing is 1074 m. A is the injector and B is the producer. From Doe et al., 2014.

Table 1. Property definitions, symbols, and values.

Property	Symbol	Value	Units
Rock Thermal Conductivity	K_r	2.5	J/m-s-°C
Rock Heat Capacity	c_r	1,045	J/kg-°C
Rock Density	ρ_r	2,650	kg/m ³
Water Heat Capacity	c_w	4,180	J/kg-°C
Water Density	ρ_w	1,000	kg/m ³
Lumped Parameter for T_d , Dimensionless Time	C_1	2.52E6	s/m ²
Lumped Parameter for X_{ed} , Dimensionless Block Thickness	C_2	1.67E6	s/m ²
Gringarten Flow Rate (per fracture per unit y)	Q	$\frac{qx_e}{yx}$	m ² /s (or kg/ms as noted)
Number of Fractures	n_f	$\frac{x}{2x_e}$	-
Reservoir Flow Rate (flow through all fractures)	q	$Qyn_f = \frac{Qyx}{2x_e}$	m ³ /s (or kg/s as noted)
Reservoir Width	x	Variable	m
Reservoir Height	y	Variable	m
Reservoir Length (Well Spacing)	z	Variable	m
Dimensionless Time	t_D	$C_1 \left(\frac{Q}{z} \right)^2 t$	-
Block Thickness	x_e	Variable (1/2 fracture spacing)	m
Dimensionless Block Thickness	x_{eD}	$C_2 \left(\frac{Q}{z} \right) x_e$	-
Injection Water Temperature	T_I	50	°C
Initial Rock Temperature	T_{RO}	250	°C
Production Water Temperature	T_P	Variable	°C
Dimensionless Temperature	T_D	$\frac{T_{RO} - T_P}{T_{RO} - T_I}$	-

Table 2. Results of multiple fracture calculations for thermal breakthrough and energy production

Number of fractures n_f	Fracture Spacing $2x_e$	Block Thickness x_e	Dimensionless Block Thickness X_{eD}	Q , flow rate per fracture per unit y ($q=0.08 \text{ m}^3/\text{s}$)	Time to 10% Decline	Rock Thermal Energy Produced at 10% Decline
-	m	m	-	m^2/s	years	$\%$
1	200	100	53.3	0.00016	0.09	1%
2	100	50	13.3	0.00008	0.44	3%
4	50	25	3.3	0.00004	1.40	11%
8	25	12.5	0.83	0.00002	5.00	38%
16	12.5	6.3	0.21	0.00001	8.60	65%
24	8.3	4.2	0.09	6.7E-06	9.70	72%

Table 3. Properties for complex DFN simulation based on Newberry (Cladouhos et al. 2011)

Heat Capacity, water	c_w	4180	J/kg°C
Heat Capacity, rock	c_R	918	J/kg°C
Thermal Conductivity, rock	K_R	2.7	J/sm°C
Density, rock	ρ_R	2500	kg/m ³
Density, water	ρ_w	960	kg/m ³
Dimensionless time, Lumped Parameter	C_1	2.6×10^6	s/m ²
Dimensionless fracture spacing lumped parameter	C_2	1.5×10^6	s/m ²

14 Two- and Three-Dimensional Hydro-Mechanical Simulations (Itasca)

14.1 Objectives of Hydro-Mechanical Simulations

The simulations in this section use coupled hydromechanical DFN simulations to explore fracture network properties, in situ stresses, and injection conditions that are favorable to creating slip on natural fractures to create the reservoir. The model capabilities evolved over the period of the panel study, and the results reported in this section were developed before the models had thermal capabilities. Thus, these simulations do not include thermal effects so the inferences of EGS performance are based on the changes in the fracture network caused by fluid injection and do not include simulations of production fluid temperature. The thermal capabilities were added over the course of this study, and those results appear in section 4.

14.2 Background and Simulation Approach

The original concept of EGS involved creating a reservoir a single artificial fracture created by hydraulic fracturing. Injection using fluid pressures greater than the minimum horizontal stress created the fracture in a plane oriented normal to the minimum stress direction. The development and application of microseismic methods at the Rosemanowes EGS research site in the UK showed that the injections were stimulating a considerable volume of rock and not a single fracture plane (Pine and Batchelor, 1984). The stimulation was apparently opening natural fractures rather than creating a single hydraulic fracture. Barton et al. (1995) introduced the concept of critical stress to show how pore pressure in its natural state could cause shear slip and dilation on natural fractures that were favorably oriented relative to the in-situ stress field. They propose that this could be a significant control on the natural permeability of fractured rocks. The concept of critically stressed fractures has become a basis for so-called hydro-shearing approaches in EGS (Cladouhos et al., 2011).

The hydrothermal calculations presented in Chapter 2 showed that EGS performance is strongly enhanced by having multiple fracture pathways contributing higher surface area and reduced flow compared with a single fracture pathway. Hydro-shearing provides an attractive approach for achieving this goal. The simulations discussed in this section were performed by Itasca and reported in Riahi and Damjanac (2013 a,b,c) and Riahi et al. (2015). The approach uses coupled hydro-mechanical models to determine the sensitivity of stimulation treatment outcomes to the existing fracture network, in situ stress, and operational factors such as injection rate and well positioning relative to the fracture network and stresses.

14.3 Two-Dimensional Simulations

15 Computational approach

The numerical analyses were performed using *UDEC*, a discrete-element modeling tool developed by Itasca and widely used in rock mechanics practice (Itasca, 2011). The *UDEC* model consists of an assembly of intact rock blocks separated by joints and fractures. The fractures are represented by smooth surfaces with a slip condition $\tau = (\sigma_n - P) \tan \varphi$, which relates the fracture shear strength (or critical shear stress), τ , to the normal stress, σ_n , the friction angle, φ , and the pore pressure within the fracture, P . Natural fractures have some roughness which causes them to dilate as the fracture slips (Figure 18). The dilational opening of fractures as a result of slip is irreversible. In *UDEC*, the fracture dilatancy is characterized by a macro-property called dilation angle. The potential for shear stimulation is determined by the magnitude of the in-situ stresses and their relative direction with respect to the fracture sets. Depending on the stress conditions, natural fractures may hydroshear under fluid pressures that are less than the minimum stress in the rock (Cladouhos et al., 2011).

Understanding the in-situ stress and fracture conditions is important for determining whether or not there is an injection pressure that will cause the natural fractures to hydro-shear while not creating a hydraulic fracture. The amount of dilation furthermore affects the overall increase in permeability of the fracture network and

the pressure requirements to establish circulation between injection and production wells.

UDEC is a fully coupled hydro-mechanical code, i.e., changes in pressure result in change in stresses, opening of fractures, displacement and straining of blocks. Also, displacement and stress change within the blocks affect pressures. In the current study carried out with *UDEC*, flow occurs only within the fractures and the blocks between the fractures are assumed to be elastic and impermeable.

The pre-existing fractures are represented explicitly as discrete, planar features. They deform both elastically and inelastically. The inelastic joint deformation can be in the form of opening and slip as a function of the fluid pressure in the fracture and the stresses in the rock. In a fully coupled model, the local stress state within the model domain reflects both the in-situ stresses of the model boundary and the local perturbations of stress due to fluid pressure and fracture deformation. The pre-existing fractures are assumed to be permeable, i.e., they are already assumed to be broken in tension. As pressure in the fractures increases, they can further open and shear. Once the stresses acting on the fractures exceed shear failure criteria, they can slip.

16 DFN model

The DFN model for this study is synthetic and is created stochastically using parameters that characterize discrete fracture network, i.e., fracture size distribution, density, and fracture orientation.

Fracture size distribution: It is assumed that fracture size distribution follows the power law. The power law distribution means that the numbers of fractures, $n(l)$ having a size greater than l follows a function $n(l) \propto l^{-\alpha}$ in which α is a positive number greater than 1 (de Dreuzy et al., 2004).

The power law distribution for fracture size is well established in the technical literature (Bonnet et al., 2001). This distribution is highly skewed towards producing a large number of small fractures and smaller numbers of larger fractures. The exponent of the power law affects the weighting among small fractures versus larger ones. Smaller exponents weight more of the total fracture area into larger fractures, while larger exponents put more weight into smaller fractures. The

simulations use a range of exponents from 2 to 3. The choice of exponent is supported by research suggesting that in 2D approximation α varies between 2 and 3; in 3D, it is in the range of 3 to 4. In these models, a minimum cut-off value of 15 m is applied for the fracture length. The minimum cut-off value is needed to limit the model computational size and the simulation time. For maximum value (used through generation curve) a cut off of 10,000 m was applied, which is significantly larger than the model size used. This effectively means that there is no maximum cut-off value. In some models, the maximum fracture length is limited to 250 m, which is about the quarter of the reservoir length. The limit on the maximum fracture length ensures more uniformity of length among fractures within the DFN and is a deviation from the power-law distribution among the larger fractures.

Fracture orientation: DFNs often consist of one or multiple fracture sets with each set having a mean orientation and some variation about the mean. The DFN model for these simulations uses two fracture sets, each with a constant orientation. For computational purposes, variation of orientation about the mean is neglected.

Fracture Density: The target density is selected through an iterative process (by iteratively increasing fracture density) such that the DFNs are at the threshold of connectivity. In other words, in these studies, unless explicitly said otherwise, the fracture network forms a cluster that extends to the boundaries of the model. Such a network is called “fully connected.” In this study, the degree of connectivity is evaluated by the size of the formed fracture cluster relative to the model dimension. A cluster is a network of connected fractures. No fracture within a cluster is intersected by a fracture outside of that cluster.

In addition to density, the exponent of fracture size distribution and variation of fracture orientation affect connectivity of the DFN. Smaller exponents result in a better fracture connectivity (Figure 19). Also, connectivity increases as variation in fracture orientation increases. Although variation in the fracture orientation within sets is neglected, the desired connectivity in the models was achieved by increasing the fracture density.

The DFNs have an approximate fracture density of approximately 0.06 m/m². There is variability in the fracture density between the models, depending on the

exponent of the fracture length distribution and the maximum fracture length cut-off value.

The fracture generation process locates fractures randomly within the model domain. This process can sometimes generate two fractures close to one another. Hence, the fracture networks are simplified by removing fractures that are less than a critical distance apart. This distance is generally 15 m, unless otherwise specified in this report.

17 Base model fracture network description

As explained in the previous section, the DFN model consist of two fracture sets each with a constant orientation. The DFN is fully connected. As this is a two-dimensional model, the fracture sets are vertical with the primary set oriented at 45° (N 45 E) and a secondary at 160° (N 20 W).

Initially, the fractures in each set have a uniform aperture. The initial apertures of fractures are selected such that equivalent permeability is in the range between 10^{-18} and 10^{-16} m². The apertures of two fracture sets are selected based on set orientation relative to the in-situ stresses. In this study, the fracture set which is oriented relative to the principal stress directions at a more favorable angle for slip is called “primary fracture set;” the other one is called “secondary fracture set.” The primary and secondary sets have apertures of 3×10^{-5} and 1.1×10^{-5} m respectively. The slip criterion for the fractures uses a Coulomb law with zero cohesion, a friction angle of 30° and a dilation angle of 7.5°. The fracture properties within a fracture set are assumed to be uniform.

The model is two-dimensional, assumed to be in a horizontal cross-section in the middle of a 350 m thick reservoir at a depth of 2.5 km. It is initially fully saturated with water. The initial water pressure in the model is assumed to be uniform and equal to hydrostatic pressure. The horizontal dimensions of the model are 2 km or 3.5km (depending on the model) in each direction (Figure 20). In the interests of computational efficiency, the model has an inner domain that is 1 km² with explicit discrete fractures (for the hydro-mechanical model presented in this section and a 2 km square domain for thermo-hydro-mechanical models (Section 4) . The outer domain has a regular fracture network with an initial permeability equivalent to that of that of the inner region. The model has the maximum initial principal stress in the

x direction (East) equal to the vertical, lithostatic stress based on a density of 2700 kg/m³, and the minimum initial principal stress in the y direction (North) equal to half of the lithostatic stress.

Throughout this study, all model parameters are those outlined in this section unless explicitly mentioned.

18 Flow conditions

The hydro-mechanical simulations include both stimulation and production phases. The stimulation is conducted by injecting fluid at a constant rate for 20 hours followed by a period of no injection to allow the pore pressures to dissipate. In the production phase, the fluid injection rate is reduced to 75% of that in the stimulation phase. All models use the stimulation phase injection rate of 2.4×10^{-4} m³/s per unit height, which is equivalent to 0.07 m³/s (70 kg/s) over the thickness (350 m) of the reservoir¹. In most studies, the selected fluid injection rate would not result in substantial growth of the hydraulic fracture.

The stimulation phase uses a single well located at the center of the model. During production phase, numerous scenarios were analyzed that include one or two production wells approximately 250 m, 500 m and 700 m from the injection well. The boundary condition applied at the injection well is constant rate, while the boundary condition applied at the production well is constant pressure equal to the hydrostatic pressure. Thus, production rate is not forced, but happens naturally as a result of pressure increase.

19 Creation of hydraulic fractures

In these studies, it was assumed that the hydraulic fracture could propagate but only along the pre-defined trajectory. Trajectories of hydraulic fractures were included in the models through injection well positions perpendicular to the minimum principal stresses.

¹

Using the 70 kg/s injection rate for stimulation, in most studies, the production rate was approximately 52.5 kg/s, although some studies with higher rates were carried out

The model does not allow for fracture initiation or propagation from tips of pre-existing natural fractures.

20 Performance indices

The hydro-mechanical study developed several indices for measuring the effectiveness of the stimulation in creating an EGS reservoir. These indices included:

- Pressure at the injection well
- The affected surface area of the DFN, which is the total surface area of fractures which experience pressure increase due to injection greater than a specified threshold value (i.e., pressure increase relative to the in-situ values due to fluid injection and pressure dissipation into the reservoir)
- The shear-stimulated surface area of the DFN, which is the total area of fractures that experience more than 0.5 mm slip; and
- The average DFN aperture, which is the volume of fluid injected into the DFN divided by the affected surface area.

20.1 Results of the Two-Dimensional Model

21 Effect of connectivity

For this study, three DFNs with different densities including those that were below the connectivity threshold were created. All DFNs were created using the maximum fracture length of 100 m and a power law exponent of 2.5; however, for each case, a different value of fracture density was selected, and the size of formed clusters were evaluated. A fully connected DFN with 694 fractures, a partially connected DFN with 650 fractures and a sparsely connected DFN with 504 fractures were created. The sizes of the formed clusters relative to the reservoir model are shown in Figure 19.

The pore pressure and apertures contours at the end of the stimulations for all three cases are shown in Figure 21. The results of the study, including the evolution of the performance indices, are summarized in Figure 22 . Due to its poor connectivity, the sparsely connected DFN builds up sufficient pressure during

injection to propagate a hydraulic fracture, which is the east-west fracture in Figure 21.

The affected surface area is relatively small mainly due to the small number of fractures that are connected to the injection well even with the propagation of the hydraulic fracture. However, in this case, nearly all the affected surface area is also shear-stimulated surface area. In the other extreme, the fully connected fracture network has the largest affected surface area; however, the fracture area that undergoes shear stimulation is relatively small because the pressure increases are relatively small due to the relatively large permeability of the DFN. In terms of the creation of shear-stimulated surface area, the partially connected DFN shows the best performance. This case appears to be an optimum between relatively large area of the fracture network connected to the injection well and sufficient pressure increase to cause its shear stimulation.

22 Effect of fracture size distribution

The fracture size distribution is an important parameter of DFN geometry. It strongly affects network connectivity and percolation. However, it is difficult to determine the fracture size distribution in the field, especially at depths of geothermal reservoirs accessed with limited number of boreholes. While it is unlikely that a candidate EGS reservoir will have a known fracture size distribution, it is nonetheless useful to investigate the effect of this parameter on EGS performance.

The fracture size study used three realizations:

- Realization I, power law exponent, $\alpha=2.0$, maximum length, $l_{\max}=250$ m,
- Realization II, power law exponent, $\alpha=2.5$, maximum length, $l_{\max}=10,000$ m, and
- Realization III, power law exponent, $\alpha=3.0$, maximum length, $l_{\max}=10,000$ m.

All realizations use the minimum fracture length of $l_{\min}=15$ m. Plan views of the three realizations with fracture apertures and slip at the end of stimulation are shown in Figure 23. In Realization I, the maximum fracture length of 250 m and low value of exponent result in a fracture distribution that is relatively uniform compared to the other two realizations. In this realization, the maximum fracture size is one fourth of

the reservoir size in the model, which ensures that no single fracture controls connectivity at the scale of the entire reservoir. On the other hand, in Realizations II and III, there are single fractures transecting the entire model domain.

The summary of the results for the three realizations, including the performance indices, are shown in Figure 24. Although smaller α values generically indicate a higher proportion of longer fractures, the use of the maximum fracture length of 250 m in Realization I means that this realization does not include long fractures relative to the reservoir size. Comparing the three realizations, the long fractures intersecting the entire reservoir are most likely in Realization II and impossible in Realization I.

This ranking controls the results. The affected area is largest for Realization II, with the longest fractures, and smallest for Realization I, with the shortest fractures. On the other hand, because long fractures lead to localization of flow and deformation, the shear-stimulated area is largest for Realization I and smallest for Realization II.

This behavior reflects the higher connectivity of the networks with longer fractures and tendency of longer fractures to localize flow and deformation. The longer fractures dissipate pressure further from the injection well and hence the affected area is greater. On the other hand, localization of flow and deformation in long fractures prevents stimulation and hydro-shearing in the rest of the fracture network.

23 Effect of dilation angle

The fracture dilatancy, which is responsible for permanent (irreversible) fracture opening under shearing, is caused by roughness of the fracture surfaces (Figure 18). Typically, it is characterized by dilation angle (also known as roughness angle). Dilatational opening of pre-existing fractures is the main mechanism of hydro-shearing. However, it is not clear how the dilation angle affects overall reservoir stimulation. A larger dilation angle means a greater increase in fracture aperture during shear and a greater increase in permeability. At the same time, dilation of fractures and resulting volumetric strain will result in increase in the mean stress that will suppress further fracture slip. Also, the dilation angle of fractures in EGS reservoirs cannot be easily characterized.

The base case for the dilation angle study is Realization I of the fracture size study (power law exponent $\alpha=2.0$, maximum length $l_{max}=250\text{m}$). Stimulations were conducted for three dilation angles, 3° , 7.5° , and 15° . Figure 25 and Figure 26 show a clear increase in aperture of stimulated fractures with increase in the dilation angle. In Figure 26, the average DFN aperture is calculated over the affected area of the DFN (i.e., part of the DFN that experiences pressure increase). On the other hand, an increase in the dilation angle results in greater volumetric strain and mean stress that reduce potential for fracture slip. Therefore, the shear-simulated area (Figure 26) is greater for smaller dilation angles.

Some fracture dilatancy is necessary for hydro-shearing as a mechanism of the reservoir stimulation. Increase in the dilation angle results in increase in the maximum slip-induced fracture aperture (i.e., permeability increase), but decrease in the shear-stimulated surface area.

24 Effect of orientation of in situ stresses

In all the simulations presented in Section 3, the fracture network consisted of two sets of parallel fractures (i.e., there is no variability in fracture orientation within each set). Both are favorably oriented with respect to the in-situ stresses for hydro-shearing. This promotes a relatively isotropic fluid dissipation and growth of the stimulated volume. Isotropic growth of stimulated region means that the increase in transmissivity remains similar in the direction of both fracture sets, and a network of well-connected stimulated fractures will continue to exist upon pressure decrease. This study focuses on the effect of having significantly different conditions for slip (e.g., due to different orientations relative to the directions of the principal stresses).

In one model, the orientation of the secondary set with respect to the principal stresses is adjusted so that it is unfavorable for slip. Both realizations have the primary set striking at 160° clockwise (-20° counterclockwise) to σ_{HMAX} . In Realization I, the second set is at 45° ; in Realization II, the second set is at 60° , which is unfavorable to shearing (Figure 27).

Plots of aperture and slip of the fractures (Figure 27) show clearly that both fracture sets are mobilized in Realization I and only one fracture set is mobilized in Realization II.

The summary of the results in terms of performance indices is shown in Figure 28. The greater shear stimulated area for Realization I is because both fracture sets are favorably oriented for slip. The affected area (Figure 28) is greater when only one set is mobilized by hydro-shearing (Realization II) mainly because of the lower storage (only one set is hydro-shearing) that causes greater fluid pressure to increase and its dissipation further into the fracture network. As with the other simulations, the affected and shear-simulated areas are inversely correlated, at least at early times.

The results of investigation of the effect of in-situ stress orientation show that hydro-shearing of fractures from multiple sets creates a fracture network with permanently increased permeability that can also provide the surface area for heat exchange in the EGS reservoir. To have favorable stress conditions for hydro-shearing on multiple fracture sets with different orientations, the in-situ stress state should have relatively large deviatoric components; that is, larger differences between the principal stress magnitudes are better. Therefore, from the practical EGS perspective, understanding of the stress state is critical for design of the EGS and prediction of effectiveness of hydro-shearing. As stresses become more isotropic, the potential for hydro-shearing decreases as does the ability to predict the hydraulic fracturing direction (i.e., for isotropic initial stress state, the hydraulic fracture direction may be random or controlled by the rock's anisotropic properties).

Hydro-shearing of multiple fracture sets with a wide range of fracture orientations promotes a more isotropic and connected network of stimulated fractures with increased permeability and facilitates creation of a large accessible fracture surface area. Hydro-shearing of only one set is not desired for reservoir stimulation because permanent increase in permeability will not be uniform, connected, and isotropic, resulting in relatively small rates or uneconomically large injection pressures during production.

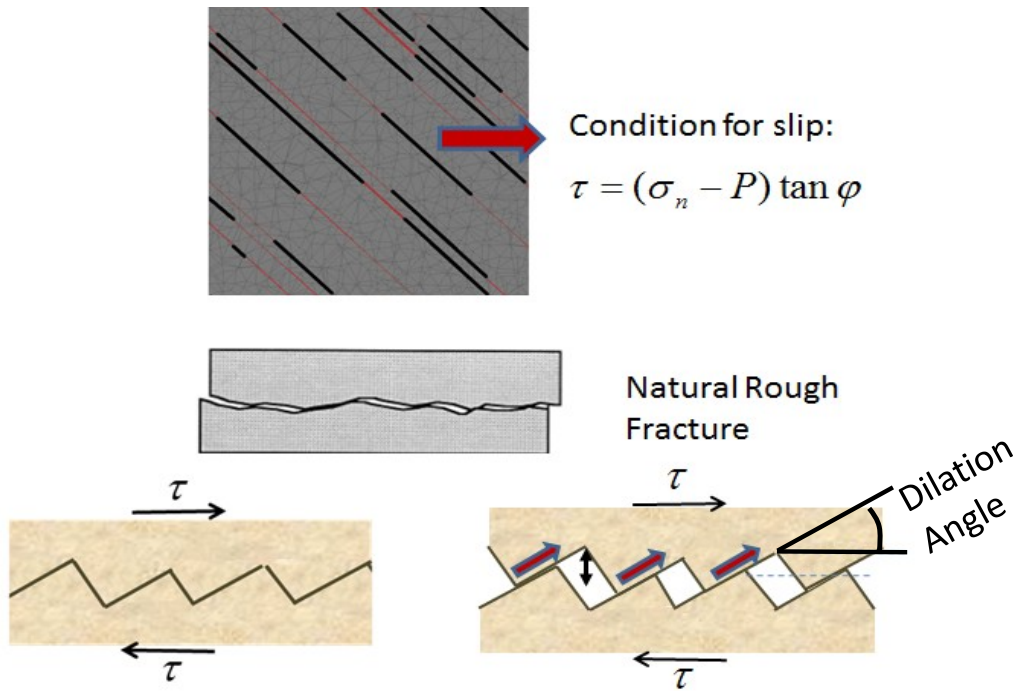


Figure 18. Conceptual model of dilation on fractures as implemented in UDEC.

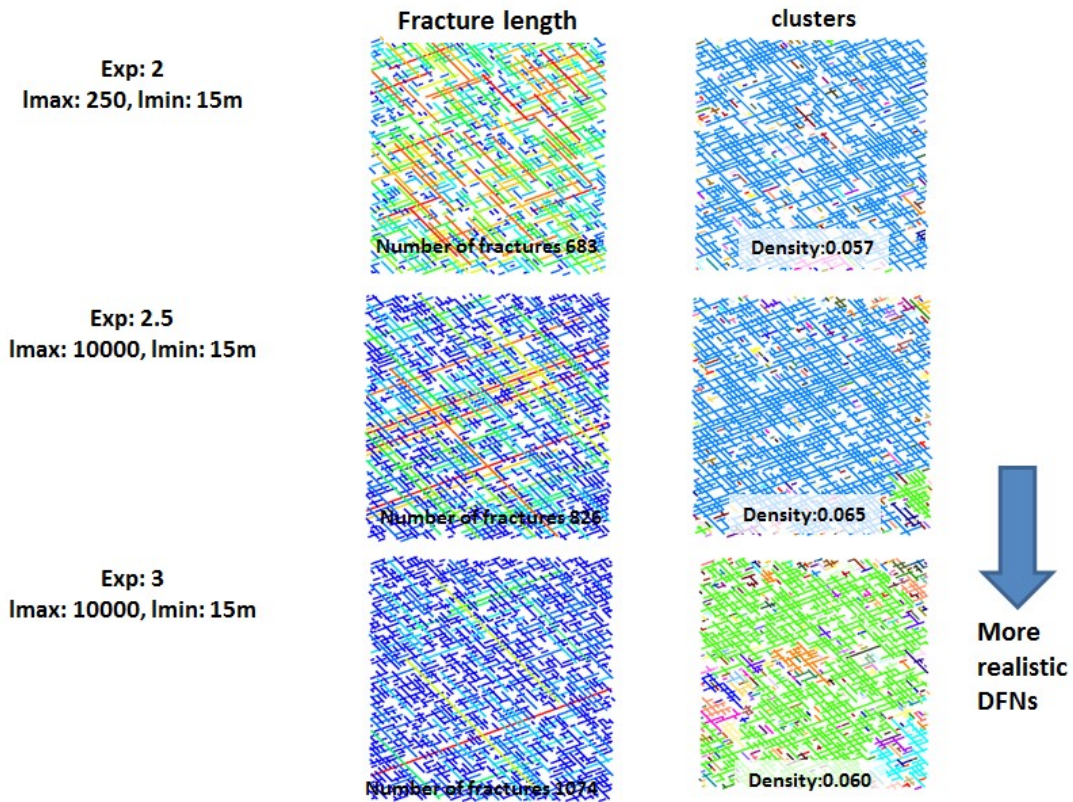


Figure 19. Effect of length exponent on fracture clustering. Left column: fractures colored based on their relative size to reservoir size, red indicates longest fractures in the reservoir while dark blue indicates shortest, right column: cluster geometry, each color within a reservoir indicates a cluster.

The inner domain is filled with a realistic representation of DFN

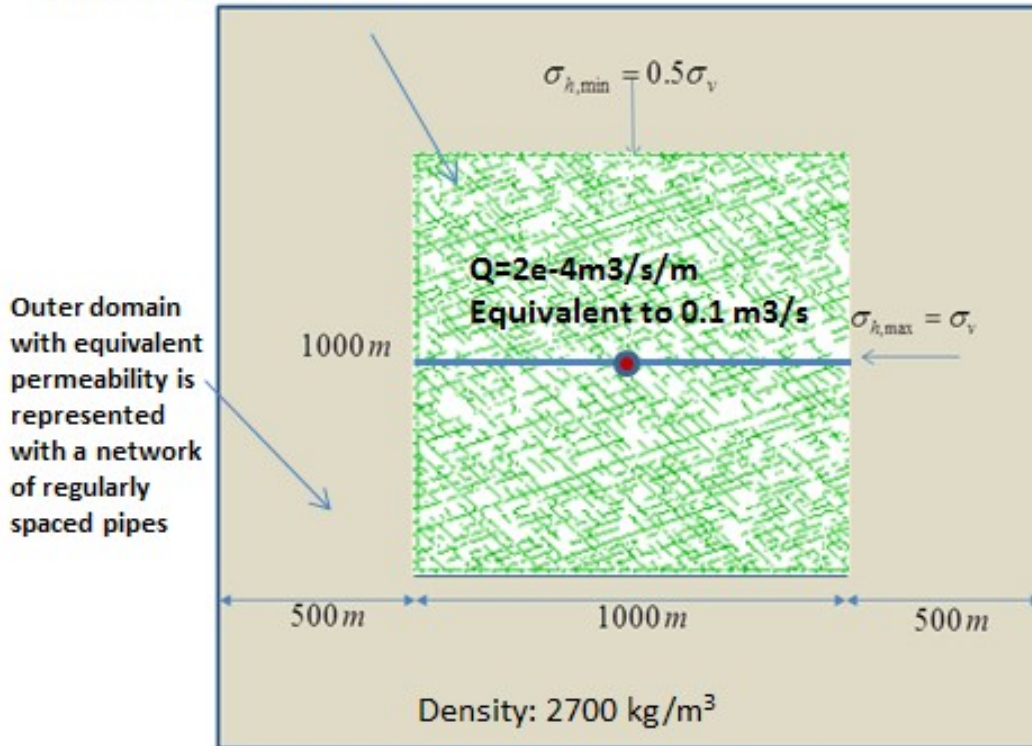


Figure 20. UDEC Model setup, DFN (core) and outer region. Red dot indicates location of injection well, and blue line is the trajectory of the potential hydraulic fracture.

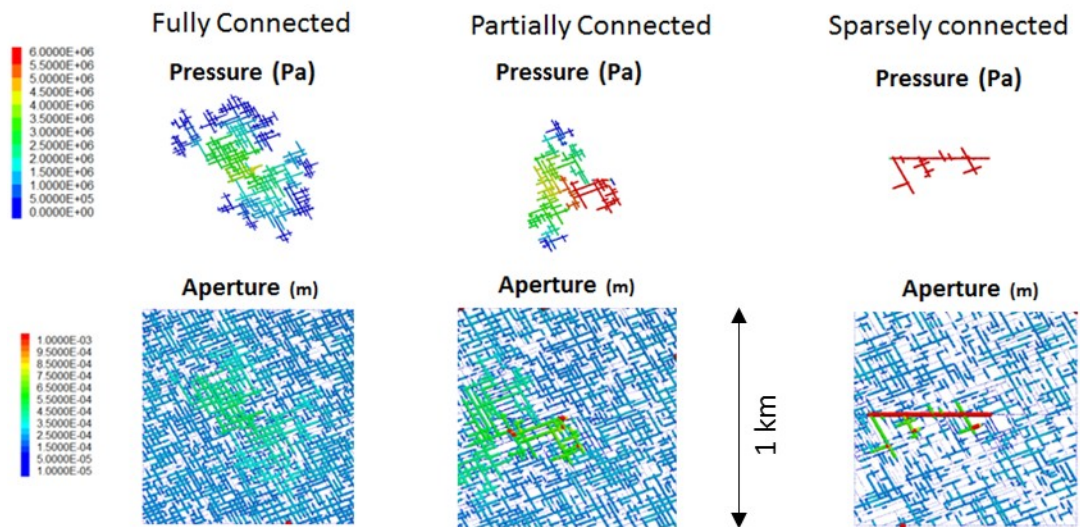


Figure 21. (a) Fracture networks for connectivity sensitivity, (b) contours of aperture increase.

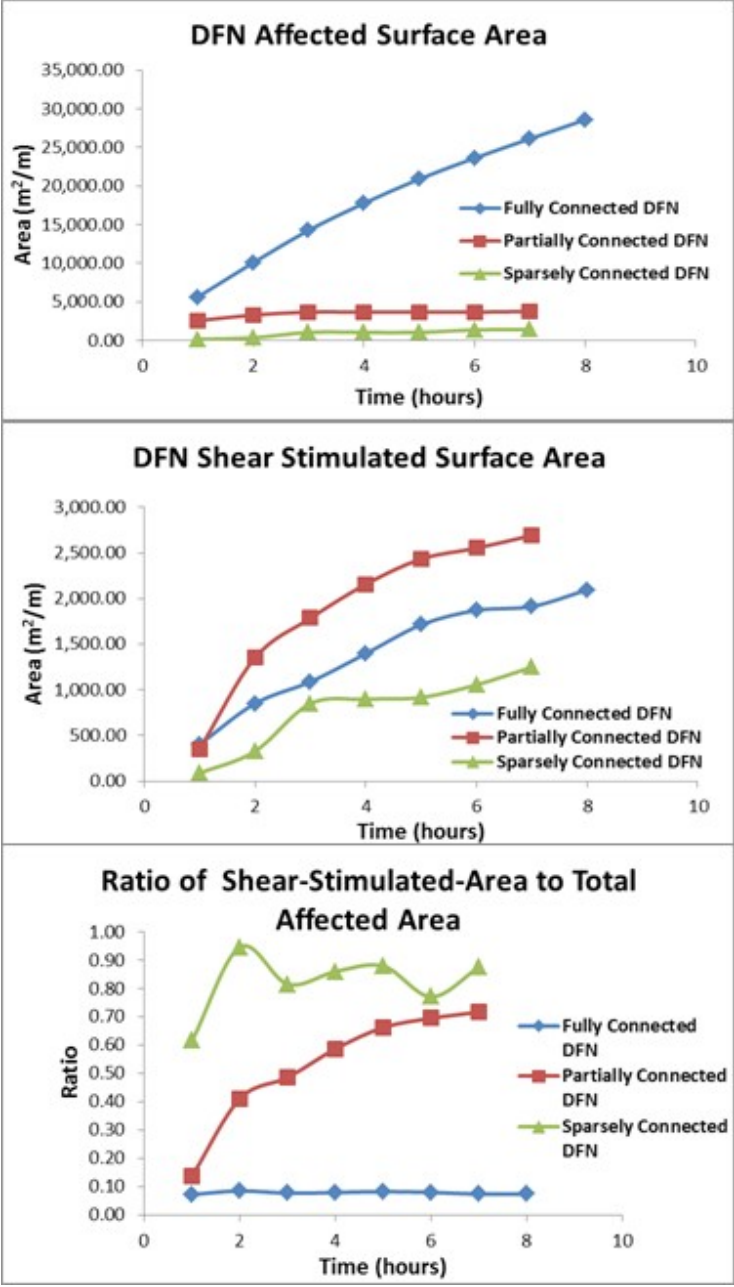


Figure 22. Performance indices for connectivity study

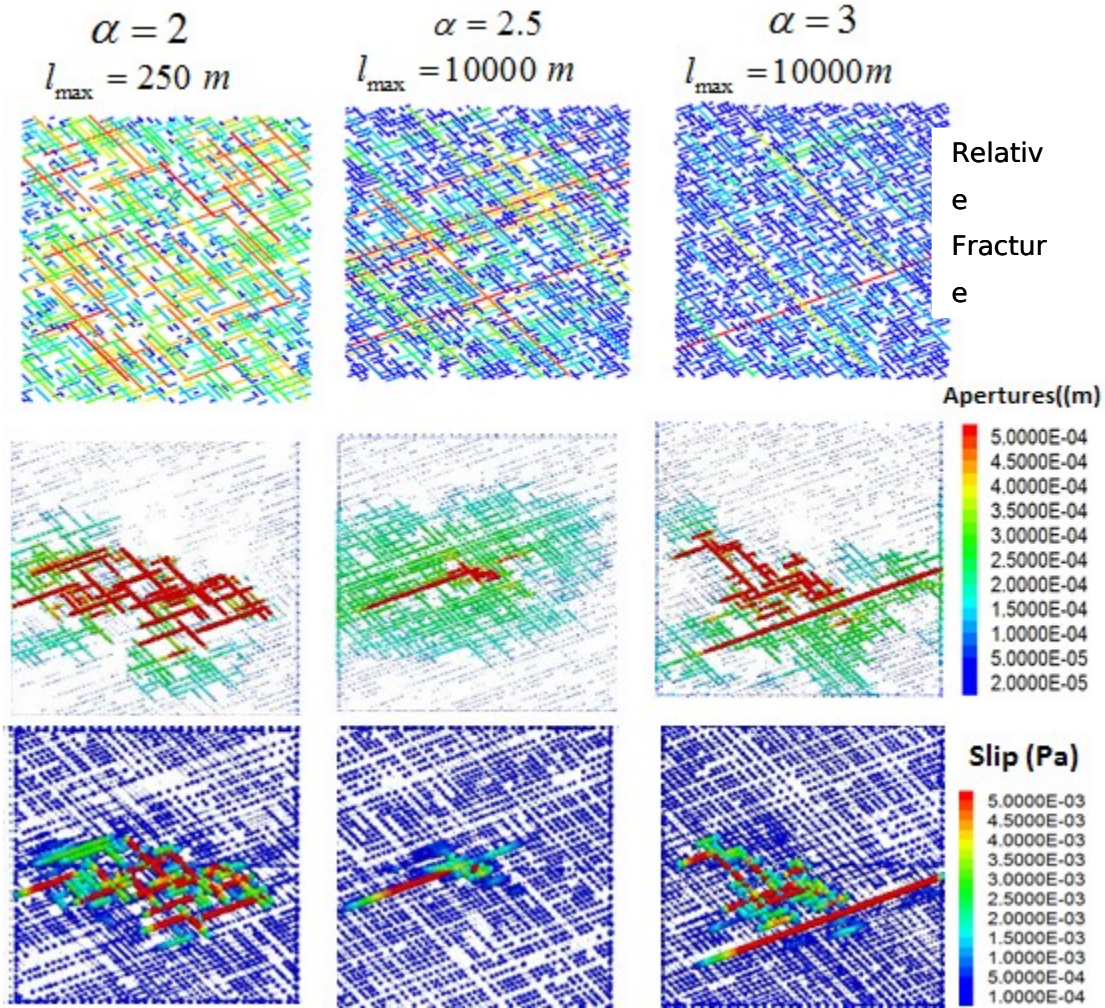


Figure 23. Fracture size exponent sensitivity study, fractures colored by their relative length to reservoir size (red indicate the longest while dark blue indicate the shortest) connectivity, fracture apertures, and fracture slip.

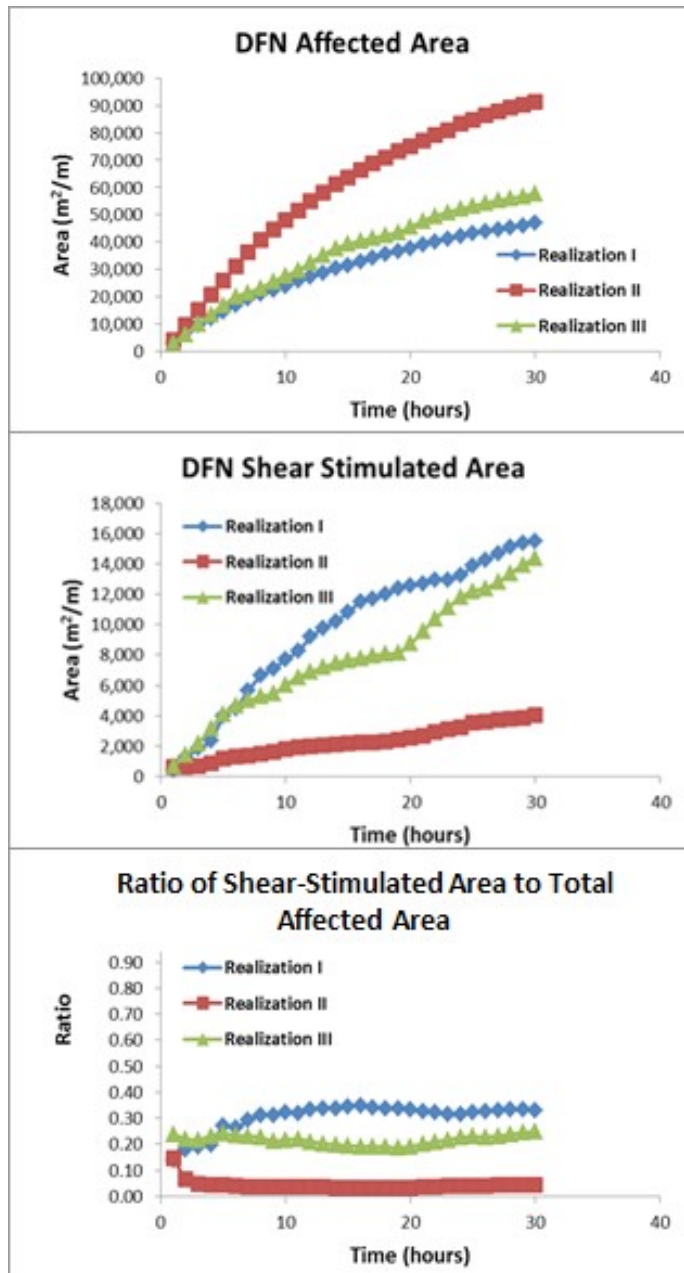


Figure 24. Effect of fracture length exponent on performance indices.

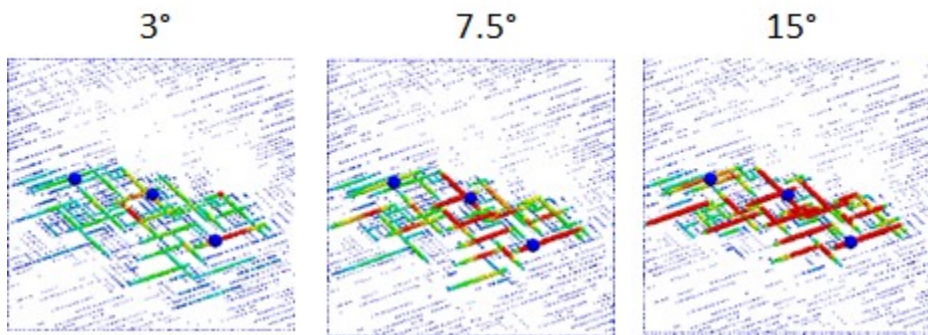


Figure 25. Permanent aperture increases after stimulation (evaluated after pressures are decreased to the in-situ value) with dilation angle

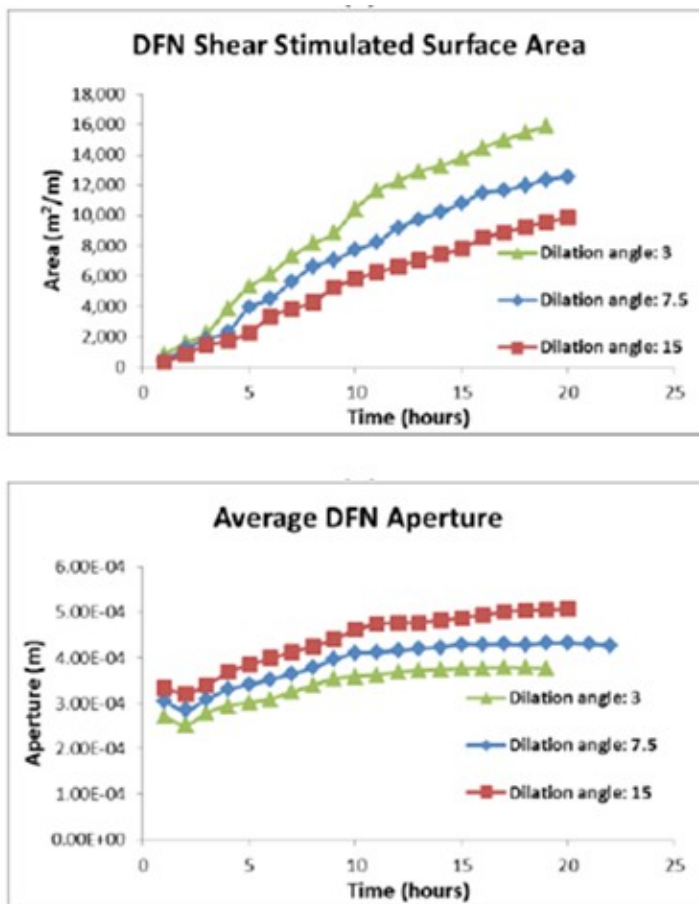


Figure 26. Effect of dilation angle on shear stimulated area and aperture.

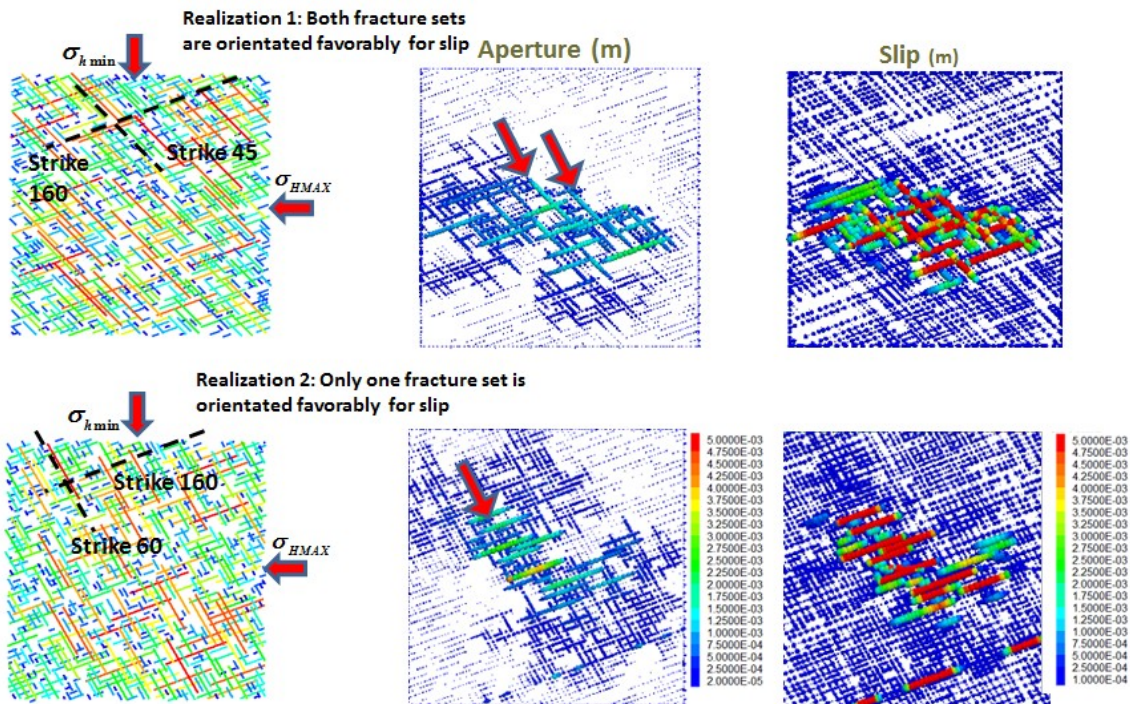


Figure 27. Effect of fracture set orientation relative to in situ stresses. (Left: fractures colored based on their relative length to reservoir size). Strike is relative to σ_{HMAX} , middle. Aperture contours, right: slip on fractures.

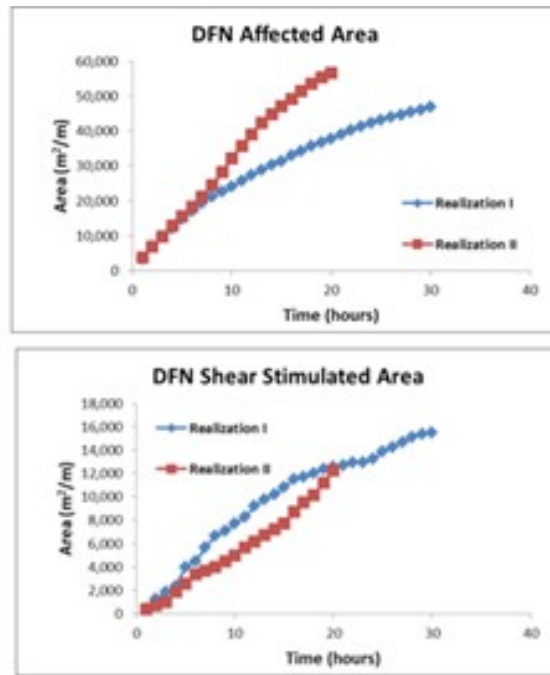


Figure 28. DFN affected and DFN shear-stimulated area for stress case.

24.1 Three-Dimensional Hydro-Mechanical Simulations

25 Three-dimensional DFN representation

The general trends observed from the results of two-dimensional investigation of reservoir stimulation presented in Section 3.3.3 are an estimate based on a 2D representation of the DFN. A three-dimensional geometry of the DFN is critical for better understanding hydro-mechanical behavior in a practical EGS reservoir. Therefore, Itasca performed three-dimensional hydro-mechanical simulations using their *3DEC* distinct element code to investigate some of the observed trends in 3D. *3DEC* accommodates a stochastic DFN model. It allows fracture propagation along pre-defined bonded contacts between blocks in the model. The model setup did not consider extension of pre-existing fractures but did include the possibility of propagating a hydraulic fracture. A hydraulic fracture plane was included in the model in a bonded state, allowing it to open only if the tensile strength at the fracture tip was exceeded.

As an extension of the two-dimensional model, the DFN in 3D occupies a region that is a 1 km square in plan view with a 350 m thickness. The DFN is embedded in a 2 km x 2 km x 2 km model domain. Stress conditions are the same as in the two-dimensional simulations, and the failure criterion is a Coulomb slip law with zero cohesion, a friction angle of 30° and a dilation angle of 7.5°.

The DFN models used two fracture sets with dip directions of 45° and 135° and constant dip angle of 75°. The stress conditions are identical to that of 2D model. The maximum horizontal stress is equal to the vertical stress (weight of the overburden) and the minimum principal stress is half of the vertical stress. The fracture sets orientations relative to the principal stress directions are selected to make them likely to slip at the injection pressures that are smaller than the hydraulic fracturing pressures (i.e., typically few mega pascals just greater than the minimum principal stress).

Fracture size distributions were generated for three cases

- Power law exponent, $\alpha=3.0$, maximum length, $l_{\max}=250\text{m}$,
- Power law exponent, $\alpha=3.5$, maximum length, $l_{\max}=10,000\text{m}$, and

- Power law exponent, $\alpha=4.0$, maximum length, $l_{\max}=10,000\text{m}$.

As in the 2D case (Section 3.4.2), the case with the smallest power law exponent uses a small maximum fracture length and, therefore, has the smallest fracture size variability of the three cases, which is contrary to the trend expected based on the exponent. In all simulations it is ensured that all realizations were fully connected, that is, forming a single cluster within the model domain. The realizations are shown in Figure 29. EGS stimulation for nine hours at an injection rate of $0.07 \text{ m}^3/\text{s}$ was simulated in these 3D models.

26 Injection method

This study investigated if some of the common stimulation practices used in oil and gas reservoirs, such as multi-stage stimulation or different completion designs (e.g., cased with perforation clusters versus openhole), would be beneficial for an EGS. Details and more studies on this work are presented in Riahi et al. (2015). In the multi-stage stimulation, the horizontal segment of the borehole is divided into multiple stages, which are stimulated sequentially. Common practice in the oil and gas industry is to use cased wells and to inject fluid into the reservoir through perforation clusters in the casing. An alternative is the open borehole completion in which fluid is injected in an uncased borehole. The models of injection through perforation clusters and open borehole segments are illustrated in . Simulations were conducted for three different DFN models, two injection rates, two completion design (open borehole and cased) and two stimulation staging designs: single-stage with nine perforation clusters, and three stages (multi-stage) with three perforation clusters.

27 Multi- versus single stage stimulation

The effect of staged stimulation on the stimulated volume is shown in Figure 31 for the injection rate of a $0.07 \text{ m}^3/\text{s}$ and the power law exponent of 3.5. In the multi-stage stimulation, each segment is isolated, and the injection rate is applied for one third of the total time assuming there are three segments. The injected volumes for multi-stage and single stage models are equal. Other rates and DFNs for different power law exponents give similar results that show a clear advantage of multi-stage stimulation over single-stage stimulation for both cased borehole and open borehole completion in creating shear-stimulated surface area (Riahi et al., 2015). Sequential

injection into isolated stages along the borehole results in a more uniform distribution of flow and stimulation of the reservoir. With the multi-stage stimulation, chances of localization of injected fluid into a few of the fractures is reduced (Figure 32). Therefore, it is expected that even under conditions of equal injection rate, and equal pressure, the stimulated volume would be greater if the multi-stage stimulation is used.

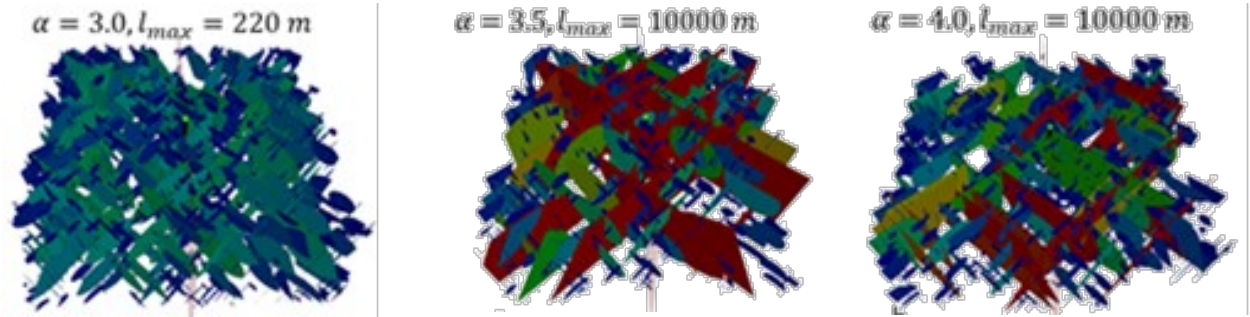


Figure 29. Three-dimensional DFNs for study

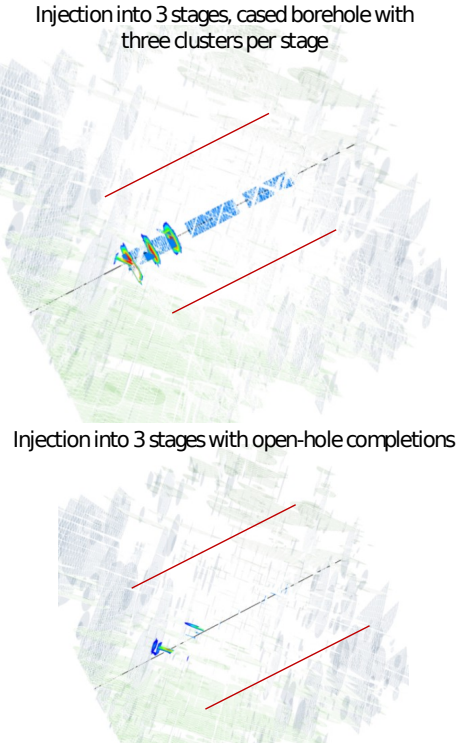


Figure 30. Multistage stimulations with horizontal borehole. Top row is multistage with cased borehole, bottom row is multi stage in an open borehole completion. Circles indicate the three stages, red lines are potential location of production well

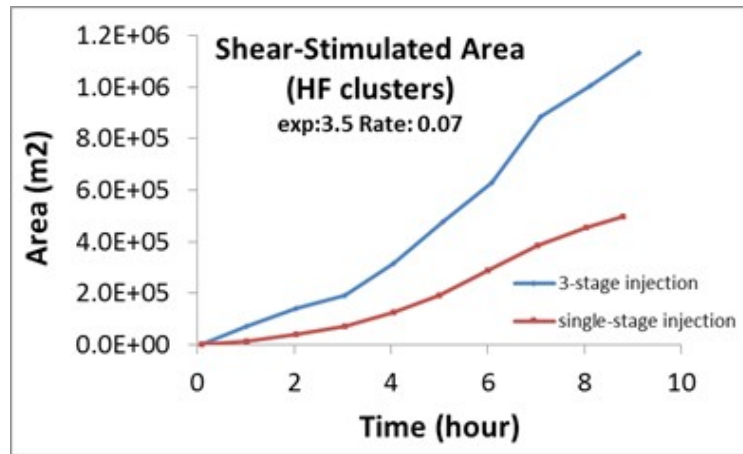


Figure 31. Shear stimulated area for multistage versus single stage stimulation, injection rate of 70 kg/s.

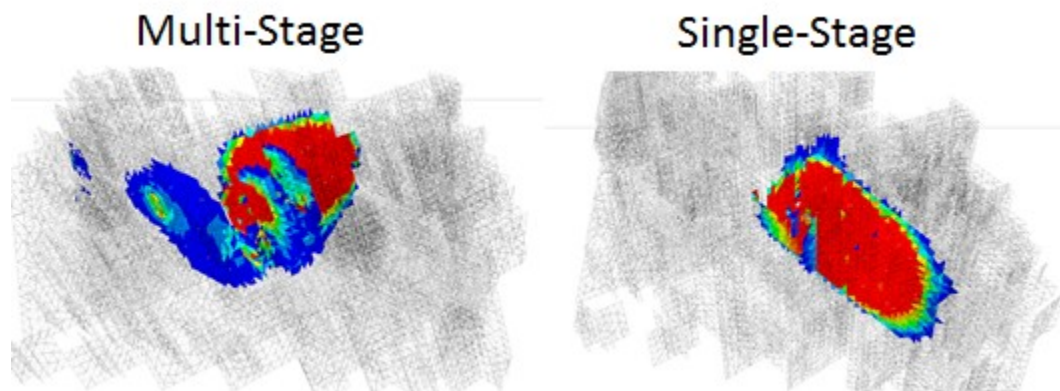


Figure 32. Visualization of multi-stage versus single stage stimulation

28 Cased borehole versus open borehole completion

The effectiveness of injection into a cased borehole with a series of clusters is compared to injection through an open-hole completion. When the borehole completion is open borehole, injection into the rock mass occurs mainly through the

intersections of the borehole with the pre-existing natural fractures. When the borehole is cased, injection occurs through the HF planes initiated from the clusters. For the purpose of these simulations, HF planes are assumed to be perpendicular to the borehole and equally spaced along the borehole. Figure 33 shows that the case borehole resulted in a higher shear stimulated area. This indicates that the opening of a hydraulic fracture can provide better connectivity to the reservoir. However, as shown in Figure 34 cased borehole results in lower injectivity because higher pressures are required to keep the hydraulic fracture open during the production phase.

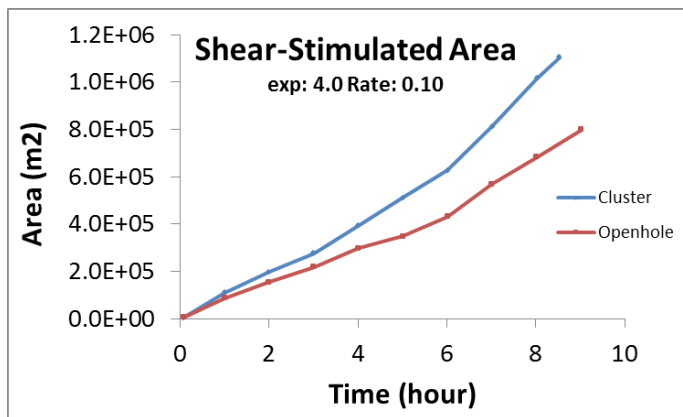


Figure 33. Comparison of shear stimulated area for cased well completion vs. open borehole completion

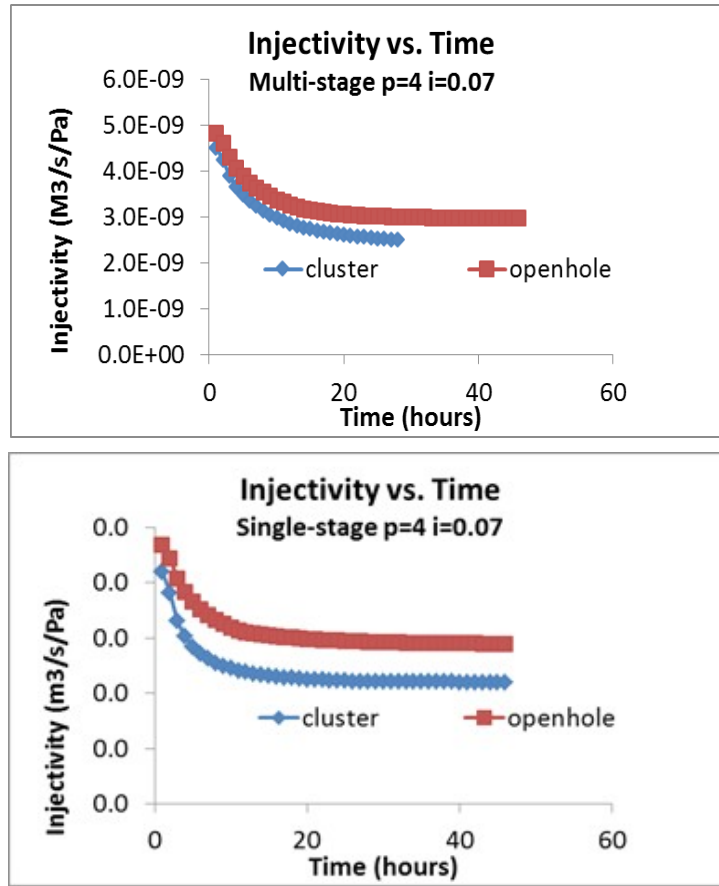


Figure 34. Comparison of infectivity during production for cases with cased borehole and open borehole completion, Left column: multi-stage stimulation, right column single stage

29 2-Dimensional Studies With Vertical Wells Using Coupled Hydro-Thermal-Mechanical Models (Itasca)

29.1 Objective

In Chapter 3, the shear-stimulated area calculated from the results of the coupled hydro-mechanically simulations was used as an evaluation index of the EGS stimulation effectiveness. This chapter extends the simulations to a fully coupled Thermo-Hydro-Mechanical (THM) model, which simulates EGS performance directly by calculation of the produced temperature, production rate, and power with time.

The numerical models include modeling of the heat transfer processes with full thermo-hydro-mechanical coupling during the production phase. Different scenarios were simulated using the fully coupled THM model. The EGS performance over a time scale of years was evaluated by comparing histories of produced temperature and power. The simulations presented here were performed by Itasca using their expanded UDEC code.

29.2 Thermomechanical behavior of fracture networks using UDEC

30 *UDEC thermal verification*

The first task was validation of the hydrothermal solution implemented in UDEC. The validation used a single fracture in an effectively infinite medium with the numerical results compared to the Gringarten solution shown in Figure 35 using properties given in Table 4. The numerical approach and verification examples are discussed by Riahi et al. (2014a,b,c).

31 *Model description*

The thermo-hydro-mechanical simulations were carried out in 2D for a 4 km square geothermal reservoir at a depth of 2500 m with a thickness of 350 m. The conditions are the same as for the base model described in Section 3.3.3. The

reservoir has an initial temperature of 200° C and the injected water temperature is at 25° C. The thermal properties of the rock are given in Table 5.

The simulations have two stages, the stimulation phase of 120 hours and the production phase of variable duration (in the range of months to years). As stated before, the injection rate during stimulation is 70 kg/s. Unless stated otherwise, the injection rate during production is 52 kg/s. All simulations were carried out with Itasca's distinct element code, UDEC (Itasca, 2011).

32 Effects of well positioning and spacing

Site characterization of an EGS reservoir will likely be able to identify the orientations and relative permeabilities of the fracture sets. Assuming a dipole configuration (i.e., one injection and one production well), this study investigates the effect of alignment of the production and injection wells with respect to the fracture sets that have different permeabilities. It is assumed that conditions are constant throughout 350 m of the reservoir thickness in the 2D model in which the vertical wells are represented as points.

The sensitivity study considered the following parameters

- Well alignment relative to the fracture sets
 - Case I: Aligned with the orientation of the primary fracture set
 - Case II: Aligned with the orientation of the secondary fracture set and perpendicular to the primary fracture set; and
 - Case III: Aligned in an orientation intermediate to the two sets
- Spacing of the wells: 250 m, 500 m, 800 m.

32.1.1.1 Well positioning relative to fracture set orientation

The temperature contours in the reservoir after 32 months of production (Figure 36) clearly show the difference in flow paths between the cases of the wells aligned in the primary fracture set direction (Case I) and in the secondary fracture set direction (Case II) and along the intermediate direction (Case III). Figure 36 does not include the results of models with 800 m wells spacing for Cases I and II, as in these simulations the production wells did not produce fluid. It can be seen for Case I that

at 800 m distance between the wells, the alignment of the wells with the primary set locates the production well outside the stimulated volume. Consequently, practically no fluid was recovered at the production well.

The temperature histories for three alignment cases, 250 m and 500 m well spacing are shown in Figure 37 and Figure 38, respectively. Alignment in the primary fracture set direction results in relatively short, direct flow paths with fast thermal breakthrough. In contrast, the Case II and Case III simulations produce highly tortuous flow paths with lengths that are considerably longer than the well spacing. For 250 m spacing, Case II has a delayed thermal breakthrough and superior performance compared to Case III. The ordering of Cases II and III reverses for 500 m well spacing. Overall, the results indicate that an offset from the primary fracture set is beneficial for creating more effective heat exchange area. However, the results do not show any trend when comparing cases of alignments between the two fracture sets or on the secondary sets. These results probably exaggerate the effect of well positioning because the DFN is simplified by neglecting variation in fracture orientation within sets.

32.1.1.2 Effects of well spacing

Figure 39 shows thermal breakthrough curves for the Case III simulations for three different well spacings of 250 m, 500 m, and 800 m. As shown in Section 2.2.2, the positive effect of surface area, or in these cases increase in well spacing, on thermal performance is clear from analytical solution for simplified cases. Using time to 10% thermal decline as an indicator, Figure 40 shows that both increased well spacing and increased tortuosity of flow path improve thermal longevity. The importance of these results lies in the fact that they show that (a) design of well positioning coupled with understanding of fracture and stress orientation can help in creating flow tortuosity and improve accessed fracture surface area, (b) DFN response deviates from the predictions based on simplifying assumptions including a model with a single or multiple parallel fracture or a continuum approach with relatively uniform permeabilities. Aligning production and injection wells in the primary set direction (Case I) at the 250 m well spacing, results in a 10% decline in less than one month and extending the well spacing to 500 m only delays the 10% decline to approximately 4 months (Table 6).

33 Effects of thermo-mechanical coupling during production

The effect of thermo-mechanical coupling during the production phase, or the secondary stimulation, is numerically investigated. Thermo-mechanical coupling (i.e., block shrinkage and expansion due to thermal effects) is studied on the time scale relevant to EGS operation and how this can affect heat production.

Figure 37 through Figure 39 compare thermal breakthrough for the models used in the previous sub-section with and without thermo-mechanical coupling. The grey curves are generated from the non-coupled simulations. For most cases, the coupled and non-coupled simulations match relatively well for the early time thermal drawdown and 10% thermal decline. That is because in most cases thermal decline occurs in time scales of less than a year, which is not long enough for propagation of temperature changes far into the rock (because of relatively small thermal diffusivity). As this is the important timeframe for assessing EGS feasibility, these results suggest that non-uncoupled simulations may be sufficient for predicting the EGS performance. A visual comparison of temperature contours after 32 months of production (Figure 41) confirms the similarity of results of the coupled and uncoupled models.

Compared with the smooth thermal decline curves of the uncoupled simulations, the jumps and non-smoothness in the temperature histories of the coupled simulations are associated with secondary stimulation (i.e., the thermal effects on aperture changes). This shows that the coupled thermo-mechanical simulations may have rather complex behaviors, with some cases of thermal recovery during the production. These complex production curves likely reflect pathways that open due to contraction of the rock during the course of production. It is important to realize that the change in the aperture is proportional to the change in temperature of rock, the overall volume of rock where temperature changed and the coefficient of thermal expansion of rock. The secondary stimulation can be important after the temperature changes diffuse far enough into the rock mass, which may take years because of relatively small thermal diffusivity of rocks. On the other hand, fracture hydraulic transmissivity is highly sensitive to fracture aperture and deformation of the rock, as fracture transmissivity is a function of aperture cubed.

Furthermore, cooling-related contraction is a self-reinforcing effect, where localized opening creates more localized cooling, leading to further localized opening.

Opening new pathways exposes additional surface area, which can provide additional thermal input between the injection and production wells. Overall, most of the completed analyses show that this effect of thermal coupling is relatively small. Case II with a 500 m well spacing (Figure 38) is an exception that appears to show a particularly pronounced effect. In this case, the large deviation between coupled and uncoupled behaviors is mainly due to the creation of a hydraulic fracture during the production phase, which added multiple new pathways.

Overall, thermo-mechanical coupling in these simulations appears to have a relatively small and possibly negligible effect on simulated performance. It is important to run the coupled models as a check but, in the interests of running a larger number of cases for sensitivity studies, uncoupled models, which run significantly faster, may be adequate.

34 Effective surface area

From a practical perspective, one of the most critical questions in predicting the EGS performance is estimating the production well fluid temperature over time. Given that the well locations and injection rates are operational parameters, the unknown factor is the volume of rock that injected fluid percolates through during production. Historically, this volume has been estimated using microseismic data obtained during reservoir stimulation, and it was hoped that the entire stimulated (seismically active) volume would be engaged during the production. Today, it is generally accepted that the key factor in evaluating EGS performance is the “effective fracture surface area”. That is the actual area that would act as a heat exchange during the production. The objective of this study is to demonstrate the role that the DFN plays in creating the “effective fracture surface area.”

Comparison of the temperature curve histories from Gringarten analytical solutions with those predicted from DFN models provides a mean to make this assessment. The Gringarten solution with one fracture is equivalent to a case with a single hydraulic fracture or a single conductive fault/fracture between injection and production well. Specifically, one may calculate the effect of surface area from the Gringarten solution and compare that result with the simulation for a complex fracture network. The differences between the Gringarten value for a single fracture surface area and calculated fracture surface area may reflect the presence of

multiple fractures, the tortuosity of the pathway between the injection and production wells, or both.

This study uses the result of well positioning study to investigate effective heat-exchange area. For each well positioning, the well spacing is considered constant and the Gringarten solution curve with one fracture using the given distance is calculated. Using an iterative curve fitting approach, the best match to Gringarten solution for multiple fracture sets is obtained. The Gringarten solution with n number of parallel fractures at distance x was fitted to the produced curve from the DFN model. In one case distance x is assumed to be equal to well spacing and number of fractures, n , is estimated. In another case, n is assumed to be one and the distance is estimated. The solution is not constrained and multiple (n, x) combinations may be found to match the curve equally well.

An example of such a match is shown in Figure 42, which compares the simulation results for Case III with 500 m well spacing with Gringarten's curves. The family of curves represents different values of dimensionless fracture spacing. The simulation matches the Gringarten solution equally well for either a single fracture with a 3000 m length and 350 m height or six fractures that have lengths equal to the nominal spacing between the two wells. Both matches have the same product of length and fracture number and therefore represent the same total fracture area.

Each of the well positioning simulations was matched to Gringarten type curves to do area calculations, and the results are presented in Table 7. Inspection of the results shows that the ratio of the nominal surface area (a single fracture with a length equal to the well spacing) to the apparent surface area is least for the Case I simulations, where the injection and production wells are in alignment with the primary fracture set. In Case I the apparent and nominal surface areas are relatively similar, having ratios of 1 and 2 for the 250-m and 500-m simulations, and thermal decline is rapid. By contrast, the Case II and Case III simulations achieve a higher ratio of effective to nominal surface area, from 3.2 to 6, due to the tortuosity and complexity of the pathways between the wells. This ratio is in direct correlation with EGS performance.

35 Effects of thermal conductivity

A sensitivity study was performed with respect to thermal conductivity and rock density. In one case, the model had a rock density of 2000 kg/m³ and a thermal conductivity of 2.2 W/m°K. In the second case, the rock has a density of 2700 m³/s and thermal conductivity of 4.0 W/m°K. The controlling factor of the rate of thermal diffusion is rock thermal diffusivity, which is provided in Table 8.

A series of simulations for the given pair of density and conductivity and for the six well-positioning cases for well spacing of 250 m and 500 m, were conducted.

The results in terms of production temperature versus time (Figure 43), show a modest improvement in the EGS performance for the higher diffusivity case. The results for all cases are summarized in Table 6. These results show an average of 15% power increase (over 30-year period) for 50% increase in thermal diffusivity.

36 Effects of fracture spacing

The fracture spacing study uses one injection-production well pair with a spacing of 700 m, and it extends the simulation to 20-30 years with no thermo-mechanical coupling.

This fracture-spacing study modifies the base case of the well-positioning study to use a power law exponent for fracture size distribution of two and a maximum fracture length of 300 m. Three values of fracture spacing are considered, 30 m, 50 m and 80 m. The DFN realization for each fracture spacing is created such that the DFN remains fully connected while the value of spacing changes. This is important for comparison, because it ensures that the flow characteristics and overall connectivity in different models remain the same.

The target time for the simulations was a production time of at least 20 years, with a maximum of 30 years. The temperature contours in the rock mass after more than 10 years of production are shown in Figure 44. All the simulations use a production injection rate of 70 kg/s.

The production temperature histories (Figure 45) show that higher fracture densities (smaller spacing) improve the thermal performance of the EGS reservoir. Using the time to 10% thermal decline as a measure, the 30 m fracture spacing (three-year break through) has nearly 4 times the thermal longevity of the 80 m case. It is

noted that even in reservoirs with low in-situ permeability, the logged fracture frequency is often much higher than that used in this study. In this study, the DFN is simplified, and smaller fractures are removed. The shown realizations are equivalent to a network of larger and unsealed fractures in the reservoir, which most probably will control flow.

The results of this study show that for the assumed design (i.e., single injection and production well) the spacing of fracture sets has a strong effect on the reservoir thermal response. The case of 80 m spacing resulted in a single flow pathway with quick thermal draw-down. As the spacing of fractures decrease then a more distributed flow network will form. With flow distributed between multiple fractures, the decline in the temperature curve becomes a function of the average fracture spacing. The models with smaller spacing show better potential of complete depletion of heat closer to the injection point, and the thermal front gradually sweeping the reservoir volume between the injection and production wells. The model with relatively large spacing results in a single flow path, very quick draw down, without that much depletion of thermal energy from the reservoir.

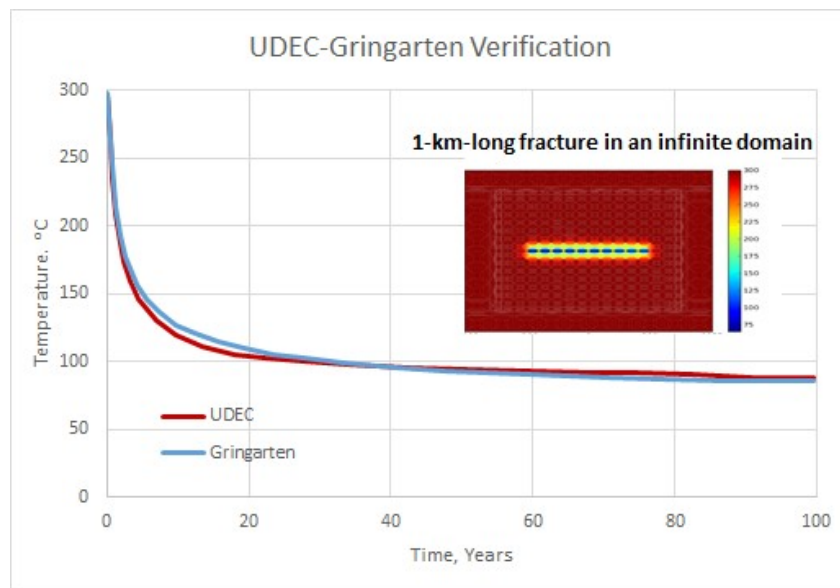


Figure 35. Single-fracture hydro-thermal verification of UDEC with Gringarten et al. (1975) solution. Mismatch due either to meshing coarseness and minor differences in Gringarten and model boundary conditions. Gringarten domain ends at fracture tip, simulation continues 500 m on either side

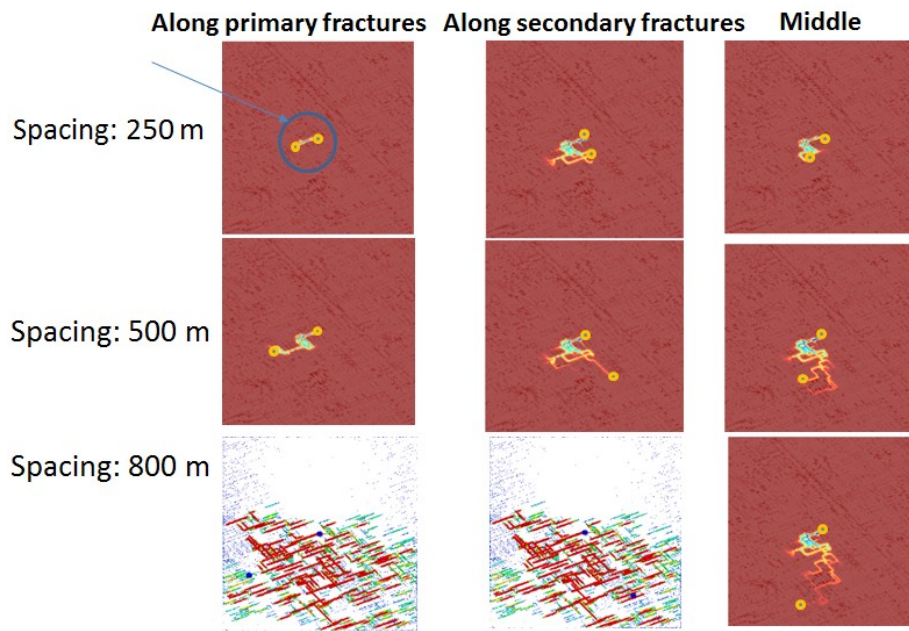


Figure 36. Temperature contours in the reservoir after 32 months of production in the well positioning study. From left to right the columns are Case I, Case II, and Case III. Cases I and II did not have well connectivity for the 800 m well spacing. Circle points out single pathway for short well spacing and orientation along primary fracture set.

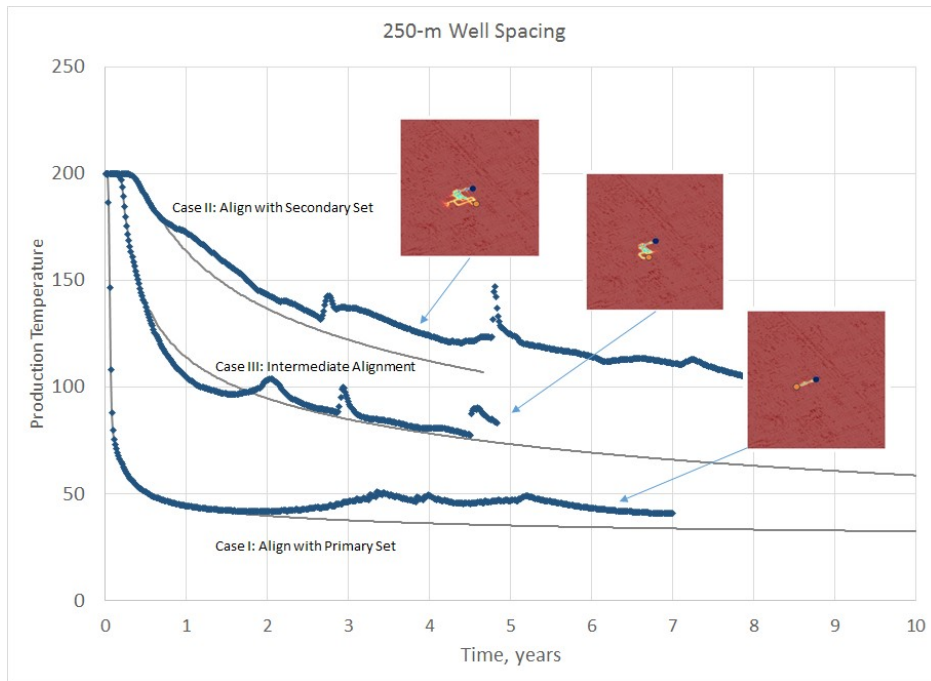


Figure 37. Production temperature, well positioning study, 250 m well spacing (gray lines are without thermomechanical coupling) Case II and III have improved performances due to pathway tortuosity compared with the direct connection along the primary fractures in Case I.

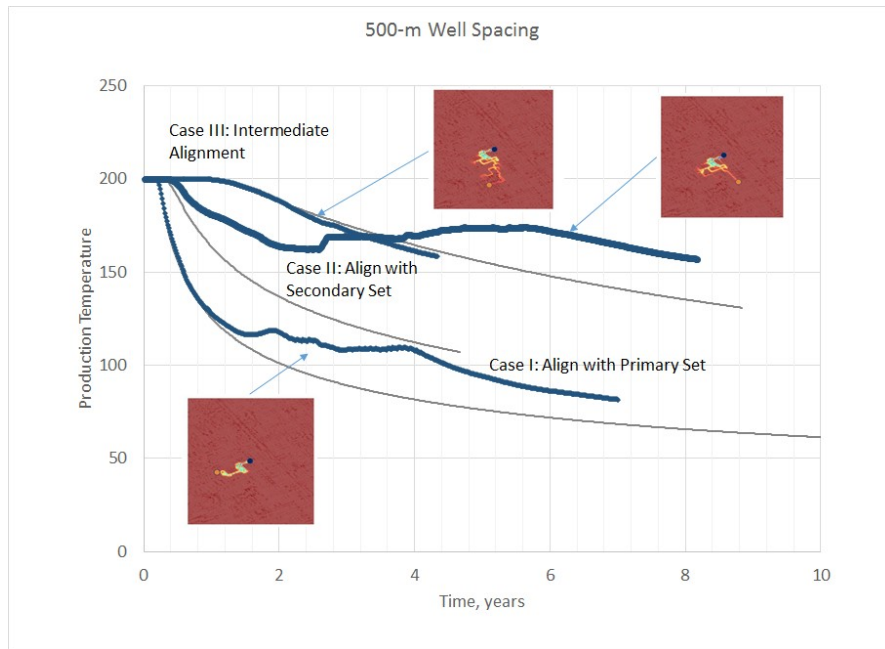


Figure 38. Production temperature, well positioning study, 500 m well spacing (gray lines are without thermomechanical coupling) Case II and III have improved performances due to pathway tortuosity compared with the direct connection along the primary fractures in Case I.

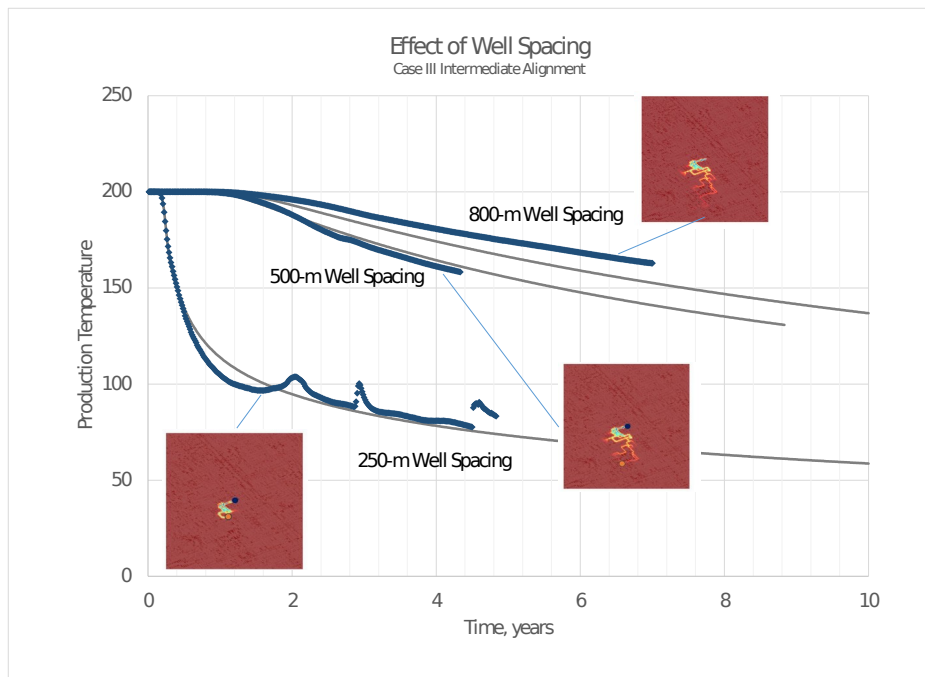


Figure 39. Effect of well spacing on thermal performance. Blue symbols are coupled thermal-mechanical model results. Gray lines are without thermomechanical coupling. Increased well spacing has better performance due to added surface area to the heat exchange.

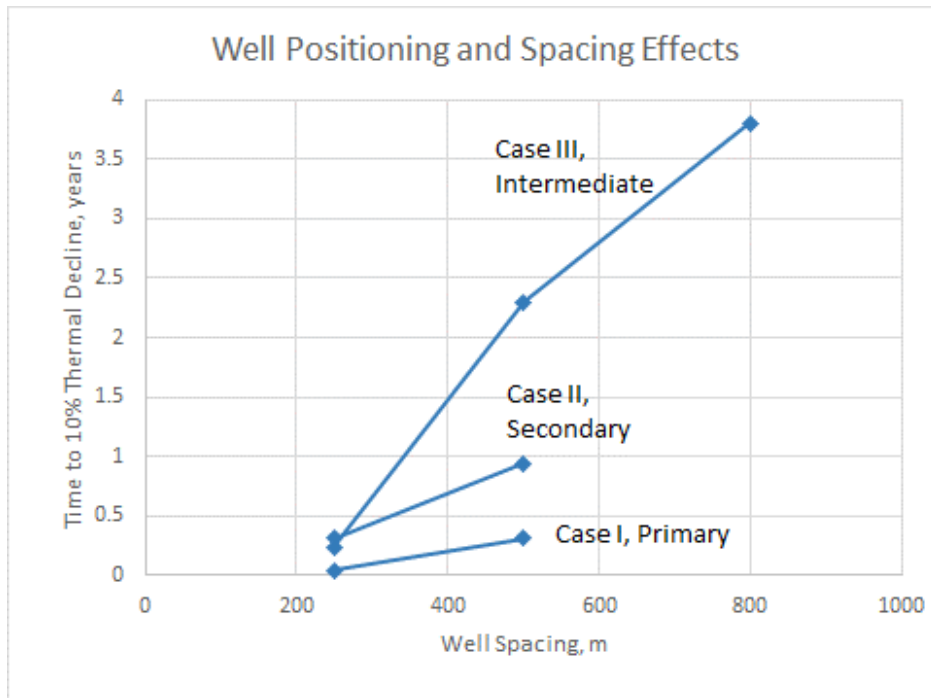


Figure 40. Time to 10% thermal decline by well position and spacing. Case II and III have improved performances due to pathway tortuosity compared with the direct connection along the primary fractures in Case I.

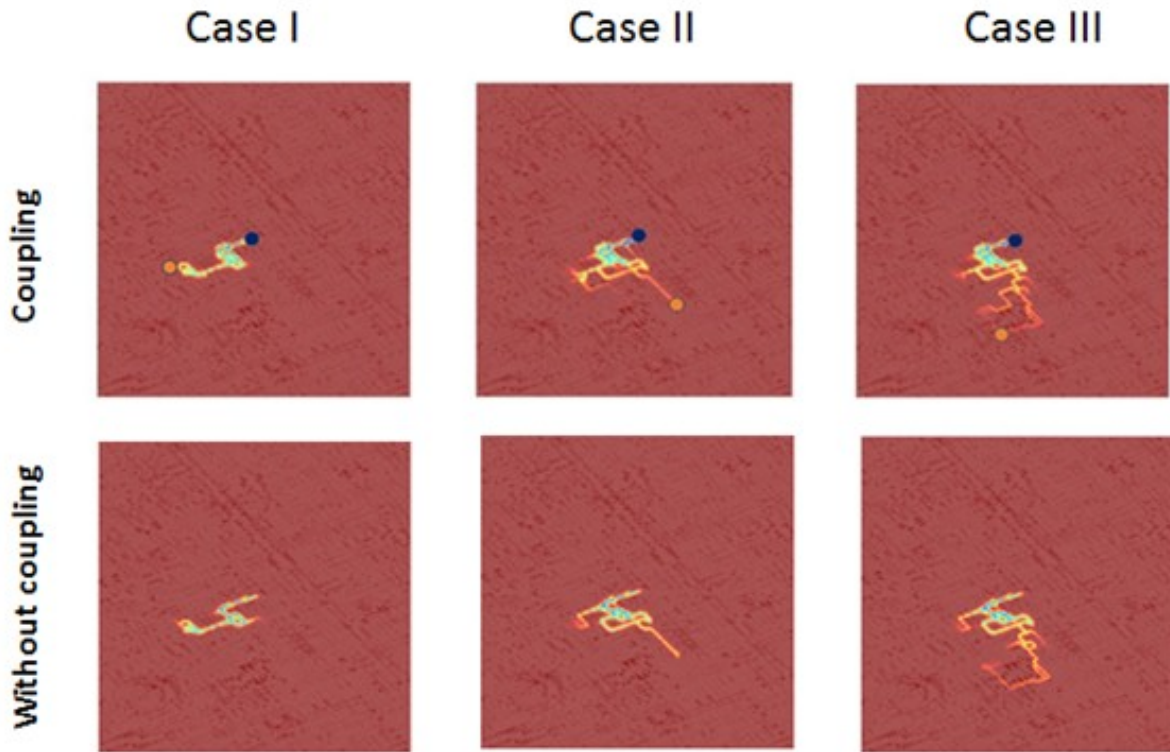


Figure 41. Comparison of thermal behavior with and without thermomechanical coupling (500 m well spacing). Coupling does not significantly affect the pathways or pattern of thermal drawdown. Comparisons of thermal performance appear in Figure 37 to Figure 39.

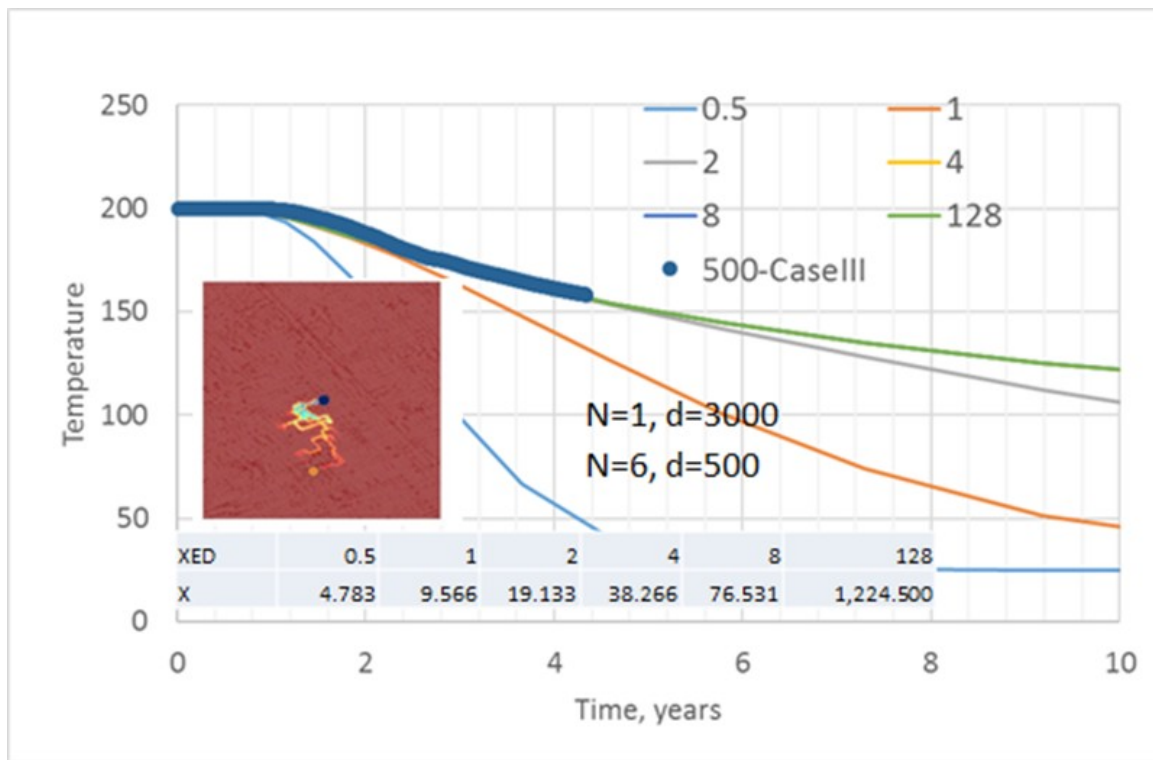


Figure 42. Match of simulation for Case III, well spacing = 500m for Gringarten et al. (1975) analytical solution. Curves are for various values of dimensionless fracture spacing, X_{eD} and inset table shows correspondence to spacing, X_e , in meters. The simulation is for a complex fracture network. The thermal behavior suggests a total interchange area of $1.05E6 \text{ m}^2$ (Area times number of fractures times 350m height). If the length is the well spacing ($d=500$), there are effectively $n=6$ fractures. If there is a single, highly tortuous, fracture, it has an effective length of 3000 m.

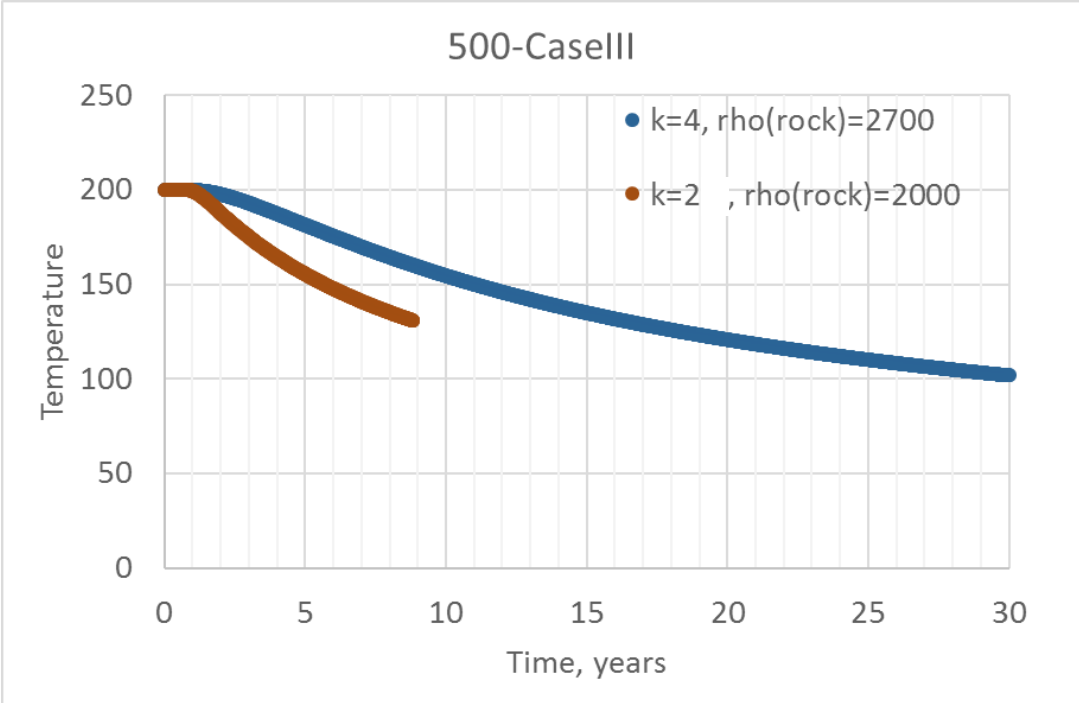
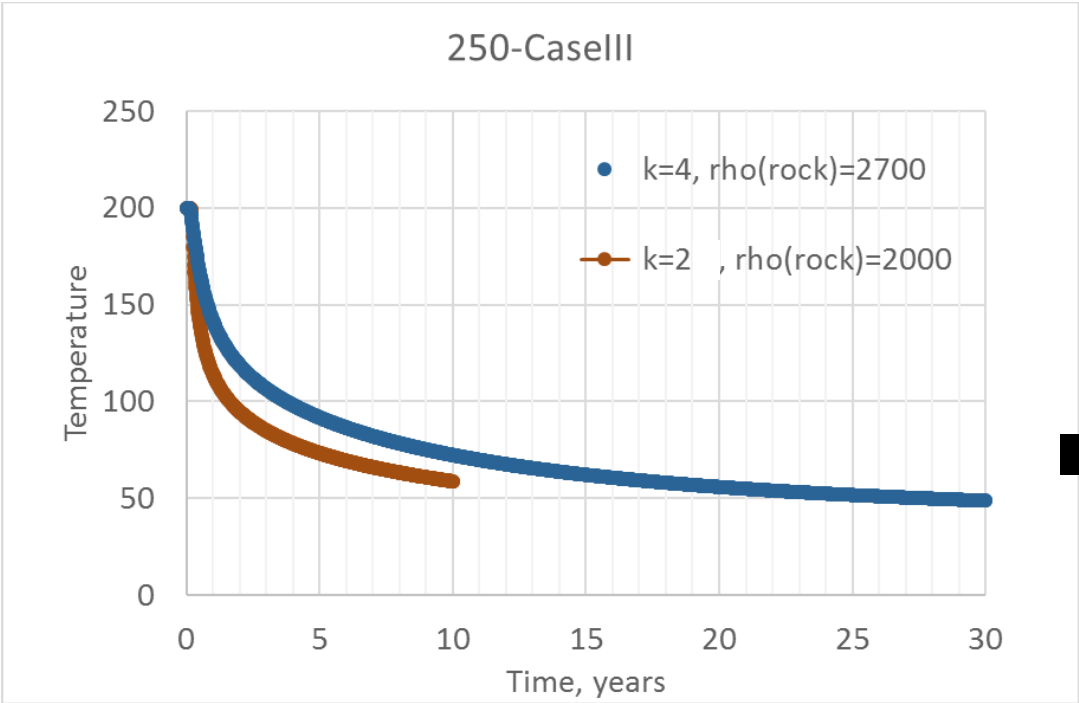


Figure 43. Sensitivity study to thermal conductivity and rock density for Case III, wells positioned intermediate to the direction of the two fracture sets. Increased density and thermal conductivity improve thermal performance.

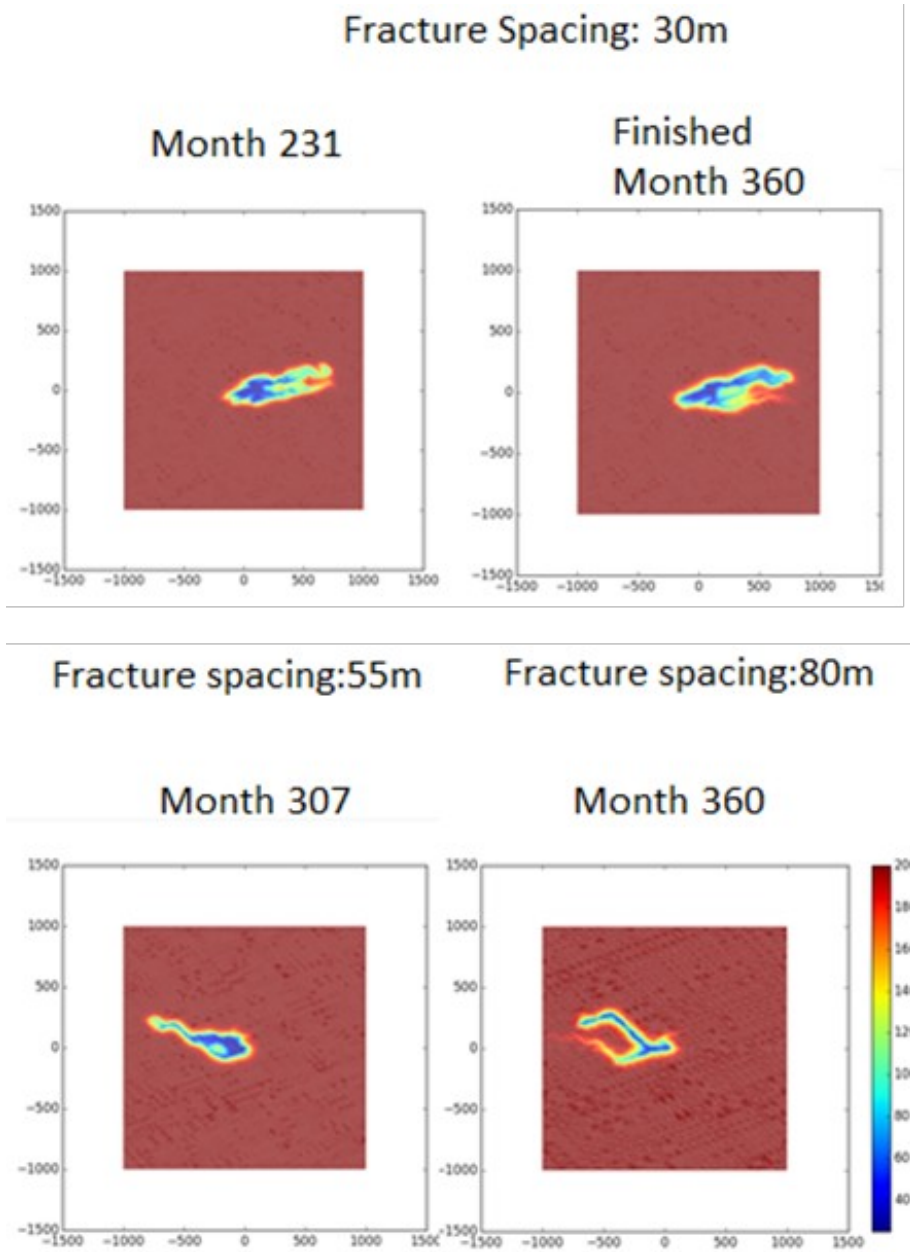


Figure 44. Visualization of thermal drawdown for fracture spacing study. Smaller spacing provides more conducting pathways between the wells. With increasing spacing the stimulated volume evolves towards pathways along individual fractures rather than through a network.

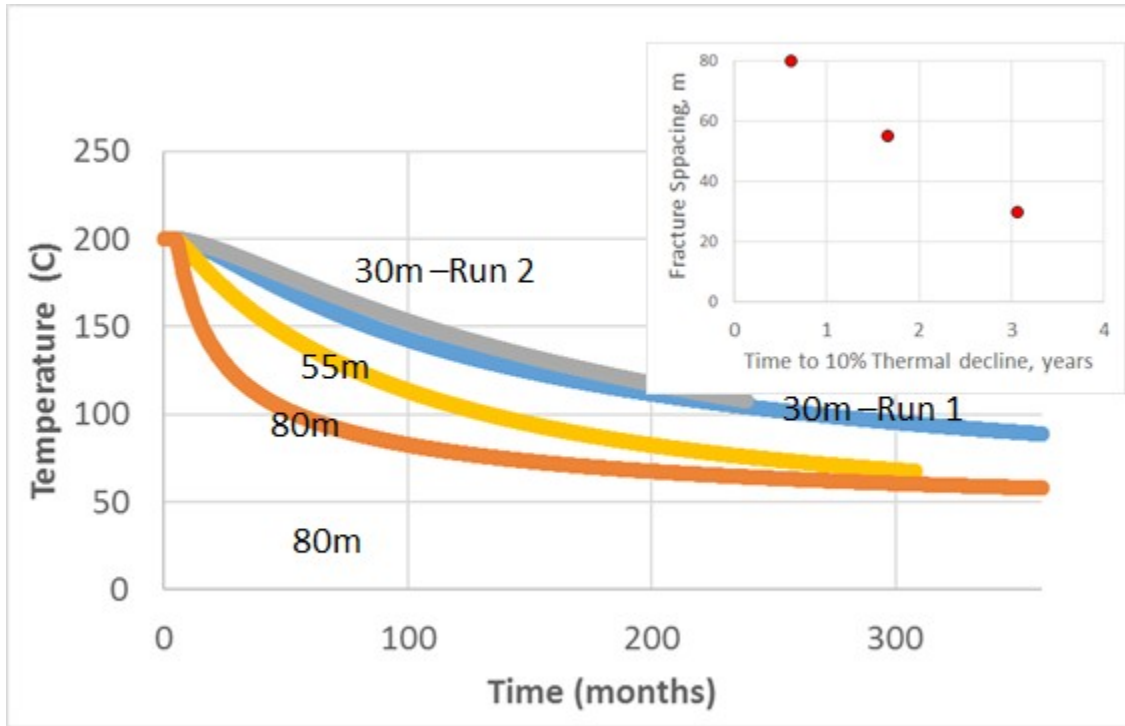


Figure 45. Production temperature versus time for fracture spacing study. The smaller spacing creates stimulated regions with more pathways and surface area for heat exchange, thus improving thermal performance. Inset shows the time to 10% production temperature decline.

Table 4. Properties for UDEC verification with Gringarten solution.

Property	Value	Units
Thermal conductivity (K_r)	2.6	J/m-s-K
Rock density (ρ_r)	2650	kg/m ³
Fluid density (ρ_w)	1000	kg/m ³
Rock Specific heat (c_r)	2600	J/kg-°K
Fluid Specific heat (c_w)	4180	J/kg-°K

Table 5. Input Rock and water mechanical and thermal properties for Itasca THM simulations

Property	Value	Units
Rock Density	2700	kg/m ³
Poisson Ratio	0.25	-
Bulk Modulus	40	MPa
Water viscosity	9e-4	Pa-s
Water density	1000.0	kg/m ³
Rock Specific heat	1000.0	J/kg-°K
Water Specific heat	4181.3	J/kg-°K
Linear Thermal Expansion	8e-6	1/°K
Rock Thermal Conductivity	3.0	J/m-s-°K

Table 6. Time to 10% thermal decline or three well positioning cases and well spacings.

Well Spacing, m	Time to 10% Decline, months		
	Case I	Case II	Case III
250	0.5	3.7	2.9
500	3.7	11.2	27.6
800	-	-	45.6

Table 7. Effective surface area for well position simulations.

Well Spacing	250			500			800
Case	Case I	Case	Case	Case I	Case	Case	Case

		II	III		II	III	III
Effective Well Spacing, m	250	1600	800	1000	2000	3000	4000
Nominal Surface Area, m ²	8.8E+04	8.8E+04	8.8E+04	5.0E+05	1.0E+06	1.5E+06	2.8E+05
Effective Surface Area, m ²	8.8E+04	5.6E+05	2.8E+05	3.5E+05	7.0E+05	1.1E+06	1.4E+06
Ratio of Effective to Nominal Surface Area	1	6.4	3.2	2	4	6	5
Average Power 30 years (MW-thermal, K _r =2.2 W/°K-m)	1.7	16.2	10.3	11.2	17.8	25.1	27.1
Average Power 30 years (MW-thermal, K _r =4 W/°K-m)	2.53	18.2	10.8	12.1	19.9	29.2	32.1
rate=70 kg/s							

Table 8. Rock thermal properties used in evaluating the effect of thermal diffusivity.

Specific Heat (C _p) (J/(kg°K))	Density (kg/m ³)	Conductivity (K) (J/m-s-°K)	Thermal diffusivity (J/(m ³ ·K))
1000	2000	2	1e-6
1000	2700	4	1.48e-6

37 LLNL Simulations with Thermomechanical Coupling

37.1 EGS Well Layouts to Mitigate Thermal Drawdown Induced Flow Channeling Overview

Thermal drawdown in a fractured reservoir may create flow channeling. Fracture networks are by nature heterogeneous, and preferential flow of cool injection water through the higher connectivity portions of the network may cause the thermal contraction of the rock along flow pathways, thus enhancing the apertures of the fractures to create flow channels. Fu and Carrigan (2014) investigate how the layouts of injection and production wells might mitigate this effect. The work was performed at Lawrence Livermore National Laboratory (LLNL) using their GEOS simulation system.

As GEOS's fully coupled modules were not yet available at the time of this work, the LLNL team used a hybrid of three models - a discrete fracture network model (GEOS), a continuum heat and fluid flow transport model (NUFT), and a mechanical finite-element model (GEOS) (Figure 46). The workflow starts by creating the fracture network and calculating the fluid flow using a discrete fracture (DFN) solver. Being essentially a 2-D model, the fractures are line segments. The two-dimensional permeability field of the DFN model is mapped to a regular Cartesian grid. NUFT (Non-isothermal Unsaturated-saturated Flow and Transport), developed by LLNL, performs the coupled heat and fluid flow simulations. The temperature changes provide a basis for calculating thermally induced stresses using a thermal stress finite-element model (FEM). The thermal stresses export back to the original DFN model to adjust fracture properties for the next time step. The heat and fluid are assumed to be steady state within each time step.

37.2 EGS Well Layouts to Mitigate Thermal Drawdown Induced Flow Channeling

38 *Description of the well-layout study model*

The study uses simulations of fluid flow and heat transport in a two-dimensional fracture network consisting of two fracture sets embedded in a 2-km-square region (Figure 47). The maximum horizontal stress on the model runs north-south with a magnitude of 25 MPa, and the minimum horizontal stress runs east-west with a magnitude of 18 MPa. One of the two fracture sets runs east-west which is normal to the maximum horizontal stress. The orientations of the east-west set vary randomly within 10° of that direction. The second set is oriented 20° clockwise to the north-south direction (N20E), also with a random variation within plus or minus 10° of that direction. Note this misalignment of the N20E set with the major principal stress running N-S. It has a significant effect on the thermal results.

The fractures have a length distribution based on a power law with an exponent of two and with 60 m and 600 m as the lower and upper truncations respectively. The total fracture density is 0.0625m/m². The fracture apertures have a reference value of 0.14 mm; however, the coupled mechanical model calculates apertures depending on the rock stress, fluid pressure, and temperature conditions up to a maximum of 1 mm. The properties for the model appear in Table 10 and the one fracture network realization used for all studies is shown in Figure 47. The well layouts for the different simulations appear in Figure 48.

The results of the well layout study appear in Figure 48, Figure 49, and Figure 50. The figures show the fluid temperatures in each production well and a map of the temperatures at 20 years of production. The thermal breakthrough times, defined as 10% decline in production temperature, are given for each simulation in Table 11.

39 *Single well pair simulations*

Scheme A and B use single well pairs compare injecting in the maximum stress direction, where the fractures are relatively open and conductive, and in the minimum stress direction, where the fractures are less open and conductive. For Scheme A the flow is along direct pathways of high fracture permeability. Scheme

B, on the other hand, follows much more tortuous pathways that combine the more open and the less open fracture sets (Figure 47). This causes a significant spreading of the flow paths and a much better thermal sweep. The time to 10% production temperature decline (Figure 49 and Table 11) is dramatically different, with 17 years for Scheme A flowing in the maximum stress direction and more than 30 years for Scheme B flowing in the minimum stress direction.

40 Well doublet simulations

Schemes C and D look at parallel injection-production pairs (Figure 48 and Figure 50). The well pairs for all these simulations are aligned north-south coincident with the maximum stress direction.

For Scheme C, both injection wells are in the south and the production wells are in the north. These are called parallel doublets, and the simulations are run with two variant spacings between the well pairs of 400-m and 800-m. The experimental objective of using two spacings is to look for interference between the well pairs.

Scheme D is the same as Scheme C except that for one well pair the injection well is in the south and the producing well is in the north, and for the other pair the injection well and production are reversed. This is called a “corner flow doublet”. This scheme is intended to introduce a component of east-west flow between the southwest injector and southeast producer and between the northeast injector and southwest producer.

The thermal breakthrough times, again defined as 10% production temperature decline, are generally very consistent among the Scheme C and D simulations having values that average 14.7 years except for the Scheme C 400-m well-pair spacing results, which are discussed further below. The flow is dominantly in the north-south direction following the open N20E fracture set. The temperature maps for the 800-m well-pair spacing simulations for both the C and D schemes (Figure 50) show the pathways are independent for each well pair. This is also the flow layout for single pair in Scheme A, which has a breakthrough time of 17 years. In summary, north-south injection pairs produce relatively consistent breakthrough times.

The outliers in this set of simulations are the Scheme C results with a 400-m doublet spacing. The objective for this simulation was to show whether there is interference between the two well pairs, and that appears to be the case. The eastern doublet develops a very direct pathway between the injection and the producer with a rapid, 7.5-year thermal breakthrough. The western doublet, on the other hand, does not have the same level of connection and breakthrough to the NW production well is 27 years. Fu and Carrigan (2014) attribute the differences in the breakthrough times to interference where the western doublet is capturing water from the eastern doublet. This diversion of injection water to the northeast production well from the northwest production well appears to be responsible for the rapid breakthrough at the northeast well compared with a slower breakthrough time at the northwest well. The average of the two breakthrough times is 17.2 years, which is not much different than the single well pair of Scheme A or the 14.9-year average of breakthroughs for all north-south well pairs (Schemes A, C, and D).

An alternative explanation for the Scheme C, 400-m spacing results could be simply heterogeneity where fracture network in the eastern doublet simply more directly connected the injector and producer, while the western network has poorer connectivity. A test of these concepts could involve running a single pair simulation for the eastern and western doublets in the locations of the 400-m spacing simulation and compare the single pair results with the doublet results. If the breakthrough times are due to heterogeneity, then the behaviors of the single pair will be similar to the doublet. If not, then the results more likely reflect interference between the pathways.

Scheme D, the corner injection scheme, sets up the possibility of flow along a longer pathway aligned with the more open fracture set as well as a shorter pathway in the direction of the less open set. The temperature maps (Figure 50) show that the well pairs are too far apart in the 800-m spacings simulations to have a significant flow in the east-west direction along the less open fracture set. For this doublet spacing the eastern and western well pairs act independently. On the other hand, for the 400-m well pair spacing simulations, the temperature maps (Figure 50) show the thermal drawdown is stronger in the east-west direction along the less-open fractures than in the north-south direction. Interestingly, the thermal breakthrough

times for the 800-m well spacing simulations are in the same general magnitude as the 800-m spacing simulations (Table 11).

41 Five-spot layout

Scheme E is a so called “five-spot” with four producing wells on an 800 m square with a central injection well. Unlike the well pairs, where the injection rates were 20 l/s, the rate for the five-spot injector is 80 kg/s (Figure 48). Like the other schemes, each production well has a -20 l/s production rate. In the five-spot, the thermal sweep takes considerable advantage of both fracture sets (Figure 51). Despite having a shorter path length between the injector and the producing wells (557 m versus 800 m), the times for thermal breakthrough are larger than both Schemes C and D, having range off from 18.0 to 26.0 years and having an average of 21.4 years.

The temperature curves are nearly identical for the SE and NW productions with a breakthrough time of 18 years, while the NE and SW wells are also strongly similar with breakthrough times of 26.0 and 27 years (Table 11). One might expect the NE and SW would have the earlier breakthrough, because those paths are more aligned with the N20E fracture set than the SE and NE production wells. But that is not the case. The stronger connection to the NW and SE production wells is likely an artifact of the specific fracture network realization.

Nonetheless, the 5-spot does outperform the doublet well pairs despite the path lengths from injector to producer being shorter. This is partly due to the pathways taking advantage of both fracture sets. Also, the power production from the 5-spot will be double the Scheme C and D well pairs because there are four production wells instead of two.

Fu and Carrigan (2014) also note the five-spot carries with it some advantages of drilling cost. If the target for a 5 MW power plant is a flow rate of approximately 80 l/s, then of these well layouts only the five-spot achieves that goal.

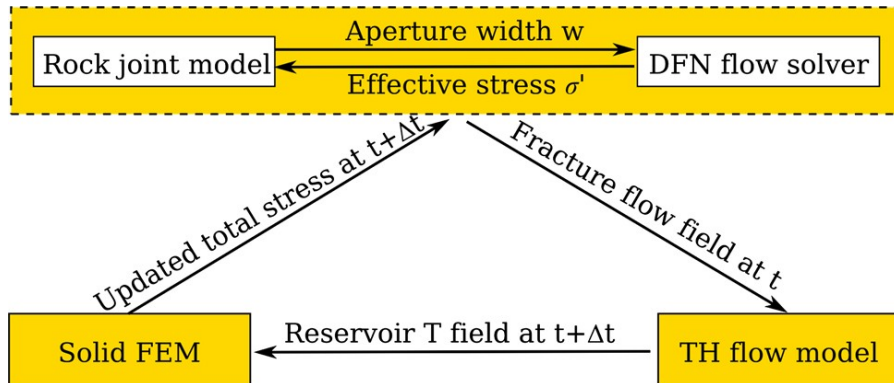


Figure 46. GEOS modeling approach for coupled hydro-thermal-mechanical simulation. GEOS involves the interaction of three separate codes, a fracture network model, continuum heat and fluid flow mode (TH flow mode), and a finite-element mechanical code (Solid FEMO. Each time step starts with the DFN/rock joint model, passes through a hydro-thermal calculation, determines the stress changes due to temperature, and finally updates the DFN model with apertures that are updated for thermomechanical effects. (Fu et al., 2016).

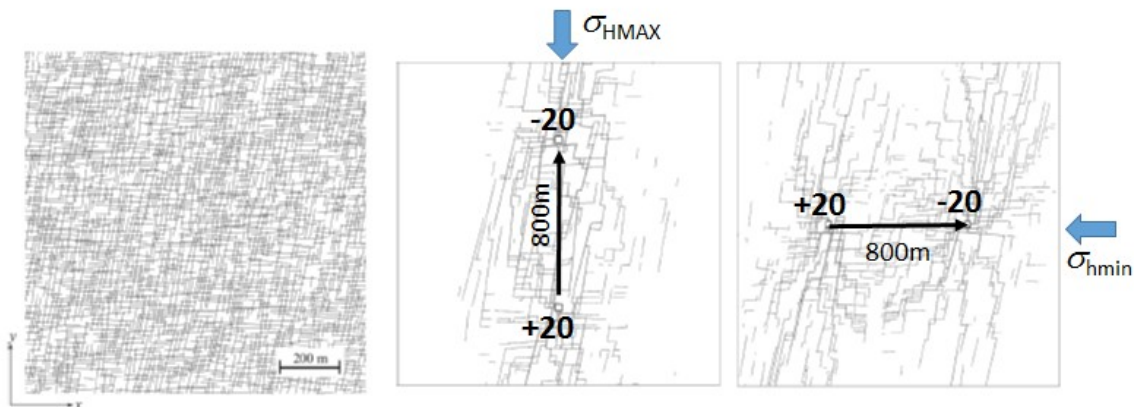


Figure 47. Fracture network for well positioning study (left); pathways from Scheme A (center) where the wells are aligned with the maximum horizontal stress, and Scheme B (right) where wells are aligned with the minimum horizontal stress.

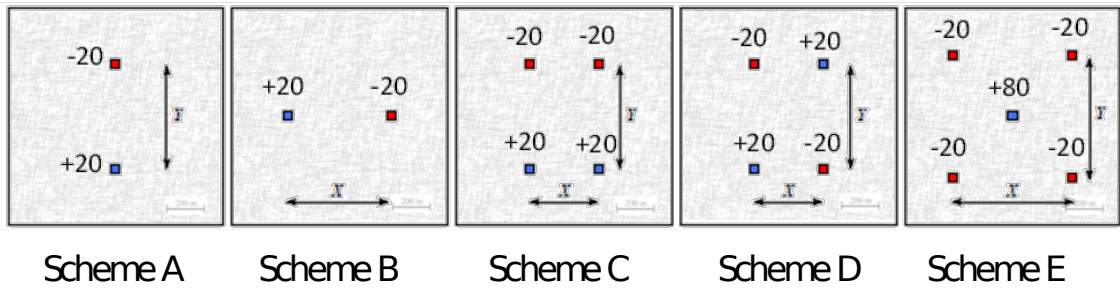


Figure 48. Well layouts and flow rates for well layout study. Injection is positive in kg/s, production is negative. Injection wells are blue, production wells are red. North is up on the page. The y well spacing is 800 m. The x well spacing is 800 m except for variants of C and D that are 400 m.

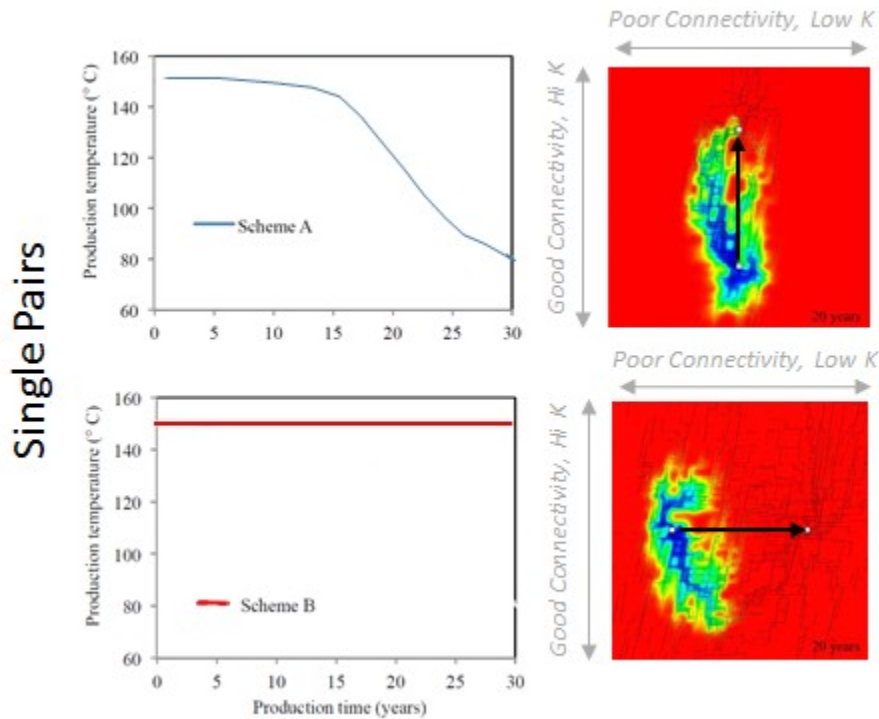


Figure 49. Well positioning study, single pairs, Scheme A (top) in the direction of the major stress, Scheme B (bottom) in the direction of the minor stress. Left, production temperature. Right, temperature visualization at 20 years with pathways. Visualizations show flow pathways as black lines. Stresses are acting N-S (N up on the page) and preferentially open the N20E set rather than the E-W set. Scheme A follows the open fractures and has early thermal breakthrough. Scheme B forces flow through the E-W set and has a much better sweep with no thermal decline in 30 years.

Parallel Doublets

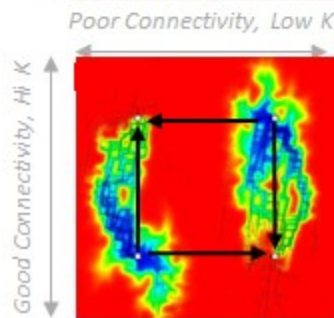
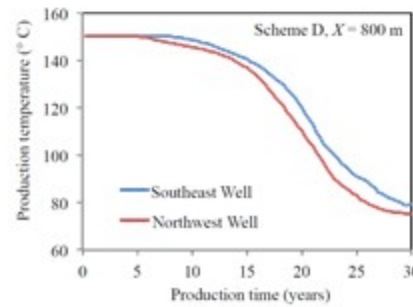
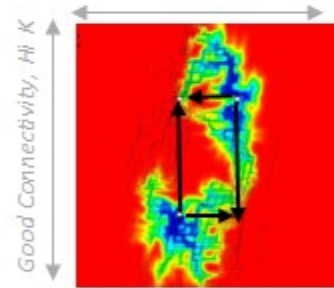
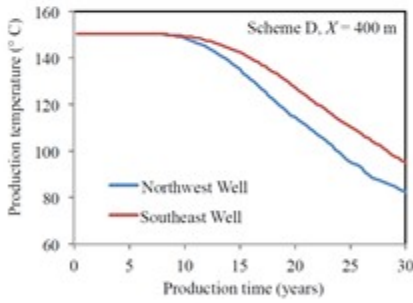
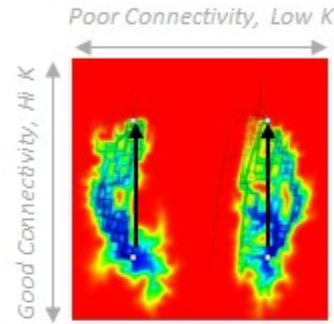
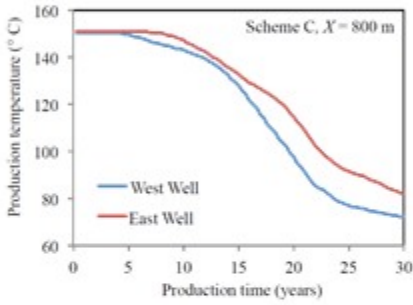
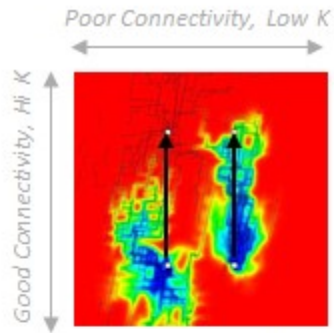
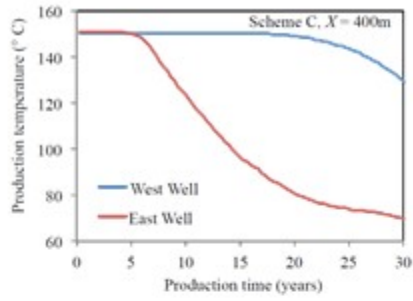


Figure 50. Well positioning study, two well pairs. Scheme C producer and injector are flowing in parallel direction with 400 and 800 m spacings on the pairs. Scheme D, injection and production are at opposite corners. Left, production temperature, Right, temperature visualization at 20 years with pathways. Scheme C with the 400-m doublet spacing shows a single pathway connecting the SW injection well with the east well pair. This capture of SW injection water results an early breakthrough at the NE producer and later breakthrough at the NW producer. Other doublet simulations show similar breakthrough times.

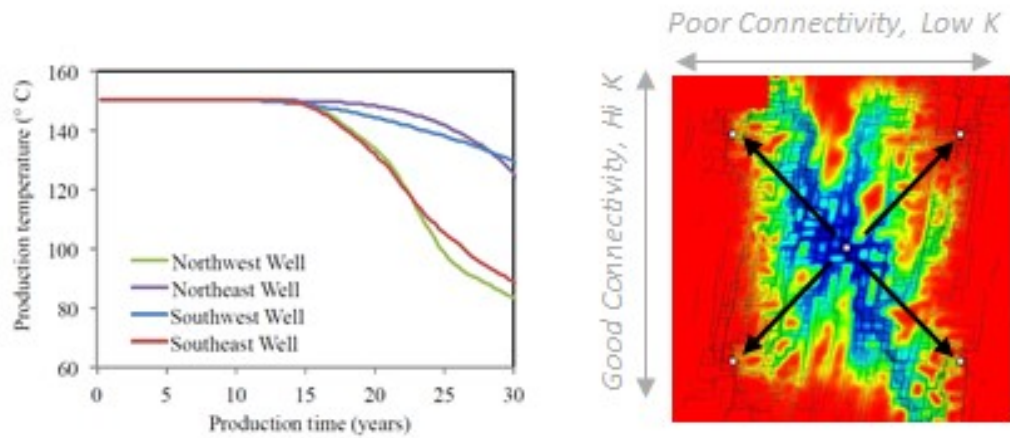


Figure 51. Well positioning study, Scheme E - center well injection well with four production wells and a central injector. Left, production temperature, Right, temperature visualization at 20 years with pathways.

Table 9. Properties for LLNL well layout study.

Original <i>in situ</i> stress	$\sigma_x = \sigma_{hmin} = 18$ MPa (east-west) $\sigma_y = \sigma_{HMAX} = 25$ MPa (north-south)
Original pore pressure	$P_0 = 15$ MPa
Rock joint parameters	$w_{max} = 1.0$ mm; $\sigma_{ref} = 20$ MPa; $w_{ref} = 0.14$ mm
Initial reservoir temperature	$T_0 = 150^\circ\text{C}$
Injection fluid temperature	$T_i = 50^\circ\text{C}$
Mechanical properties of rock	Young's modulus $E = 20$ GPa; Poisson's ratio $\nu = 0.2$; Linear thermal expansion coefficient $\alpha_L = 8 \times 10^{-6}$
Thermal properties of rock	Thermal conductivity $K_r = 3$ W/m/ $^\circ\text{C}$ Heat capacity $c_r = 2.5$ MJ/m ³ / $^\circ\text{C}$
Fluid properties	Those of water.

Table 10. Dimensions and injection/production pressures for LLNL well layout study.

Lay out	Dimension	Net Production Pressure* (MPa)	Net Production Pressure* (MPa)
A	$Y = 800$ m	1.9	-6.5
B	$X = 800$ m	2.4	-4.4
C	$X = 400$ m $Y = 800$ m; $X = 800$ m; $Y = 800$ m	2.3/1.5 2.1/1.6	-4.3/-6.8 -3.8/-6.3
D	$X = 400$ m; $Y = 800$ m $X = 800$ m; $Y = 800$ m	2.1/2.0 1.9/1.9	-2.4/-3.3 -2.5/-2.6
E	$X = 1,200$ m; $Y = 1,200$ m	4.1	-2.8/-3.5/-3.0/-2.1

Table 11. Well layout study, time to 10% production temperature decline

Well Layout Study Time to 10% Production Temperature Decline				
Description	Scheme	t _{10%}	t _{10%} Averages	Notes
One Pair in Major Principal Stress	A		17	
One Pair In Minor Principal Stress	B		>30.0	
Parallel Doublet 400-m Spacing	C-400-NW	27.0	14.7	Injection and Production Holes Aligned with Major Principal Stress
	C-400-NE	7.5		
Parallel Doublet 800-m Spacing	C-800-NW	11.8		
	C-800-NE	12.9		
Corner Flow Doublet 400-m Spacing	D-400-NW	13.5		
	D-400-SE	15.9		
Corner Flow Doublet 800-m Spacing	D-800-NW	13.5		
	D-800-NE	15.1		
Central Injection, 4 production wells	E-NE	26.0	24.9	NE-SW Direction, Less aligned with N20E set
	E-SW	23.7		
	E-SE	18.0	18.0	NW-SE Direction, Better aligned with N20E Set
	E-NW	18.0		

41.1 Flow Channeling in 2-D Fracture Networks Using a Single Well Pair With and Without Thermomechanical Coupling

42 Model description

Compared with the well layout study, the simulations described in this section introduce the following variations:

- Different length distributions for the two fracture sets, and therefore different expectations for connectivity
- Multiple realizations of the fracture network
- Thermomechanical coupling for the flow simulations.

A GEOS model very similar to the one used for the well-layout study discussed in Section 4.3 uses a single well pair to explore the effects of fracture network properties, well spacing, and thermal-mechanical coupling (Fu et al., 2016). A description of the fracture network properties appears in Table 12. The initial model, Fracture Network A, uses uniform, regularly spaced orthogonal fractures. The stochastic fracture networks (Figure 52) use lengths drawn from a uniform distribution that may be either long (between 150 m and 300 m) or short (between 60 and 120 m). Fracture Network B uses the long distribution with a single, randomly oriented fracture set. The remaining fracture networks (C-F) have two sets, a secondary set oriented $\pm 5^\circ$ with direction of the maximum stress and primary set oriented $\pm 5^\circ$ to a direction 10° clockwise to the maximum stress direction. The four fracture network cases consider both sets being long (Fracture Network C); the primary set long and secondary short (Fracture Network D); the primary network short and the secondary long (Fracture Network E); or both sets being short (Fracture Network F). All fracture networks have the same intensity (that is fracture length per unit area), with a value of 0.1 m^{-1} . The number of intersections along each fracture, n_i , provides a measure of connectivity. Longer sets have on average approximately 7 intersections per fracture, while shorter sets have about 2.5.

The base apertures for all fractures are 1 mm; however, these are modified according to the applied in situ stresses and change over time due the coupled hydro-thermomechanical stresses. The well spacing for these simulations was 600 m.

Simulations of EGS production were carried out for each fracture network under both uncoupled and coupled thermomechanical conditions. The uncoupled visualizations in Figure 52 show strong effects of the length variations among the fracture networks. Network E, with long fractures in the secondary set, shows considerable lateral spreading compared with simulations that have long fractures on the primary set oriented more in alignment with production and injection wells. This spreading follows the fracture connectivity. The fracture network with both sets having short lengths, Fracture Network F, have relatively poor connectivity between the injection and production wells.

Applying thermomechanical coupling focuses the flow into channels that align with the orientation defined by the injection and production wells, and thermal decline is concentrated along the channels (Figure 53). Times to 10% thermal decline for the fracture network cases (Figure 54) show this clearly. Alignment of the long fracture set with the production and injection wells (as well as the maximum stress direction) produces relatively direct pathways with earlier thermal breakthrough for Fracture Networks B, C, and D. On the other hand, the spreading of flow caused by aligning the long fracture set at 90 degrees from the well alignment spreads the flow through more of the fracture network and results in later thermal breakthrough. The simulation with two short fracture sets (Fracture Network F) has poor connectivity between the wells. Flow focusses along one pathway connecting the wells, producing the poorest thermal performance among the cases.

Fu et al. (2016) conclude from their simulations that fracture networks having more diffuse and less direct pathways between injection and production wells produce later thermal decline and better EGS performance. In their models, the diffuse behavior results from creating preferential connectivity along fractures that are not aligned with the direction between the injection and production well. Thermomechanical coupling promotes channelization along pathways between the injection and production wells, which causes earlier thermal breakthrough and

degrades EGS performance. Nonetheless, they conclude that fracture networks that begin with more diffuse pathways will retain an advantage for EGS behavior.

43 Importance of multiple realizations

Fu et al. (2016) complemented their simulations of the five stochastic fracture-network cases by running an additional five realizations of the statistics for Fracture Network B. This is the case with one fracture length distribution and random fracture orientations. A comparison of thermal performance, as measured by time to 10% temperature decline (Figure 54, right) shows that the variability produced among single realizations of different fracture networks is not greatly different than the variability produced by different realizations from the same fracture network statistics. The general overlap of these results illustrates why it is difficult to draw conclusive observations from stochastic simulations with few realizations.

Fu et al. (2016) note, however, that all of the Fracture Network B simulations have earlier thermal decline than the one realization of Fracture Network E, which aligns the longer fracture set to create more spreading with respect to the alignment of the injection and production well. Similarly, all of the Fracture Network B realizations have later thermal decline than the one realization of Fracture Network F, where both sets are short, the inter-well connectivity is poor, and flow reduces to one or a few pathways.

44 Effects of single pair well spacing

For four of the fracture networks (B through E), Fu et al. (2016) ran single realizations using 400- and 800-meter distances between the wells in addition to the 600 m well spacing of the base case. There are too few realizations to define quantitative trends; however, there is a clear improvement in the thermal performance (Figure 55) with increased well spacing. The behavior of Fracture Network E shows an earlier thermal decline at 800 meters than 600 meters, which may be a behavior specific to this realization.

45 Effect of thermomechanical coupling on impedance

The channeling effects of thermomechanical coupling are clearly evident in the evolution of impedance over production time (Figure 56). For constant-rate

injection, the increase in fracture aperture that accompanies preferential cooling along flowing pathways reduces the injection pressure over time.

45.1 Thermally Induced Channeling in a Single Fracture (LLNL)

46 Model description

The channeling of flow as a consequence of aperture heterogeneity within fracture planes is a well-established concept (Tsang and Neretnieks, 1998). The fracture network of an EGS system may experience an enhanced channelization as thermal contraction around flowing channels creates a positive feedback loop. The more a fracture is channeled the more it becomes locally cooled and the more it becomes further channeled.

LLNL, using their numerical model, GEOS, performed a series of simulations on a horizontal EGS reservoir represented as the single heterogeneous fracture shown in Figure 57 (Guo et al., 2016). The simulation is intended to loosely resemble the Habanero project in the Cooper Basin, Australia. The fracture is conceived as having a diameter of 1000 m at a depth of 3000 m. There is a single injection and production well with an inter-well distance of 500 m. The initial rock temperature is 200°C and the model circulates fluid at an initial temperature of 50°C at a rate of 12.5 l/s. Properties for the simulation appear in Table 13. The aperture within the fracture is variable, following a lognormal distribution with a mean value of 0.24 mm and a standard deviation of 0.17 mm. The aperture assignments use a geostatistical algorithm to create spatial correlation. All of the values are assigned quasi-randomly with the stipulation that values are more likely to be similar to nearby locations than to be purely random. This spatial correlation tends to create channels within the fracture.

47 Model results

The experimental test matrix for the simulations included

- Homogeneous versus heterogeneous initial aperture
- Presence or absence of thermomechanical coupling
- Aperture standard deviation and
- Aperture correlation length.

An example set of simulations compares the homogeneous-aperture case with a heterogeneous case having a correlation length of 50 m and a lognormal standard deviation of 0.24 mm and 0.17 mm. The set includes the results of simulations with and without thermal coupling for both the homogeneous and heterogeneous cases. Visualizations of the change in aperture, flow paths, and temperature are shown for one year and thirty years in Figure 58. In contrast to the homogeneous case, where the injection fluid sweeps the entire fracture surface, a heterogeneous case produces a highly channelized flow field. Even without the thermomechanical coupling one can observe strong non-uniformity of the temperature sweep, which becomes even more channelized with the addition of thermomechanical coupling.

The production temperature versus time curves for these cases (homogeneous, heterogeneous, no thermomechanical coupling, thermomechanical coupling), show that the best performance case is a homogeneous aperture field without thermal stress (Figure 59). Heterogeneity and thermomechanical coupling both serve to localize flow and result in earlier thermal breakthrough and poorer EGS performance. These model results reflect the role of channelization in reducing the effective area for heat transfer between the rock and the fracture.

Although the results are highly scattered, increasing the correlation length of the apertures or standard deviation of the aperture distribution reduces the production life of the reservoir (Figure 60). Note that Guo et al. (2016) define production life as a reduction from 250° C to 120° C, which is a 53% thermal decline for an injection temperature of 50° C. This is a larger thermal decline than the 10% used elsewhere in this report. The trends resulting from more pronounced heterogeneity should hold for the 10% thermal decline as well.

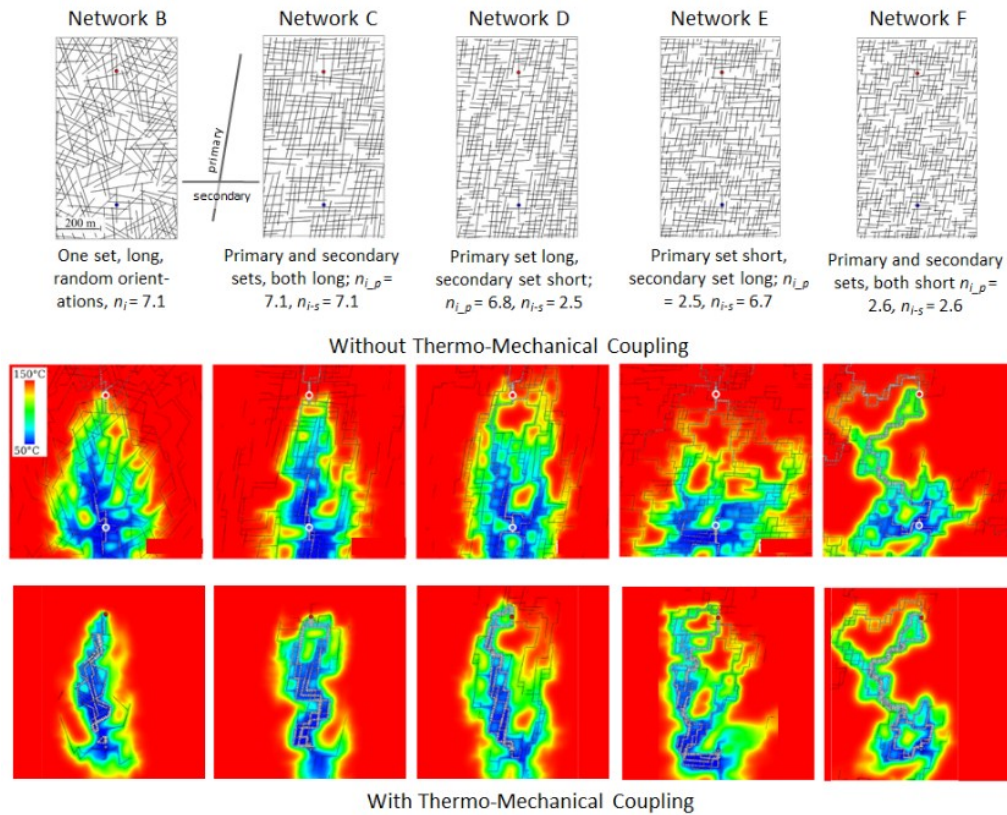


Figure 52. Fracture networks for Flow Channeling Study (Fu et al., 2016). The injection well (blue) and production well (red) are 600 m apart. All networks have the same intensity 0.1 m^{-1} . Network A (not shown) uses regularly spaced fractures with lengths that extend to the model boundaries. Top: central portion of network with descriptions, Middle: Temperature at 20 years with no thermomechanical coupling, Bottom: Temperature at 20 years with thermomechanical coupling. n_i is the average number of intersections along each fracture and is a measure of connectivity with the subscripts indicating primary and secondary sets.

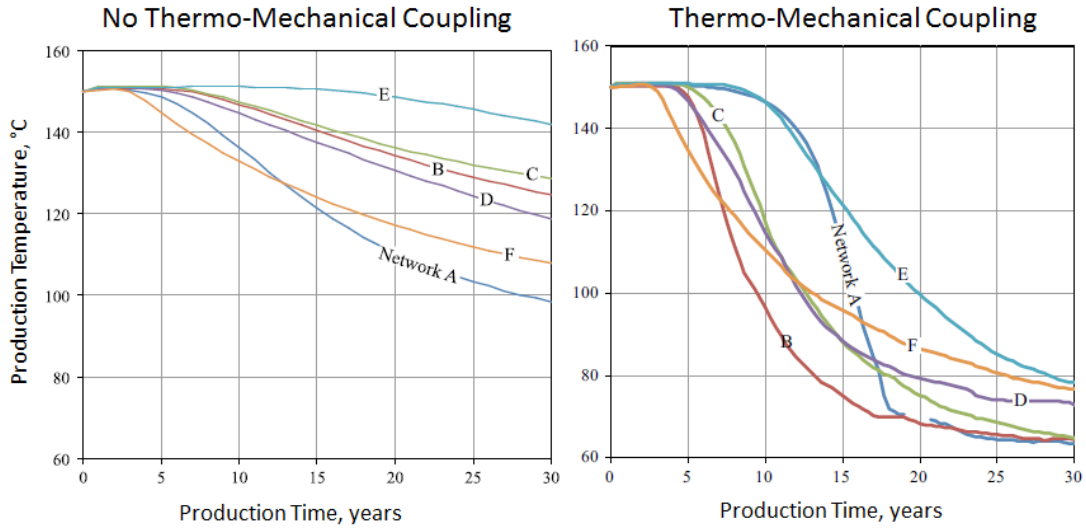


Figure 53. Thermal performance of networks for single well-pair study (Fu et al., 2016). Left: no thermomechanical coupling; right, thermomechanical coupling.

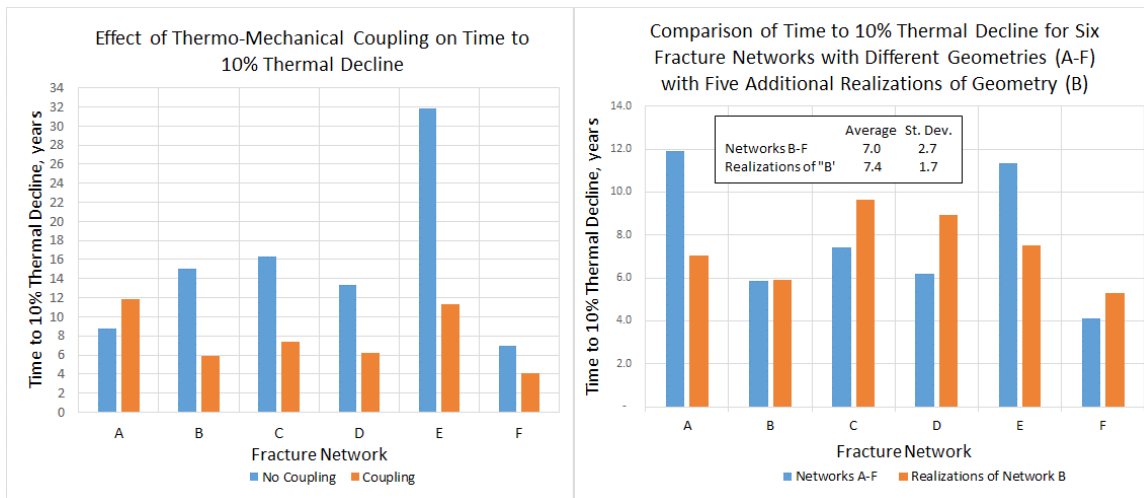


Figure 54. Left: Effect of thermomechanical coupling on time to 10% thermal decline for each fracture network. Except of for Network A, the coupling significantly reduces time to thermal decline. Right: Comparison of time to 10% thermal decline for all networks with six realizations of Fracture Network B. Variability of different realizations of a single network is similar to variability among single realizations of six different networks. Data are replotted from Fu et al. (2016).

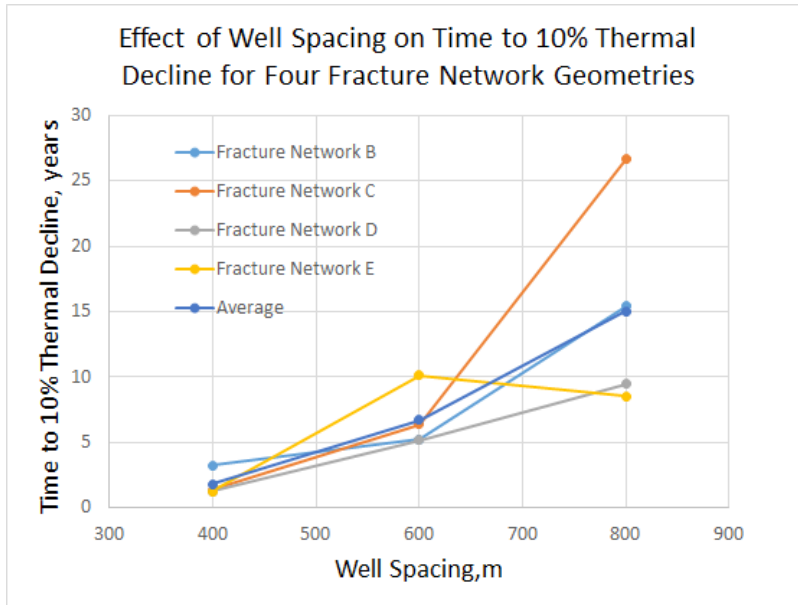


Figure 55. Effect of well spacing on time to 10% thermal decline for Fracture Networks B - E. Increasing well spacing improves EGS performance. Decrease in Fracture Network E time from a spacing of 600 m to 800 m is likely an effect of a single realization. Data replotted from Fu et al. (2016).

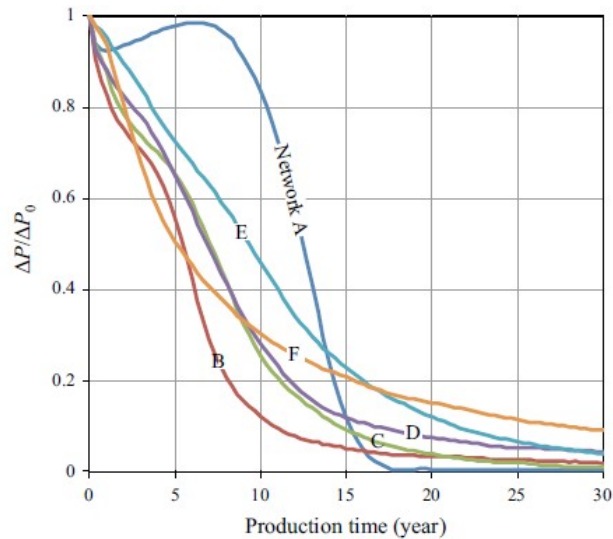


Figure 56. Evolution of injection well impedance over time. Decrease in impedance reflects the increasing apertures of fractures with cooling due to thermomechanical coupling. Impedance measured as the pressure difference between the wells at a given time divided by the initial pressure difference (Fu et al., 2016).

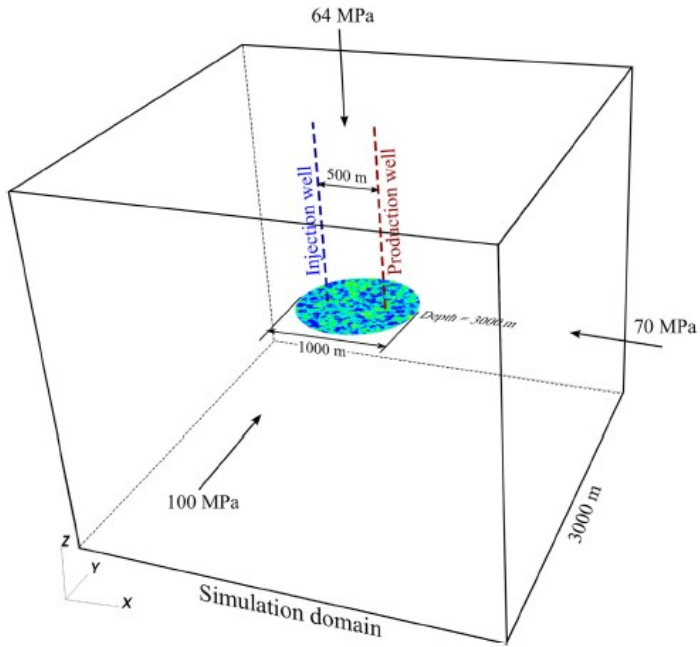


Figure 57. Single fracture channeling simulation sketch (Guo et al., 2016)

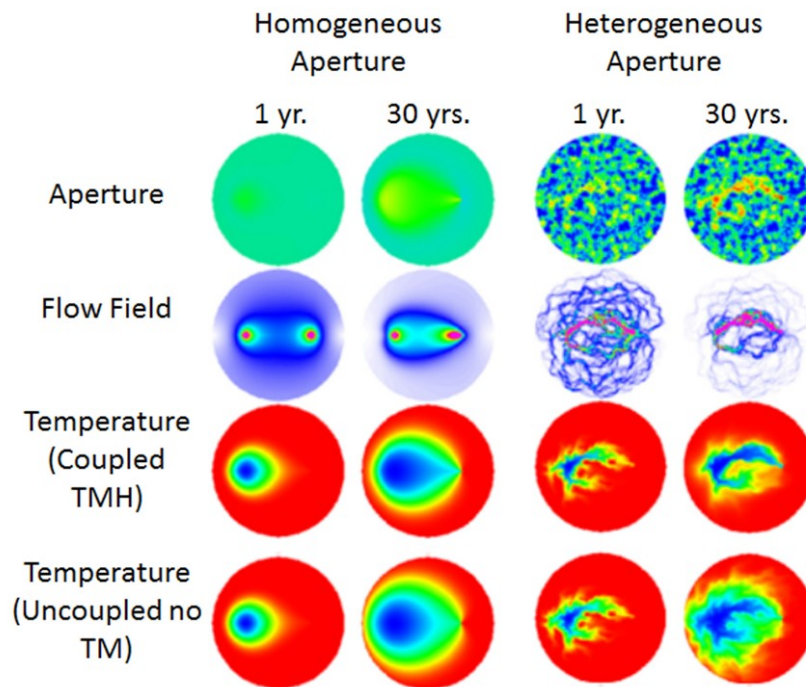


Figure 58. Visualizations of single fracture channeling study.

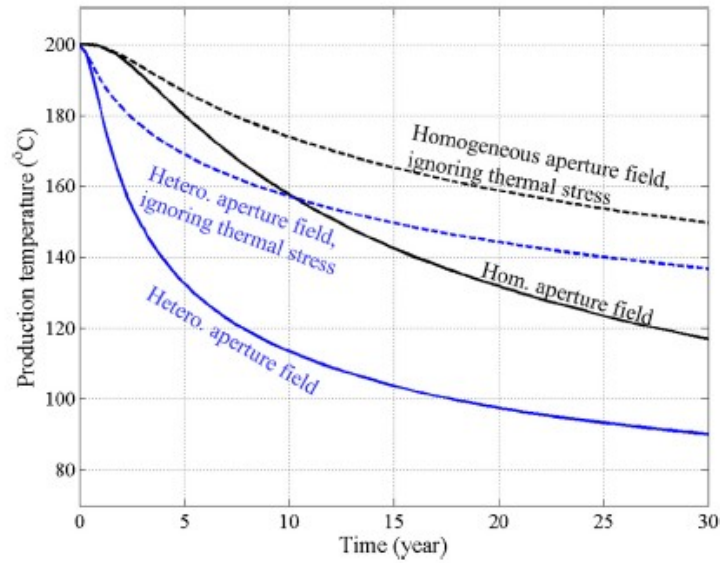


Figure 59. Production temperature versus time, channeling study

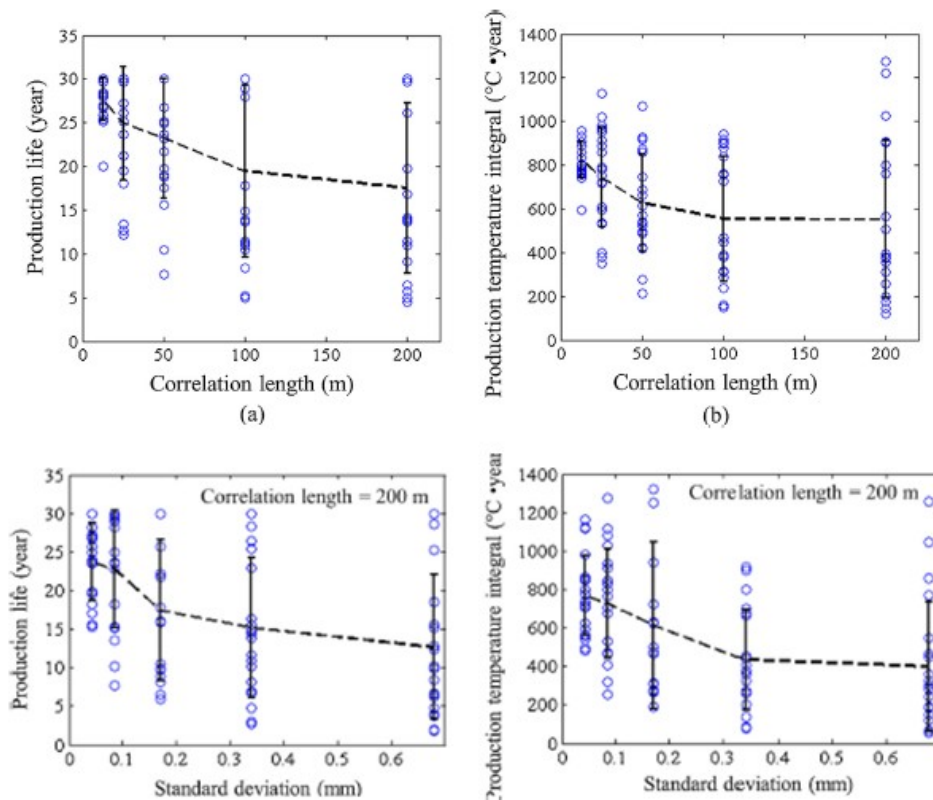


Figure 60. Variation in production life (defined as 53% thermal decline) versus correlation length and aperture standard deviation.

Table 12. Model descriptions for 2-D channeling studies (data from Fu et al., 2016). Fracture network parameters from the well layout study (Fu and Carrigan, 2014) are given at the bottom of the table for comparison.

		Intensity	Set 1 Strike		Set 2 Strike		Set 1 Length ¹		Set 2 Length ¹		Aperture
		m ⁻¹	Clockwise to 0				m				m
			min	max	min	max	min	max	min	max	initial
2-D Channeling (Fu and others, 2016)	A	0.10	90	90	0	0	infinite		infinite		
	B	0.10	75	85	-5	5	150	300	150	300	0.001
	C	0.10	75	85	-5	5	150	300	60	120	0.001
	D	0.10	75	85	-5	5	60	120	150	300	0.001
	E	0.10	75	85	-5	5	60	120	60	120	0.001
	F	0.10	75	85	-5	5	150	300	60	120	0.001
	G	0.17	75	85	-5	5	150	300	60	120	0.001
	H	0.17	75	85	-5	5	60	120	60	120	0.001
Well Layout (Fu and Carrigan, 2014)	A	0.06	75	85	-5	5	60	600	60	600	0.001
	B	0.06	75	85	-5	5	60	600	60	600	0.001

¹Length in the 2-Channeling study is a uniform distribution. For the well layout study, it is a power law with exponent 2.

Table 13. Properties for single fracture channeling study (Guo et al., 2016)

Property name	Value
Porosity of the rock matrix (φ_m)	0.01
Permeability of the rock matrix (k_m)	$1 \times 10^{-20} \text{ m}^2$
Rock solid density (ρ_s)	$2,500 \text{ kg/m}^3$
Rock bulk modulus (K)	33.3 GPa
Rock shear modulus (G)	20 GPa
Specific heat capacity of rock solid (C_s)	790 J/kg/K
Specific heat capacity of fluid (C_f)	$4.46 \times 10^3 \text{ J/kg/K}$
Linear thermal expansion coefficient of rock matrix (α_r)	$8.0 \times 10^{-6} \text{ K}^{-1}$
Reference fluid density (ρ_f)	887.2 kg/m^3
Reference pressure for fluid density (P_f)	34 MPa
Reference temperature for fluid density (T_f)	200 °C
Fluid dynamic viscosity (μ)	$1.42 \times 10^{-4} \text{ Pa}\cdot\text{s}$
Fluid compressibility (β_f)	$5.11 \times 10^{-10} \text{ Pa}^{-1}$
Volumetric thermal expansion coefficient of fluid (α_f)	$7.66 \times 10^{-4} \text{ K}^{-1}$
Thermal conductivity of rock matrix (K_m)	3.5 W/m/K

47.1 Studies on Horizontal Wells with Multiple Stimulation Zones and Completions

48 Description of EGS using horizontal wells

This chapter presents the results of otherwise unpublished work performed at Lawrence Livermore National Laboratory (LLNL) for an EGS concept of multiple fractures or stimulated zones created between two horizontal wells. The assumption in the analysis is that the production and injection wells are horizontal, and the stimulation produces vertical fractures that are oriented normal to the wells' orientation. This production concept closely mirrors that which has been applied in so-called unconventional oil and gas production from very low permeability reservoirs (Figure 61).

A major revolution in oil and gas production arose from the development of directional drilling, in which the combination of downhole drilling motors and systems for steering the drill bit greatly enhanced the ability to drill wells into any orientation including horizontal. The combination of directional drilling with two technologies that arose in part from early EGS studies -- large-scale hydraulic fracturing in multiple stages and microseismic monitoring -- enabled the unconventional oil and gas industry to become a significant portion of American fossil fuel production. The application of directional drilling to EGS has been hampered by temperature limits on directional drilling equipment. For the purposes of studying EGS feasibility, we will assume that restrictions on directional drilling will eventually be overcome.

The major difference between unconventional oil and gas production and EGS applications is the number of wells and the inter-well circulation. An unconventional oil or gas well layout uses a single production well, relying on the reservoir pressure to drive the fluid flow. By contrast, the horizontal-well EGS system will have at least two wells, an injector and producer, or possibly three wells where the central well is used to create the stimulations.

The simulations are similar in concept to the analytical solutions for multiple hydraulic fractures presented in Section 2.3 in that they are two-dimensional, but they add the solution of coupled, hydro-thermomechanical flow. The simulations use

similar properties and conditions as the single fracture simulations described in Section 4 with the following exceptions:

- The model consists of eleven hydraulic fractures created between two horizontal wells that are 200 m apart with horizontal legs that are 1000 m long. The eleven fractures are assigned random initial transmissivities as shown in Figure 62. The simulation assumes a 100 m thick rock formation with the wells at mid-height. There is a constant flow rate of 30 kg/s circulating between the two wells, with an injection temperature of 50° C and an initial reservoir temperature 150° C.
- The simulations addressed two production design options. The first set of simulations applies a constant production over a 30-year period without any changes over time. The second allows for sealing the most conductive fractures as they thermally break through to the production well. The second set of simulations also use a constant rate of 30 kg/m, but the flow redistributes among the remaining fractures as the most transmissive fractures are blocked. The term “active reservoir management” applies to these simulations.

49 Horizontal well simulation results

49.1.1.1 Simulations without active reservoir management

As with the LLNL single-fracture simulations, and unlike the simulations in Section 2.3, the GEOS code includes thermomechanical coupling. Similar to the single-fracture cases, thermomechanical coupling results in thermal contraction of the rock, which increases the apertures of the most conductive fractures over time. The larger the flow rate, the greater the thermomechanical effect. Thus, the highest transmissivity fractures not only carry a larger portion of the flow between the two wells initially, but the portion of flow in those fractures increases over time.

The production history has major effects on both the thermal behavior and the pressure behavior. The production temperature remains roughly constant for about five years and then goes into thermal decline after thermal breakthrough (Figure 63). The pressure difference between the production and injection wells decreases

with time as thermomechanical coupling increases the apertures of some fractures and reduces overall flow impedance.

The exit temperatures and flow rates of individual fractures further show the effects of thermomechanical coupling (Figure 64). The highest-transmissivity fractures, that is, the ones with the largest apertures, experience the earliest thermal breakthroughs. The flows in these fractures (especially fractures #6 and #8) increase with time, while other fractures are nearly steady or declining. The largest fractures act as short-circuits, providing most of the early thermal decline (Figure 65), an effect that the thermomechanical coupling enhances.

49.1.1.2 Simulations with active reservoir management (ARM)

Active reservoir management (ARM) involves blocking the higher transmissivity fractures at the injection well as they thermally breakthrough to the production well. In this set of simulations, the two largest aperture/transmissivity fractures (#6 and #8) are blocked and stop taking flow after 15 years. A second management intervention blocks the next two highest transmissivity fractures (#3 and #5) at 20 years. A constant flow rate of 30 kg/s is maintained through the production history, but the flow redistributes among the remaining fractures.

Blocking results in an immediate increase in the production temperature (). The amount of thermal improvement is 10°C or more, restoring more than half the thermal decline. The blocking of fractures also increases the injection pressure. However, because the coupled thermomechanical effects had been increasing aperture and decreasing the pressure difference, the injection pressures after blocking do not exceed the initial values at the beginning of production (Figure 66).

Individual fracture performance (Figure 67) reflects shifting the major portion of the flow from fractures #6 and #8 to fractures #3 and #5 at 15 years. Flow rates in fractures #3 and #5 begin to increase as they in turn experience aperture enlargement with cooling. Similarly, when fractures #3 and #5 are blocked at 20 years, fractures #7 and #10 see increased flow rates as they take the major portion of the flow.

A comparison of the thermal fields at 30 years without and with ARM (Figure 68) shows that the overall thermal decline is much more distributed with the active reservoir management approach. There is even some thermal recovery, especially around fractures #6 and #8, which were blocked at 15 years.

Even with the active reservoir management approach, there is a considerable volume of rock that is not thermally affected by production at thirty years. Reducing the fracture spacing, with additional fractures along the 1000-m lateral wells, would not only tap the thermal resources more effectively, but would delay the thermal breakthrough by distributing flow to more fractures and reducing the flow rate in each fracture.

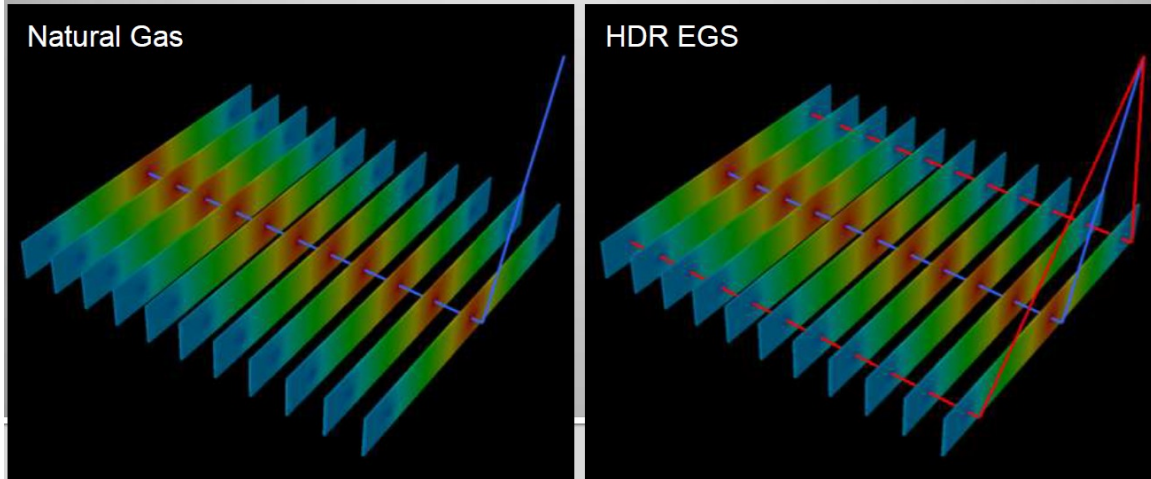


Figure 61. Comparison of unconventional natural gas system of hydraulic fractures with a multiple fracture EGS system using horizontal wells.

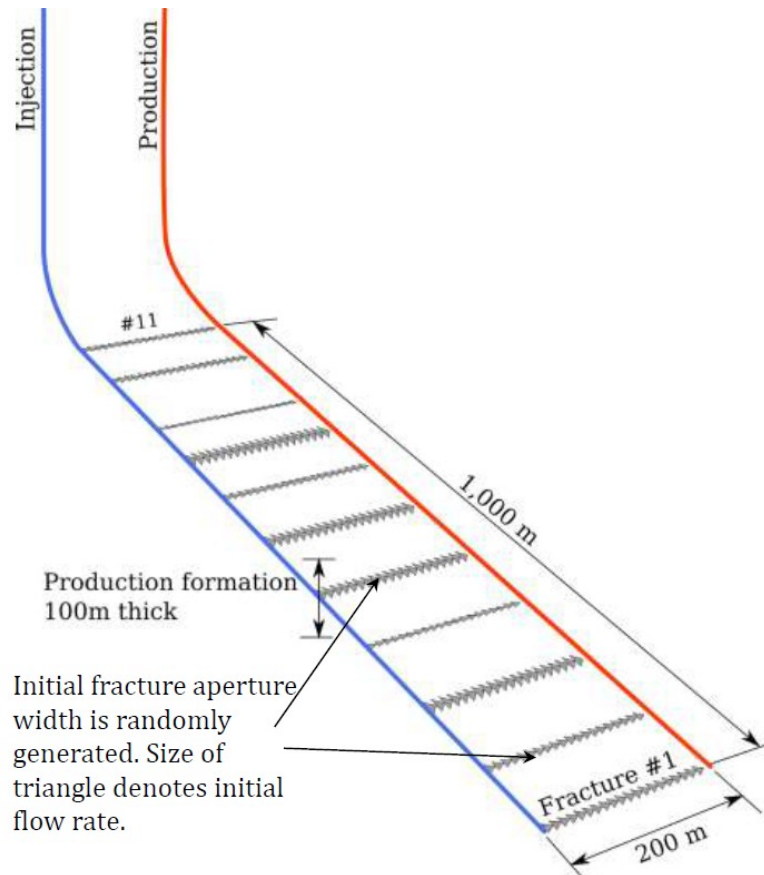


Figure 62. Well layout for multiple fracture EGS simulations.

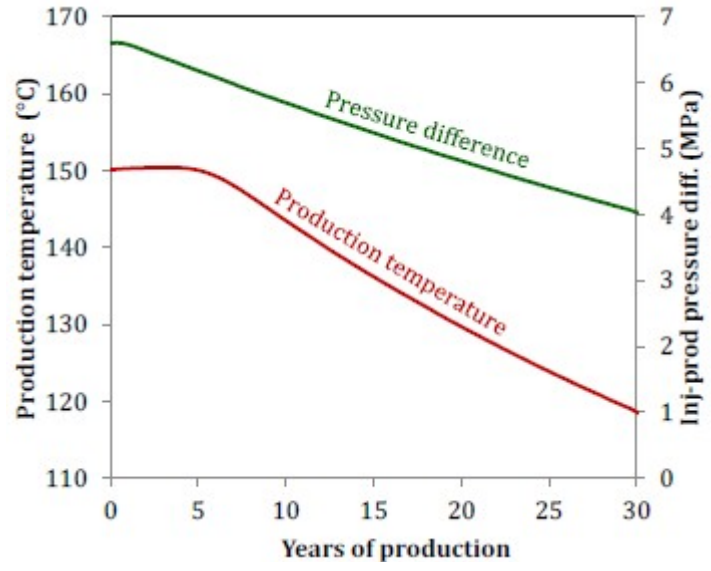


Figure 63. Production temperature and pressure difference versus time.

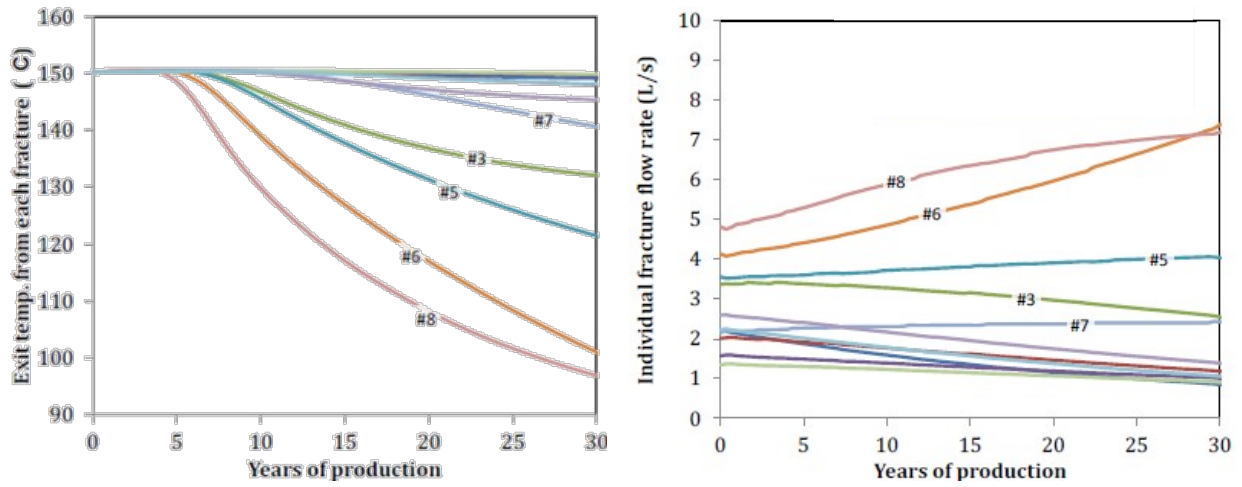


Figure 64. Exit temperature and flow rate for each fracture.

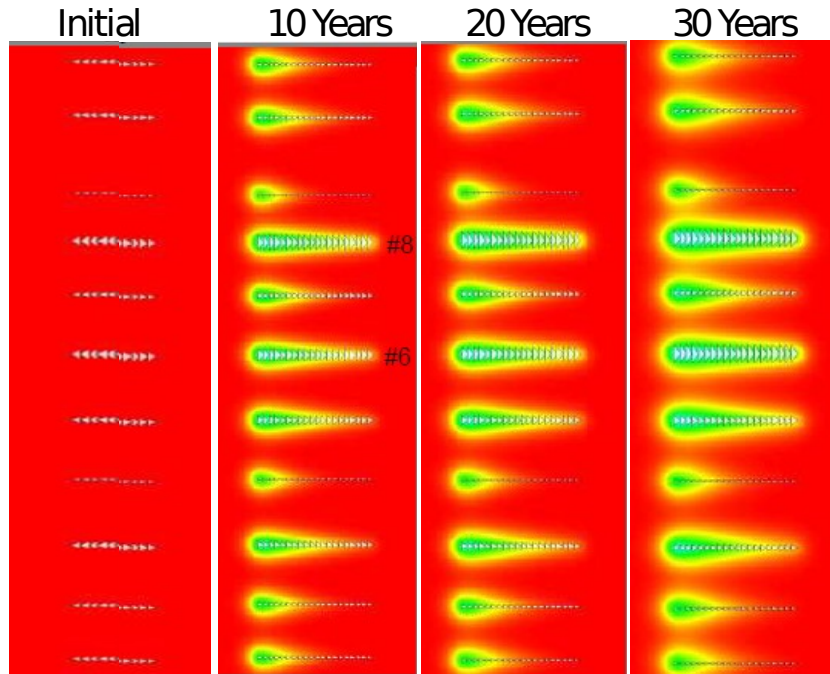


Figure 65. Thermal drawdown visualization for production with no fracture blocking.

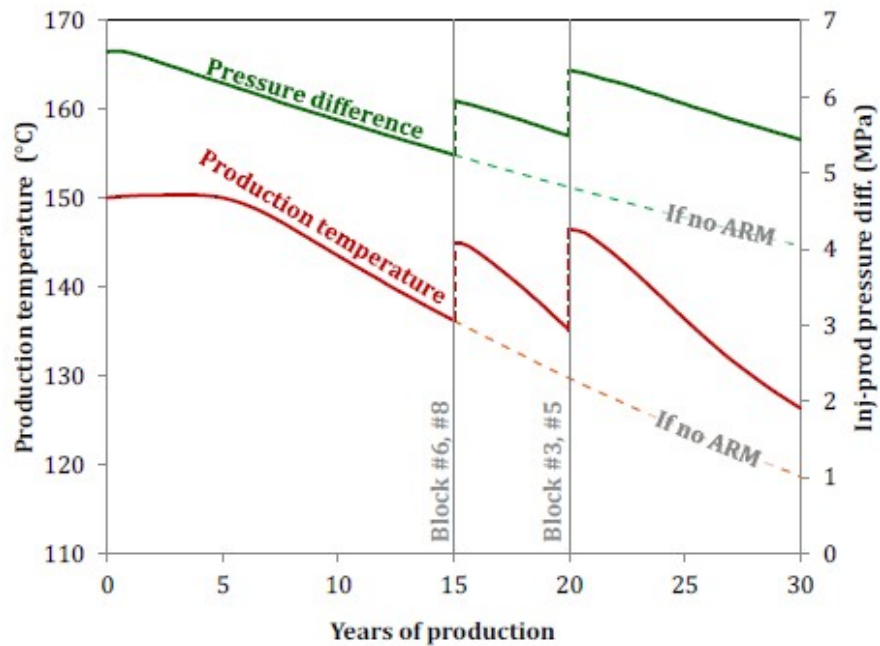


Figure 66. Production temperature and pressure versus time blocking single fractures as they have thermal breakthrough.

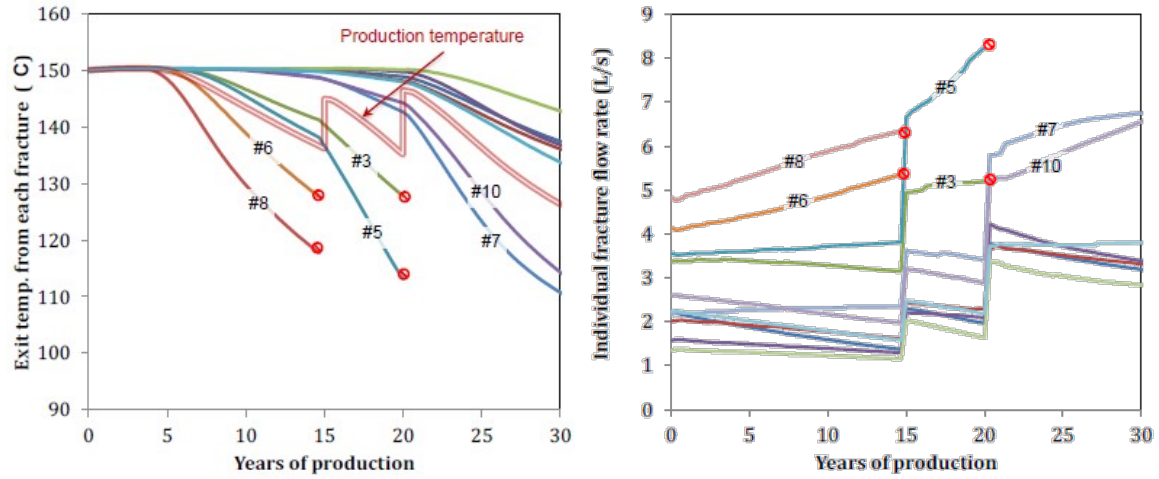


Figure 67. Single fracture exit temperature blocking single fractures as they exhibit thermal breakthrough.

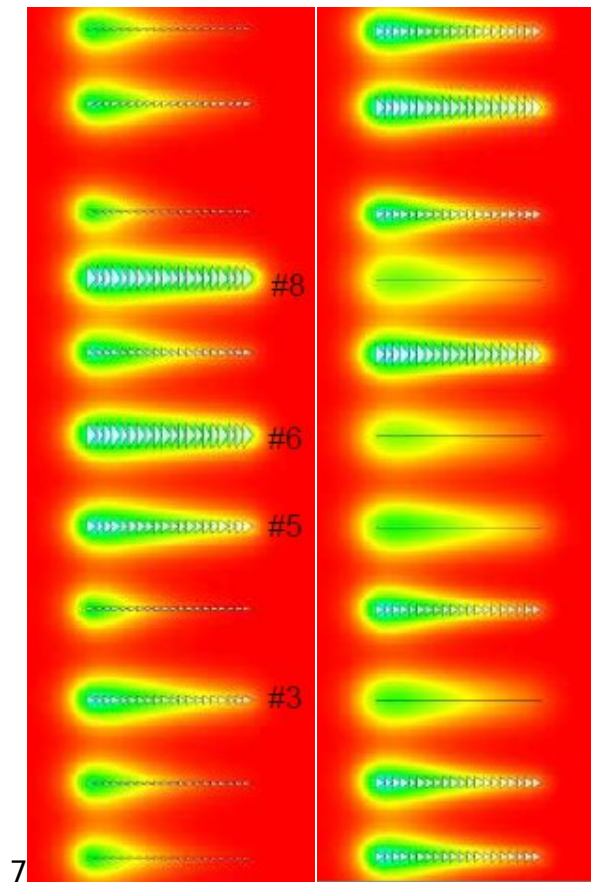


Figure 68. Temperature visualization at 30 years for a reservoir with no management intervention (left) and active reservoir management (right) which blocks fractures #6 and #8 at 15 years and fractures #3 and #5 at 20 years).

50 Thermal-Hydrological-Chemical Processes Simulations Using Discrete Fracture Networks (LBNL)

50.1 Overview

Most of the work for this panel report involved thermal-hydrological-mechanical coupled simulations. These models did not consider geochemical reactive transport, which includes changes to water and gas chemistry, simulation of reactive and conservative tracers, mineral precipitation/dissolution, and geochemically induced fracture porosity and permeability changes, all coupled to multiphase fracture and rock matrix fluid and heat transport. The purpose of the work reported in this section was to couple the aperture changes induced by hydro-mechanical stimulation of fractured rock in an EGS using a distinct element approach (UDEC) with the coupled thermal-hydrological-chemical (THC) processes (TOUGHREACT) following the initial fracture stimulation.

Geochemical and isotopic effects are critically important for reservoir characterization as well as influencing fracture surface area creation, fracture-matrix interaction, and changes in connectivity (e.g., channelization or bifurcation) during EGS stimulation. Over longer time periods, understanding and controlling mineral dissolution/precipitation are necessary for optimizing geothermal reservoir performance from the injection well through the reservoir to power plant operation (e.g., wellbore/pipe scaling, corrosion, gas discharges). The capability to effectively plan, and in essence "validate" the approaches developed to create an economically viable EGS, will require physically based and rigorously tested models of THMC processes.

Lawrence Berkeley National Laboratory (LBNL) is the developer of the TOUGH family of porous-continuum simulators (Pruess, 1990; Finsterle et al., 2014). TOUGH-based codes have been used extensively for geothermal reservoir exploration and management for over 30 years (Dobson et al., 2003, 2004). They include multiphase equation of state capabilities, an integrated finite difference (IFD)

approach allowing rigorous mass and energy conservation, and unstructured 3-D gridding capabilities. TOUGH-based codes can treat hydrothermal processes in fractured rock with single to multiple interacting continuum (MINC) methods (Pruess, 1990; Pruess et al., 1999; Battistelli et al. 1997; O'Sullivan et al., 2001; Finsterle et al., 2014). The reactive transport simulator TOUGHREACT was developed by adding transport of aqueous and gaseous species and mineral-water-gas reactions (kinetic and equilibrium) to the TOUGH2 V2 core, with particular emphasis on simulating hydrothermal processes in fractured rock (Xu and Pruess, 2001a,b; Xu et al., 2001, 2006, 2011; Sonnenthal et al., 2015). Coupled THC simulations in this report were performed using the most recent parallel TOUGHREACT V3.3-OMP that has many improvements for simulating geothermal reservoir THC processes (Sonnenthal et al., 2015).

50.2 Coupled Thermal-Hydrological-Chemical (THC) Model Development

The overall tasks for THC model development were to:

- Implement reactive transport processes into results of discrete fracture THM models
- Use well-described EGS thermal, hydrological, and geochemical properties as initial conditions (i.e., Newberry Volcano EGS)
- Simulate injection and production effects on water chemistry and mineralogy and porosity and permeability changes, with predictions of thermal and tracer breakthroughs over the lifetime of an injector-producer pair.

Like the UDEC simulations, TOUGHREACT simulations for this study are two dimensional, with a reservoir domain located perpendicular to the injecting and producing wells. LBNL worked with Itasca to extract UDEC-derived fracture networks into a TOUGHREACT mesh used for coupled thermal-hydrological-chemical (THC) simulations.

The methodology in creating a THC (or THMC) model is key to the results, because reactive-transport processes are much more sensitive to numerical errors inherent in spatial (gridding) and temporal (time step) discretization than simulation of pressures and temperatures in typical geothermal reservoir models. Because the

methodology must be designed for the specifics of each problem and is not a standard approach, it is described in some detail in this section.

Itasca simulated the aperture field post-stimulation and post-production. For the TOUGHREACT simulations, the post-stimulation aperture field was used as initial conditions to develop a permeability field. TOUGHREACT can consider a discrete fracture network, or a "Multiple Interacting Continuum" (MINC) mesh. However, these are more computationally intensive, so the simpler equivalent continuum was employed but on a relatively finely discretized polygonal mesh.

The stimulated aperture field generated by UDEC was used to create an equivalent permeability field for a single continuum mesh. Because the form of the UDEC mesh geometry and its representation of fractures is very different from that in TOUGHREACT, several levels of abstractions of the UDEC geometry and fracture data were required. The codes and tools for this abstraction were developed as part of the EGS validation and are available for future EGS applications such as FORGE.

Geometric attributes of the UDEC model relevant for a TOUGHREACT mesh consist of the following:

- **Zone** (mesh element)
- **Grid Points** (nodes of zones)
- **Sub-contact** (nodes/edges at the interface between two interacting surfaces); these represent the discretization of a fracture
- **Domain** (nodes that are formed at the intersection of pipes that contain the fluid)

First, a 2D grid was generated by Delauney triangulation of subsampled UDEC block centers (blowup of one region shown in Figure 69a) using the program AMESH (Haukwa, 1999). A fractured region with denser sampling is in the center of the domain. Typical TOUGH2 meshes generated with the program AMESH often appear as shown in

. In some cases, these meshes are adequate for thermal-hydrological simulations; however, accurate reactive transport simulations require a smoothly varying mesh with more equant polygons. To smooth the grid, a technique known as Centroidal Voronoi Tessellation with Lloyd's iteration (Du et al., 1999) was applied until the polygons were nearly equant and the transition between the interior fractured

reservoir and the outer boundary region was smoother (Figure 69b and Figure 69c). Ten iterations were sufficient.

The final 2D smoothed TOUGHREACT mesh is shown in Figure 70a, with original UDEC fracture locations and a blowup of the transition region showing the original UDEC subcontacts and fracture locations (Figure 70b).

The next step was to calculate an equivalent permeability field from the UDEC stimulated fracture apertures. The equivalent permeability grid blocks are assumed to start with the same zone grid points from the UDEC model. Subcontact coordinates are then used to determine fracture locations embedded in the TOUGHREACT mesh. Apertures at subcontacts are used to calculate an equivalent permeability field using the cubic law. The permeability field was assumed to be locally isotropic (within a grid block), but spatially anisotropic.

The detailed methodology is as follows:

- For each fracture subcontact find the enclosing polygon
- Using fracture aperture at each subcontact, calculate grid block permeability using a modified cubic law
- Unfractured rock is assumed to have a permeability equal to 10^{-18} m^2
- The maximum permeability is found at intersecting fractures of large aperture ($\sim 10^{-10} \text{ m}^2$)
- An injector was placed in a high permeability block (domain center) and a producer 500 m away

The contoured permeability field of the center of the stimulated fracture region is shown in Figure 71. The permeability outside the stimulated fracture region was assumed to be uniform.

The main input parameters for the ITASCA UDEC and LBNL TOUGHREACT-based models are listed in Table 14. Some parameters are not used in both codes. TOUGHREACT parameters such as fluid density and viscosity are shown as "EOS1" because they are calculated as a function of changing temperature and pressure using the TOUGHREACT equation-of-state module for pure water (EOS1), whereas UDEC assumed constant fluid properties.

Table 14. THM Input Parameters

PARAMETER	ITASCA (UDEC)	LBL (TOUGHREACT)
X - Dimension	3500 m	3600 m
Y - Dimension	3500 m	3600 m
Length of core region in X	2000 m	2000 m
Length of core region in Y	2000 m	2000 m
Assumed depth of reservoir center	2500 m	3000 m
Depth of water table	2500 m	0 m
Rock density (grain density in TOUGHREACT)	2700 kg/m ³	2700 kg/m ³
Water density	1000 kg/m ³	EOS1
In-situ pressure	9.81 MPa	24.52 MPa
Minimum principal stress (in y direction)	33.1 MPa	NA
Minimum principal stress (in x direction)	66.2 MPa	NA
Poisson ratio	0.25	NA
Bulk Modulus (1/pore compressibility in TOUGHREACT)	40 GPa	40 GPa
Pore thermal expansion coefficient	NA	3.0 x 10 ⁻⁵ /°C
Water viscosity	8.9x10 ⁴ Pa s	EOS1
Initial aperture of primary fractures	3e-5 m	NA
Initial aperture of primary fractures	1e-5 m	NA
Porosity	NA	0.05
Fluid thermal conductivity	6.20E-03 cal/cm	EOS1
Fluid density	1000 kg/m ³	EOS1
Rock specific heat (grain Cp for TOUGHREACT)	0.25 Cal/g/cm	1000 J/kg/°C
Fluid specific heat	1 Cal/g/cm	EOS1
Rock thermal conductivity	3 W/m/K	3 W/m/K
Rock initial temperature	200°C	200°C
Injection temperature	25°C	~7°C
Injection Rate	80 kg/s/km	80 kg/s/km

50.3 Simulations using Newberry Volcano EGS Site Geochemical Data

Previous modeling of the DOE Newberry Volcano (Oregon) EGS Demonstration Site (Sonnenthal et al., 2012) used TOUGHREACT to develop a three-dimensional calibrated model of the initial temperatures and water chemistries based on a postulated intrusive igneous body acting as a heat source; the reaction-transport model used the pre-alteration mineralogy and shallow groundwater chemistry as

the initial geochemical conditions. The model assumed that temperature and pressure distributions had been relatively constant over several thousand years (approximate steady-state condition). The initial pore water and injected groundwater chemistry and mineralogy from this model were used for the EGS Validation Project THC simulations. TOUGHREACT requires an extensive set of thermodynamic data (based on Reed and Palandri, 2006) and kinetic data for minerals, aqueous species, and gases. Kinetic data for minerals were compiled from a wide range of sources (i.e., Palandri and Kharaka, 2004; Carroll et al., 1998).

Initial primary mineral abundances (volume fractions of solid mineral assemblage), kinetic data (rate constants, activation energies, transition state law exponents), and assumed reactive surface areas are given in Table 15. Dissolution and precipitation kinetics are assumed to be the same unless specifically noted. Potential secondary mineral kinetic data and reactive surface areas are given in Table 16. Note that secondary mineral abundances are given about an order-of-magnitude greater surface area since these are formed primarily on fracture surfaces in contact with flowing water, in contrast to the bulk rock minerals, most of which are embedded in the low permeability rock matrix.

Table 15. Primary Mineral Volume Fractions and Kinetic Data used in the THC Model (based on Bargar and Keith, 1999; Keith and Bargar, 1988). Kinetic data include the rate constant at 25°C (k_0), activation energy E_A , the transition state law exponents (n and m), and the reactive surface area A_i .

Primary Minerals	Volume Fraction	k_0 mol/ m²/s	E_a kJ/ mol	n	A_i cm²/ g
Albite-high	0.14	7.08e-13	67.7	0.333	1.0
Anorthite	0.10	3.16e-15	67.7	0.5	1.0
Microcline	0.20	1.78e-13	36.	0.333	1.0
Sanidine-high	0.02	1.78e-13	36.	0.333	1.0
Diopside	0.01	2.82e-13	22.	0.5	1.0
Hedenbergite	0.01	2.82e-13	22.	0.5	1.0

Phlogopite	0.01	2.82e-13	22.	0.5	1.0
Annite	0.01	2.82e-13	22.	0.5	1.0
Muscovite	0.04	1.994e-10	0.0	0.333	1.0
Quartz	0.35	4.52e-14	90.1	1.0	1.0
Cristobalite	0.02	3.45e-13	68.9	1.0	20.

Table 16. Potential Secondary Mineral Kinetic Data used in the THC Model (based on Bargar and Keith, 1999; Keith and Bargar, 1988)

Secondary Minerals	k_0 mol/ m ² /s	E_a kJ/ mol	n	$k_{0,H+}$ mol/ m ² /s	$E_{a,H+}$ kJ/ mol	n_H +	A_i cm ² / g
Calcite	1.2598e-9	41.87	1.0	6.4565e-4	36.1	0.5	10.
Siderite	1.2598e-9	62.76	1.0	6.4565e-4	36.1	0.5	10.
Ankerite	1.2598e-9	62.76	1.0	6.4565e-4	36.1	0.5	10.
Amor. Silica (diss)	7.32e-13	60.9	1.0	-	-	-	20.
Amor. Silica (prec)	1.00e-10	0.0	m=4.4	-	-	-	20.
Chalcedony (diss)	7.32e-13	60.9	1.0	-	-	-	20.
Chalcedony (prec)	1.00e-10	0.0	m=4.4	-	-	-	20.
Illite	1.52e-16	58.6	0.2857	-	-	-	20.
Nontronite-Ca	3.02e-13	88.0	0.2725	-	-	-	20.
Nontronite-Mg	3.02e-13	88.0	0.2725	-	-	-	20.
Nontronite-Na	3.02e-13	88.0	0.2725	-	-	-	20.
Nontronite-K	3.02e-13	88.0	0.2725	-	-	-	20.
Kaolinite	1.0e-13	7.1	0.5	-	-	-	20.
Epidote (ordered)	3.02e-13	88.0	0.333	-	-	-	10.
Daphnite	3.02e-13	88.0	0.333	-	-	-	10.
Clinochlore	3.02e-13	88.0	0.333	-	-	-	10.

Heulandite	5.66e-13	58.0	0.14 29	-	-	-	20.
Analcite	2.37e-13	58.0	0.5	-	-	-	20.
Magnetite	3.98e-14	90.9	1.0	-	-	-	20.
Hematite	3.98e-14	40.	1.0	-	-	-	20.
Goethite	1.17e-11	0.0	1.0	-	-	-	20.
Pyrite	1.0e-8	50.	1.0	-	-	-	20.
Pyrrhotite	1.4e-9	100.	1.0	-	-	-	20.

The initial reservoir water chemistry and injection water chemistry (in parentheses where different) are based on the groundwater chemistry injected into Newberry 55-29 well (Sonnenthal et al., 2012, 2015). Reservoir and injection water chemistry were assumed to be same, except for the added sodium 1,5-naphthalene disulfonate tracer and LiCl tracers (Table 17) in the injection water.

The groundwater chemistry is not initially in equilibrium with the reservoir mineral assemblage. Typically, the system would be run to steady-state over a long period in a 3-D hydrothermal model with different deep geothermal water or magmatic inputs to bring the minerals and fluids to a steady-state (potentially close to equilibrium) with the flow regime. In this case, because the purpose was not to describe an actual hydrothermal system and owing to the model geometry as a simple 2-D planar layer, the reservoir fluid composition was not initially run to a pseudo-steady-state with the minerals. However, prior to fluid injection the reservoir fluid was speciated at the reservoir temperature and then added to reservoir. A pseudo-steady-state is attained in the first time step, thus nearly equilibrating the fluid with the minerals. Thus, a small amount of some minerals dissolve (e.g., feldspars) and some precipitate (e.g., calcite), which bring the fluid to near equilibrium nearly instantaneously, owing to the high reaction rates at 200 °C. Therefore, the reservoir fluid chemistry becomes quite different chemically from the injected water chemistry, and is similar to the producer chemistry shown in Table 15.

The sodium 1,5-naphthalene disulfonate tracer is a thermally degrading tracer at temperatures over 300°C (Rose et al., 2001), and therefore was conservative in

these simulations. Final in-situ reservoir fluid compositions at the injector and producer are also shown and discussed later.

Table 17. Initial, Stimulation (Parentheses), Final Reservoir Injector and Producer Water Chemistry

Component	Initial and (Injection Water) Total Conc. (mg/kg H₂O)	Injector 30 Years	Producer 30 Years
Na+	1.8269e-3	1.8257e-3	3.8706e-3
K+	1.2788e-4	1.2778e-4	3.3723e-5
Ca+2	4.7408e-4	4.7261e-4	1.4486e-5
Mg+2	9.8745e-4	9.8438e-4	4.8637e-10
Al+3	1.0e-8	9.6045e-11	8.5618e-5
Fe+2	1.0e-9	8.0628e-9	6.1009e-11
SiO ₂ (aq)	9.9859e-4	2.4472e-4	4.6897e-3
Cl-	8.4619e-5 (2.2256e-2)	2.2241e-2	1.4878e-2
F-	2.6318e-5	2.6300e-5	2.6297e-5
HCO ₃ -	3.7694e-3	3.7669e-3	1.1180e-3
HS-	1.0e-10	8.9523e-11*	2.0756e-5*
SO ₄ -2	2.6024e-5	2.4120e-5*	3.5918e-10*
Li+	1.0e-10 (2.2256e-2)	2.2241e-2	1.4850e-2
Br-	1.0e-12	9.9933e-13	9.9920e-13
Napthalene Sulfonate 2,15	1.0e-12 (5.9159e-4)	5.9119e-4	3.9472e-4
pH	7.97	8.30	8.20
Temp. (°C)	200. (25.)	7.5	196.4

**HS⁻ and SO₄⁻² concentrations in final reservoir and produced waters are given as actual species concentrations rather than total concentrations, since reduction of SO₄⁻² to HS⁻ results in totals that are not similar to species*

concentrations (owing to the mathematical representation of redox species in TOUGHREACT).

The simulation was performed by injecting into a high permeability feature in the after-stimulation aperture field at a rate of 80 kg/s along a fully penetrating vertical well in a 1 km thick domain. The production well was assumed to produce at the same rate at an arbitrary location 500 m from the injector, also in a high permeability feature. The simulation was run for 30 years of injection and production.

A sodium 1,5-naphthalene disulfonate tracer was used to monitor breakthrough of injected water in the production well (Figure 72). The simulations show channeling along the permeability pathways derived from the UDEC-generated DFN fractures, particularly in the one-year timeframe. Note that the tracer flows down through the most permeable pathway and then is drawn along a more direct path to the producing well. However, the tracer is also transported in several other circuitous pathways as the flow field organizes into a typical dipole field. The tracer breakthrough occurs (Figure 72 lower right) after approximately seven months of injection and the tracer concentration at the production well begins to level out after approximately 2 years, increasing slowly thereafter.

Even though tracer breakthrough is observed after less than one year of production, the temperatures at the producing well (Figure 73) are fairly stable over the first 20 years of production and decline only slightly to a final temperature of 196.4°C after 30 years (Table 17). Over the first year the injection pressure steadily increases (not shown), and the production pressure steadily decreases (Figure 73b). From about 5 to 15 years production, the pressure at the producer stays relative constant, and then declines slowly. As will be seen in later figures, mineral precipitation along the pathway away from the injector reduces the permeability, thus causing the pressure to decline at a constant production rate.

Temperatures for the reservoir region are shown after 2 and 30 years in . As seen from the temperature curve at the producer in Figure 73a, temperatures are only declining slightly near the producer, even though there is a large decline around the injector and along the most permeable main pathway. In Figure 75 a blow-up of the injector region is shown with the fluid flux vectors superimposed. Multiple pathways

are evident in the temperatures and in the flux vector field. The cooling of the region around the main pathway extends to a width of about 50 meters once the flow field has switched from being dominated by the injector to being influenced strongly by the producer.

The TOUGHREACT simulations also produce chemical and porosity changes over time which result in permeability changes. Reactive species concentrations such as Ca^{+2} and Mg^{+2} are shown in Figure 76. The high calcium concentrations in the injected groundwater result in calcite precipitation in the reservoir owing to its reverse solubility with temperature. However, continued injection cools the region where calcite has precipitated, and eventually re-dissolution of calcite takes place. In Figure 77 the highest Ca concentrations are seen in the outer regions of the flow pathway, where calcite previously dissolved closer to the injector has given rise to higher concentrations than those in the injector. Figure 77 shows that the regions of greatest calcite precipitation (blue) migrate further from the injector over time.

Dissolution of primary minerals such as plagioclase and potassium feldspar also demonstrates the large region affected by fluid flow (Figure 78). In both cases the greatest amount of dissolution takes place some distance away from the injector, mainly because cooling directly near the injector decreases the solubilities and reaction rates of most silicate minerals.

Precipitation of chlorite and pyrite are shown in Figure 79. Chlorite is primarily formed by injection of Mg-rich groundwater (Figure 76) with the maximum amount also occurring away from the injector along the flow pathway. Pyrite is formed predominantly by release of Fe from primary minerals (pyroxenes) and reduction of sulfate in the groundwater to sulfide. Final fluid chemical compositions in the reservoir at the injector and at the producer are given in Table 17. The composition in the reservoir at the injector is close to but not exactly the same as the injection fluid, and the producer is quite evolved containing some injected components (tracers) et al. derived solely by reaction with the primary reservoir minerals.

The chemical changes show the complexity of the fracture networks in that they do not lie upon a direct path between the injection and production wells. This is an effect of the discrete fracture network. The permeability changes (k/k_0) over time mirror the changes in the mineral abundances (Figure 80), with about a 40%

increase along the paths near the injector (dark blue) and a smaller change along the main pathway to the producer (pale red). Hence, over time, while there may be a small decrease in pressure at the injector owing to increased permeability, the pressure at the producer is also dropping because it becomes slightly harder to produce from the reservoir region where permeability is declining. For a constant pressure at the producer, this would be reflected in lower flow rates over time.

The equivalent permeability method captures the main geochemical effects and trends in permeability; however, it likely underestimates the effect on fracture permeability. Mineral precipitation and dissolution are likely affecting a smaller total volume (< 1%) than the 5% equivalent continuum porosity used in the simulations. Therefore, permeability changes given the same model geochemistry and DFN apertures could result in much larger permeability increases and declines. These types of model assumptions inherent in all approaches can only be evaluated by comparison to data from a range of spatial scales from lab-scale to near well-bore scale, to reservoir-scale.

50.4 Coupled THC Simulation Conclusions

The results of the TOUGHREACT simulations demonstrate that the simulation of chemical effects coupled to mechanical stimulation can yield valuable information regarding the initial stimulation effectiveness as well as the long-term evolution of an EGS reservoir. The complexity of the pathways shows the value of integrating a DFN-based permeability field into a continuum model.

At this point, the simulations serve strictly as a demonstration and cannot yield generalized conclusions. It is clear that changes in reservoir pressures and temperatures can be affected by mineral precipitation and dissolution, and that the resulting patterns can be highly complex and variable in time and space. However, the magnitude of geochemically driven permeability changes is likely underestimated because most flow is through small aperture widely spaced fractures that likely are in temperature and pressure disequilibrium with the rock matrix. Multiple-continuum methods could address these issues and are likely necessary in such systems. Even more complex patterns will certainly emerge in three-dimensional simulations. In particular, fracture networks in 3-D result in

anisotropic permeabilities and flow is likely to be channeled along preferred pathways and fracture intersections. Aside from such heterogeneity, injection leads to significant effects on 3-D reservoir pressures and modifications in the stress regime, which can only be treated in 3-D (Ingebritsen et al., 2010). Increasing permeabilities may potentially drive buoyant convection in systems that were initially characterized by conductive thermal gradients. The simulations to this point in time show, however, that useful numerical experiments can be developed using the hybrid DFN-continuum approach. Fully coupled THMC approaches are available to investigate EGS stimulation processes (Kim et al., 2015; Smith et al., 2015; Sonnenthal et al., 2015).

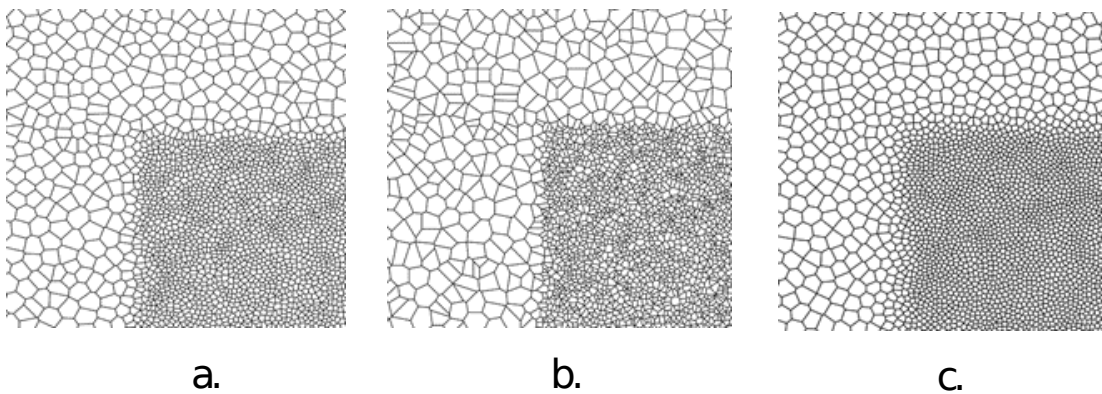


Figure 69. (a) 2D TOUGHREACT mesh generation using Delaunay triangulation of UDEC subcontacts. (b) Remeshing using Centroidal Voronoi Tessellation with 5 Lloyd's iterations. (c) Final smoothed mesh after 10 Lloyd's iterations.

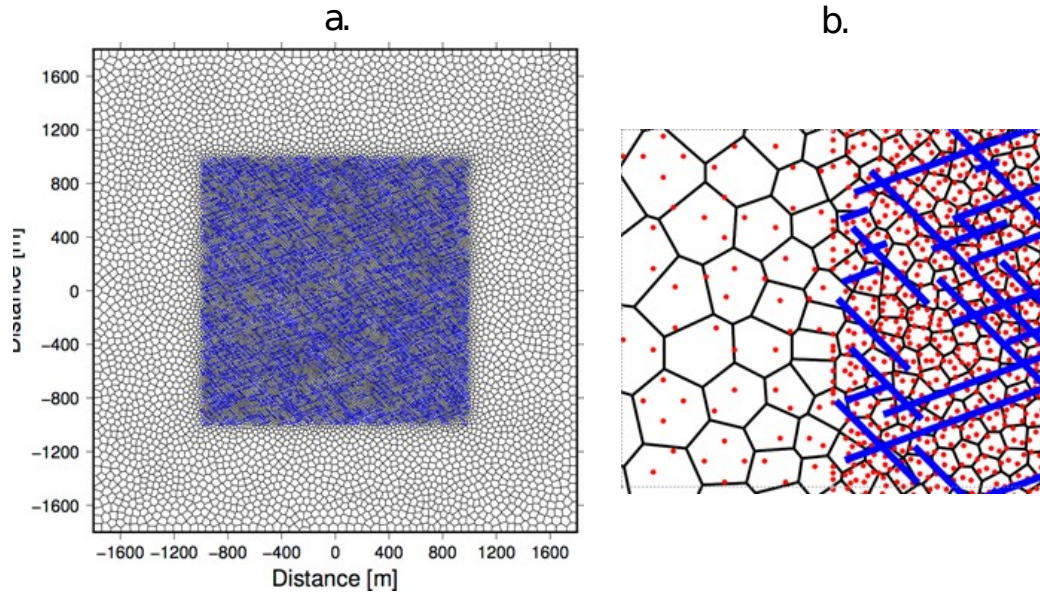


Figure 70. (a) Final 2D TOUGHREACT mesh of entire domain showing overlain UDEC stimulated fracture network. (b) Blow-up of edge of fractured region showing smoothed TOUGHREACT mesh with original UDEC subcontacts (red points) and UDEC fracture network (blue lines).

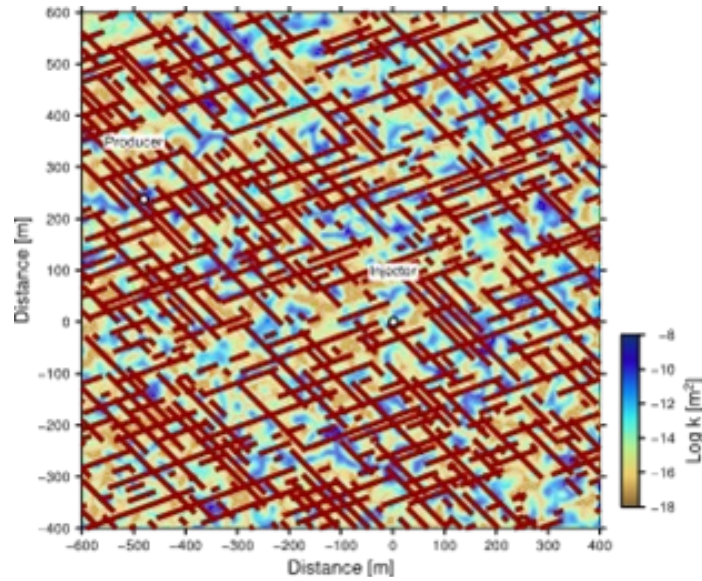


Figure 71. Contoured equivalent permeability field of interior stimulated reservoir region. UDEC fracture network superimposed (dark red). Equivalent permeability was field calculated using the cubic law applied to the UDEC fracture aperture distributions weighted over polygonal TOUGHREACT mesh elements. The permeabilities vary from about 10^{-9} m^2 (dark blue) to 10^{-17} m^2 (brown).

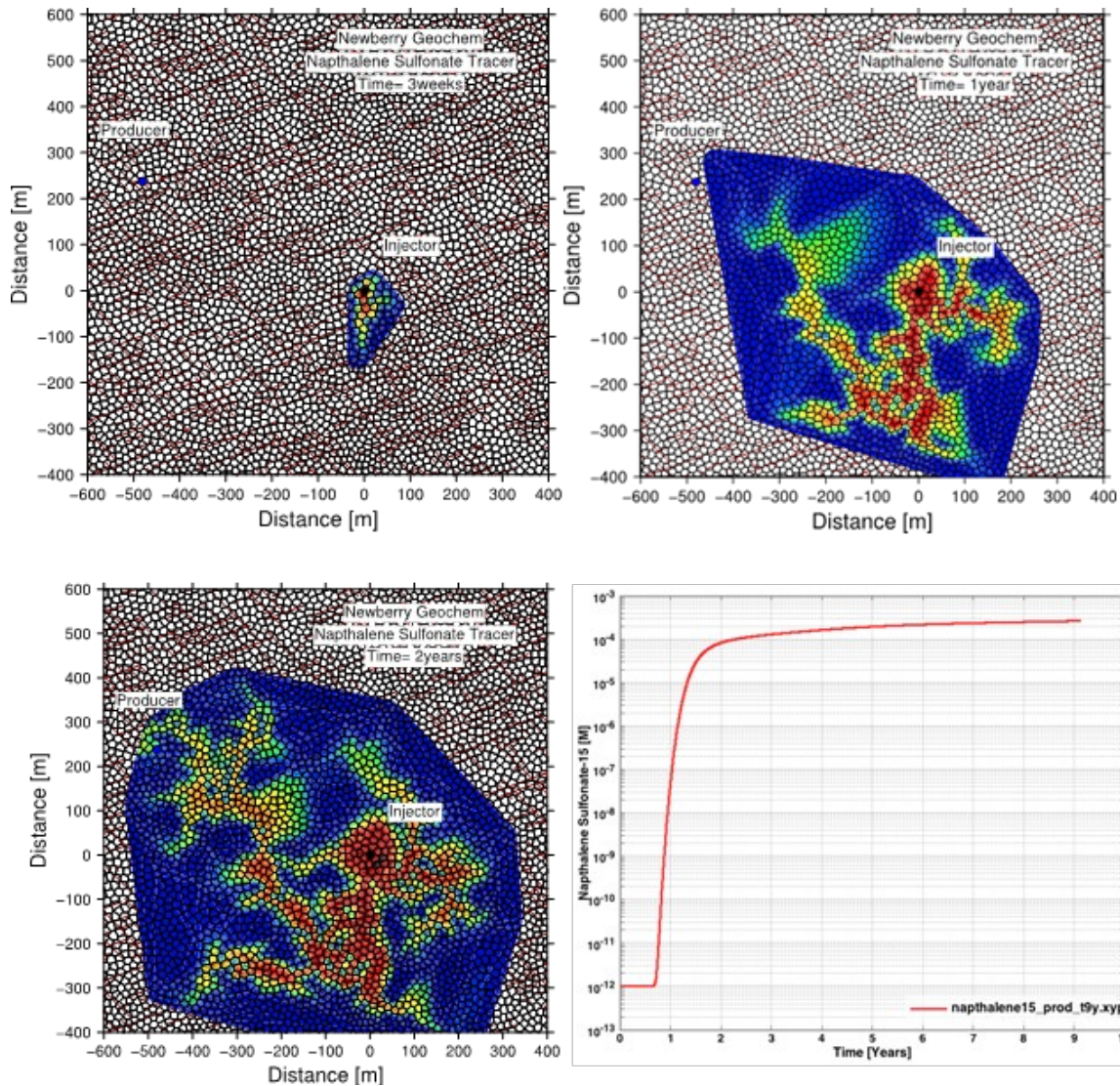


Figure 72. Sodium 1,5-naphthalene disulfonate tracer concentrations after 3 weeks, 1 year, and 2 years of injection and production. The figure shows the simulation grid for TOUGH as well as in dark red the DFN model developed in UDEC. At lower right, the naphthalene sulfonate-2,15 tracer concentration at the producing well is shown over nine years of injection and production.

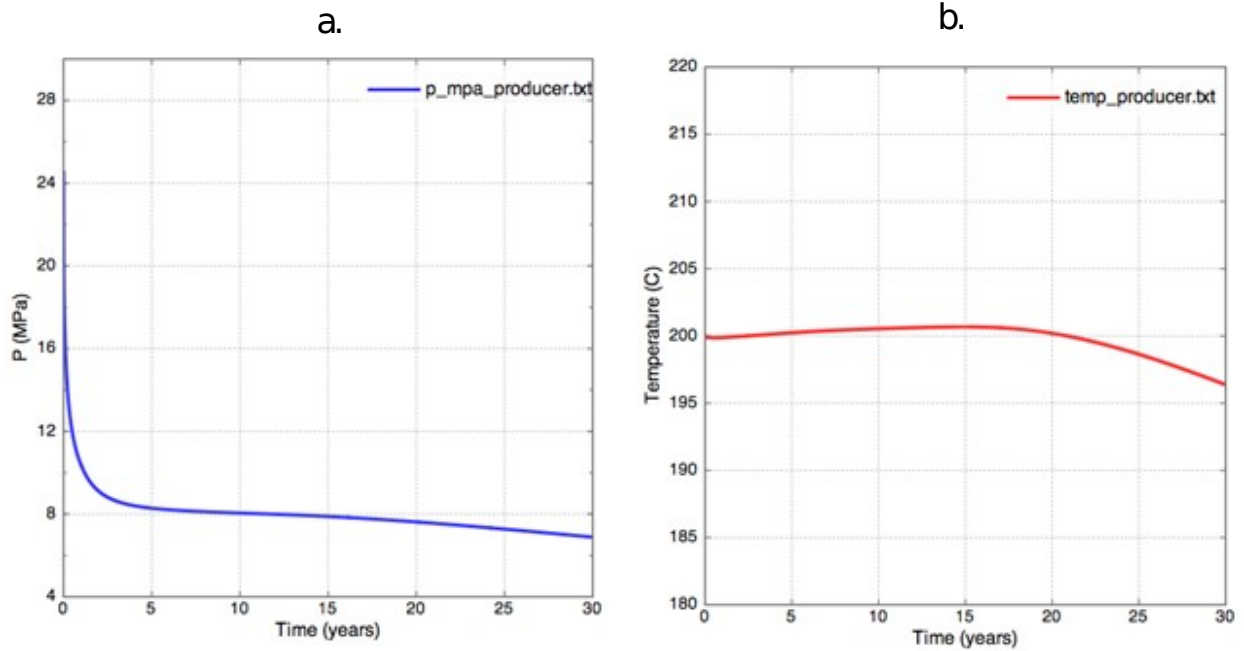


Figure 73. a) Temperature at producing well over 30 years injection and production at 80 kg/s. Note that temperatures only start declining after 20 years, and by 30 years have only dropped to 196 °C. b) Pressure at producing well over 30 years. Note the early pressure drop, followed by fairly stable pressures, and then a more gradual decline after 15 years.

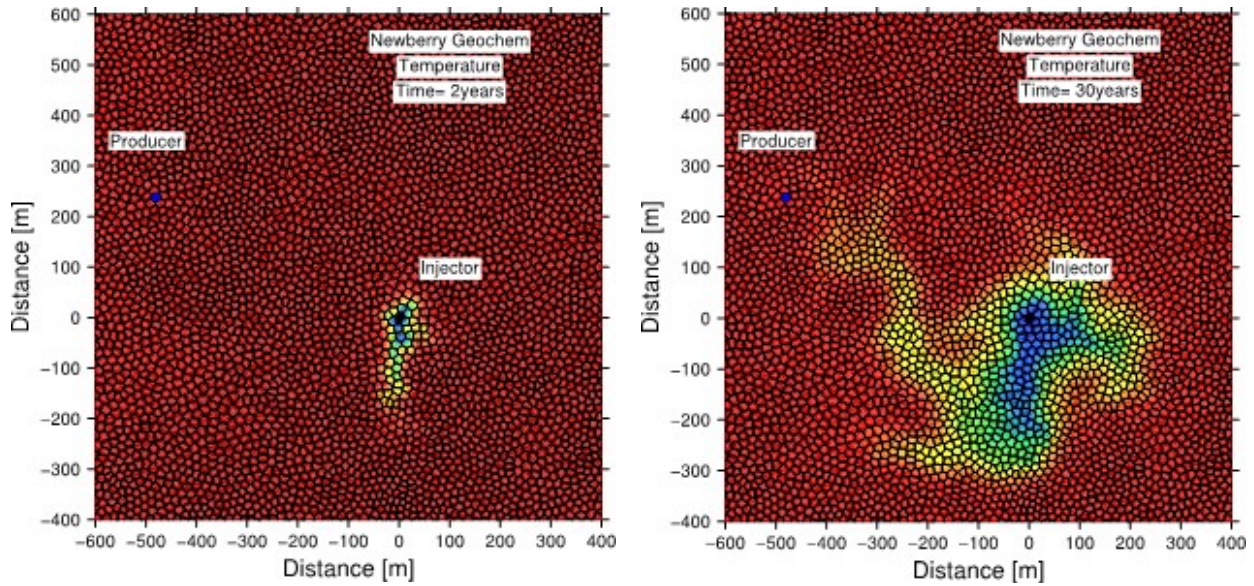


Figure 74. Temperature field in reservoir with simulated injection and production. Note that even though a large region around the injector has cooled significantly after 30 years, the production well is still close to the initial reservoir temperature. a) 2 years. b) 30 years

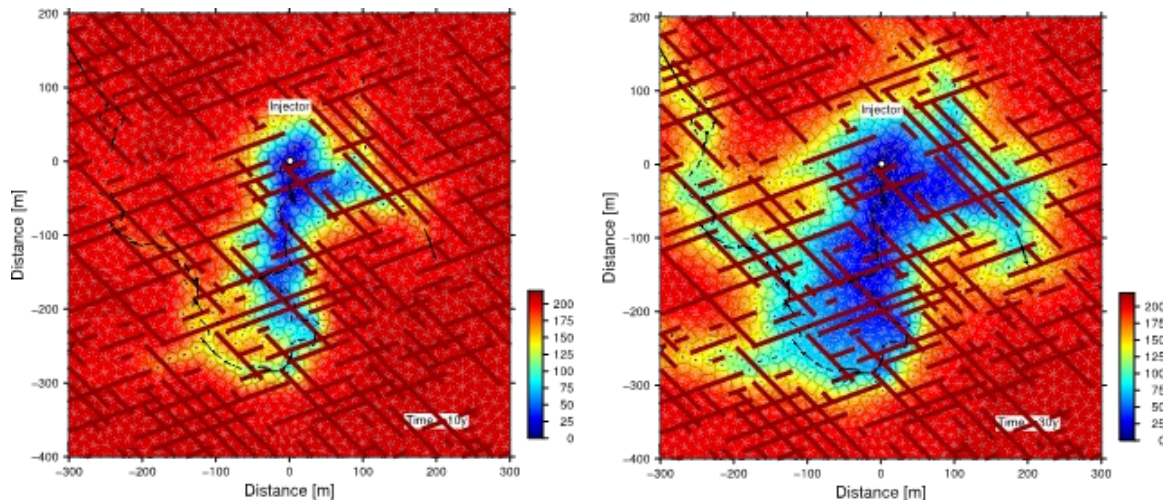


Figure 75. Temperature field around injector of simulated injection and production. Flux vectors show fluid flow focused in preferred permeability pathways. UDEC fracture network superimposed (dark red). a) 10 years. b) 30 years

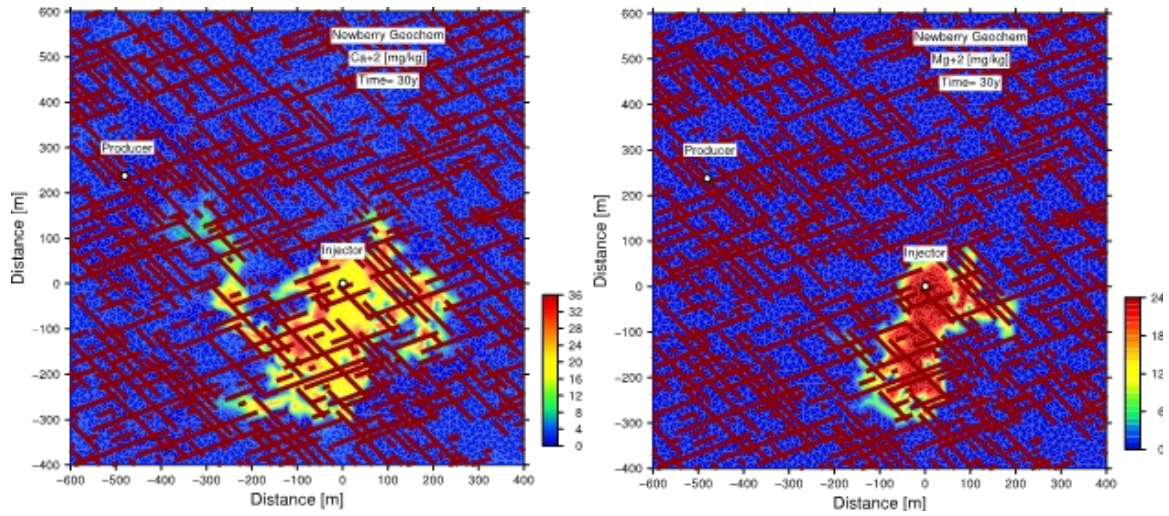


Figure 76. Calcium and magnesium concentrations (mg/kg H₂O) in reservoir after 30 years.

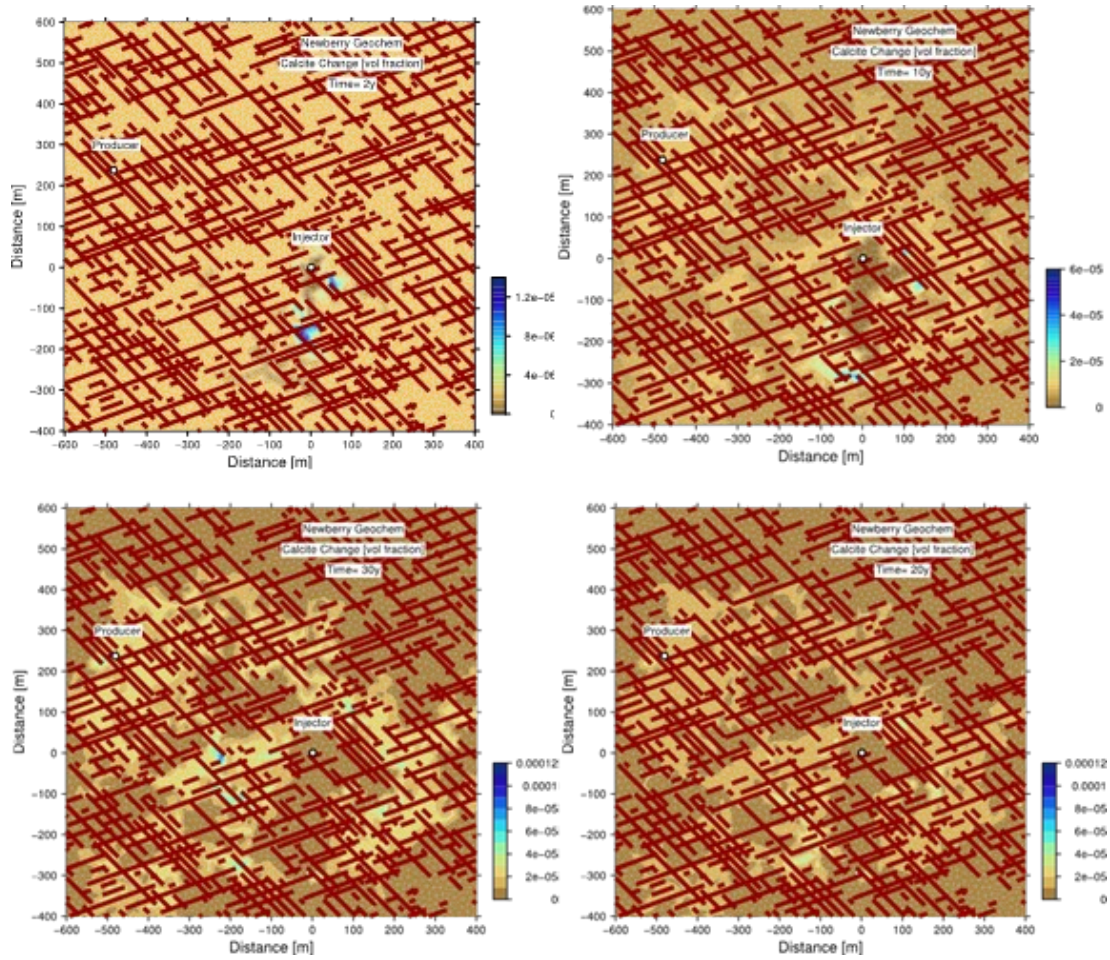


Figure 77. Calcite precipitation after 2, 10, 20, and 30 years.

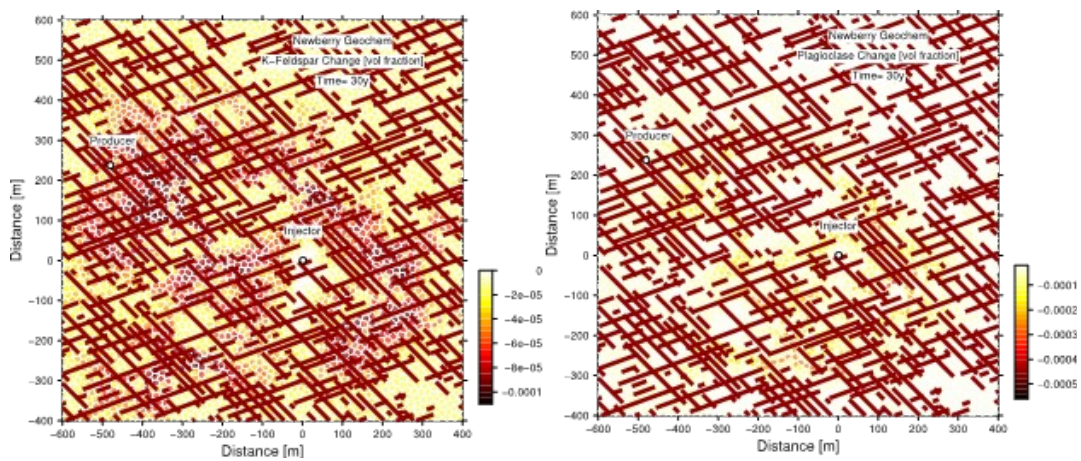


Figure 78. Plagioclase (albite+anorthite) and potassium feldspar (microcline+sanidine) dissolution after 30 years.

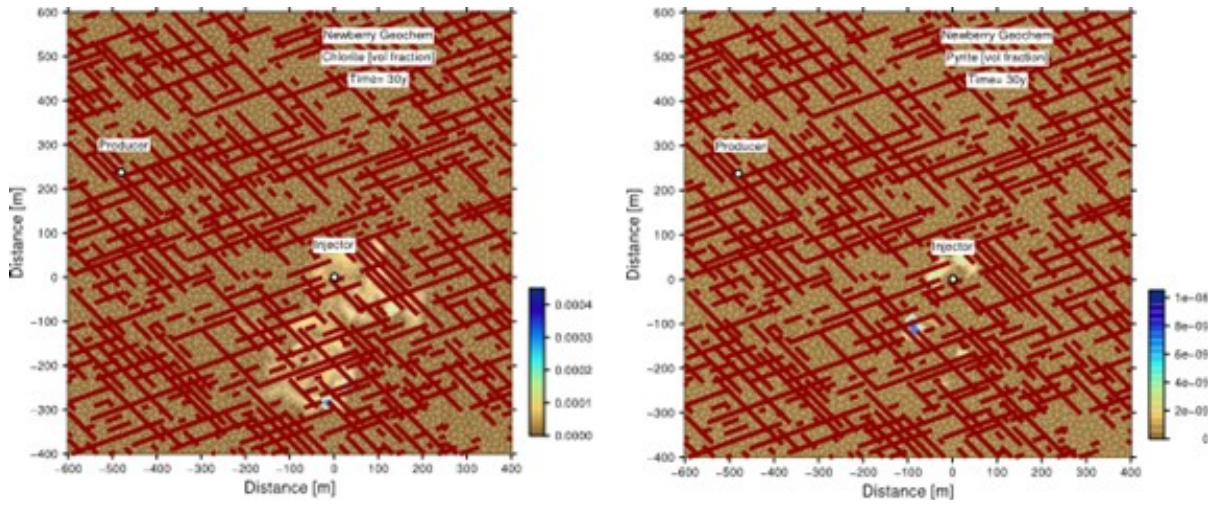


Figure 79. Chlorite (daphnite+clinochlore) and pyrite precipitation after 30 years.

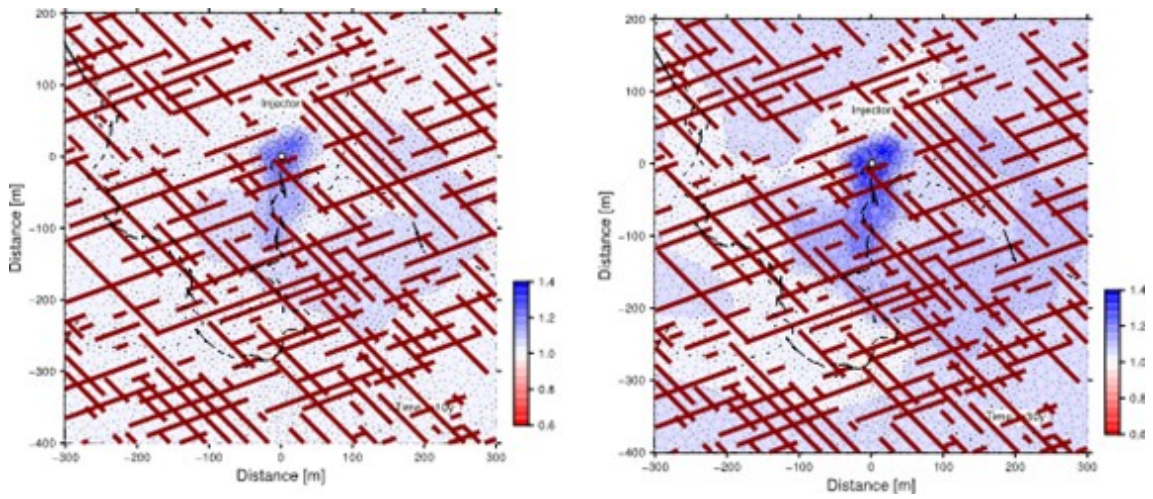


Figure 80. Permeability ratio (k/k_0) after 10 and 30 years.

51 Three-Dimensional Hydro-Thermal Simulations Focusing on the Role of In Situ Stress State

51.1 Stress State and EGS Development

A major appeal of EGS is the possibility of tapping geothermal energy anywhere. Two key variables for assessing the regional feasibility of EGS are the state of in situ stress and the geothermal gradient. The stress state controls the orientation of artificial fractures and the potential for reopening natural fractures. It also has practical implications for wellbore stability and drilling feasibility. The geothermal gradient determines the drilling depth necessary to reach exploitable thermal resources.

A brief review of in situ stress, faulting, and fracture stimulation is helpful to understanding the design and results of the numerical experiments. The classic model of faulting and stress (Anderson, 1951) relates the style of faulting -- normal, thrust, and strike-slip -- to the relative magnitudes of the three principal stresses (Figure 81). Particularly important are the orientations of the greatest principal stress, σ_1 , relative to the least principal stress, σ_3 . In portions of the Earth's crust where deformation is extensional, the greatest principal stress is vertical, the least principal stress is horizontal, and the dominant style of faulting is normal. Where the crust is being shortened or compressed horizontally, the greatest stress is horizontal and acting in the direction of compression, and the least stress is vertical. This stress state produces thrust faults. Where the greatest and least principal stresses are both horizontal, and the vertical stress is the intermediate principal stress, the mode of faulting is strike-slip involving horizontal displacements.

The stress state controls the orientation of induced hydraulic fractures. Hydraulic fractures will grow perpendicular to the least principal stress as shown in Figure 81. Hydraulic fractures will be horizontal in thrust-faulting regimes, where σ_3 is vertical. Hydraulic fractures will be vertical in normal and strike-slip faulting regimes where σ_3 is horizontal.

EGS development is also concerned with developing reservoirs by stimulating natural fractures under so-called "critical stress" conditions. The optimal natural

fracture orientations for critical stress (Zoback, 2007), or hydro-shearing, are on two conjugate planes that contain the intermediate stress direction, σ_2 , and lie at an acute angle to the maximum stress direction, σ_1 (Figure 81). Faults will occupy one or both conjugate fracture orientations.

Critical stress is a very important design factor in EGS development (see also Section 3.2). It refers to the relationship between fault and fracture shearing due to fluid pressures in the fractures, and stems from research that gained momentum from observations of injection-well induced seismicity in the 1970's (Zoback, 2007). If the fractures are rough, shearing may cause dilation and greatly enhance their permeability (Figure 18). The shear dilation will occur at pressures that are usually lower than those required to create new hydraulic fractures, provided the natural fractures are oriented within a range about the optimal orientations. This range is determined by the stress state, fluid pressure in the fractures, and the frictional and roughness properties of the natural fractures. Depending on the stress state, some fractures may be in a state of critical stress under reservoir fluid pressure conditions and be open without any additional hydraulic stimulation.

As induced hydraulic fractures are generally thought to act as short circuits in the EGS circulation, one approach to EGS design has been to shear-stimulate a network of natural fractures with larger effective surface area and tortuosity than a single induced hydraulic fracture. A design approach that favors natural fracture stimulation will use stimulation pressures that are sufficient to cause shearing on natural fractures but not so great as to create induced hydraulic fractures.

Stress state also has a large effect on the optimal drilling direction. The optimal well orientation will usually be the maximum stress direction, both for intersecting hydraulic fractures and natural fractures that are optimally oriented for shear stimulation. That direction is vertical only for thrust fault regimes. It will be horizontal for both normal and strike-slip dominated regions.

51.2 Stress State, and EGS Development

52 Description

Finnila et al. (2015, 2016) developed models of EGS performance for three faulting terrains in the United States. The simulations used a mixture of actual data and

assumptions for a normal faulting site (Desert Peak, Nevada: Robertson-Tait and Johnson, 2005; Davatzes and Hickman, 2009; Swyer and Davatzes, 2013; Dempsey et al., 2014), a strike-slip faulting site (Salton Sea, California: Kilb, 2010; Holland, 2002), and a thrust faulting site (Mirror Lake, New Hampshire: Johnson and Dunstan, 1993; Bennett et al., 2006). The full list of properties for the simulations appears in Finnilla et al. (2015). Although they use some site-specific information, the simulations are not intended to assess any specific location's performance or any region's suitability for EGS development.

The models targeted a depth where rock temperature would be 200°C, which put the simulations at different depths depending on the thermal gradient. Like the analyses in Chapter 2, the models targeted an EGS performance of 70 kg/s rate with a thermal decline of less than 10% over 20 years. The simulations also looked at impedance, with a target of limiting the surface injection pressures to 70 MPa (~10,000 psi).

The list of rock types, stresses, and thermal gradients for the three models appears in Table 18.

53 Regional stress and heat flow

Maps of heat flow and stress state in the United States (Figure 82) show that heat flow and stress state are often correlated. Lower heat flows occur in the eastern half of the US, where EGS reservoirs need to be deeper in order to attain sufficiently high temperatures for electricity production.

Each faulting terrain model included both a hydraulic fracturing scenario involving induced fractures normal to the minimum stress, and a hydro-shearing scenario where the circulation system relied upon stimulated critically stressed fractures. The simulations also looked at issues of impedance based on assumed permeability enhancement from the hydro-shearing stimulation. The hydro-shearing model used Golder Associates' FracMan DFN code, which contains a module for hydraulic fracture growth and shear stimulation of natural fractures (Dershowitz et al., 2010; Cottrell et al. 2013).

Table 18 presents the rock types, thermal gradients, and in situ stresses. The target temperature for the simulations was 200° C, which, given the different thermal

gradients in the three faulting terrains, led to simulations at quite different depths. The strike-slip faulting terrain had the highest thermal gradient leading to a shallow 2.2 km depth. The normal faulting terrain is only somewhat deeper at 3.3 km, while the thrust faulting terrain in the much lower heat flow region of the northeast US required a depth of 8.3 km.

The natural fracture transmissivity values were assumed to decrease with increasing stress (depth). The normal faulting and strike-slip faulting models used fracture transmissivities in a range between 10^{-8} and 7×10^{-7} m²/s. The deeper thrust faulting model used transmissivities of 10^{-9} m²/s for all fractures. Hydro-shearing was assumed to increase the transmissivity of the natural fractures by a factor of 1000 based on Miller (2015). The transmissivity values and their changes during the stimulation primarily affect the impedance calculations.

The natural fracture networks for simulating the archetypical faulting terrains appear in Figure 83, which shows a 2 km² region with 1 km thickness including the fracture network model, a stereographic projection of poles to the fractures within the model, and the well layouts. Each simulation uses three wells, a central well for stimulating the fracture network and injection and production wells, which are one kilometer apart and 500 meters from the stimulation well. Wells are horizontal for the normal faulting and strike-slip faulting scenarios and vertical for the thrust faulting scenario. The orientations of critically stressed fractures are distinctive for each archetypical terrain as shown in stereographic pole plots of critical fractures for the models in Figure 83 and Mohr stress diagrams (Figure 84).

54 Archetypical faulting terrain simulation results

The regional fault terrain simulations produced several significant observations:

- Faulting terrains control the optimization of borehole layouts
- Faulting terrains correlate with heat flow and determine the depth of the reservoir
- Gradients of stress and fluid pressure may drive fracture growth vertically, creating preferential flow paths that may be into either cooler rock at shallower depth or into hotter rock at greater depth.

54.1.1.1 Stress state and well layouts

The relationship of stress state to borehole layout is straightforward and illustrated in Figure 83 and Table 18. Thrust faulting terrains produce either horizontal hydraulic fractures or shallow dipping, stimulated natural fractures. By contrast, normal and strike-slip faulting terrains both produce vertical hydraulic fractures and steeply dipping stimulated natural fractures. Due to temperature constraints on directional drilling equipment, most geothermal development has used vertical or steeply inclined wells in contrast to oil and gas reservoirs where directional and horizontal drilling have become routine. Only thrust faulting terrains produce fractures that are optimally oriented for vertical and steeply inclined drilling. The development of EGS in other faulting terrains will be greatly enhanced by the ability to drill horizontal wells in the maximum horizontal stress direction. The thermal simulations for this study assumed that directional drilling was available and utilized horizontal wells for the strike-slip and normal faulting simulations.

54.1.1.2 Heat flow and reservoir depth

As discussed above, heat flow in the United States (Figure 82) is highly variable, with the highest heat flows in the Basin and Range province and lower heat flows in the eastern half of the United States. Assuming a target of 200° C for a commercial EGS operation, the reservoir depth in a low heat flow region such as the northeastern US will be several kilometers. For the specific case in the simulations, the New Hampshire generic site has a depth of 8.3 km. By contrast, target depths in a high heat-flow region in the Basin and Range province such as Desert Peak, Nevada, or in strike-slip faulting regimes such as the Salton Sea, California, will be only a few kilometers. The shallower depth of the reservoir decreases drilling costs lowering pumping requirements for both reservoir creation and operation. Such stress conditions also lead to lower impedance, as fracture opening and stimulation must overcome lower pressures due to the lower in situ stresses.

54.1.1.3 Effects of stress and fluid pressure gradients

A significant feature of the simulations is the preferential opening of fractures at shallower depth. This appears in the hydro-shearing simulations for the thrust faulting case () where the flow lines predominantly pass through the upper,

shallower fractures. The thermal simulation of the normal faulting hydraulic fracturing case shows the preferential growth of the fracture to shallower depths and the preferential cooling of upper parts of the fracture ().

The source of this behavior is the contrast between the fluid pressure in the fracture and the in-situ stress and the stress normal to the fracture faces. Secor and Pollard (1975) identified this behavior, which occurs when the gradient of minimum stress, which controls the stress acting normal to the fracture face, is steeper than the hydrostatic gradient, which is the pressure inside the fracture (Figure 87). At the depth of injection, the fluid pressure in the fracture must equal or exceed the minimum stress in order for the fracture to open. As the fracture opens, the pressure gradient inside the fracture will parallel the hydrostatic gradient with depth. At depths greater than the injection depth, the pressure falls below the injection pressure (if the fracture grows that way at all), while at depths shallower than the injection depth, the difference between the pressure in fracture and the stress normal to the fracture will increase. This difference will cause apertures to be larger at shallower depths, thus creating preferential pathways at shallower depths. The increase in aperture with shallower depth appears in Secor and Pollard's (1975) illustration of this phenomenon (Figure 87). Depending on the relative gradients of stress and fluid pressure, the preferred growth and opening may also occur at greater depth rather than shallower depths. This phenomenon was observed in the Rosemanowes EGS site in the UK, where microseismic activity migrated downward during stimulation (Pine and Batchelor, 1984).

The preferential opening of a fractures at shallower depth has a strong effect on EGS thermal performance. The normal faulting hydraulic fracture is the worst performing of all the faulting simulations (Figure 88). It has an early thermal breakthrough and rather odd inflection in the thermal decline, at around three years and 185 °C. A similar inflection appears, with less thermal decline in the hydro-shearing simulation of the normal faulting case. This behavior appears to be associated with a circulation pathway that follows the larger fracture apertures, which occur in shallower, cooler rock. Thus, not only does the aperture enhancement create some short circuiting, but the short circuit passes through cooler rock.

The effects of vertical gradients in stress, fluid pressure, and temperature also affect the thrust fault case. While the initial reservoir temperature at the injection depth is 200°C, the initial production temperature is cooler at around 190°C. The lower production temperature appears to reflect pathway connectivity that intersects the production well at a shallower depth than the injection well. Because there is a thermal gradient, inflow points at shallower depths, and pathways that pass through shallower depths, will produce at cooler temperatures than are present at the injection depth.

54.1.1.4 Simulation of impedance

Stimulation was assumed to multiply the transmissivity of critically stressed fractures by 1000². After simulating the stimulation process, the fracture network model for each regional simulation was reduced to the 10% most transmissive fractures. An investigation of impedance in these regional models used this reduced network to calculate the injection well pressure assuming an injection rate of 0.07 m³/s and production rate of -0.07 m³/s. A review of impedance values from current and historical EGS sites shows a range from approximately 3 MPa/l/s at Fenton Hill and Newberry to 0.2 to 0.3 at Soultz-sous-Forêt (Finnila et al., 2015, Table 6). The decrease in impedance due to stimulation in the simulations (Table 18) produces ranges that are very roughly comparable to observations, between 0.04 and 0.44 MPa/l/s for nearly all simulations. Higher impedance for hydraulic fracturing in the thrust faulting regime reflects stresses at the depth of the reservoir, which are due both the high horizontal stress gradients with depth and the depth required to reach rock with exploitable temperatures.

55 Simulations with constant material properties and depths

55.1.1.1 Model description

Finnila et al. (2017) examined the effects of natural fracture set orientation and regional stress state EGS impedance and thermal evolution keeping lithology,

2

For lack of a better source the stimulation factor was based on Miller's (2015) analysis of Basel, Switzerland information. In general, understanding the enhancement of transmissivity

thermal gradient, well geometries and both original and hydro-sheared fracture transmissivity constant.

Simulations using the same depth, temperature, and material property values isolate more the effect of stress on EGS performance. This study assumed that there were two fracture sets which could be either aligned or not aligned with the in-situ stresses. The three fracture cases were (1) two aligned sets where both fracture sets were oriented for shear stimulation (see Figure 81), (2) one aligned set, and (3) no aligned sets, where neither set would be capable of shear stimulation.

The Constant Material Property models use an initial reservoir temperature of 210° C at 3500 m, and the injection water has a temperature of 75°. The well spacing is 875 m and the open lengths of the wells are 600 m. The normal faulting and strike-slip faulting simulations use horizontal wells at depth of 3500 m. The thrust-fault simulations have open intervals spanning a depth range from 2950 m to 3550 m. Unlike the horizontal wells which have constant initial temperature over their length, the vertical wells have a temperature range from 177° to 213°C. Other model properties and stress conditions are documented in Finnila et al. (2017).

55.1.1.2 Natural fractures and critical stress

Aligned sets strike symmetrically about σ_1 with a conjugate angle of 30° (Figure 89). The orientations are not constant but have a variability that produces a dispersion of orientations about the mean trend. For the in-situ stresses shown in Table 19, Mohr diagrams (Figure 89) show the orientations of the critically stressed fractures and the percentages of the fracture populations that are critically stressed. Critical stress is based on a Mohr-Coulomb failure criterion with a friction angle of 30°. Alignment of a fracture set in one of the conjugate directions results in approximately 85% to 90% of the fractures in that set being critically stressed. If both sets are aligned, the percentage of critically stressed fractures lies between 85 and 90% of the total fracture population. If only one set is aligned, 45% to 50% of the total population of fractures is critically stressed. If neither set is aligned with the principal stresses, only 4% to 16% of the fractures are critically stressed. The normal faulting model with no fracture sets aligned produced the lowest percentage

of critically stressed fractures yet resulted in insufficient connectivity and conductivity to produce a 70 l/s flux between the injection and the production well.

55.1.1.3 Impedance results

Impedance is alternatively defined by the injection pressure divided by either a mass (MPa/kg/s) or a volume flow rate (MPa/l/s). All fractures are assigned an initial mean transmissivity of $4.6E-8$ m²/s. The transmissivity of critically stressed fractures is assumed to increase by a factor of 1000, as with the Archetypical Faulting Terrain simulations.

As the results in Table 19 show, the alignment of fractures relative to the stresses has a large effect on the impedance. Decreasing the number of aligned sets from 2 to 1 increases the impedance by a factor of approximately 3. Having no aligned sets increases the impedance by a factor of approximately 6 relative to a single aligned set and by 20 with respect to having two aligned sets. A target impedance for this study was 0.15 MPa/l/s, which requires approximately 10 MPa service injection pressure to create a flux of 70 l/s. The simulations with a single aligned fracture set met this criterion for all faulting cases despite having higher impedance. The simulations with no aligned sets produced impedance values that exceeded the target.

55.1.1.4 Thermal Results

The thermal results in Figure 90 have several notable features. First, there is no result for normal faulting with no aligned sets, because this simulation did not produce a connected fracture network with sufficient conductivity. For the normal faulting and strike-slip faulting simulations, the differences between one aligned set and two aligned sets are minor. This is not surprising because both simulations use vertical fracture sets aligned with the same conjugate angle about the intermediate principal stress.

It is useful to compare the three fracture-set cases for a single faulting regime, and also to compare the same fracture set cases between different faulting regimes.

For the normal stress simulations (Figure 90, upper left) and strike-slip simulations (Figure 90, middle left), there is very little difference between behaviors for two aligned sets and a single aligned set. The two aligned sets perform slightly better,

probably due to better access to the surface areas of both sets. Having neither set aligned produces either a higher rate of thermal decline, as in the strike-slip model, or no connectivity, as in the normal stress model. These behaviors may be specific to the realizations used and not necessarily a unique feature of the normal strike-slip faulting stress state.

55.1.1.5 Summary of three-dimensional hydro-thermal simulation results

A major finding of the three-dimensional simulations was the effect of differences in fluid pressure and in situ stress gradient with depth. Depending on the relative magnitudes of these gradients, both hydraulic fractures and shear-stimulated natural fractures may have a preference for propagating either upward or downward, and to have apertures that increase in size with the vertical direction of propagation. For the simulations developed here, the preference was for upward propagation, which meant that fracture pathways had a tendency to develop into shallower, cooler rock. This has an effect on EGS performance. While the results cannot be used in a quantitative manner for EGS design, they do point out the importance of understanding the relative magnitudes of the stress and fluid pressure gradients.

The Constant Material Property models show the advantages of sites where the natural fractures are preferentially aligned for critical stress stimulation. Multiple fracture sets with favorable orientations produce the best EGS results, but even a single set in a favorable orientation may produce acceptable results. Potential development sites where there are no favorable natural fractures will require the creation of induced hydraulic fractures to develop sufficient connectivity for EGS circulation, with the potential pitfall of creating short circuits.

Stress Regimes and Fault Types

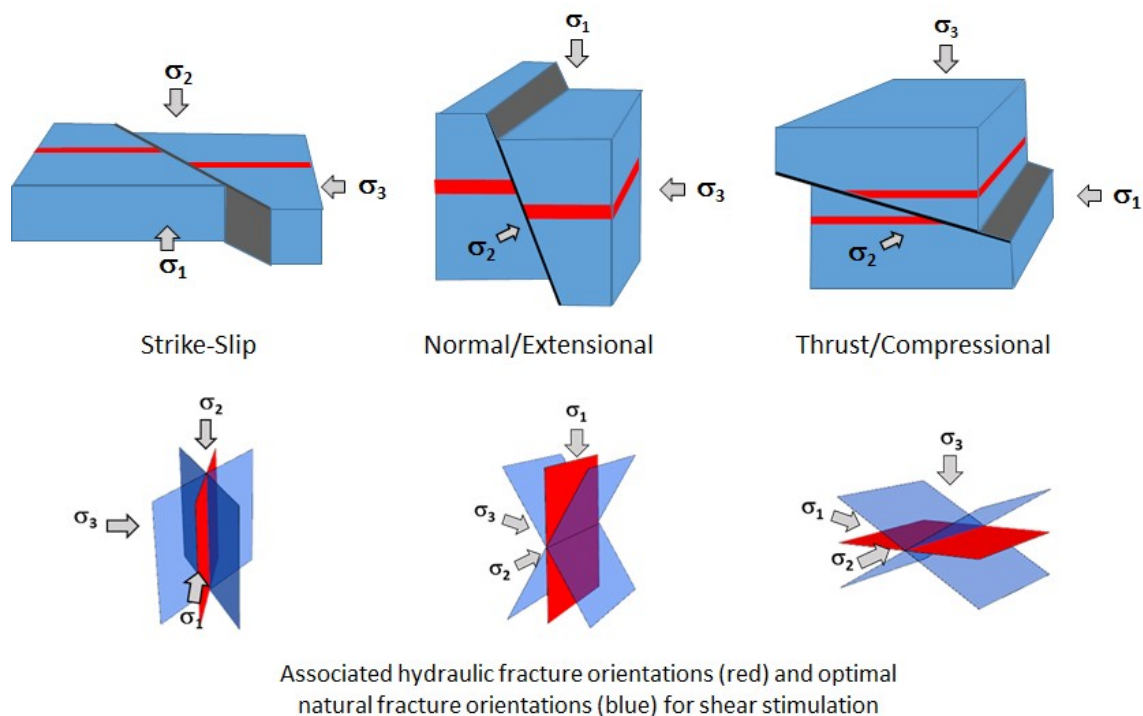


Figure 81. In situ stress states and their relationship to faulting, hydraulic fracturing, and favorability of natural fracture orientation for hydro-shearing. The three regional stress regimes appear in the upper panel with the orientation of principal stresses (σ_1 largest) and the associated fault geometries. The lower panel shows the orientation of hydraulic fracture for each regime (perpendicular to the least principal stress, σ_3) and the most favorable orientation to create hydro-shearing, which is two orientations at an acute angle to the maximum principal stress (σ_1)

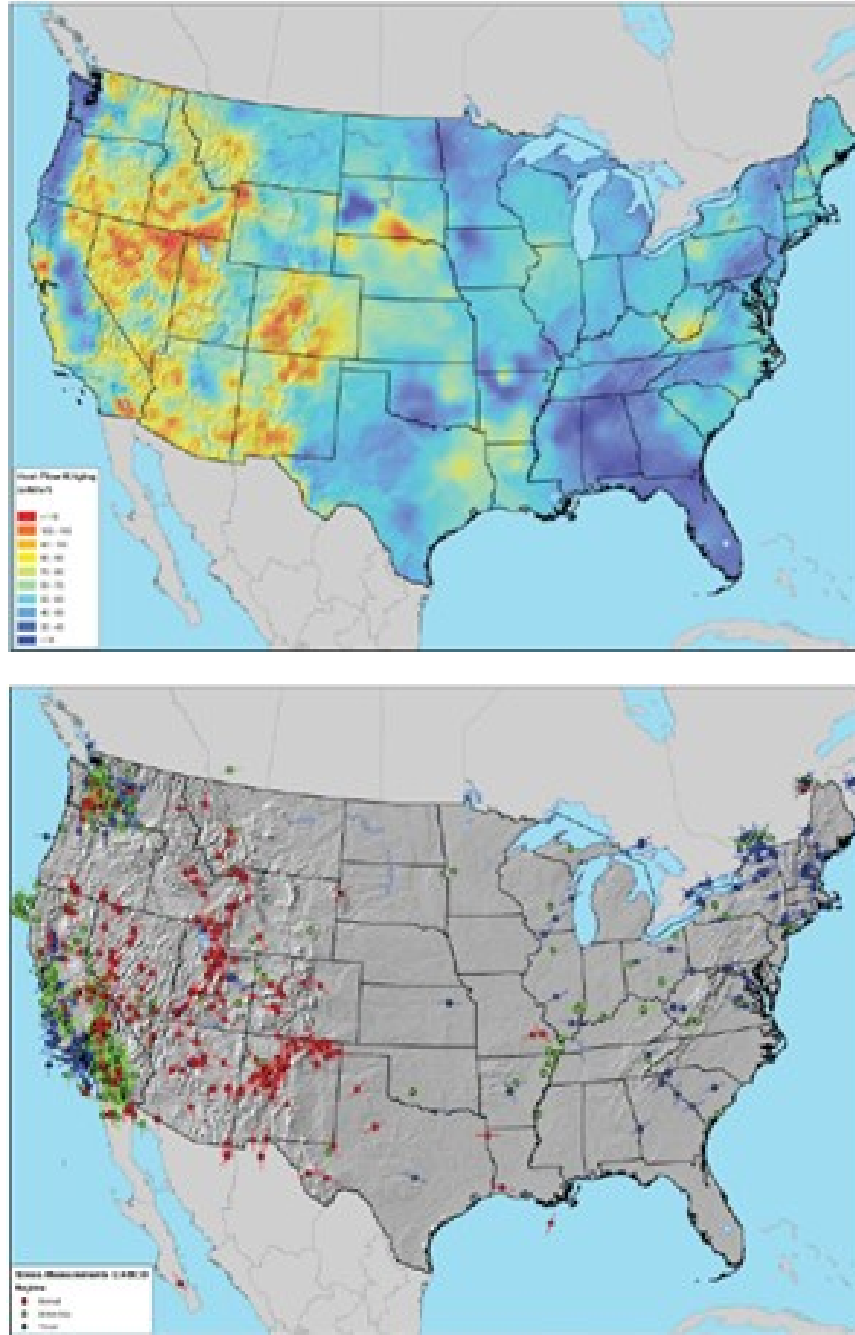
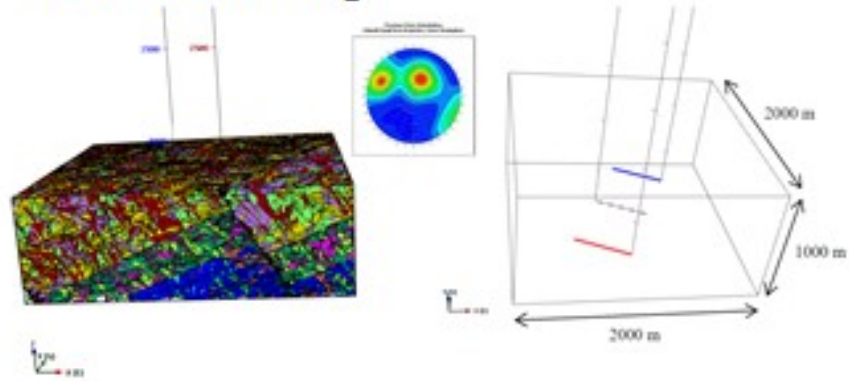
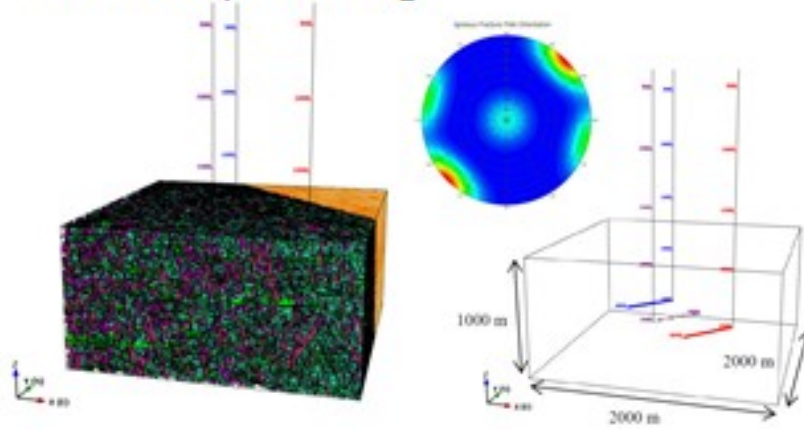


Figure 82. Maps of heat flow (top) and stress state (below) (Reinecker et al., 2005) in the lower 48 states of the United States (from Williams and DeAngelo, 2015). Higher heat flows are in red. Regional stress regimes are divided into normal faulting (red), strike-slip (green) and thrust faulting (blue) on the figure on the right. High heat flows associate most with normal faulting (west, basin-and range province) and least with thrust faulting (east and north-east)

Normal Faulting



Strike-Slip Faulting



Thrust Faulting

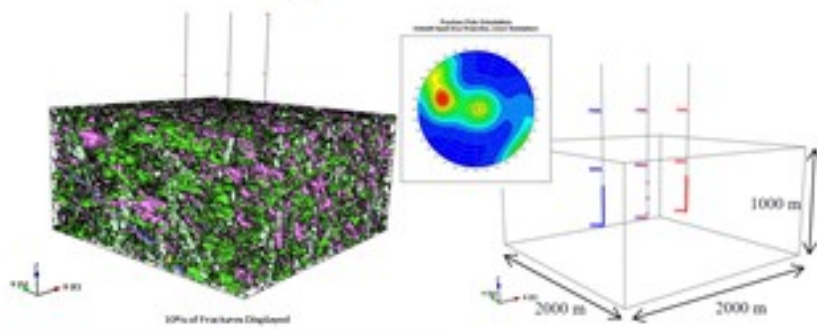


Figure 83. DFN model for Normal, Strike-Slip, and Thrust faulting with stereographic plots of fracture poles and orientations of wells.

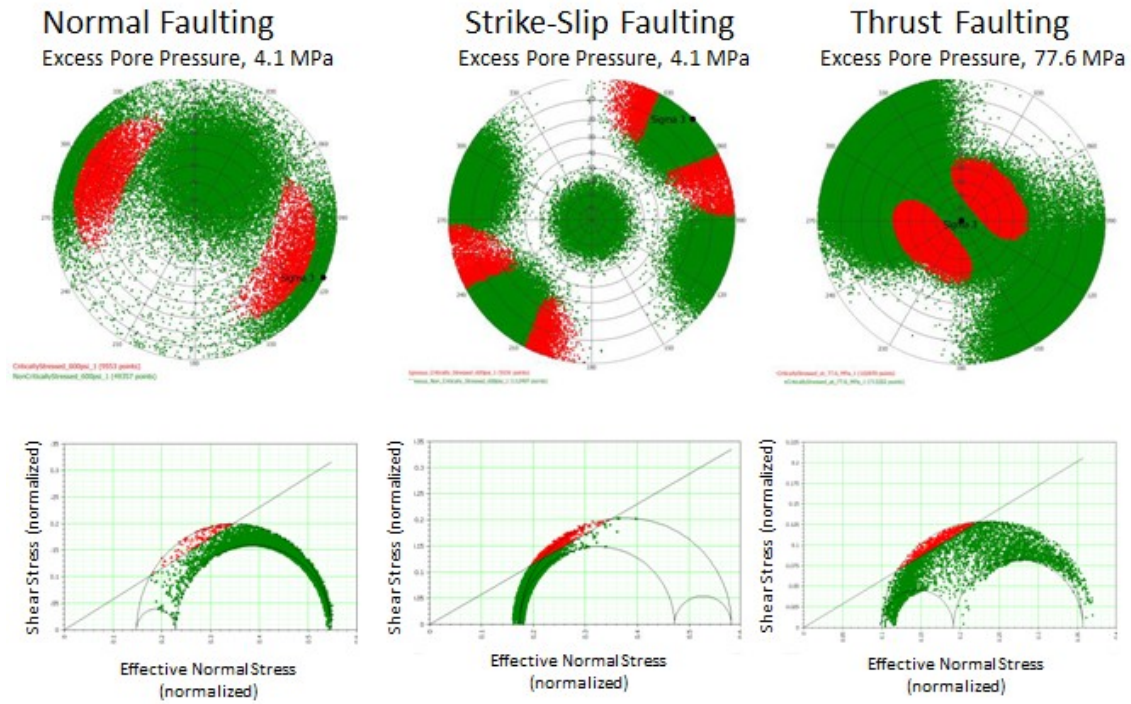


Figure 84. Critically stressed (hydro-sheared) fractures in archetypical models. Upper: pole stereographic plots of all fractures (green) and critically stressed fractures (red). Lower: Mohr diagrams of shear and normal stress with shear and normal stresses on all fractures (green) and critically stressed fractures (red).

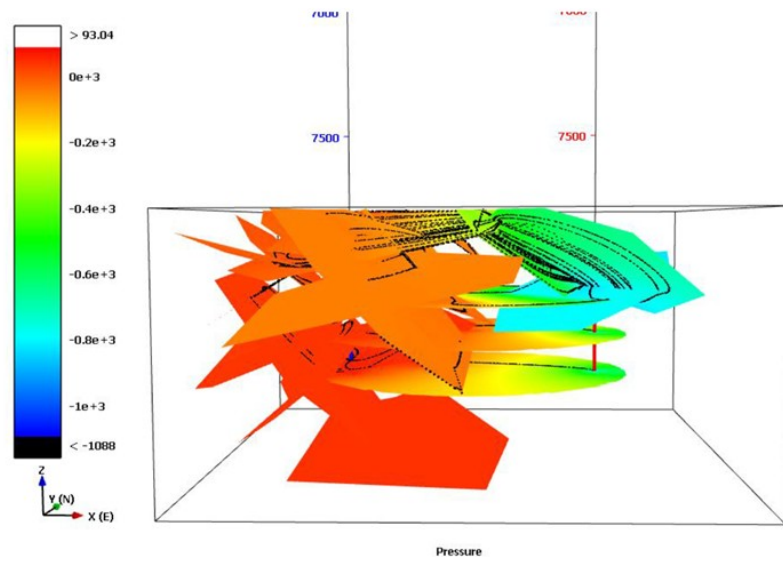
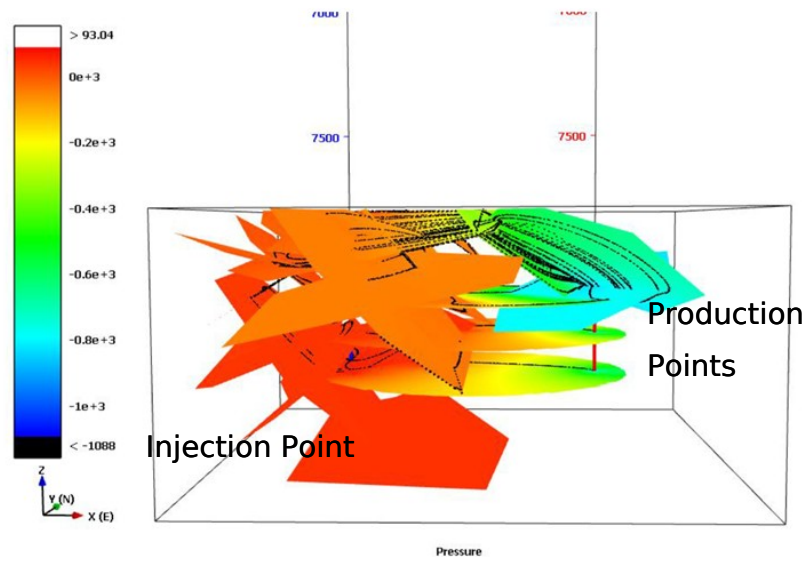


Figure 85. Extracted fractures for flow and thermal simulation in thrust faulting model. Color shows pressure, and dashed lines are flow lines. Note the preferential flow due to larger fracture opening (apertures) at shallower depth. The major portion of the production passes through shallower, cooler rock and enters the production at a shallower depth than the injection point.

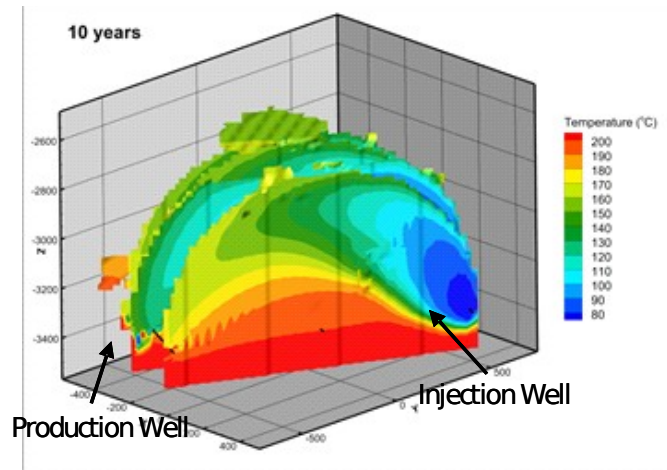


Figure 86. Water temperature in vertical hydraulic fractures of normal faulting regional model after 10 years. Injection well located on right side with Production well located on left side of figure (scale is in meters). Note preferential cooling due to larger opening (apertures) of fractures at shallow depths. (Finnila et al., 2015).

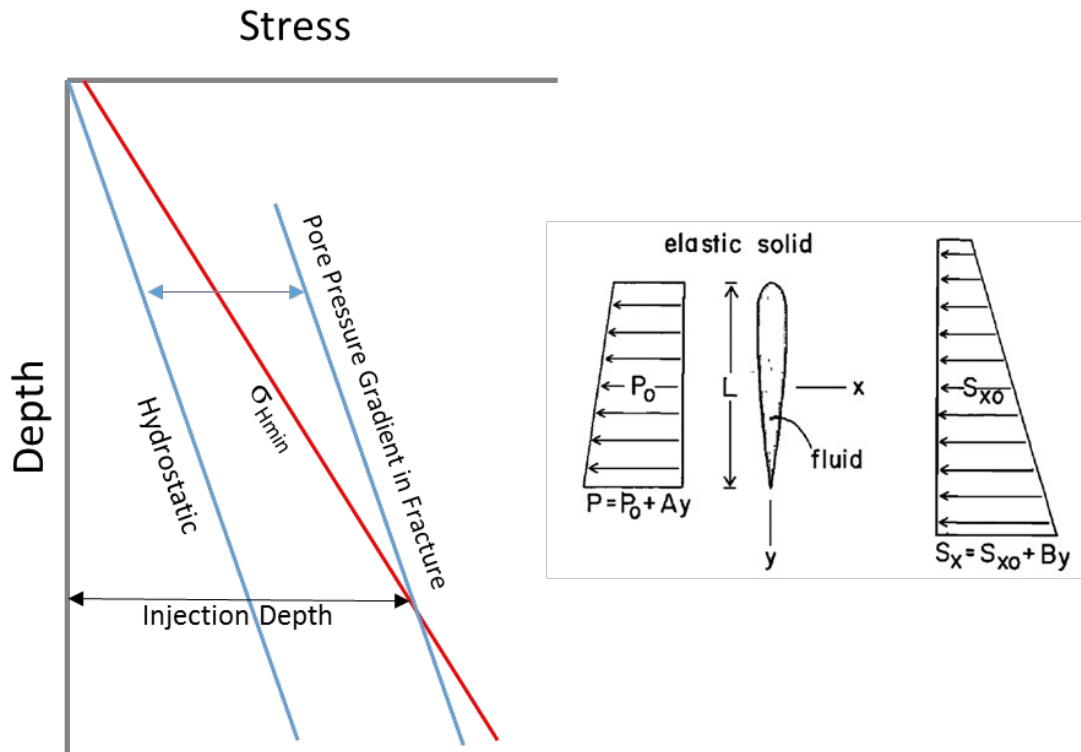


Figure 87. Left: Comparison of pore pressure gradient in the fracture with minimum stress. To open fractures, pore pressure (or pressure inside fractures) must equal the minimum stress. However, the pressure gradient within the fracture is based on the fluid density and parallels the hydrostatic gradient. The difference between the fluid pressure in the fracture and the stress normal to the fracture increases with shallower depth causing the fracture to be more open at shallow depth. Right: Illustration of apertures opening with shallower depth from Secor and Pollard (1975). P_0 is the gradient of fluid pressure and S_{x0} is the gradient of rock stress. The “teardrop” shape shows the variation in fracture aperture with depth, which is controlled by relative difference between fluid pressure and rock stress.

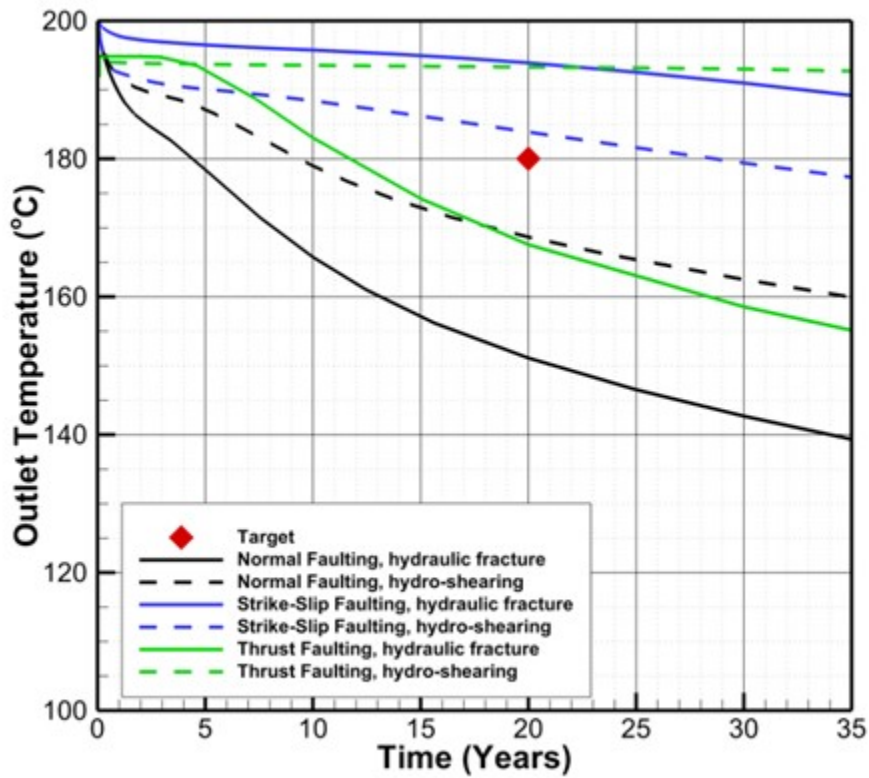


Figure 88. Thermal performance of hydraulic fracture and hydro-sheared fracture models for each faulting terrain. Poor performance of the Normal faulting hydraulic fracture model comes from preferential circulation in shallower, cooler parts of the model due to enhanced fracture aperture at shallower depth.

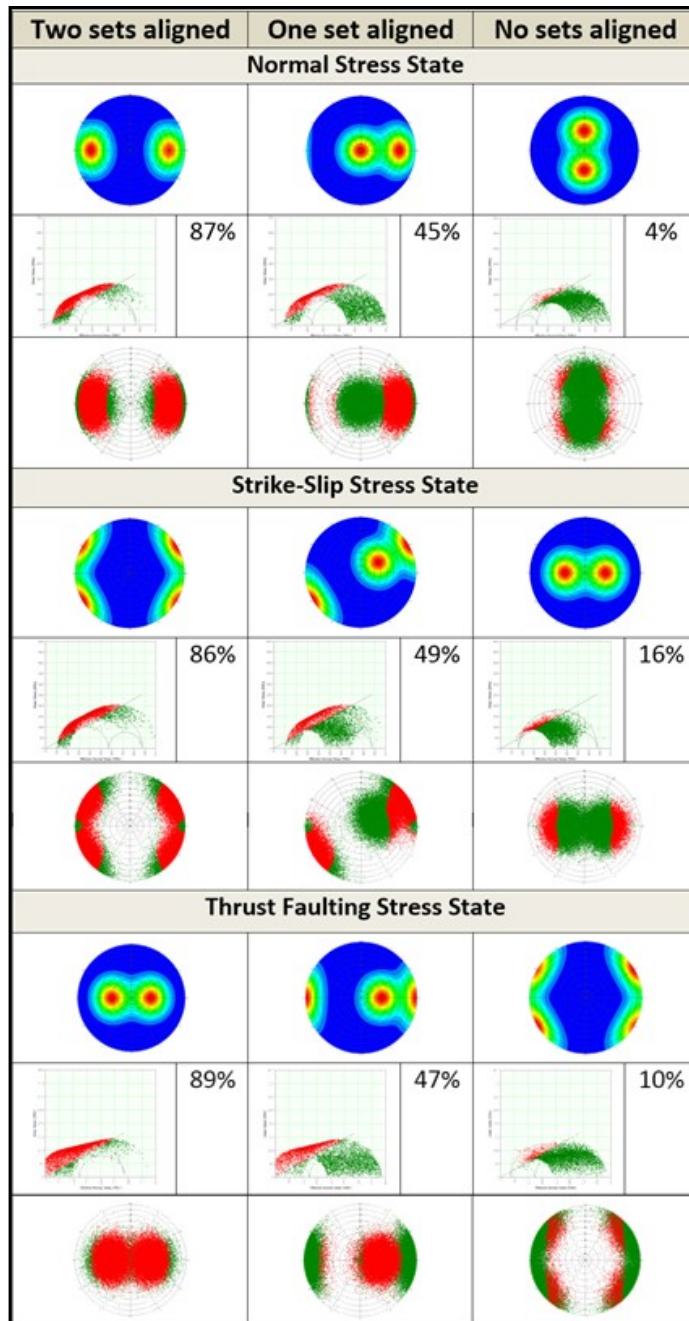
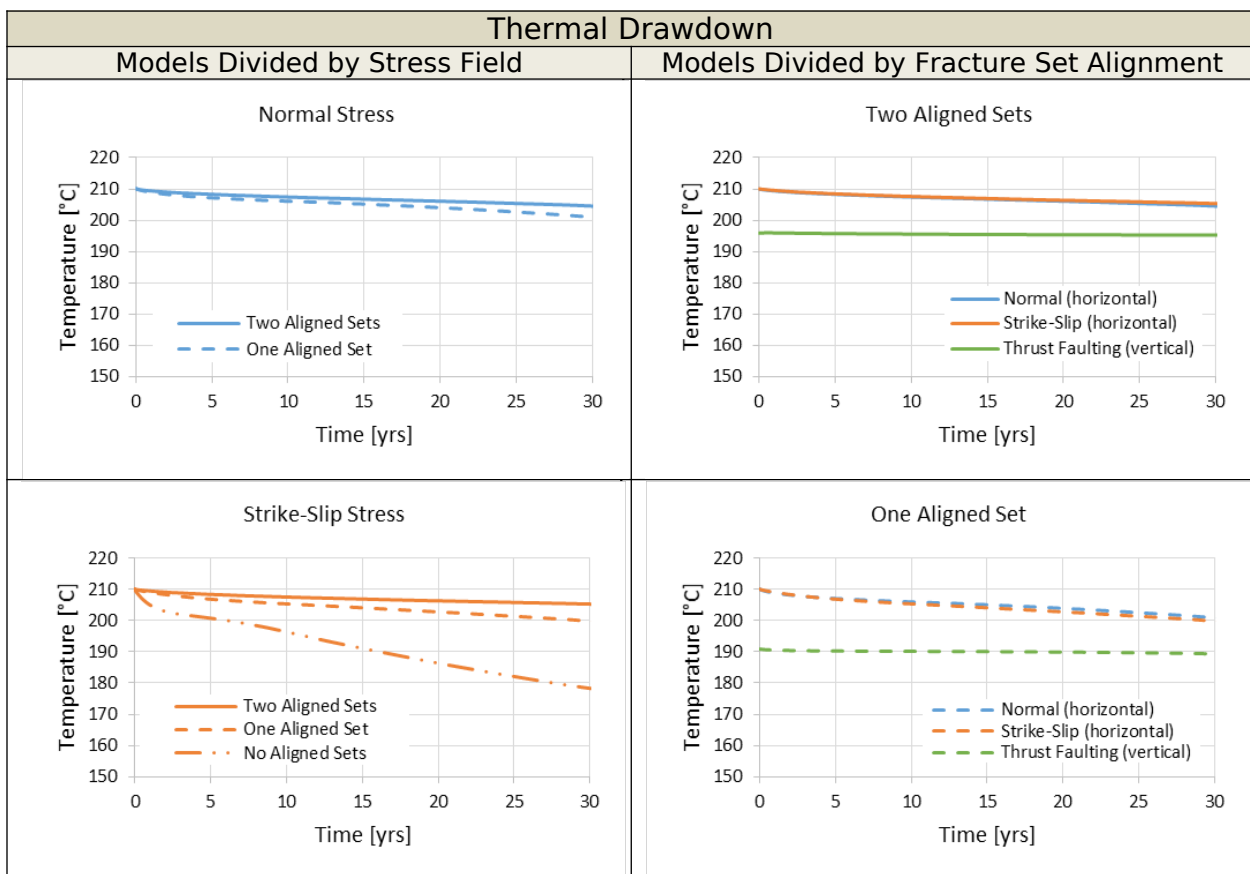


Figure 89. Summary of Constant Material Property model. For each stress state (normal, strike-slip, thrust), there is a DFN model with two sets aligned for shear stimulation, one set aligned and one not, and no sets aligned (top row of stereographic projections). The second row for each stress state shows a Mohr diagram of shear versus normal stress with critically stressed fractures (red) and non-critically stressed fractures (green) with percent critically stressed. The bottom row for each stress state is a stereographic projection of poles to the fractures with critically stressed in red and not critically stressed in green.



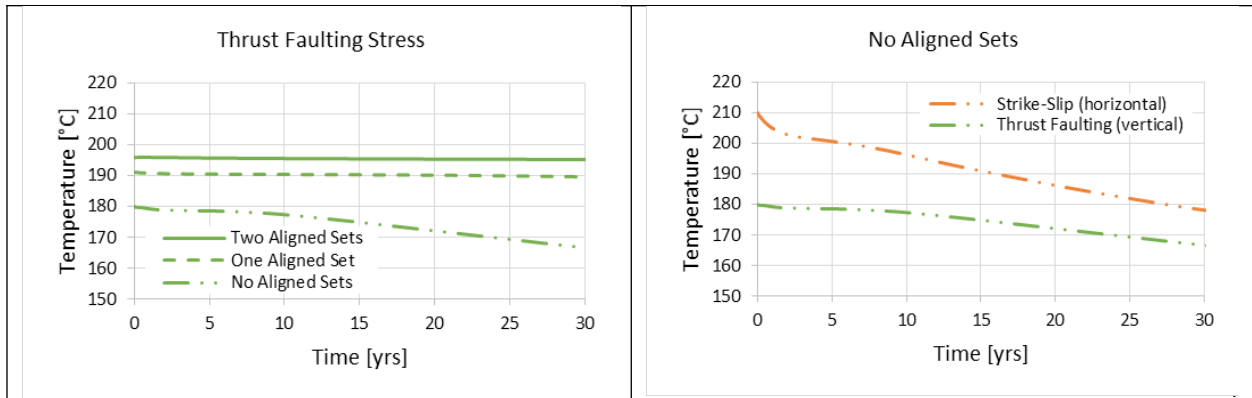


Figure 90. Thermal behaviors in three regional faulting terrains (normal, strike-slip, and thrust) for constant material properties and thermal conditions. There are a total of nine combinations of stress state and fracture orientation. Simulations assume two fracture sets where both sets are optimally aligned for shear stimulation (two aligned sets), one set is optimally aligned and the other set is not (one aligned set), and where neither set is optimally aligned (no aligned sets). The normal stress model with no aligned sets produced no connectivity and has no thermal curve.

Table 18. Parameters and impedance results for Archetypical Faulting Terrain models.

	<i>Normal Faulting</i>	<i>Strike-Slip Faulting</i>	<i>Thrust Faulting</i>
<i>Generic Site</i>	<i>Desert Peak, Nevada</i>	<i>Salton Sea, California</i>	<i>Mirror Lake, New Hampshire</i>
<i>Rock Type</i>	<i>Metavolcanic</i>	<i>Basalt</i>	<i>Granite</i>
<i>Depth to Reservoir (km)</i>	3.3	2.2	8.3
<i>Thermal Gradient (°C/km)</i>	60	90	24
<i>Maximum stress gradient, σ_1 (MPa/km) and orientation to clockwise to N</i>	25, vertical	27, horizontal at 135°	30, horizontal at 50°
<i>Intermediate stress, σ_2 gradient(MPa/km) and orientation to N</i>	17, horizontal at 25°	24.1, vertical	25, horizontal at 140°
<i>Minimum, stress, σ_3 gradient (MPa/km) and orientation to N</i>	15, horizontal at 115°	16, horizontal at 45°	22.3, vertical
<i>Impedance with no stimulation(MPa/kg/s)</i>	32.0	8.0	25.0
<i>Impedance, hydro-shearing only (MPa/kg/s)</i>	0.22	0.39	0.17
<i>Impedance, hydraulic fracture only (MPa/kg/s)</i>	0.26	0.44	8.1
<i>Impedance, hydraulic fracture and hydro-shearing (MPa/kg/s)</i>	0.06	0.04	0.17

Table 19. Description of Constant Material Property models with impedance results.

	<i>Normal Faulting</i>	<i>Strike-Slip Faulting</i>	<i>Thrust Faulting</i>
<i>Rock Type</i>	<i>Granite</i>		
<i>Depth to Reservoir (km)</i>	<i>3.5</i>		
<i>Thermal Gradient (°C/km)</i>	<i>60</i>		
<i>Maximum stress gradient, σ_1 (MPa/km) and orientation to clockwise to N</i>	<i>22.3, Vertical</i>	<i>27, horizontal at 0°</i>	<i>30, horizontal at 90°</i>
<i>Intermediate stress, σ_2 gradient(MPa/km) and orientation to N</i>	<i>17, horizontal at 90°</i>	<i>22.3, vertical</i>	<i>25, horizontal at 0°</i>
<i>Minimum, stress, σ_3 gradient (MPa/km) and orientation to N</i>	<i>15, horizontal at 0°</i>	<i>16, horizontal at 90°</i>	<i>22.3, vertical</i>
<i>Impedance, 2 sets aligned(MPa/kg/s)</i>	<i>.019 horizontal well</i>	<i>.027 horizontal well</i>	<i>.013 vertical well</i>
<i>Impedance,1 set aligned (MPa/kg/s)</i>	<i>.082 horizontal well</i>	<i>.059 horizontal well</i>	<i>.048 vertical well</i>
<i>Impedance, no sets aligned (MPa/kg/s)</i>	<i>No connectivity</i>	<i>.356 horizontal well</i>	<i>.358 vertical well</i>

56 Synthesis and Conclusions

56.1 Objectives and Basic Criteria of EGS Performance

57 Purpose of this Panel Report

This report presents the results of discrete fracture network (DFN) models to assess EGS performance. Discrete fracture network models are distinct from the porous continuum models conventionally used for EGS stimulation. They represent fractures explicitly as individual, fluid-conducting features rather than averaging and homogenizing fractures into a continuous porous medium (see Figure 3 and Figure 4).

The primary goals of the DFN simulations were the following:

- Determine under what conditions EGS may or may not be viable,
- Guide analyses, including coupled hydro-thermo-mechanical-chemical modeling, to understand critical parameters and sensitivities, and
- Provide input to future field operations and EGS demonstrations.

The panel's efforts included DFN simulation studies by Itasca Consulting Group, Inc., Golder Associates Inc., Lawrence Livermore National Laboratory (LLNL), and Lawrence Berkeley National Laboratory (LBNL).

DFN models capture more efficiently than porous continuum models the potential for localization of deformation and flow; the heterogeneity of flow from networks with variable transmissivities, sizes and connectivities; and the anisotropy of flow arising from preferred fracture orientations. Furthermore, recent advances in DFN modeling capabilities allow simulation of coupled mechanical, thermal, and chemical processes including shear stimulation of natural fractures. These characteristics of fracture networks have a strong influence on EGS performance as they determine the surface area for heat exchange, the sizes and shapes of the rock blocks that contain stored thermal energy, and the impedance (flow resistance) of the network to fluid circulation.

The DFN modeling efforts in this report do not simulate specific EGS development sites. Rather, they are numerical experiments that look at the influence of fracture networks on EGS performance. They attempt to look at generic characteristics of fractures to determine which among these characteristics most strongly influence EGS performance.

The following sections address these three tasks in turn, but here are some major conclusions that arise from this work.

- A viable EGS requires several square kilometers of effective fracture area for heat exchange. Creating a reservoir with this surface area will likely require multiple fractures or stimulations.
- Heterogeneity of transmissivity between fractures in a multi-stage stimulation EGS and within single fractures reduces the effective heat exchange area; heterogeneous EGS systems may lead to further localization of deformation and flow resulting in short-circuited systems that have early thermal breakthrough at the production well without significantly depleting the rock's stored heat.
- EGS developments may utilize shear-stimulated natural fracture networks that have multiple fracture-sets favorably oriented relative to anisotropic in-situ stress state. Among other factors, well placement to create circulation pathways through multiple fracture sets may enhance access to fracture surface area for heat exchange.
- Chemical effects can be effectively simulated in continuum models (TOUGH) to show permeability changes with dissolution and precipitation during EGS production.
- Three-dimensional simulations are required to capture the effects of DFN and stress and fluid pressure gradients that may drive preferential vertical growth into cooler or hotter portions of the reservoir.
- EGS development strategies may regionally depend on the geothermal temperature gradients, the natural fracture network geometries, and the natural fracture hydro-mechanical properties, and especially the orientations of natural fractures relative to the principal stress directions and magnitudes.

The following sections describe each of these findings along with their implications for EGS viability and effect on field operations and EGS demonstrations.

58 Criteria for EGS Viability

Two basic EGS performance criteria guided the modelling efforts –

- a circulating flow rate that would achieve 5 MW_e power production, and
- the sustainability of the production water temperature over time, or thermal longevity.

The circulating flow rate criterion for 5 MW_e power production was a volumetric flow rate of 0.08 m³/s (80 liters/s) or mass flow rate of 80 kg/s based on

$$W_e = \eta \rho_f q \Delta T c_w$$

- the temperature difference, ΔT , between the injection fluid and initial reservoir rock
- the circulating fluid density, ρ_f , and specific heat capacity, c_w (J/kg/°C),
- the thermal efficiency of the generating system, η , which is number between 0 and 1, and
- a fluid density of 1000 kg/m³, fluid heat capacity of 4180 J/kg/°C, a temperature difference of 150°C, and efficiency of 10% (§1.4).

The second requirement was thermal longevity. The EGS system should produce for twenty years with a temperature decline no greater than 10% of the temperature difference between the injection fluid and the initial reservoir temperature³. Ideally thermal longevity depends on the rate of depletion of the stored thermal energy in the rock; however, early thermal breakthrough may occur due to “short circuits” in the fracture circulation system. Short circuits are fracture connections where the circulation rate outpaces the heat exchange from the rock

3

In this summary section the term “thermal breakthrough” is defined as the time to a 10% decline in the production well temperature relative to the initial reservoir temperature and the injection well temperature or $(T_R - T_P)/(T_R - T_I) = 0.1$ where the subscripts signify *P* for production well, *I* for injection well, and *R* for initial reservoir.

resulting in production temperature drops without significant depletion of the heat stored in the rock.

An additional concern is the stability of the heat exchanger over time with respect to chemical or biological fouling. Circulating fluids may create dissolution or precipitation conditions (or both). Chemical and biological effect may reduce, enhance, or redistribute permeability within the heat exchanger. Chemical effects not only affect the impedance of the system but also change the characteristics of the heat exchanger. Section 6 addresses approaches to simulating coupled hydro-thermal-chemical processes in fracture networks.

58.1 Fracture surface area required for an EGS Heat Exchanger and need for multifracture EGS

59 Lessons from analytical solutions

Analytical solutions provide simple approximations of the surface area required to meet the power production and thermal longevity. A rearrangement of the definition of dimensionless time in the analytical solution of Gringarten et al. (1975 and described in §2.2.1 and §2.2.4) provides this approximation of the required surface area, A :

$$A = q \sqrt{\frac{t_l}{t_{D10}}} C_1$$

where

t_l is the target thermal longevity (assume 20 years or 6.3×10^8 seconds),

t_{D10} is the dimensionless time corresponding to a 10% decline in the production well temperature (Figure 6. t_{D10} is approximately 0.74 for a single fracture ($x_{eD} = \infty$) and reduces to 0.5 for a closely-spaced fractures, ($x_{eD} = 0.5$)

q is the volumetric flow rate ($0.080 \text{ m}^3/\text{s}$),

C_1 is a lumped parameter containing the rock and water properties ($\sim 2.6 \times 10^6 \text{ s/m}^2$, based on Table 3).

The area of a single fracture that satisfies these performance criteria is $3.4 \times 10^6 \text{ m}^2$ (3.4 km^2) for the viability criteria of a 20-year thermal longevity (time to 10% thermal decline in the production well), 80 liter/second flow rate, and material properties like those for the Newberry, Oregon, experimental EGS

site (Cladouhos et al. 2011, and Table 3 in this report). This area is equivalent to a fracture that is 0.5 km high and 6.8 km long assuming a 100% effectiveness in the surface area for heat transfer (Figure 91). The spacing of the injector and producer wells for such a single fracture is an unrealistically large 6.4 km (Figure 91).

60 Second power dependency of thermal breakthrough on rate and area and need for a multifracture EGS

An important implication of analytical solutions is the second power relations of thermal longevity to surface area and flow rate. Rearranging the equation in previous section gives

$$t_b = \frac{t_{D10}}{C_1} \left(\frac{A_e}{q} \right)^2 .$$

Decreasing the flow rate or increasing the effective surface area has second power effect on increasing the thermal longevity. Conversely, increasing the flow rate or having less surface area decreases the thermal longevity also shortens the time to thermal breakthrough by a second power. For example, doubling the flow rate in an EGS system will decrease thermal longevity by a factor of four.

If the spacing between injector and producer wells is limited to a range of 500 m to 1 km, a single fracture may be unlikely to support both the rate and thermal longevity criteria. The design approach may require determining the flow rate within a single fracture or stimulation that will produce the desired thermal longevity. If this flow rate is less than the desired power production, then the EGS design will require multiple stimulations whose cumulative production meets the power production criterion (Figure 92).

As an example, an EGS system producing from a single 524-m square fracture (Figure 93) will have a thermal breakthrough of 51 days producing at 80 liters/second. The same fracture with a flow rate of 7.6 liters per second will have a thermal longevity of 20 years. A desired production of 80 liters/second will need to come from 12 fractures producing 6.7 liters each to meet both the power production and thermal longevity criteria.

61 Input for future field operations and EGS demonstrations

The prediction of surface area is a critical need for EGS design. Overestimating the surface area may lead to unexpectedly early thermal breakthrough. The simple models also demonstrate the need for robust models and calculations to determine flow rates that will assure thermal longevity.

Validating the second power relationships of flow and thermal longevity would be good targets for in situ experimentation at all scales. Early breakthrough is not an indicator that the rock is thermally depleted. Methods for mitigating the effects of early breakthrough could include reducing flow rate or allowing time for thermal recovery before restarting, albeit at the lower flow rate. Early thermal breakthrough in one stimulation might indicate a need to change the circulation to another existing or new stimulation zone.

The need for characterizing surface area and validating predictions is discussed further in section 8.4.4.

61.1 Effects of Heterogeneity Between Fractures and within a Single Fracture

62 The problem of heterogeneity

The hydraulic properties of fractures are not uniform. The transmissivity⁴ may vary both among fractures and within a single fracture. The variability of transmissivity distributes flow non-uniformly over the fracture surfaces, which concentrates flow in the most transmissive fractures in a multi-fracture EGS system and in transmissive channels of heterogenous single fractures.

63 Heterogeneity within a single fracture

The heterogeneity of flow within a single fracture reduces the time to the thermal breakthrough and causes a significant degradation of thermal performance (§5.5

⁴

flow rate per unit fracture width per unit hydraulic head

and Figure 94). Thermal-mechanical coupling further enhances heterogeneity (localization) of flow and the degradation effect.

Consider a homogeneous fracture where the injection and production wells are 500 m apart (Fu et al., 2016). With a 12 liter/s flow rate, the thermal breakthrough occurs in 5.8 years. Adding heterogeneity to the fracture reduces the breakthrough time ~70% to 1.7 years.

Thermal-mechanical coupling increases the aperture of the fracture in the areas of greatest cooling, creating channelization effects. A fracture that is initially homogeneous therefore becomes heterogenous along the main flow lines reducing the breakthrough time to 4.2 years. The thermal-mechanical coupling effects are even more dramatic in the heterogenous case, where the breakthrough time reduces to 0.92 years.

64 Heterogeneity between fractures in a multiple stimulation EGS

Heterogeneity of transmissivity among the fractures in a multifracture stimulation has a significant effect on thermal breakthrough time. Consider a 12-fracture case identical to the homogenous system in §8.3.2 except one fracture is taking 50% of the flow, a second fracture is taking 25%, and remaining 25% of the flow is distributed uniformly among the other ten fractures (Figure 94). Assuming these fractures have a large enough spacing that they are not thermally interacting, the Gringarten solution provides a basis for calculating the production well temperature. For this example, the thermal breakthrough occurs in eleven months compared with 20 years for a set of homogenous fractures.

65 Input for future field operations and EGS demonstrations

65.1.1.1 Understanding effective surface area

Heterogeneity reduces the effective surface area for heat exchange in an EGS. A critical need for predicting EGS performance will be having a means of identifying this heterogeneity and estimating an “effective” surface area for heat exchange. Among the possible characterization methods could be geophysical monitoring and tracer testing.

Microseismic monitoring of fracture behavior during stimulation and production is well established for determining the spatial extent of fracture stimulation; however, it may not be able to determine the total fracture surface area or the heterogeneities within the fractures to a resolution necessary to make performance predictions. Other forms of tomographic characterization may be capable of resolving heterogeneities within fractures, but these would need to be checked against actual thermal circulation tests.

Tracer tests provide a direct means of assessing heterogeneity mainly using tracers with behaviors that depend on interacting with the rock over the fracture surface area. Estimates of both sorption onto surfaces and diffusion of tracers into the rock will constrain the effective surface area.

Whatever methods may be used, the effect of heterogeneity on thermal circulation requires testing at multiple scales, including laboratory, 10-100-meter field scale, and in EGS test sites. These experiments need to include thermal circulation to compare estimates of total fracture surface area with those coming from geophysics and tracer tests. One approach for designing EGS systems could be the development of “rules of thumb” from thermal circulation experiments. Such experiments would compare the calculated surface areas from the production versus time behaviors with the fracture surface areas known from geomechanical calculations and geophysical characterization.

Using proppants may provide some homogenization to the fracture transmissivities. The heterogeneity of fractures will likely be less in dilated fractures where the walls are separated than in rough fractures where flow occurs in channels between the asperities that in contact with one another. Maintaining fractures in a dilated state requires pressures that exceed the normal stresses on the fracture unless proppants can be emplaced to maintain the wall separations. Comparisons of effective surface area in propped versus unpropped fractures can be investigated at multiple scales from laboratory tests at sub-meter scale to field experiments at scales from tens to hundreds of meters.

65.1.1.2 Controlling flow to multiple stimulations in an injection well

Heterogeneity among fractures in a multifracture stimulation causes the most transmissive fractures to take most of the flow in an open-hole injection. The dominance of the more transmissive fractures (flow-paths) results in early thermal breakthrough.

A critical need may be the development of zonal isolation strategies that allow separate control of each stimulation stage in the well to ensure the stages are taking uniform rates, albeit at different injection pressures. This will also require characterization methods including flow logging that clearly show the rates being taken by each stimulated fracture.

Testing strategies for multiple completions and separate control of stimulation stages will be a key technology development for EGS if multiple stimulations will be employed.

65.2 Stimulation of Natural Fracture Networks and Optimizing EGS Performance

66 *Natural fractures and EGS*

Fracture surface area is the key to a successful EGS development. The previous sections showed that ~3 square kilometers of effective surface area are required to sustain 5MW_e power production over 20 years. Furthermore, that heterogeneity of permeability within and between fractures reduces the effective heat exchange area.

The stimulation of natural fractures may be one approach to creating the large surface areas necessary for a successful EGS development. Under the right conditions of in situ stress and fracture orientation, fluid injection may cause these fractures to dilate and shear to create the pathways necessary for EGS circulation. The effective surface of the natural fractures may be further enhanced if

- the stimulated networks contain fractures with multiple orientations and
- the wells are positioned to create tortuous pathways through these networks.

67 Well positioning and fracture networks

The positioning of wells in a reservoir with multiple stimulated fracture sets has a very strong influence on thermal performance especially if the fracture sets vary in their transmissivity. For a reservoir with two sets – a major and a minor set – this alignment is crucial in determining the sweep of the circulation through the fracture network (Figure 95).

Alignment of the wells with the major fracture set (that is, the set with greater in-situ permeability) creates a limited number of direct pathways between the injection and production wells. The short circuiting along the major fractures results in early thermal breakthrough and inefficient heat production from a relatively small portion of the reservoir.

Well alignments in the minor fracture set direction or in a direction intermediate to the two sets create tortuous pathways that enhance the effective surface area for heat exchange. These pathways improve the sweep of the circulating fluids through the fracture network. The main drawbacks of positioning wells in the direction of the minor fracture set are the possibility of higher impedance and poorer connectivity. The poor connectivity may create challenges for establishing circulation between the wells, especially if the inter-well distances are large.

These drawbacks may be mitigated by positioning the wells in an alignment intermediate to the two fracture sets. Numerical simulation using fracture networks models may assist in optimizing heat exchange area, impedance, and connectivity for specific sites.

Itasca (§4.2.3) investigated the effects of well placement and spacing. The Itasca 2-D network contained two fracture sets, a major set which was more conductive and continuous and a minor set which was less so. The production and injection wells were laid out in three configurations, one parallel to the major set, one parallel to the minor set, and a third positioned in a direction intermediate to the two sets.

The intermediate well positioning produced the best production performance based on thermal longevity (time to 10% thermal decline). For a spacing of 500 m, the well pair aligned with the major declined by 10% in temperature in roughly 4 months, while the intermediate well alignment took 28 months to decline that

amount. The well pair aligned in the secondary set direction behaved between the intermediate and major set alignments breaking through in about 12 months.

The LLNL well positioning studies (§5.3) also used two fractures sets. Like the Itasca simulations, the alignment in the minor set direction performed considerably better than the alignment in the major set direction. Single well pairs spaced 800 m apart with 20 kg/s flows had thermal break through times of 17 years for circulation in the major fracture-set direction and greater than 30 years for the minor set direction. LLNL did not specifically simulate flow in a direction intermediate to the two sets, however, they did look at a so-called 5-spot configuration with four production wells at the corners of an 800-m square and an injector at the center (Figure 51). The overall pattern of the wells aligned two of the production wells more closely with the major fracture set, and the other two more closely with the minor set. The wells aligned more closely with the major set had breakthrough in 18 years compared with nearly 25 years for the wells aligned more closely with the minor set.

68 Optimizing shear stimulation for fracture surface area

The DFN simulations of Itasca and LLNL explored the creation of fracture surface by shear stimulation and its effects on heat transfer. Among the factors these simulations considered were fracture network geometry, fracture properties, and in situ stress conditions.

Itasca's two-dimensional simulations used a fracture network with two stochastic sets to investigate the effects of fracture network geometry and properties on shear-stimulated area and thermal performance during fluid circulation. The simulations took two forms — coupled hydromechanical models without thermal coupling and coupled hydro-thermo-mechanical models. The hydromechanical models mainly investigated factors that affected stimulated fracture surface area during stimulation of EGS, while the hydro-thermal-mechanical models were used to simulate the production phase to predict produced temperature and energy versus time.

Among the variables considered by hydromechanical models were fracture size and intensity⁵, fracture dilation angle, and in-situ stress conditions. The fracture size and intensity variation studies found that these parameters strongly influenced the

5

connectivity of the fracture network over the model space. Simulations with longer fractures tended to localize deformation and flow along single pre-existing fracture resulting in relatively short breakthrough time during production. Networks of shorter fractures with multiple sets favorably oriented to slip during stimulation resulted in a connected network of fractures relatively uniformly stimulated in shear.

The models applied a major and a minor principal in situ stress at the boundaries. The ratio of these stresses influences the shear stimulation potential, where a large difference allowed shear stimulation at lower injection pressures for a wider range of fracture orientations, while more equal stresses required higher stimulation pressures for a limited range of fracture orientations.

Itasca's coupled hydro-thermo-mechanical simulations identified several factors that increase the surface area for heat exchange and improve thermal performance. Increasing the distance between the injection and production wells is one of these effects provided the distances are not too large for fracture networks to retain their connectivity. Higher fracture intensity (more fracture per unit area) increases the surface area for heat exchange.

69 Three-dimensional DFN simulation of multi-stage stimulation

Itasca compared multi-stage and single-stage stimulation strategies (§3.5.3) using 3D DFN simulations. Single stage stimulation injects over the entire open hole section of the well. In such a case, the most naturally conductive zones take most of the stimulation fluid to the detriment of less conductive zones. Multi-stage stimulations use multiple isolated sections, which distribute the injection fluid more evenly along the length of the well resulting in a larger number of fractures being stimulated. The area of shear stimulated fractures from multi-stage stimulation was more than double that of single-stage stimulation.

Fracture length per unit area in two dimensions or fracture area per unit volume in three dimensions.

70 Effects of Thermal-Hydro-Mechanical Coupling

70.1.1.1 Basic Effects

During EGS production the rock thermally contracts as it cools. A portion of that contraction increases the apertures of the fractures. The opening of fractures, in turn, increases the transmissivity of the fracture and decreases the flow impedance. Both Itasca and LLNL compared EGS simulation with and without thermal-mechanical coupling.

70.1.1.2 LLNL DFN simulations

The LLNL simulations found that thermal effects increase the heterogeneity of the flow properties significantly. These effects follow a positive feedback where cooled portions of fracture network become more transmissive as apertures increase. The localization of thermal contraction further concentrates flow enhancing channeling effects both among fractures (§5.4) and within single fractures (§5.5). As discussed above, thermal-mechanically induced channeling reduces the effective heat-exchange area and results in early thermal breakthroughs.

70.1.1.3 Itasca DFN simulations

Itasca performed their simulations of well positioning and spacing effects using both coupled and non-coupled models (§4.2.4 and Figure 37 to Figure 39). The uncoupled production-well temperature curves have a smooth decline with time. The coupled results, while following the general trends of the uncoupled curves, include occasional jumps and reversals in decline trends (i.e., non-monotonic histories). The similarity in the coupled and uncoupled trends seems to indicate that coupling (which is computationally more demanding) was not necessary to determine the overall trends in production performance. Sometimes non-monotonic temperature and produced energy histories predicted by these DEM models imply the complex coupled behaviors with fractures opening (secondary stimulation) or closing relatively quickly in different parts of the fracture network (potentially shutting off or opening entire flow paths between the wells) with sudden effects that can explain jumps in the production temperature. This effect is overstated in a 2D approximation in which fracture closure at a single point on a flow path can shut-off that entire path and divert the flow.

70.1.1.4 Discussion and further work

The LLNL and Itasca models use fundamentally different approaches to stimulation. Itasca's codes explicitly included the fractures and intervening rock blocks in the discretization of the simulation. LLNL, on the other hand used a DFN-informed approach to production simulation rather than directly performing simulations on the fracture networks. This approach maps (or upscales) the fracture properties into the grid of a continuum solver.

These two approaches produce production thermal histories that are fundamentally different, where LLNL's DFN-informed approach produces smooth, monotonically decreasing production temperatures, and Itasca's explicit modeling of the fractures and matrix blocks produces both jumps in production temperature and occasional reverses in production temperature trends, as discussed in §8.5.5.3 and shown in Figure 37.

The work in this report did not include any common problems for code cross verification. An additional study of the irregular thermal behaviors predicted by DEM simulations seems to be warranted. The resolution of these issues requires further work.

71 *Input for future field operations and EGS demonstrations*

DFN simulations show the value of stimulating multiple fracture sets and positioning wells to optimize the circulation through the stimulated fracture networks for enhancing heat-exchange surface area. This is an important topic for both field operations and EGS demonstrations and it has several components including:

- Identifying natural fracture sets that are prone to shear stimulation
- Knowing the in-situ stresses well enough to accurately predict the conditions for shear-stimulating one or multiple sets
- Understanding the tradeoffs in fracture connectivity and impedance associated with positioning wells to avoid localization of deformation and flow along the major fracture sets and exploit tortuous pathways including minor fracture sets.

- Validating fracture exploitation strategies using production temperature behaviors in field experiments.
- Validating in field experiments the ability to create and characterize hydro-sheared natural fracture pathways for EGS circulation.
- Cross-verification and validation of DFN modeling approaches including discrete fracture modeling codes and methods for upscaling fracture properties to continuum models.

71.1 Simulation of Coupled Chemical Effects

72 *Importance of chemical effects*

Coupled chemical effects have importance both in the characterization and operation of an EGS reservoir. The successful production of the EGS reservoir requires recognizing, predicting, and mitigating changes in the flow circulation caused by the chemical processes that locally reduce or enhance the openings of fractures.

The coupled chemical simulations discussed in Section 6 use a hybrid modeling process that maps fracture properties from a DFN model into TOUGHREACT, a well-established continuum code for geothermal applications. The simulations were based on fracture data and conditions from the Newberry, Oregon, geothermal development site (Cladouhos et al., 2011).

The Newberry simulation results clearly show that the circulation system evolves over time due to chemical processes.

73 *Input for future field operations and EGS demonstrations*

The results presented in this report serve primarily as a demonstration of a simulation approach that upscales fracture properties from a DFN model to a well-established continuum code (TOUGH). As such, this report does not provide major conclusions regarding chemistry other than acknowledging progress that has been made to date and recognizing the need to develop further the ability to predict chemical effects in EGS production from fracture networks.

A successful EGS development requires not only the existence of a fracture network with sufficient area for heat exchange, but also the ability to maintain that surface area through the production life of the reservoir. Chemical effects are extremely important to the sustainability of the reservoir and should be a focus of EGS field demonstrations and further model development.

73.1 Three-Dimensional DFN Models in Different Regional Settings

74 Regional settings

A major attraction of EGS development is the possibility of producing geothermal energy anywhere that rock with sufficient temperature exists and not just the few places where there is a naturally conductive geothermal reservoir. Hot rock exists in the subsurface everywhere; however, the depth to an exploitable thermal reservoir will vary depending on the geothermal gradient.

This section of the report considered regional variations of EGS performance within the continental United States. The approach simulated EGS power production using 3D DFN models of fracture networks of three archetypical regional settings:

- A thrust faulting setting in granitic rock in the northeastern US with low geothermal gradient
- A normal faulting setting in metavolcanics rock in western basin and range province with a high geothermal gradient (based on Desert Peak, Nevada), and
- A strike-slip faulting setting in basalt proximal to California's San Andreas Fault in the Salton Sea Basin with a very high geothermal gradient.

The ability to shear stimulate varied greatly among the three cases. The normal and strike-slip settings were very close to critical stress conditions even before stimulation, while the thrust faulting case proved very difficult due to the high stress conditions and depths required to reach the target reservoir temperature of 200°C.

75 Estimating the effect of shear stimulation on transmissivity

A significant area of uncertainty in the modeling was the transmissivity increase due to shear stimulation. The modeling used multipliers of 10, 100, and 1000 over the natural fracture transmissivity. Flow simulations targeted an impedance of 0.15 MPa/l/s, which could be achieved with multiplier of 10 in the strike-slip setting but required multipliers of 100 or more for the normal and thrust fault setting. Achieving low impedance was particularly challenging for the thrust faulting case where initial fracture transmissivity values were very low due to the depths and stresses. In general, at least one fracture set needs to be optimally aligned for shear stimulation to achieve acceptable impedance values.

76 Three dimensional behaviors

The three-dimensional modeling revealed two key behaviors that would not be evident in two-dimensional modeling. For the thrust-faulting case, shear stimulation favored shallow-dipping fractures at shallower depths. This negatively affected thermal performance as shallower fractures are also cooler fractures.

The second key behavior in three-dimensional modeling appeared in the normal faulting stimulations where fracture growth also was favored by shallower stress conditions. Simulations of hydraulic stimulation for a basin and range, normal faulting environment (§ 7.2.3.3, Figure 87) can result in upward growth of hydraulic fractures and hydraulically stimulated natural fractures. The vertical growth depends on the relative gradients of the minimum horizontal stress and the fluid pressure. Assuming the reservoir temperature is decreasing with shallower depth, the upwards growth means that the circulation system will produce from cooler rock than at the depth where the stimulation initiates. Preferential vertical growth was also observed at the Rosemanowes test site in the United Kingdom (Pine and Batchelor, 1984) albeit in a downwards direction. The vertical migration was attributed to the stress and fluid pressure gradients.

77 Input for future field operations and EGS demonstrations

The results of the three-dimensional modelling in different regional settings reinforce several key points including the following:

- Understanding the in-situ stress conditions
- Characterization of the major fracture set orientations with respect to critical stress and shear stimulation.

Additionally, these simulations point out the needs for the following:

- Better estimation of the transmissivity changes that result from shear stimulation from field data and
- Better understanding of the influence of stress and pore pressure gradients with depth and their effect on vertical growth of stimulated fracture networks.

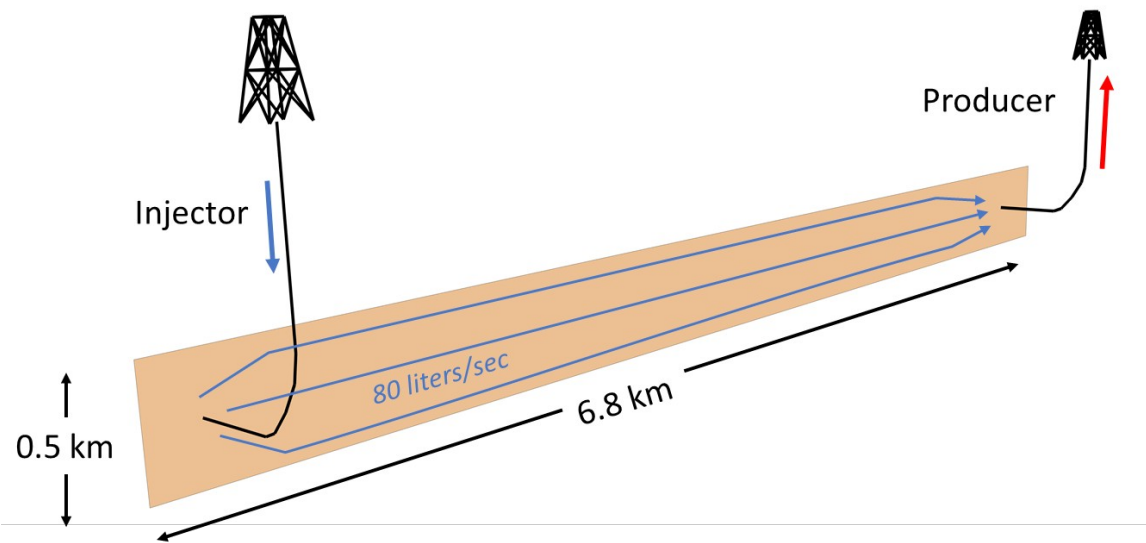


Figure 91. Example of a single fracture EGS capable of producing 5 MW_e for 20 years.

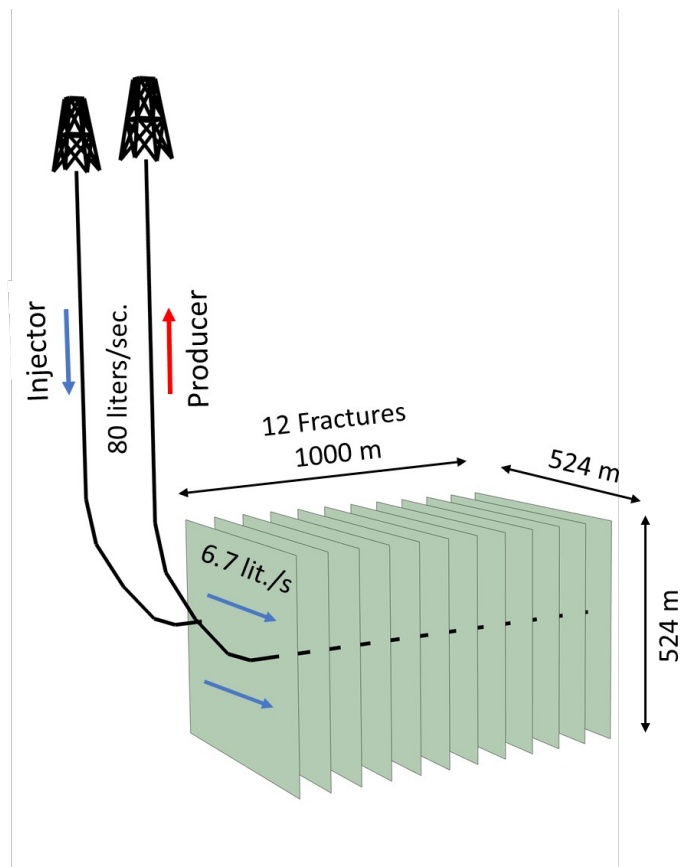


Figure 92. Example of multifracture EGS capable of producing 5 MW_e for 20 years.

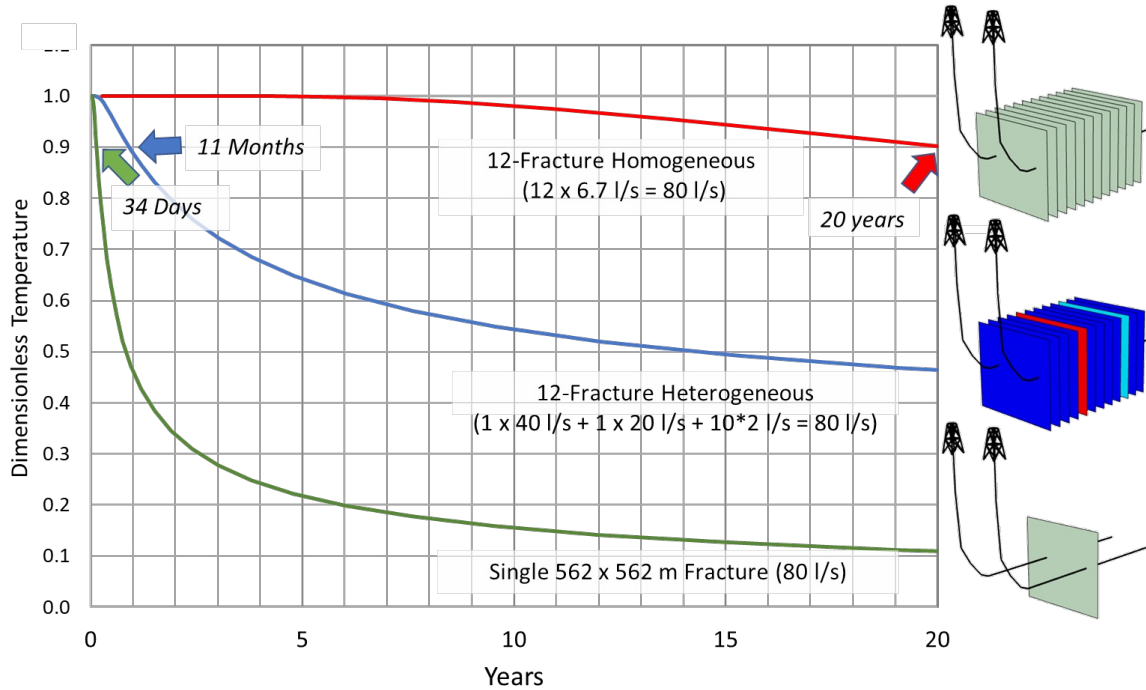


Figure 93. Comparison of production temperature histories for an EGS using multiple homogenous fractures, multiple heterogeneous fractures, and a single fracture with same dimensions as one of the fractures in the multiple fracture case. Arrows point out the time to thermal breakthrough (10% production temperature decline or dimensionless temperature equals 0.9). The heterogeneous and single fracture cases see much earlier thermal breakthrough than the homogenous case.

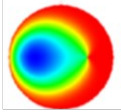
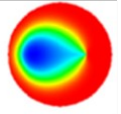
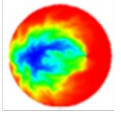
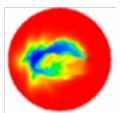
		10 % Production Temperature Decline	30-year Temperature Field
Homogeneous	No Coupling	5.8 years	
	Thermal Coupling	4.2 years	
Heterogeneous	No Coupling	1.7 years <i>(~70% reduction from homogeneous)</i>	
	Thermal Coupling	0.92 years <i>(~80% reduction from homogeneous)</i>	

Figure 94. Thermal performance in a homogeneously and heterogeneously transmissive fracture with and without thermal-mechanical coupling. Heterogeneity channelizes the flow resulting in earlier thermal breakthrough. This channelization increases with thermal-mechanical coupling. Results from Fu et al. (2016).

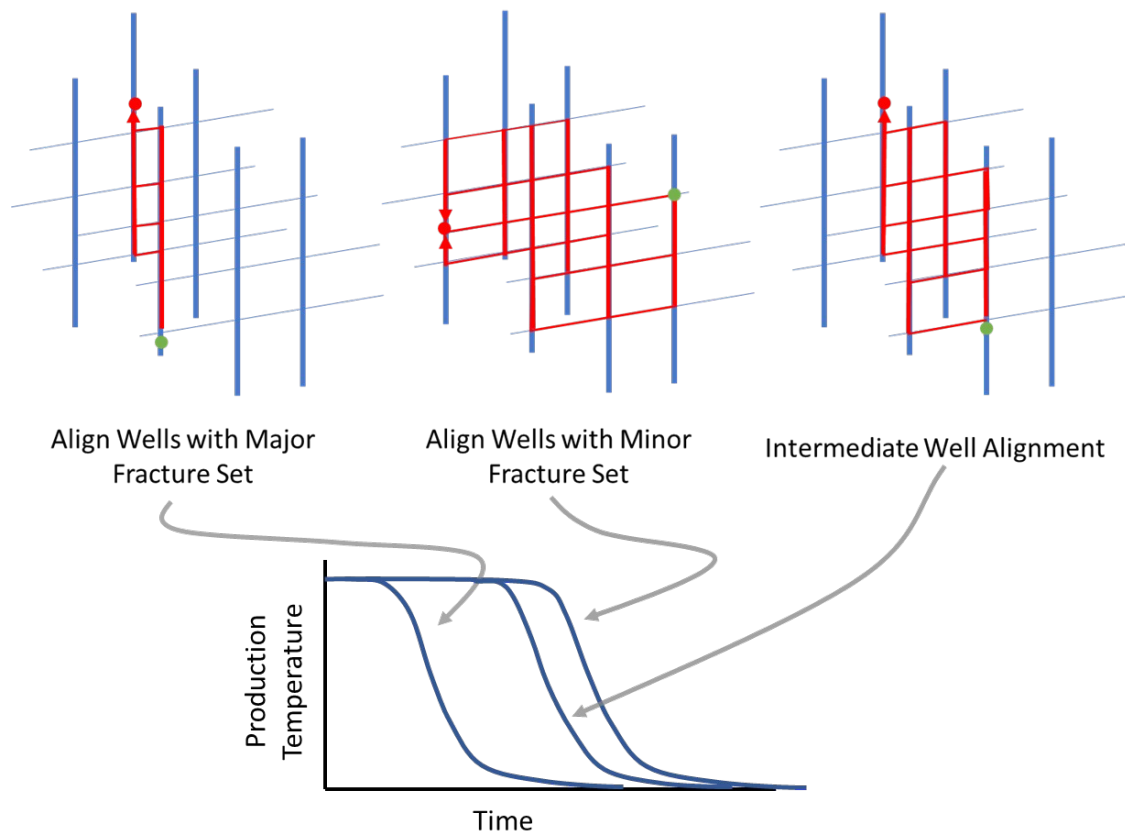


Figure 95. Conceptual model of the effects of well positioning with respect to major and minor fracture sets. Thermal performance improves when the well layout exploits tortuous pathways through multiple fracture sets.

78 Acknowledgements

Special thanks to Susan Sprinkle (LBNL) and Patrick Dobson (LBNL) for assistance with editing and report finalization.

This work was supported by the Assistant Secretary for Energy Efficiency and Renewable Energy (EERE), Office of Technology Development, Geothermal Technologies Program, of the U.S. Department of Energy under Contract No. DE-AC02-05CH11231 with LBNL, contract DE-NA0003525 with SNL, and contract DE-AC52-07NA27344 with LLNL.

79 References

- Anderson, 1951. *The Dynamics of Faulting*, Oliver and Boyd, Edinburgh, 206 p.
- Bargar, K.E., and Keith, T.E., 1999. Hydrothermal mineralogy of core from geothermal drill boreholes at Newberry Volcano, Oregon, U.S. Geological Survey Professional Paper 1578.
- Battistelli, A., Calore, C., and Pruess, K., 1997. The simulator TOUGH2/EWASG for modelling geothermal reservoirs with brines and non-condensable gas. *Geothermics*, 26, 437-464.
- Barton, C., Zoback, M., and Moos, D., 1995. Fluid flow along potentially active faults in crystalline rock, *Geology*, 23, 683-686.
- Bennett, D. S, Wittkop, C.A., and Dicken, C.L., 2006. Bedrock Geologic Map of New Hampshire - A Digital Representation of the Lyons and others 1997 map and ancillary files: U.S. Geological Survey Data Series 215, scale 1:250,000, CD-ROM.
- Bonnet E., Bour, O., Odling, N., Davy, P., Main, I., Cowie, P., and Berkowitz, B., 2001. Scaling of fracture systems in geologic media, *Reviews of Geophysics*, 39, 347-383.
- Breede, K., Dzebisashvili, K., Liu, X., and Falcone, G., 2013. A Systematic Review of Enhanced (or Engineered) Geothermal Systems: Past, Present and Future, *Geothermal Energy*, 1, 1-27.
- Brunner, P., and Simmons, C., 2012. HydroGeoSphere: a fully integrated, physically based hydrological model, *Ground Water*, 50, 170-176.
- Butler, S., Sanyal, S., and Robertson-Tait, A., 2004. A numerical simulation study of the performance of enhanced geothermal systems, *Proceedings, 29th Workshop on Geothermal Reservoir Engineering*, Stanford University, Stanford, California, January 26-28, 2004, SGP-TR-175.
- Carroll, S., Mroczek, E., Alai, M., and Ebert, M., 1998. Amorphous Silica Precipitation (60 to 120°C): Comparison of Laboratory and Field Rates, *Geochim. Cosmochim. Acta*, 62, 1379-1396.
- Cladouhos, T., Clyne, M., Nichols, M., Petty, S., Osborn, W., and Nofziger, N., 2011. Newberry Volcano EGS demonstration stimulation modeling, *Geothermal Resources Council Transactions* 35, 317-322.
- Cottrell, M., Hosseinpour, H., and Dershowitz, W., 2013. Rapid discrete fracture analysis of hydraulic fracture development in naturally fractured reservoirs, *Unconventional Resources Technology Conference*, SPE-168843-MS.
- Davatzes, N.C., and Hickman, S.H., 2009. Fractures, stress, and fluid flow prior to stimulation of well 27-15, Desert Peak, Nevada, EGS project. *Proceedings, 34th Workshop on Geothermal Reservoir Engineering*, Stanford University, Stanford, California, 11p.
- de Dreuzy, J.R., Darcel, C., Davy, P., and Bour, O., 2004. Influence of spatial correlation of fracture centers on the permeability of two-dimensional fracture

- networks following a power law length distribution, *Water Resources Research*, 40, W01502, doi: 10.1029/2003WR002260.
- Dempsey D., S. Kelkar, N. Davatzes, S. Hickman, D. Moos, and E. Zemach, 2014. Evaluating the roles of thermoelastic and poroelastic stress changes in the Desert Peak EGS stimulation. *Proceedings, 39th Workshop on Geothermal Reservoir Engineering*, Stanford University, Stanford, California, 14p.
- Dershowitz, W.S., Cottrell, M.G., Lim, D.H., and Doe, T.W., 2010. A Discrete Fracture Network Approach for Evaluation of Hydraulic Fracture Simulation of Naturally Fractured Reservoirs, *American Rock Mechanics Association (ARMA) Conference*, United States.
- Dobson, P.F., Kneafsey, T.J., Sonnenthal, E.L., Spycher, N.F., and Apps, J.A., 2003. Experimental and numerical simulation of dissolution and precipitation: Implications for fracture sealing at Yucca Mountain, Nevada. *Journal of Contaminant Hydrology*, 62-63, 459-476.
- Dobson, P.F., Salah, S., Spycher, N., and Sonnenthal, E.L., 2004. Simulation of water-rock interaction in the Yellowstone geothermal system using TOUGHREACT, *Geothermics*, 33, 493-502.
- Doe, T., McLaren, R., and Dershowitz, W., 2014. Discrete fracture network simulations of enhanced geothermal systems, *Proceedings, 39th Workshop on Geothermal Reservoir Engineering*, Stanford University, Stanford, California, SGP-TR-202.
- Doe, T., and McLaren, R., 2016. Discrete fracture network analysis of controlling factors for EGS performance, *Proceedings 41st Workshop on Geothermal Reservoir Engineering* Stanford University, Stanford, California, SGP-TR-209.
- Du, Q., Faber, V., and Gunzburger, M., 1999. Centroidal Voronoi tessellations: applications and algorithms. *SIAM Review*, 41(4), 637-676.
- Finnila, A., Dershowitz, W., Doe, T., and McLaren, R., 2015. Hydro-shearing and hydraulic fracturing for enhanced geothermal systems in archetypical normal, strike-slip and thrust faulting terrains, *Geothermal Resources Council Transactions*, v. 39.
- Finnila, A., Dershowitz, W., and McLaren, R., 2016. Geomechanical analysis of egs reservoir development in normal, strike-slip and thrust faulting terrains, *Proceedings, 41st Workshop on Geothermal Reservoir Engineering*, Stanford University, Stanford, California, SGP-TR-209.
- Finnila, A., Doe, T., and McLaren, R., 2017. Dependency of EGS development on the alignment between natural fracture set orientations and regional stress state, *Proceedings, 42nd Workshop on Geothermal Reservoir Engineering*, Stanford University, Stanford, California, SGP-TR-212.
- Finsterle, S., Sonnenthal, E.L., and Spycher, N., 2014. Advances in subsurface modeling using the TOUGH suite of simulators. *Computers & Geosciences*, 65, 2-12.
- Fu, P., Hao, Y., Walsh, S., and Carrigan, C., 2016. Thermal drawdown-induced flow channeling in fractured geothermal reservoirs, *Rock Mech Rock Eng*, 49, 1001-1024.

- Fu, P., and Carrigan, C., 2014. Exploring EGS well layouts that mitigate thermal drawdown-induced flow channeling, Proceedings, 39th Workshop on Geothermal Reservoir Engineering, Stanford University, Stanford, California, SGP-TR-202.
- Gringarten, A.C., Witherspoon, P.A., and Ohnishi, Y., 1975. Theory of heat extraction from fractured hot dry rock, *Journal of Geophysical Research*, 80, 1120-1124.
- Guo, B., Fu, P., Hao, Y., Peters, C., and Carrigan, C., 2016. Thermal drawdown induced flow channeling in a single fracture in EGS, *Geothermics*, 61, 46-62.
- Hartley, L., and Roberts, D., 2012. Summary of discrete fracture network modelling as applied to hydrogeology of the Forsmark and Laxemar sites, Svensk Kärnbränslehantering Report R-12-04.
<http://www.skb.com/publication/2656007/R-12-04.pdf>
- Haukwa, C.B., 1999. AMESH: A mesh creating program for the Integral Finite Difference Method. User's Manual. Earth Sciences Division, E.O. Lawrence Berkeley National Laboratory, Berkeley, CA, MOL.19990519.0191.
- Holland A., 2002. Microearthquake study of the Salton Sea Geothermal field, California: Evidence of stress triggering. INEEL/EXT-02-00191, 77p.
- Ingebritsen, S.E., Geiger, S., Hurwitz, S., and Driesner, T., 2010. Numerical simulation of magmatic hydrothermal systems. *Reviews of Geophysics*, 48, 1-33.
- Itasca, 2011. Itasca UDEC (Universal Distinct Element Code), Version 5.0, Itasca Consulting Group, Inc., Minneapolis.
- INL (Idaho National Engineering Laboratory), 2006. The Future of Geothermal Energy Impact of Enhanced Geothermal Systems (EGS) on the United States in the 21st Century. INL/EXT-06-11746, 372p.
- Johnson, C.D., and Dunstan, A.H., 1998. Lithology and fracture characterization from drilling investigations in the Mirror Lake Area, Grafton County, New Hampshire. USGS Water-Resources Investigations Report 98-4183, 211p.
- JASON, 2013. Enhanced Geothermal Systems, JSR-13-320, 141 pp., MITRE Corporation, McLean, VA.
- Keith, T.E.C., and Bargar, K.E., 1988. Petrology and hydrothermal mineralogy of US Geological Survey Newberry 2 drill core from Newberry Caldera, Oregon, *Journal of Geophysical Research*, 93, 10,174-10,190.
- Kilb, D., 2010. State of stress at the southernmost end of the San Andreas fault: integration of seismicity patterns and focal mechanisms with fault structure observed in seismic reflection data beneath the Salton Sea., USGS/NEHRP G09AP00098, 11p.
- Kim J., Sonnenthal, E., and Rutqvist, J., 2015. A sequential implicit algorithm of chemo-thermo-poro- mechanics for fractured geothermal reservoirs. *Computers & Geosciences*, 76, 59-71.
- McClure, M., and Horne, R., 2013. Discrete Fracture Network Modeling of Hydraulic Stimulation: Coupling Flow and Geomechanics, Springer Briefs in Earth Sciences, Springer, 89p.

- Miller, S.A., 2015. Modeling enhanced geothermal systems and the essential nature of large-scale changes in permeability at the onset of slip. *Geofluids*, v. 15, p. 338-349.
- O'Sullivan, M.J., Pruess, K., and Lippmann, M.J., 2001. State of the art of geothermal reservoir simulation. *Geothermics*, 30, 395-429.
- Palandri, J., and Kharaka, Y.K., 2004. A compilation of rate parameters of water-mineral interaction kinetics for application to geochemical modeling. US Geol. Surv. Open File Report 2004-1068. 64 pp.
- Pine, R.J., and Batchelor, A., 1984. Downward migration of shearing in jointed rock during hydraulic injections. *International Journal of Rock Mechanics and Mining Sciences*, 21, 249-263.
- Pruess, K., 1990. Modeling of geothermal reservoirs: Fundamental processes, computer simulation and field applications. *Geothermics*, 19, 3-15.
- Pruess, K., Oldenburg, C., and Moridis, G., 1999. TOUGH2 User's Guide Version 2. Lawrence Berkeley National Laboratory, (November), 210. Retrieved from <http://escholarship.org/uc/item/4df6700h.pdf>
- Reed M. and Palandri, J., 2006, SOLTHERM.H06, A Database of Equilibrium Constants for Minerals and Aqueous Species, Available from the authors, University of Oregon, Eugene, Oregon.
- Reinecker J., Heidbach, O., Tingay, M., Sperner, B., and Müller, B., 2005. The release 2005 of the World Stress Map. (available online at www.world-stress-map.org).
- Riahi, A., and Damjanac, B., 2013. Numerical study of hydro-shearing in geothermal reservoirs with a pre-existing discrete fracture network, 38th Workshop on Geothermal Reservoir Engineering, Stanford University, Stanford, California, 9p.
- Riahi, A., Damjanac, B., and Furtney, J., 2014a. Thermo-hydro-Mechanical Numerical Modeling of Stimulation and Heat Production of EGS Reservoirs, Proceedings, 48th US Rock Mechanics Symposium ARMA-2014-7741.
- Riahi, A., Damjanac, B., and Furtney, J., 2014b. Discrete element modeling of thermo-hydro-mechanical coupling in enhanced geothermal reservoirs, Proceedings, 39th Workshop on Geothermal Reservoir Engineering, Stanford University, Stanford, California, 9p.
- Riahi, A., Furtney, J., and Damjanac, 2014c, Evaluation of optimum well positioning in enhanced geothermal reservoirs using numerical modeling, *Geothermal Resources Council Transactions*, 38, 325-330.
- Riahi, A., Radakovic-Guzina, Z., Damjanac, B., and Katsaga, T., 2015. Three-dimensional numerical investigation on the effect of injection method on shear stimulation of enhanced geothermal reservoirs, Proceedings, 49th US Rock Mechanics/Geomechanics Symposium, (San Francisco, June 28-July 1 2015), ARMA-2015-869.
- Robertson-Tait, A. and Johnson, S., 2005, Progress on the Desert Peak EGS project, *Geothermal Resources Council Transactions*, 29, 117-213.
- Rose, P.E., Benoit, W.R., and Kilbourne, P.M., 2001. The application of polyaromatic sulfonates as geothermal tracers in geothermal reservoirs. *Geothermics*, 30, 617-640.

- Sanyal, S., and Butler, S., 2005. An analysis of power generation prospects from enhanced geothermal systems, Proceedings, World Geothermal Conference 2005.
- Secor, D., and Pollard, D., 1975. On the stability of open hydraulic fractures in the earth's crust, *Geophysical Research Letters*, 2, 510-513.
- Settgast, R.R, Fu, P., Walsh, S.D.C, White, J.A., Annavarapu, C., and Ryerson, F.J., 2017. A fully coupled method for massively parallel simulation of hydraulically driven fractures in 3-dimensions. *International Journal for Numerical and Analytical Methods in Geomechanics*, 41(5): 627-653, DOI: 10.1002/nag.2557.
- Smith, J.T., Sonnenthal, E.L., and Cladouhos, T., 2015. Thermal-hydrological-mechanical modelling of shear stimulation at Newberry Volcano, Oregon. Proceedings of the 49th Rock Mechanics / Geomechanics Symposium of the American Rock Mechanics Association, ARMA2015-000680.
- Sonnenthal, E., Spycher, N., Callahan, O., Cladouhos, T., and Petty, S., 2012. A thermal-hydrological-chemical model for the enhanced geothermal system demonstration project at Newberry Volcano, Oregon, Proceedings, 37th Workshop on Geothermal Reservoir Engineering, Stanford University, SGP-TR-194
- Sonnenthal E.L., Smith, J.T., Cladouhos, T., Kim, J., and Yang, L., 2015. Thermal-hydrological-mechanical-chemical modeling of the 2014 EGS stimulation experiment at Newberry Volcano, Oregon. Proceedings, 40th Workshop on Geothermal Reservoir Engineering Stanford University, Stanford, California, January 26-28, 2015. SGP-TR-204.
- Swyer M.W., and Davatzes, N.C., 2013. Evaluating the role of the Rhyolite Ridge fault system in the Desert Peak geothermal field with robust sensitivity testing through boundary element modeling and likelihood analysis. 38th Workshop on Geothermal Reservoir Engineering, Stanford University, Stanford, California, 16p.
- Therrien, R., and Sudicky, E.A., 1996. Three-dimensional analysis of variably-saturated flow and solute transport in discretely-fractured porous media, *J. Cont. Hyd.*, 23, 1-44.
- Tsang, C.-F., and Neretieks, I., 1998. Flow channeling in heterogeneous fractured rocks, *Reviews of Geophysics*, 36, 275-298.
- Williams C.F., and DeAngelo, J., 2015. Developing improved methods for the assessment of enhanced geothermal systems. Proceedings, 40th Workshop on Geothermal Reservoir Engineering, Stanford University, Stanford, California, 9p.
- Xu, T., and Pruess, K., 2001a. On fluid flow and mineral alteration in fractured caprock of magmatic hydrothermal systems, *J. Geophys. Res.*, 106, 2121-2138.
- Xu, T., and Pruess, K., 2001b. Modeling multiphase fluid flow and reactive geochemical transport in variably saturated fractured rocks: 1. Methodology, *Am. J. Sci.*, 301, 16-33.
- Xu, T., Sonnenthal, E., Spycher, N., Pruess, K., Brimhall, G., and Apps, J., 2001. Modeling multiphase fluid flow and reactive geochemical transport in variably saturated fractured rocks: 2. Applications to supergene copper enrichment and hydrothermal flows, *Am. J. Sci.*, 301, 34-59.

- Xu, T., Sonnenthal, E.L., Spycher, N., and Pruess, K., 2006. TOUGHREACT - A simulation program for non-isothermal multiphase reactive geochemical transport in variably saturated geologic media: Applications to geothermal injectivity and CO₂ geological sequestration, *Computers & Geosciences*, 32, 145-165.
- Xu, T., Spycher, N.F., Sonnenthal, E., Zhang, G., Zheng, L., and Pruess, K., 2011. TOUGHREACT Version 2.0: A simulator for subsurface reactive transport under non-isothermal multiphase flow conditions, *Computers and Geosciences*, **37**, 763-774.
- Zoback, M., 2007. *Reservoir Geomechanics*, Cambridge University Press, 449 p.